UAlg
UNIVERSIDADE DO ALGARVE

UNIVERSIDADE DO ALGARVE

GIS and Palaeontology integrated application for the recognition of tsunamigenic events in Doñana National Park

Liliana de Castro Dias Guerra

Projeto para obtenção do Grau de Mestre em Geomática

Trabalho efectuado sob a orientação de:
Professor Dr. Francisco Ruiz
E
Professora Dr. Cristina Veiga-Pires

2013/2014

Declaração de autoria de trabalho

Declaro ser a autora deste trabalho, que é original e inédito. Autores e trabalhos consultados estão devidamente citados no texto e constam da listagem de referências incluída.

(Setembro 2014)

Acknowledgements

My master thesis wouldn't have been possible without the help and support of many people within the University faculties and of course my family.

First I would like to thank my parents, that gave me the opportunity of studying far from home, that trusted me to complete a bachelor and master degrees, and always supported my choices and paths throughout the years. Without them, definitely none of these would have been possible. Thank you very much mom and dad, to whom the love I feel cannot be measured.

A special thanks to Sónia Oliveira, my partner in this master throughout the years. Times were tough mainly in the first year, and the second year wasn't a piece of cake either! Your support, patient and friendship made the master so much easier and fun. You were the best team mate that I had the pleasure to work with, and I know we will be great investigators in the future and friends for a very long time, hopefully forever!

My deep gratitude to Professor Cristina Veiga-Pires, who always had my back and was always available to help me with everything! Our field trip to Doñana National Park was one of the best experiences of my life, one that I will never forget, and will always be thankful for sharing it with her. It was a lot of fun! Not only is she a great teacher, as well a great person, very funny, and always available to share her big heart! Thank you very much! I wouldn't have chosen any other person to come along with me in my master's journey!

I can't thank enough to the Centro de Investigação Marinha e Ambiental (CIMA) for enabling me to work in the Micropaleontology laboratory, especially to investigators Isabel Mendes and Francisca Rosa that taught me everything I know today about foraminifera and made me fell in love with this wonderful tiny and beautiful world! You two are the people I most admire and I am very grateful to have been given the opportunity of learning and working with both of you!

I would also like to thank Ana Isabel Gomes for all the friendship and support given to me throughout these years, which was very important to me! Thank you for all your patient helping me with my doubts and for welcoming me to the laboratory as if I was

part of the house! I was honored to have been able to share the Sevilla experience with you, to get to know you better and see the great person you are!

A special thanks to technician Paulo Santana, a funny and peculiar guy, who was always available to help me in the treatment of my samples, and with who I became a great friend within the University.

Thank you also to Professor José Rodrigues for teaching me everything I know in the ArcGIS software and his guidance along the way, which was very helpful for the accomplishment of my master thesis.

Last but not least, a special thanks to Professor Francisco Ruiz for the opportunity of working with his data and to get to know Huelva and Doñana National Park!

A huge thanks to Manuel Abad, who while away, was always available for any doubt and very helpful! For his company and guidance in the Doñana National Park field trip! It was an honor to get to know you and work with you!

Thank you also to Professor María Luz González-Regalado Montero for helping me at the Universidade de Huelva, reviewing my taxa identification and preparation for SEM photography! It was a pleasure working with you, thank you for your availability and patient!

I hope I haven’t forgotten anyone! A last thanks to all my friends who are always present in my mind, and to my colleagues within the master degree.

Abstract

The present work aimed to characterize the actual and past environments at Doñana National Park (SW Spain) throughout the study of benthic foraminifera assemblages at two drill holes (cores C and D, from Ruiz et al., 2004) and twenty surface samples, as well as to recognize and confirm the occurrence of extreme energy events (storms/tsunamis) around 2165 yrs B.P. (215 yrs BC).

The studied tsunamigenic beds have between 8 to 26 cm in Core C and 40 to 10 cm in Core D. Almost all the variables studied in the present work concur with previous works on tsunamigenic layers found worldwide. These variables include the foraminifera species found in the tsunamigenic layer, the composition of sand beds (suggesting strong waves and currents), the presence of reworked molluscs, marine foraminifera taxa, high values for planktonic/benthic ratio, and high Shannon H, Fisher Alpha and Species richness diversity indexes.

In our case the diversity index that evidences the most the occurrence of a tsunami seems to be Fisher Alpha, which value is much higher than the other registered in both cores.

Regarding foraminifera species, results with relative abundance >1% were considered in the present work, rather than abundances >5% as used by many authors. These results show the presence of marine foraminifera at the tsunamigenic layers, and their absence in the remaining records, which appeared extremely important for the recognition of the occurrence of these high energy events.

From the twenty surface samples studied, only eight presented foraminifera content, which did not allow to compare the actual environments with the palaeoenvironments recorded in Cores C and D.

Finally, ArcGIS software and Geosoft Target extension helped the micropalaeontological study, enabling to confirm the palaeoenvironmts description made for Doñana National Park by other authors, as well as the occurrence of palaeotsunamis in this area.

Keywords: palaeotsunamis, benthic foraminifera, GIS, Doñana National Park

Resumo

O presente trabalho teve como objectivo caracterizar os ambientes passados e presentes no Parque Nacional de Doñana (SO Espanha) através do estudo de associações de foraminíferos bentónicos em dois furos (Cores C e D, de Ruiz et al., 2004) e vinte amostras superficiais, bem como reconhecer e confirmar a ocorrência de eventos energéticos extremos (tempestades/tsunamis) por volta de 2165 anos B.P. (215 anos BC).

As camadas tsunamigénicas estudadas têm entre 8 a 26 cm no Core C e entre 40 a 10 cm no Core D. Quase todas as variáveis estudadas no presente trabalho estão em concordância com trabalhos prévios feitos em camadas tsunamigénicas encontradas em todo o mundo. Estas variáveis incluem as espécies de foraminíferos encontradas na camada tsunamigénica, a composição das camadas arenosas (sugerindo fortes ondas e correntes), a presença de moluscos retrabalhados, foraminíferos tipicamente marinhos, valores elevados do ratio planctónicos/bentónicos, e valores elevados dos indíces de diversidade de Shannon H, Fisher Alpha e Riqueza específica.

No nosso caso o índice de diversidade que pareceu mais evidenciar a ocorrência de um tsunami foi o de Fisher Alpha, cujo valor foi muito superior a outros registados em ambos os cores.

Em relação às espécies de foraminíferos, os resultados das abundâncias relativas >1% foram considerados no presente trabalho, ao invés de abundâncias >5% como utilizado por vários autores. Estes resultados mostram a presença de foraminiferos marinhos nas camadas tsunamigénicas, e a sua ausência nas restantes, o que pareceu ser extremamente importante para o reconhecimento da ocorrência destes eventos energéticos extremos.

Das vinte amostras superficiais estudadas, apenas oito apresentaram conteúdo em foraminíferos, o que não permitiu a comparação dos ambientes actuais com os paleoambientes registados nos Cores C e D.

Finalmente, o software ArcGIS e a extensão Geosoft Target auxiliaram o estudo micropaleontológico, permitindo confirmar a descrição dos paleoambientes feitos para o Parque Nacional de Doñana por outros autores, bem como a ocorrência de paleotsunamis nesta zona.

Palavras chave: paleotsunamis, foraminíferos bentónicos, SIG, Parque Nacional de Doñana

Index

Figure Index

Table index

List of abbreviations and symbols

AD – Ano Domini

Aspi – Relative abundance of species

BC – Before Christ

BP – Before Present

CA – Cluster Analysis

CCA – Canonical Correspondence Analysis

D.N.P. – Doñana National Park

DCA – Detrended Correspondence Analysis

DMT – Digital Model Terrain

ED50 – European Datum 1950

EWE – Extreme Wave Events

GIS – Geographic Information System

GPS – Global Positioning System

Hs or H – Shannon Index of Diversity

J – Equitability Index of Diversity

Ka – Kiloyears = 1000 years

N - North

N – Total number of individuals in the sample

NE - NorthEast

Ni – Total number of inidividuals in the samples

NOOA - National Oceanic and Atmospheric Administration

NW - NorthWest

OIS - Oxygen Isotope Stages

S - South

S – Fisher Alpha Index of Diversity

S – Species Richness

SE - SouthEast

SW - SouthWest

TIN - Triangulated Irregular Network

USGS – United States Geological Survey

UTM - Universal Transverse Mercator

Xspi – Number of individuals of species *i* in the samples

I. Introduction

1 – Tsunamis

1.1- Tsunamis (general overview)

Tsunamis were described by Lapidus (1990) as “the gravity-wave system that follows any short-duration, large-scale disturbance of the free sea surface”.

Most tsunamis are produced by earthquakes with a magnitude higher than 6.5 and a focal depth between 20 and 40 km, never reaching 80 km (Fig. 1a, Iida, 1963). The tsunami magnitude is also controlled by the fault type, the aftershock area and the distance between the epicenter and the coast (cf. Ben-Menahen and Rosenman, 1972, Abe, 1973, Catalán et al., 1979, Hatori, 1995). Active dip-slip faults are potentially more dangerous than strike-slip structures because they move the ocean floor and the overlying water column vertically.

The magnitude of a tsunami (which is proportional to its energy) can be calculated from the height of the breaking wave crest above the still water level and from the length of the run-up (Fig. 1b , Iida, 1963). Iida (1963) found a direct relationship between earthquake and tsunami magnitudes (Fig. 1c) and Hatori (1995) demonstrated that the magnitude of tsunamis decreases with increasing distance from the source area.

Tsunamis are usually small and barely noticed in deep oceans, but as waves approach the coastline, the speed of the waves decreases as they are deformed within shallower water depths (Lapidus, 1990).

In terms of stages, a tsunami can be divided into three phases: the generation, the propagation to the coast and the run-up at the shoreline.

Within several minutes after the generation process, the initial tsunami is split into a tsunami that travels towards the nearby coast (called local tsunami) (Lapidus, 1990).

As the tsunami wave travels from the deep-water, continental slope region to the near-shore region, tsunami run-up occurs. Run-up is a measurement of the height of the water onshore observed above a reference sea level.

After run-up, part of the tsunami energy is reflected back to the open ocean. In addition, a tsunami can generate a particular type of wave, called edge waves, which travel back and forth, parallel to shore. These effects result in successive arrivals of waves at a particular point on the coast rather than a single wave.

Destruction from tsunamis is the direct result of inundation, wave impact on structures and erosion.

1.2- Tsunamis in the Iberian Peninsula – the case of 1755' Tsunami

Tsunamis are not frequent in Europe, although some coastal regions of the Mediterranean and of the Atlantic have been struck by several tsunami events. The eastern Mediterranean is the region of Europe where most tsunamis have been detected (Cita and Rimoldi, 1997). On the other side, the main tsunamigenic zone that affects the Iberian Peninsula is the Gorringe Bank, located at 200 km Southwest of Cape Saint Vincent (Figure 1.1).

According to Campos (1991) in the Iberian Atlantic coasts, we can consider three main seismotectonic areas and, as consequence, three main tsunamigenic areas (Figure 1.1):

"Zone A- from the Mid-Atlantic ridge to 25ºW. It is an area of expansion of the oceanic crust because of the mid-Atlantic ridge. It is unlikely that it would generate tsunamis because earthquakes are of small magnitude and their focal mechanism solution is not associated with vertical displacement.

Zone B- from Gloria fault (24ºW) to 18ºW. It is an area of friction where large-magnitude earthquakes occur, which are however associated with dextral horizontal displacements along a fault orientated E-W (Udias et al., 1985). This kind of displacement generates small tsunamis that are not generally observed on the South-western coast of the Iberian Peninsula.

Zone C- The Cadiz Gulf is the main source of tsunamis. This is a zone of intense interaction between the African and the Eurasian plates that undergo strong deformations in approaching and compressing. The most important tsunamis were generated in that area, located from 12º to 6ºW along the 36ºN parallel (which includes the Gorringe Bank). Possibly, the 1755 earthquake had its epicenter in this area."

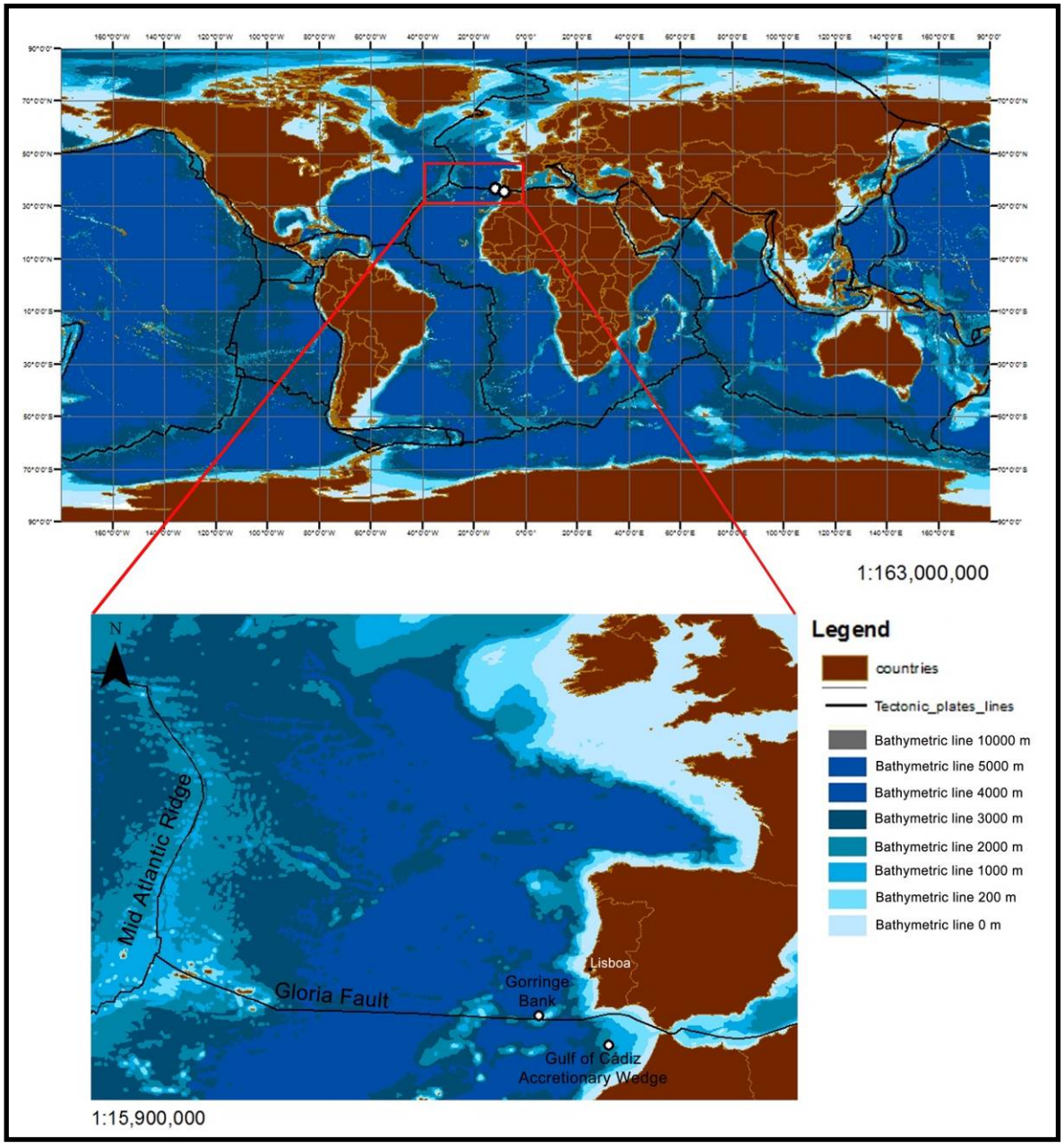

Figure 1.1. Three main tsunamigenic areas in the Iberian Peninsula, according to Campos (1991), see text for more details

Although the coasts of the Iberian Peninsula cannot be considered as very tsunamigenic, up to 27 tsunamis have been documented between the 3rd century BC and 1900 AD (Luque et al., 2001). Of these, 18 struck the Spanish and Portuguese Atlantic coasts (Galbis, 1932, 1940, Campos, 1991, 1992) (Table 1.1).

Table 1.1 - Historical Tsunamis in Portugal and Spain (from Galbis, 1932; Campos, 1991)

Historical Tsunamis	Zone
218 BC – 216 BC	Cádiz
210 BC – 209 BC	Cádiz
60 BC	Portugal and Galicia
382 AD	Portugal
881 AD	Cádiz
949 AD	Portugal
1531 AD	Lisbon – Southern Portugal
1722 AD	Southern Portugal
1731 AD	Cádiz
1755 AD	Portugal – Southern Spain
1756 AD	Portugal
1761 AD	Lisbon – Galicia
1816 AD	Portugal
1848 AD	Portugal

This was the case of the 1755 Lisbon tsunami, which was associated with an earthquake of an estimated Ms of 8,5-9 (Udías et al., 1976, Campos, 1992). The 1755 Lisbon earthquake generated several tsunami waves that struck the coasts of Portugal, Northern Morocco and Spain, and even the Sicily Islands (SW UK) as it has been demonstrated by distal deposits interbedded with lagoonal and coastal shallow-lacustrine peat sequences (Foster et al., 1991).

Tsunami waves attained the maximum registered height along the Portuguese coast (Pereira de Sousa, 1919), leaving deposits in estuarine outlets and breaching barrier islands whose associated surficial forms are still preserved in many cases. Most Portuguese studies concern the remobilization of sand from the beach barriers and the redeposition of sand, cobbles and boulders on the sheltered muddy intertidal salt marsh of Boca do Rio, Martinhal, and Ria Formosa (Andrade,1992, Andrade et al., 1994, 1997, 1998, Dawson et al., 1995, Hindson et al., 1996, Kortekaas et al., 1998a, 1998b, Hindson and Andrade, 1999, Font et al. 2013) .

Approximately one hour after the earthquake, the coasts of Cádiz and Huelva in Spain were also affected by three tsunami waves. In some places the number rose to approximately 20, and the irregular movement of water surface lasted for 24 hours (Real Academia de la Historia, 1756). Wave heights varied along the coast, with the

most frequently reported values between 3 and 4 m. Luque et al. (1999) related the sedimentary sequence of the Valdelagrana (Cadiz, south western Spain) washover deposits to the three consecutive waves that breached the sand ridge, flooding the marshes inland.

Within the area of the North-East Atlantic and Mediterranean, Spain is one of the countries with a higher tsunami risk, not only because of the danger and exposure of its coasts, but also because of its high population density and the importance of tourism infrastructure to the country's economy.

The understanding of the genesis and impact of palaeotsunamis in coastal areas is crucial to evaluate the tsunami hazard and to prevent the consequences of future tsunamis (Leroy, 2006).

2 - Geological and biological tracers

2.1 - Distinguishing Tsunamis and Storms deposits

It is important to be able to distinguish storm and tsunami deposits to reconstruct patterns of coastal change and for an accurate assessment of the hazard frequency. The study of sediments deposited by tsunamis is crucial because it will increase the knowledge and understanding of the frequency and magnitude of past events.

Tsunamis are major events in terms of sedimentary record, but identifying tsunami deposits is not easy. The enormous quantity of sediments brought inland by tsunami waves are usually contrasting in coastal stratigraphy, usually being coarser than underlying sediments. Some layers are composed of several upward-fining sequences interpreted to represent successive wave pulses, whereas other deposits are massive. However, sand beds are also deposited in intertidal and marsh environments by channel migration, river floods and storms, so some criteria are needed for distinguishing between tsunami sand and non tsunami sand deposits (Dawson et al., 1991; Einsele et al., 1996; Nayama et al., 2000; Pinegina et al., 2003).

Intensive research (Atwater, 1986; Atwater & Moore, 1992; Atwater et al., 1995; Bruzzi & Prone, 2000; Dawson et al., 1991, Kortekaas, 2002; Liu & Fearn, 1993, Nanayama et al., 2000) has been done in this fundamental aspect of how to distinguish tsunamic sedimentary formations from other marine invasive deposits (Table 1.2).

Table 1.2 - Different characteristics found in tsunami and storms, from Kortekaas (2002)

Evidence	Tsunami	Storm
Morphological	- Wash-over fans behind breached barriers	- Wash-over fans behind breached barriers
Stratigraphical	- Thins inland and becomes discontinuous - Fines inland - Erosional basal contact - Large inland extent	- Thins inland - Fines inland - Erosional basal contact - Relative smaller inland extent
Sedimentological	- BouldersOne or more finning upward sequences, sometimes homogeneous - Intraclasts from underlying material - Loading structures at base - Bi-directional imbrication - Poorly sorted (particle size from mud to boulders) - Sedimentary structures seldom found	- Boulder deposition has been reported - Finning upward or homogeneous - Not found - Not found - Unidirectional imbrication - Relatively better sorted - Sedimentary structures more common
Geochemical	- Increase in geochemical elements indicating marine origin	- No information found, but similar signature is expected because of marine origin
Paleontological	- Marine fossils - Increased diversity (mixture marine and brackish fossils) - Relative well to poorly preserved fossils - Plant fragments - Shell rich units - Rafting light material - Buried plants at base	- Marine fossils - Mixture marine and fresh water fossils - Poorly preserved fossils - Plant fragments - Shell fragments - Not found - Buried plants at base

The main conclusion of Kortekaas (2002) is that tsunami and storm deposits (as well as coseismic subsidence) have very similar geological characteristics and that only a multi-proxy approach might allow the distinction between tsunami and storm deposits such as proposed by Chagué-Goff et al. (2011).

2.2 - Foraminifera as tsunami tracers

2.2.1 - What are Foraminifera?

Foraminifera are single celled, heterotrophic protists possessing a mineralized test (shell) and granular pseudopodia, which extend through apertures of the test wall.

Classification of foraminifera is largely based upon the composition and morphology of the test. Four main compositions are currently recognized: agglutinated (test composed of cemented detrital material) (Lee and Anderson, 1991); calcareous (test composed of secreted calcium carbonate) (Haynes, 1981); proteinaceous (organic-walled test) and siliceous (test composed of silica) (Sen Gupta,1999). The first two however, are the most commonly encountered. Both the proteinaceous and siliceous forms are relatively rare and are confined to very specific environments (low salinity shallow water and deep sea settings respectively) (Sen Gupta, 1999).

Agglutinated foraminifera are those that construct their test from foreign particles, cementing them together using either proteinaceous, carbonate or ferric oxide cements (Lee and Anderson, 1991). Calcareous foraminifera secrete a test composed of calcium carbonate. Traditionally, they have been divided into two groups: the porcelanous forms and the hyaline forms. An extinct group of calcareous foraminifera, the micro granular forms, is also recognized.

Porcelanous foraminifera have imperforate tests consisting of randomly oriented rods of calcite with an ordered inner and outer layer (his structure gives the test a porcelain-like appearance (Haynes, 1981)). Hyaline forms possess perforate tests where the framework of calcite rods that compose the test have a preferred orientation, usually radial, giving the test a glassy appearance (Haynes,1981).

More recent classification schemes (Loeblich and Tappan, 1987, 1992; Sen Gupta,1999) have further subdivided the calcareous foraminifera into a number of suborders based upon chemical composition and the structure of the test (see Sen Gupta (1999) for an overview).

2.2.2 - Foraminifera as palaeoenvironmental tools

Due to foraminifera small size (between $<$100 µm–2 cm), abundant incidence, high preservation potential within the sediment record after death and distinctly diagnostic test shape, they are unsurpassed stratigraphical, palaeoecological and

palaeoenvironmental tools for statistical and systematic analysis in environmental reconstruction (Loeblich and Tappan, 1987; Hayward et al., 1999; Sen Gupta, 1999).

Assemblage composition is influenced by both abiotic (temperature, salinity, dissolved oxygen availability, nutrient flux, sedimentology, current flow, etc) and biotic (food, predation, inter- and intra-specific competition) conditions of an area (Murray, 1991). Both pelagic and benthic are abundant within the entire marine realm and some freshwater environments (and sediments). Any change in assemblage composition within a sedimentary sequence, whether it is the disappearance or introduction of a particularly indicative species, points to a shift in marine environmental conditions at the location where the tests are subsequently preserved (Mamo et al., 2009).

Foraminifera, as a group, have an ubiquist distribution, found throughout the entire marine realm. However, individual taxa are extremely restricted to specific environmental niches (for instance, marsh and brackish environments), and it is this characteristic that makes foraminifera instrumental in palaeogeographic analysis and palaeoenvironmental reconstruction (Mamo et al., 2009)

Changes in the composition of a foraminiferal assemblage can reflect migrations (Murray, 1991), extinctions (Groves et al., 2007), glaciation events (Herguera and Berger, 1991; Wells et al., 1994), marine transgression/regression (Narayan et al., 2005), the effects of biotic competition and environmental adaptation (Linke and Lutze, 1993), changes in primary productivity, seasonality (Sunet al., 2006) and even, extreme events (such as earthquake subsidence (Alvarez-Zarikian et al., 2008), storms (Palma et al., 2007) and tsunamis (Hawkes et al., 2007)).

Analyzing foraminiferal assemblage composition has the capacity to enable inferences about palaeosea levels and environmental conditions if appropriate indicative species are identified. For example, marsh assemblages are defined by low diversity assemblages containing an abundance of agglutinated taxa (Scott et al., 2001), whereas hypersaline settings are dominated by assemblages consisting of mainly porcellanous forms (Lynts, 1971).

In addition to examining ‘gross’ assemblage composition, the use of systematics (the classification of organisms with the aim of reconstructing evolutionary relationships) for individual foraminifera found within a deposit, can also provide significant information about local environmental conditions (Hayward et al., 1999; Strotz, 2003). Similarly, palaeotemperatures and other palaeogeographical

characteristics can be inferred from foraminiferal assemblages (Miao and Thunell, 1993).

2.2.3 - Foraminifera as tsunami tracers

The value and application of foraminifera coupled with palaeoenvironmental analysis, assuming that they can be recovered from the deposit, should be of relevance to tsunami geologists seeking to resolve questions about the nature, character and origin of tsunami sediments. For example, information about the composition of foraminiferal assemblage within the tsunami deposit might tell us something about the depth of water from which the sediments were entrained, or their distance of transport before deposition at the location at which they are now found (Uchida et al., 2004, 2007a,b).

Preservation and taphonomic character (post-depositional factors that directly affect the preservation of fossilized remains) of individual tests may reveal something of the flow velocity, turbidity, abrasion and post depositional environmental processes of a tsunami in terms of the nature and the severity of abrasion and disarticulation a test has undergone (Dawson et al., 1995; Hindson et al., 1996; Andrade et al., 1997; Dominey-Howes et al., 1998; Hindson and Andrade, 1999; Hindson et al., 1999; Hawkes et al., 2007; Kortekaas and Dawson, 2007; McMurty et al., 2007; Satyanarayana et al., 2007; Alvarez- Zarikian et al., 2008).

Lastly, dating foraminiferal tests contained within the tsunami deposit has the potential (depending on test wall composition and the dating methods used) to provide robust and very well constrained dates (and chronologies) for tsunami sediments where other techniques may prove problematic or are limited by available datable material. However, care must be taken, as tsunami deposits consist of sediments that often represent a chaotic reworked mixture derived from several sources and stratigraphic layers (Mamo et al., 2009).

In rare cases where no foraminifera are present in coastal or shelf waters, then none will be available for a tsunami to deposit and a significant amount of laboratory preparation and analysis time will be lost (Andrade et al., 1997; Kortekaas and Dawson, 2007; Ramirez-Herrera et al., 2007). However, a lack of foraminifera in tsunami deposited sediments is more likely due to taphonomic effects, given the ubiquitous distribution of foraminifera in the marine realm. Therefore, tsunami

geologists should use multiple techniques and palaeoenvironmental indicators such as foraminifera, diatoms and ostracods and not rely on just one group (Mamo et al., 2009).

Where tsunami geologists have investigated foraminifera, a wide range of characteristics have been advocated to demonstrate tsunami provenance. These characteristics include; changes in assemblage composition (Hindson and Andrade, 1999; Hindson et al., 1999; Hawkes, 2007) for example, marine shelf species within a lagoon or brackish environment; changes in test size or juvenile to adult ratios (Guilbault et al., 1996); a shift in population numbers (Cundy et al., 2000; Hawkes et al., 2007; Kortekaas and Dawson, 2007); or a change in the taphonomic character of the tests (Hindson et al.,1999; Hawkes et al., 2007).

This diversity (or lack of consistency) of viewpoints makes it difficult to identify a specific characteristic that might be diagnostic. In reality, it may be that a combination of characteristics (taken together with other 'diagnostic' criteria for tsunami) will be needed to positively attribute a sedimentary sequence to deposition by a tsunami. Further, given that the exact composition of an assemblage varies from location to location (even at the same latitude, water temperature etc), it is impossible to expect to see a specific 'diagnostic' species or assemblage in association with tsunami-deposited sediments. Those sediments being rather site specific.

The capacity of a tsunami to transport deep water foraminiferal assemblages in particular, may be governed by several specific factors including proximity of deepwater to the locations where the tsunami sediments are deposited; or the near-shore current flow and its potential to bring fossilized foraminifera tests into shallow water for the tsunami to redeposit. This possibility would have to be carefully examined and discarded to avoid giving a false impression of the distance of sediment transport and depth from which tsunami sediments had been derived.

Either way, it is clear from empirical work (Dominey-Howes et al., 1998; Nanayama and Shigeno, 2006; Uchida et al., 2007b) that tsunami have deposited deeper water species that would not otherwise be expected from the shallow water, coastal settings where the tsunami deposits are now found. Consequently, the occurrence of deep water assemblages may be one of the key diagnostic characteristics for tsunami-deposited sediments, given the ideal conditions. This is an hypothesis that should be tested.

The maximum possible ocean depth from which landward transport of sediments and foraminiferal assemblages might occur is currently unknown. Uchida et al. (2007b) report that assemblages indicative of water depths between −90 and −130 m were moved and deposited on land by tsunami whereas Dominey-Howes et al. (1998) noted the deposition of species associated with outer shelf to upper bathyal waters to a depth of −200 (or more) metres were deposited by a tsunami. The work of Uchida et al. (2005, 2007b) and Weiss (2008) indicates that wave amplitude and wave period are likely important parameters in determining what range of particle sizes (and by analogy, foraminifera) may be entrained and transported landward during a tsunami (keeping in mind that this also depends on the sediment size available to be entrained). Therefore, future research could seek to explore these issues.

3 - Objectives of the present work

The present work aims to evaluate the potential use of foraminiferal assemblages as proxies for recording the occurrence of extreme energy events such as storms or tsunamis in shallow coastal environments, such as in Doñana National Park. In order to achieve this main objective, the present work intends to characterize the present and past environments at Doñana National Park (SW Spain) throughout the study of benthic foraminiferal assemblages. Accordingly, two drill holes (cores) and twenty surface samples were studied, and some extreme energy events (storms/tsunamis) that occurred between 2168-2159 yrs cal B.P. (218-209 yrs BC) in this area were identified and described. The palaeoenvironmental analysis is combined with a GIS analysis (ArcGIS software and its extensions) for better representation and interpretation of sedimentary and palaeontological data.

II. Study area

1 – Location and general description

Doñana National Park was created in 1969, due to the convergence of a great amount of natural and cultural values. Doñana was successively recognized as Biosphere Reserve (1981), Wetland of International Importance by the Ramsar Agreement (1982), Certificate of the Council of Europe to the Management and Preservation (1985, renovated in 1990, 1995 and 2000) Special Birds Protection Area (ZEPA, 1988), Human Heritage (1994), among others.

Doñana National Park is one of the largest wetlands in Europe (53,790 ha) located between Huelva and Seville Spanish provinces, on the southwest part of the Iberian Peninsula (Figure 2.1 a,b).

The climate there shows the characteristic variability of a Mediterranean climate (Siljestrom & Clemente, 1990), i.e. even though the temperature is quite regular between years, the rainfall shows an irregular distribution. The irregular rainfall distribution is apparent between as well as during the years. In fact, 50% of the total precipitation falls during winter, while, in summer, a level of 5% is seldom reached (Siljestrom, 1985).

The winter is short and presents mild temperatures (seldom reaching 0°C) while the summer, long and warm, reaches temperatures over 40°C quite frequently. The extremely high temperatures in summer and scarce rainfall cause a deficit of water in summer, and rainfall that exceeds evapotranspiration occurs only during 3-4 months of the year (Siljeström & Clemente, 1990).

According to the Water Plan of the National Park, the accumulated water produces the progressive flooding of the marshes in the months of October to November, reaching its peak in January or February (Casas and Urdiales, 1995). When the marsh reaches its maximum capacity (approximately 135 hm^3), excess water is evacuated towards the Guadalquivir River. Beginning in spring, evaporation losses are not offset by the river inputs, leading to dry out the marsh in the summer (Navarro, R. 2009).

The Guadalquivir River (Figure 2.1) is the most important fluvial stream of this zone. This river is the main sediment source of the southwestern Spanish coast, with a mean annual discharge of 164 m^3/s. The highest runoff (>1000 m^3/s) occurs from January to February, when the propagation velocity of the discharge peaks rises up

to 1 m/s (Vanney, 1970; Menanteau, 1979). The tidal regime is mesotidal and semidiurnal, with an average tidal range of approximately 3.6 m (Borrego et al., 1993). Dominant waves associated with the Atlantic circulation come from the southwest with medium wave energy, as 75% of the waves do not exceed 0.5 m in height.

These conditions favor the development of broad lowlands, usually sheltered by spits, where tidal flats and freshwater marshes extend several kilometers inland. Littoral drift currents transport sand-size sediments from the Portuguese coast to the Spanish nearshore zone, determining the form of each coastal stretch (C.E.E.P.Y.C., 1979; Cuena, 1991).

Under natural conditions, most of the contributions of water were coming from several rivers and streams (Guadalquivir, Guadiamar, La Rocina Stream, El Partido Stream, etc.) including regular entries through the Guadalquivir estuary (ICONA, 1994; MMA, 2001; García Novo and Marín, 2005; García Viñas *et al*, 2005).

Groundwater, although quantitatively less important, were crucial for the maintenance of rivers and wetlands of Doñana (Navarro, R. 2009). The aquifer system of Almonte-Marismas pours its waters at various points on the periphery of Doñana, allowing the formation of temporary pools characteristics of these areas (Hondón and Sopetón), as well as springs that drain into the marsh of Doñana (García Novo and Marín, 2005).

Water availability, depth of the water-table and topography are the most import factors for the majority of the variations in the vegetation within the geomorphological units of Doñana National Park.

2 - Ecological and Geomorphological characterization

From a geological point of view the Doñana National Park is characterized by the great development of littoral and fluvio/littoral formations. The most significant littoral formations are the great sandy barriers (sandy spits) and the extensive fields of dunes. The fluvio/littoral formations are constituted by the marshes of Guadalquivir, that fill the wide sector located behind the sandy spits (Figure 2.1c). The geomorphological characterization of Doñana National Park described in this chapter was based on Rodríguez-Ramirez (2008) due to its simple description of a very complex system, making it easier for the reader to understand.

Doñana National Park also presents a great variety of ecosystems and landscapes, whose quality is reflected in the diversity and abundance of its flora and fauna. Here we can find some exclusive plants and animal species, as the imperial eagle and Iberian lynx, and also numerous migratory bird species. The faunal and floral description made in the present work was based on Jiménez (2011).

Doñana is further to be understood as an environment partially shaped by human presence and its traditional activities, where diferent units can be distinguished.

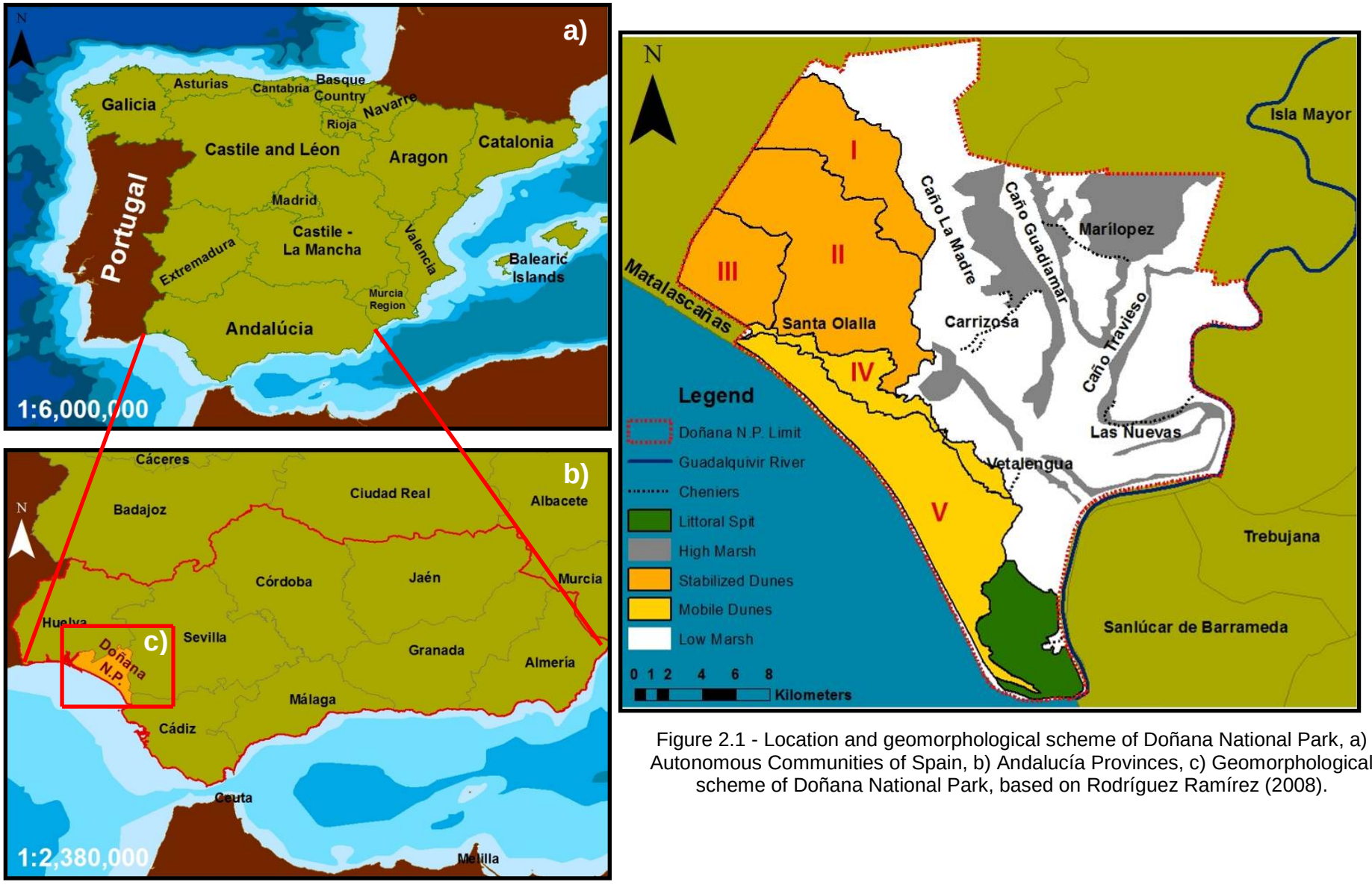

Figure 2.1 - Location and geomorphological scheme of Doñana National Park, a) Autonomous Communities of Spain, b) Andalucía Provinces, c) Geomorphological scheme of Doñana National Park, based on Rodríguez Ramírez (2008).

2.1 - Sandy spit

The Doñana sandy spit extends from NW to SE, with a maximum of 25 km of length and untill 5 km in width, constituted by successive streams of active dunes and a series of offshore bars.

In the areas where the dunes do not fossilize the previous formations (La Marismilla), the littoral barrier that originally formed the littoral spit can be observed, with a NW-SE orientation (Figure 2.2). The depressions that separate them are locally called “nazavos”, and are only flooded in the winter.

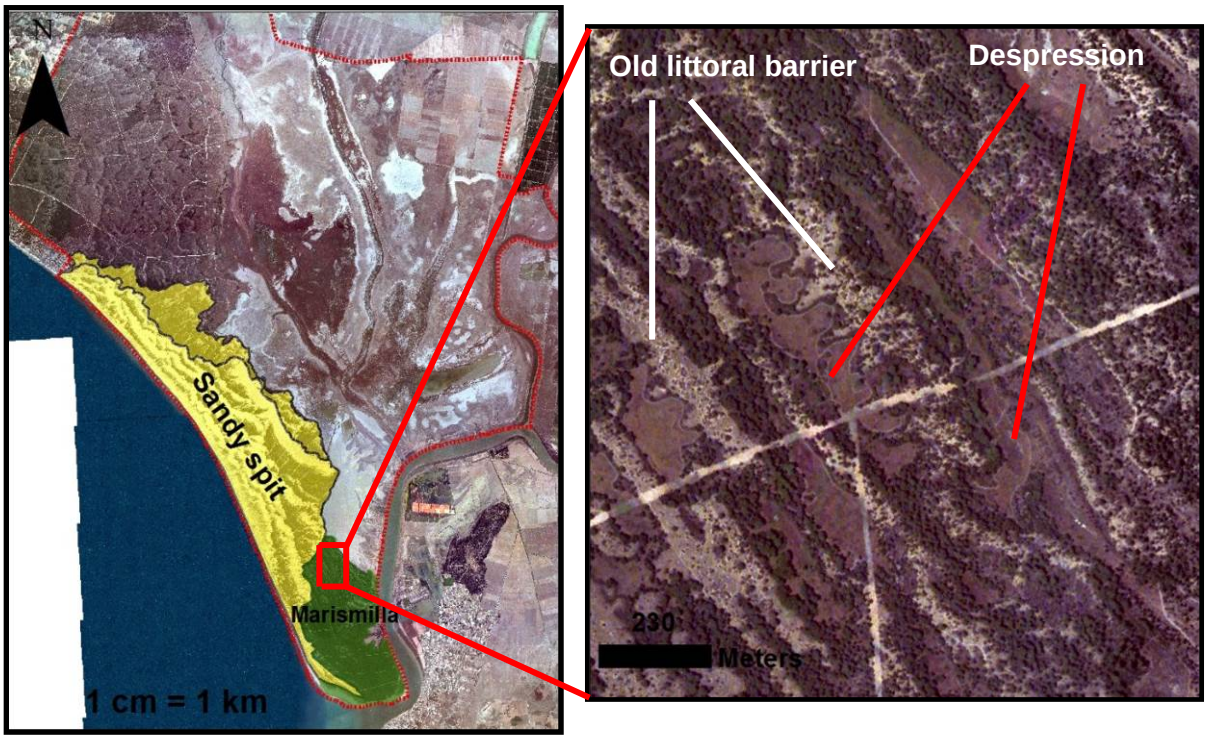

Figure 2.2 - Old shoreline and depressions in La Marismilla (based on ortophoto map 1998- 1999)

The old littoral barriers represent the successive phases of growth of the littoral spit. These generate due to the effect of the littoral drift currents which give rise to a great sedimentary supply from the West. The origin of these sediments is related to the supply from the fluvial network and to the erosion of the adjacent coastal cliffs. The result of

Figure 2.3 - Today’s beach ridge (Picture from L. Guerra 2013)

this dynamic is the formation of successive subtidal bars that migrate towards the coastline, emerging and constituting the corresponding beach ridges (Figure 2.3). Immediately after its emersion, the ridge is altered by the aeolian activity, configuring the incipient dunes and constituting the littoral barriers.

These beach ridges are constituted by fine and soft sand slopes under the intense influence of the sea and winds, with a vegetation of prickly saltwort (*Salsola kali*), sea holly (*Eryngium maritimum*), barrón (*Ammophila arenaria*) and other plants, and a fauna composed by mollusks, some stuck cetaceans or turtles, marine birds as the Common Tern (*Sterna*) or seagulls (*Larus*), and other like the black kite (*Milvus migrans*).

The normal growth (progadation) of the littoral spit in successive littoral barriers oriented NW-SE, has been interrupted several times, giving place to sandy barriers called “cheniers” that prograde towards the NE (Carrizosa, Vetalengua) (Figure 2.1). These are related to erosive high energy episodes (storms or tsunamis) that acted on the preexistent littoral spit.

2.2- Aeolian system

Doñana has five Aeolian systems, of which three are stabilized (I, II and II, Figure 2), therefore older, and two more recent and active (IV and V, Figure 2.1).

The stabilized systems have a vegetation mainly constituted by the maritime juniper (*Juniperus oxycedrus* subsp. *macrocarpa*), armeria (*Armeria gaditana*) and sea daffodil (*Pancratium maritimum*); and a fauna of reptiles, birds like the peregrine falcon (*Falco peregrinus*) and gooses (*Anser anser*), and some mammals.

The active systems move from SW to NE direction and are related to different littoral progadation phases. The dominant morphology is the successive transversal streams that rise up to 30 m of height, although there are also some parabolic dunes, in the V system. The interdune depressions located between the different dune streams are called “corrales” (Figure 2.4a). In these depressions elongated relieves (also called “gusanos”) are observed, with low height, and subparallel to the back side of the dune, indicating the progressive dune movement (Figure 2.4b).

In the “corrales”, islands of life surge in the middle of the sands, with different shades according to their size, level of moisture and vegetation. The stone pine (*Pinus pinea*) is the central tree species that occurs in the dry “corrales”, along with a vegetation of white rockrose (*Halimium halimifolium*) that gives it the appearance of a

white hill (Figure 2.4a). The more wet “corrales” have the appearance of black hills due to their predominant vegetation of heathers (*Erica scoparia*, *E. ciliaris*), gorse (*Ulex minor*), etc. In the “corrales” numerous species of reptiles, raptors, mammals and herbivorous can be found.

The elongated aquifers hanging the dune fronts feed a group of lagoons in the deflation cuvettes of the stabilized Aeolian systems, that act as small endorheic areas, being the most important the Santa Olalla (Figure 2.4c), as well as “La Vera” in contact with the marsh.

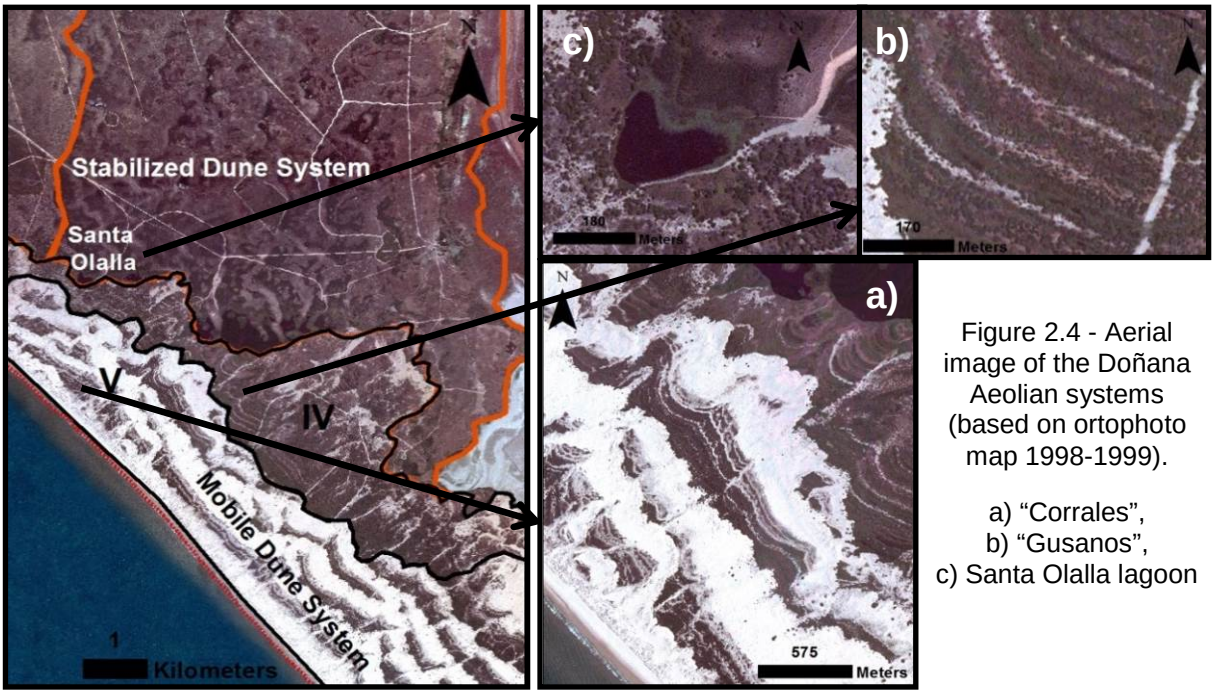

Figure 2.4 - Aerial image of the Doñana Aeolian systems (based on ortophoto map 1998-1999).

a) “Corrales”,
b) “Gusanos”,
c) Santa Olalla lagoon

2.3- Marshes

The marshes of Doñana National Park have around 35.000 ha. Its soft relieve has great hydrological and ecological significance, once it determines the floods, the salinity variations and the faunal and floral distributions. These spaces’ relieve have formed basically at the base of fine detritus (clays and silts) transported by the fluvial and marine networks. In its geography many geomorphological elements can be distinguished.

The levees of the fluvial courses constitute the most elevated topographic portions, being denominated as high marsh (also known as “pacil”). These are constituted as natural dams that separate the channel from the rest of the floodplain (Caño del Travieso, Figure 2.1). They have an important role in the rainy season (winter), once it elevates the floodplain and avoid the drain towards the sea. They also avoid the entrance of tidal flows. The most important is the high marsh of Guadalquivir, called “Montaña del Rio” (Figure 2.5). The best conserved places of the high marsh are constituted by steppes covered by halophytes (mainly *Arthrocnemum macrostachyum*), and are important seasonal habitat nesting grounds for numerous species of birds.

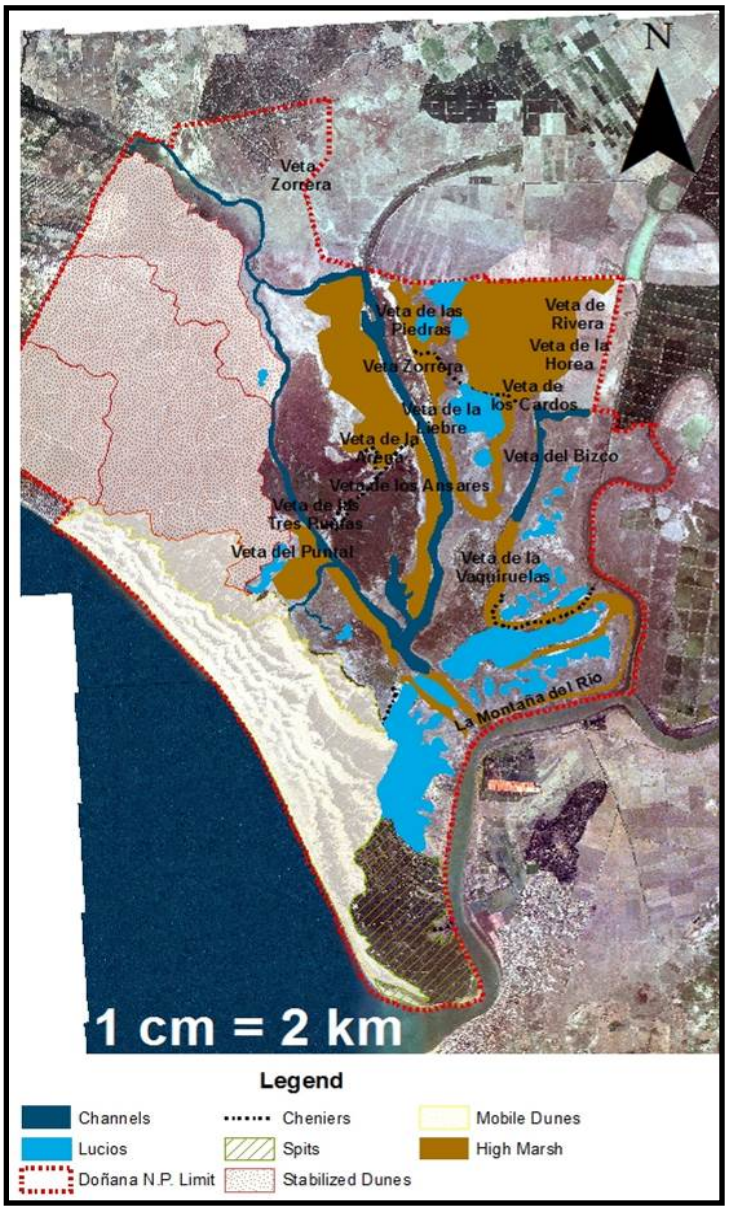

Figure 2.5 - Actual distribution of ecogeomorphologic units (see text for details)

When these high marshes are eroded by the surface flooding, they give place to oval morphologies, called “vetas” (Figure 2.5), in which human settlements take place.

The local fluvial marshes delimitate a series of depressed areas, locally called “lucios” (Figure 2.5), which stay flooded the longest. There, the vegetation is represented by the saltmarsh bulrush (*Scirpus maritimus and Scirpus lacustris*), together with *Ranunculus* and other plants. It is an optimum place for many marine

birds, embracing dozens of species (geese, ducks, swans, coots, herons, spoonbills, flamingos …) as well as fish, amphibians and reptiles.

The “cheniers” are sand or shell accumulations with little thickness, generated by the fluvial/marine currents, storms, etc (Figure 2.1 and 2.5).

The channels or “caños” (Figure 2.5) are fluvial/marine networks, responsible for the redistribution of the liquid element, either being fluvial, marine or pluvial. The working channels are the Guadalquivir and the Brazo de la Torre, where the tide and the actual river flows circulate.

3 - Origin and Evolution of Doñana National Park

The Pleistocene-Holocene geological record of littoral areas has received an increasing attention in the last decades. The multidisciplinary analysis of cores collected in lagoons, estuaries, salt marshes or deltas has revealed broad information about the palaeoenvironmental evolution of these environments, global or regional sea-level changes, palaeoclimatology or the effects of anthropogenic actions during this period (Borrego et al., 2004; Vilanova et al., 2006; Selby and Smith, 2007).

The palaeogeographical evolution of Doñana National Park was described by many authors, like Ruiz et al. 2010, that included numerous data obtained by Lario (1996), Zazo et al. (1999) and Yll et al. (2003) in other cores of the Doñana National Park; the analysis of several boreholes drilled near the Guadiamar River mouth by Salvany et al. (2001); the palaeogeographical interpretation of numerous seismic profiles effectuated in the Cádiz Gulf (Lobo et al., 2001; 2002); and previous analyses of short cores by Ruiz et al. (2004; 2005a).

The comparison and compilation of these data with other obtained by different investigation teams in the Doñana National Park and the adjacent areas allowed to drawn a tentative palaeogeographical evolution of this zone, where six main facies were delimitated (Table 2.1).

Facies	Description	Interpretation
FA-1	**Laminated Silt** It consists mainly of clayey silt, with up to 65 % of sediments included in the 40 μm-4 μm grain size interval. These sediments show a fine parallel lamination, with alternation of greyish to greenish and blackish layers. Some layers of sandy-clayey silt (sand ~10- 15 %) are also interbedded within this general pattern. The microscopic analysis reveals the presence of numerous reddish, oxidized fragments of roots and phanerogams, scarce gyrogonites of characeans (Chara sp., Nitella sp.) and isolated fragments of undifferentiated bivalves	These main features have been observed in temporary ponds and surrounding freshwater marshes of the Doñana N.P., with similar ostracod and characean assemblages (Ruiz et al., 1996; Santos et al., 2006). These ponds are very shallow (< 1 m) and contain alkaline, fresh to oligohaline waters (Serrano and Toja, 1995). Fine laminations indicate a calm environment with a cyclic sedimentation suggested by the alternating color shades, probably due to alternating dry or wet periods, pulses from small tributaries or the vegetation distribution (Whittecar et al., 2001; Harter and Mitsch, 2003). The higher grain size of Facies FA-1 and the absence of faunal remains are attributed to increasing fluvial inputs.
FA-2	**Greyish silt** This facies is constituted by silt and clay (silt: 55-70 %; clay: 26-43 %) with greyish to greenish colours. Up to 70 % of sediment is comprised between 15 and 2 μm, with high percentages of fine and very fine silt. They are massive or show a very tenuous lamination. The palaeontological record includes low densities of a high brackish ostracoda assemblage (mainly C. torosa, Loxoconcha elliptica, Leptocythere castanea), salt marsh foraminifers (Ammonia tepida, Jadammina macrescens, Haynesina germanica, Trochammina inflata), scarce pulmonate gastropods and undifferentiated fragments of stems and roots. Reworked specimens of planktonic foraminifers, spines of echinoderms, bryozoans and marine or brackish bivalves (Cardium edule, Venerupis decussatus) are frequent.	This facies has intermediate characteristics between FA-1 and FA-3. The microfossil assemblages are characteristic of brackish marsh or surrounding margins of a brackish lagoon. Tidal flows introduced marine faunas toward the more protected areas of this lagoon. Both mineralogical and palaeontological records are very similar to those observed in the inner areas of perimediterranean lagoons (Carbonel and Pujos, 1982; Montenegro and Pugliese, 1996; Ruiz et al., 2006b).

FA-3	**Green silt and clay** It consists of greenish clayey silt or silty clay, with up to 70 % of sediment (dry weight) comprised between 30 μm and 1 μm and very low sand contents (< 4 %). This facies exhibits a fine parallel lamination, with coarse laminae (5-10 cm thick) well defined and scarce evidence of bioturbation. Macrofauna is composed of brackish (mainly Cardium edule) and marine (Venerupis decussatus, Chamelea gallina) bivalves, together with less frequent specimens of marine gastropods (Rissoa, Hinia). Ostracods (C. torosa, L. elliptica, L. castanea) and foraminifers (A. tepida, H. germanica) are frequent to very abundant in these sediments. The reworked marine faunas of ostracodes, planktonic foraminifers, spines of echinoderms, fragments of bryozoans or central diatoms may be locally abundant, composing 20-40 % of the paleontological record.	The most representative species of both ostracodes and foraminifers are well represented in the deeper, subtidal areas of brackish lagoons (salinity up to 15-20 SI), located near a river mouth. In these coastal areas, the tidal renewal is conditioned by the outlet dimensions that cross the external and elongated sandy spits (Marocco et al., 1996; Samir, 2000; Ruiz et al., 2006a). This marine influence is contrasted by the presence of reworked faunas derived from the adjacent infralittoral zone (Pérez Quintero, 1989; Ruiz et al., 1997).
FA-4	**Yellow silt** It is constituted by off-white to pale yellow, sandy-clayey silt, poorly sorted, with very low to moderate percentages of sand (4-20 %). They present a very tenuous low-angle cross stratification, parallel lamination or absence of patent sedimentary structures. Macrofauna is abundant, with numerous valves and fragments of marine molluscs, including bivalves (C. gallina, V. decussatus, Acanthocardia tuberculata), gastropods (Rissoa spp., Hinia reticulata, Lemintina arenaria) and scaphopods (Dentalium vulgare, D. sexangulum). Benthic marine foraminifers (Ammonia beccarii, Quiqueloculina spp., Elphidium crispum) and ostracodes (Palmoconcha turbida, Pontocythere elongata, Urocythereis oblonga) are dominant over brackish species. Fragments of bryozoans, plates of barnacles, claws of crabs, or planktonic foraminifers	The most abundant assemblages of molluscs, ostracodes and foraminifers of this facies characterize the shallow areas (< 40 m depth) of the southwestern Spanish shelf (Pérez Quintero, 1989; Ruiz et al., 1997; González-Regalado et al., 2000). These assemblages and some brackish specimens (C. torosa, L. castanea) are usually found in the marine zones of perimediterranean lagoons, very close to the natural or artificial inlets and subjected to moderate to high hydrodynamic gradients (Ruiz et al., 2000; 2006, a; b).

	(Orbulina, Globigerina, Globigerinoides) are also abundant.	
FA-5	**Bioclastic silt and sand** This facies is the main constituent of several bioclastic ridges located in the margins of recent or former tidal channels (Veta la Arena, Las Nuevas). These sedimentary beds are characterized by a large lateral extension (3- 6 km) and a narrow width (20–30 m). Thickness (5-70 cm in most cases) decreases landward, being disposed usually over FA-2 or FA-3. They display an erosive base, with vegetation remains and intraclasts of the underlying sediments in the lower centimetres. In the upper part, bioclasts were disposed in thick laminae (3-5 cm) or present a disorganized disposition, being fragmented in most cases. Molluscs represent an important proportion (10-40 % dry weight) of the sediment. Shell debris and disarticulated bivalve shells of estuarine (mainly Cardium edule) and marine (mainly Acanthocardia tuberculata, Donax vittatus and Spisula solida) are abundant. Gastropods are represented by freshwater (Gyraulus laevis, Melanopsis) and marine (Rissoa, Lemintina, Hinia) specimens. Fragments of barnacles, scaphopods and bryozoans are also frequent. Microfauna is represented by brackish ostracodes (C. torosa, L. elliptica) and foraminifers (A. tepida, H. germanica), together with marine specimens of both groups (Basslerites berchoni, Carinocythereis whitei, Urocythereis britannica, Ammonia beccarii, Elphidum crispum). Some marine miliolids are also abundant (Triloculina, Quinqueloculina), with a frequent loss or rupture of the last chambers. Brackish ostracodes present a high-energy population structure, with numerous individuals (>70 % in most of samples).	These ridges show numerous features that have been described in tsunamigenic deposits (Bryant et al., 1992; Bryant, 2001; Costa et al., 2004; Dawson and Steward, 2007): a) an erosional base; b) presence of intraclasts plant remains near the base; c) finer sediments toward the top; d) finer sediments landward; e) presence of higher sand percentages (near the Doñana spit) in relation to the underlying sediments; f) strong changes of fauna in relation to the underlying layers; g) presence of numerous marine species of both macrofauna and microfauna with evidence of reworking; or h) high-energy population structures of ostracodes. Consequently, a tsunamigenic origin has been attributed to these beds.

FA-6	**Yellow sand** This facies is represented in the uppermost part of the sandy ridges (Carrizosa, Vetalengua) and the dune system of the Doñana spit. These layers consist of well sorted, fine to very fine sand with intense yellow shades. Up to 60 % of sediment presents a grain size comprised between 500 μm and 80 μm. Both macrofauna and microfauna are virtually absent, with exception of some isolated and fragmented remains of the bivalve Corbula gibba.	These sediments constitute the dune systems of the Doñana spit. The mineralogical records obtained coincide with those indicated by Flor (1990) and the Spanish Environmental Ministry (2005) in these aeolian beds. The sandy ridges of Carrizosa and Vetalengua show the same textural, mineralogical and faunal features. They occupy the margins of former meanders within the old lagoon system and are disposed at high angles in relation to the Doñana spit. The contact with this sandy bed coincides with the presence of an erosive surface within the dune systems of the spit (Rodríguez Ramírez et al., 1995) and a remarkable slimming of its width. The presence of these sand layers over FA-2 or FA-3 may be indicative of old tsunamis, with a partial rupture or erosion of the spit and the deposit of washover fans in its inner side. In a second episode, these washover fans would be reworked by the tidal fluxes and deposited in the margins of old tidal channels, constituting the sandy ridges of Carrizosa and Vetalengua. Simultaneously or in a later stage, a part of these washover fans would be dismantled and their almost azoic sands were introduced toward the inner areas of the lagoon, being deposited (as FA-5) over fluvial levees or marshes.

Table 2.1 - Six main facies described by Ruiz et al., 2010

The palaeogeographical evolution of Doñana National Park presented in this work is based on the palaeogeographical evolution described by Ruiz et al. 2010 which is compared with the general description of the Holocene Climate Change phases' on the Iberian Peninsula since the "Atlantic period" to the "SubAtlantic period to present".

To better complete the goals of the present work, data from historical records of high-energy events in Portugal and southern Spain and described by other authors were also taken in consideration (Galbis, 1932; Campos 1991).

During the Atlantic period (8000 B.P. to 6000-5000 B.P.) the Iberian Peninsula was under the influence of the subtropical high-pressure belt in the summer months, whereas the impact of the west wind drift shifts to higher latitudes (*Lamb* 1971). This period corresponds to phases 4 and 5 described by Ruiz et al., 2010 during which the Cádiz Gulf river mouths were inundated around 6.5 cal ka (Zazo et al., 1994; Borrego et al., 1999; Dabrio et al., 2000) and Doñana National Park was occupied by an open lagoon, partially protected in its westernmost part by aeolian units (Zazo et al., 2008)(Figure 2.6a).

After this maximum transgression, the Doñana spit began to grow (Goy et al., 1996), with the progressive emersion of the inner side of the incipient barrier. The bottom sediments of the adjacent, quiet lagoon were composed of clayey silt (FA-3) with variable bioclastic contents. Furthermore, between 5100 and 4800 cal BP, there is a record of a tsunami causing the erosion of this spit and the deposition of aeolian sand (FA-6) over the new salt marsh (Figure 2.6b).

After the end of the "postglacial climate optimum" (Holocene Maximum) and slight global cooling, there was a temporary southward shift of the northern hemispheric high west wind drift during the Sub-Boreal period (5000 – 3000 B.P.). As a result of the increasing meridional temperature gradient the circulation gained a stronger zonal component (*Lamb* 1971). The west wind weather conditions now prevailing over the Iberian Peninsula between autumn and spring brought rain to all parts of it. The water balance improved in all parts of the Iberian Peninsula.

Temporary perennial lakes formed in the endorheic basins of central Spain and erosion rates dropped beneath the growing plant cover (*Gutiérrez Elorza* and *Peña Monné* 1992: 109). In a global view this Sub-Boreal phase of improved hydric conditions corresponds to the Mid-Holocene wet-phase as known for example in wide areas of the Sahara desert (*Goudie* 1996, *Petit-Maire* et al. 1997).

Phases 6 and 7 of Ruiz et al., 2010 are included in this period, during which the central part of the Doñana National Park was still occupied by an open lagoon, whereas the Doñana spit grew towards the southeast (Figure 2.6b). There is record of one or two tsunami-like events (or very strong storms) that caused the erosion of the Doñana spit (3700-3000 B.P.; Figure 2.6b) and the deposition of bioclastic, sandy-clayey silt over the lagoon bottom. In a latter period, new high-energy events induced the emersion of the very shallow, southwestern areas of the lagoon, with the deposits of FA-5 over intertidal sediments.

In the Sub-Atlantic period (3000-1500 B.P.), historical sources reveal that the climate involved global warming of about 1.5°C (*Dansgaard* et al. 1969) and generally wetter conditions in central Europe (*Schönwiese* 1995). During this phase the Iberian Peninsula at first remained under the influence of Atlantic-cyclonic conditions as a result of the increasing meander wave-length of the high west wind drift (*Lamb* 1971). However, generally higher temperatures resulted in deteriorating water balance conditions, and an Iberian continental semi-arid climate prevailed in central Iberia after the end of the Iron Age, at the latest.

Global cooling, probably accompanied by a (on the average) southward shift of the west wind drift and thus a more regular occurrence of cyclonic winter rainfall, brought a temporary rise in humidity over the Iberian Peninsula.

The Sub-Atlantic period includes phases 8 to 10 of Ruiz et al. (2010) paleoreconstruction, during which the southwestern part of the Doñana National area remained emerged, between 3000-2200 B.P., whereas the central and southern ones were occupied by a very shallow lagoon (Figure 2.6c). The continuous growing of the Doñana spit and the progressive infilling induced the creation of new brackish marshes (Zazo et al., 1999) or the transition from marine conditions to more restricted scenarios (Ruiz et al.,2010).

During 2200-1900 B.P., several tsunamis eroded the Doñana spit (Figure 2.6c) with the creation of small washover fans constituted by aeolian sediments and the accumulation of bioclastic ridges over the lagoon borders.

Additional sedimentary evidence of these events include erosive surfaces in the Doñana spit (Rodríguez Ramírez et al., 1995), washover fans near the Gibraltar Strait (Luque et al., 2002), limestone boulders located at +4 to +15 m asl near Lisbon (Scheffers and Kelletat, 2005) or a turbiditic layer in the SW Portuguese Margin (Vizcaino et al., 2006a). These tsunamis may be assimilated to the historical

tsunamis that devastated the southwestern Iberian coasts between 2168-2159 B.P. and 2010 B.P. (218-209 BC and 60 BC) (Campos, 1991).

From 1900 B.P. to present times, there was an increasing infilling of the lagoon, with a progressive transition towards intertidal-supratidal conditions (Figure 2.6d). This tendency was interrupted by a new introduction of marine sediments and, to a lesser extent, aeolian sediments in the southern part of the park, owing to new high-energy events. Ages of these phenomena coincide with those of an historical tsunami (1568 B.P. = 382 BC; Campos, 1991). The posterior palaeoenvironmental evolution of the Doñana National Park (1500 B.P. untill present) (Figure 2.6e) is marked by the creation of new wetlands with temporary ponds and the growing of the Doñana and La Algaida spits, with aeolian sands covering intertidal sediments.

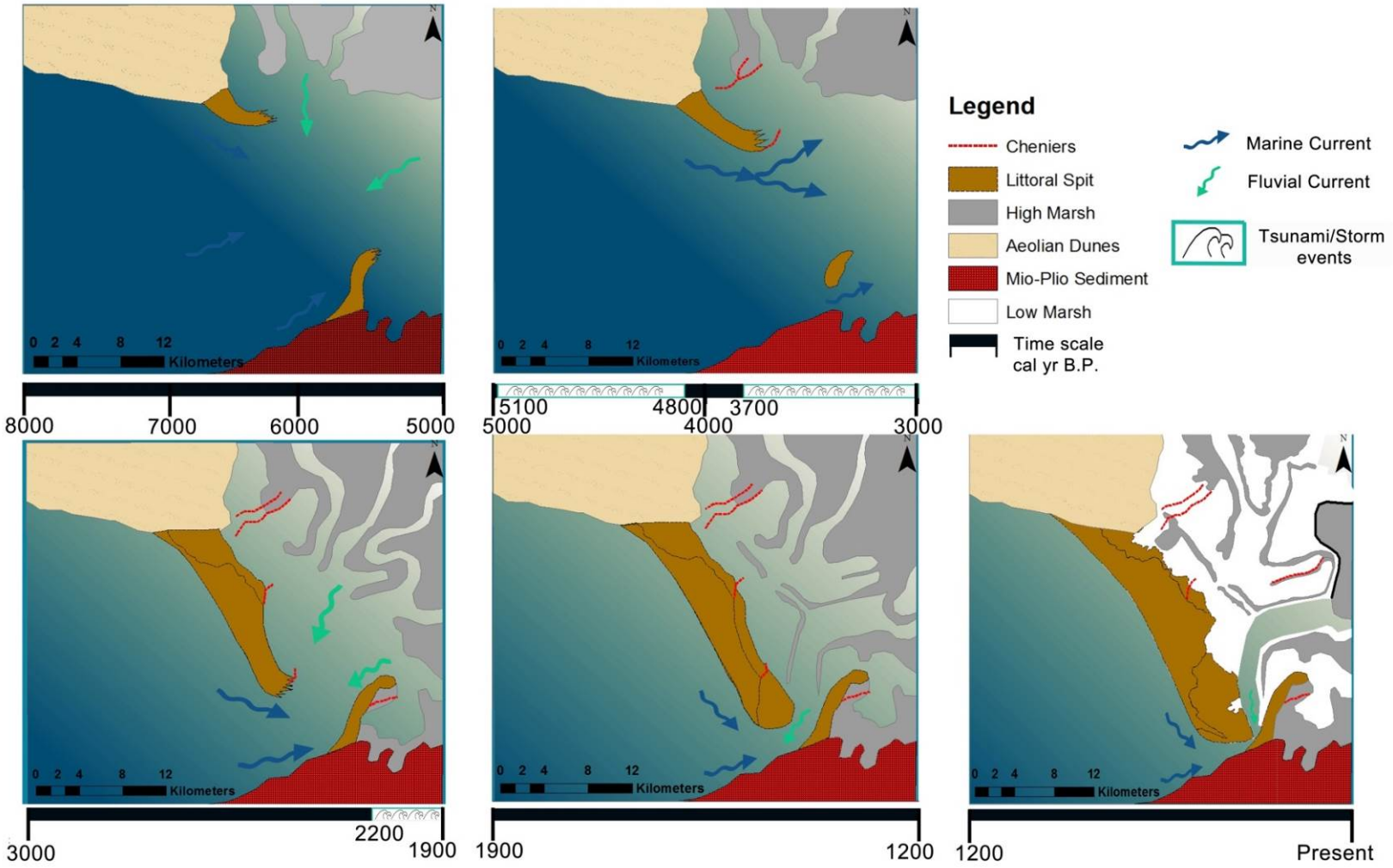

Figure 2.6 - Palaeogeographical evolution maps adapted from Rodríguez-Ramírez 2008 and showing palaeogeographical environments during a) the Atlantic Climatic period, b) the Sub-Boreal Climatic period and, c)-e) the Sub-Atlantic Climatic period until present

III. Methodology

1- ArcGIS

ArcGIS10 software, and several of its extensions, was used to create new maps based on several base maps as shown in this section. Two schemes (Figs. 3.1 and 3.2) are thus presented here for better understanding which maps were used as a basis, and which were created from these (see further information about the creation of each map in chapter IV).

Figure 3.1 shows the maps that used the 1998 - 1999 ortophoto map as a basis (Fig. 3.1a) and resulted on the geomorphological scheme of Doñana National Park (Fig. 3.1b, and b1), the location of surface samples (Fig. 3.1c) and a DMT and floodable areas analysis (Fig. 3.1d). The geomorphological map was then used as a basis for the location map of cores C and D (Fig. 3.1b2) and for the maps representing the abiotic parameters measured in situ, relative abundances of foraminifera species and diversity indexes, for surface samples (Fig. 3.1b3).

Figure 3.2 shows the maps that were created using the Geosoft Target extension for ArcGIS based on specific Collar and From-to data files for each analysis (Fig. 3.2a), namely section maps for cores C and D and for all nine cores from Ruiz et al., 2010 (Fig. 3.2b), lithology 3D voxels for surface samples analysis (Fig. 3.2c) and the group of plan maps, section maps and 3D voxels for the palaeogeographic evolution analysis of the Doñana National Park for all cores (Fig. 3.2d).

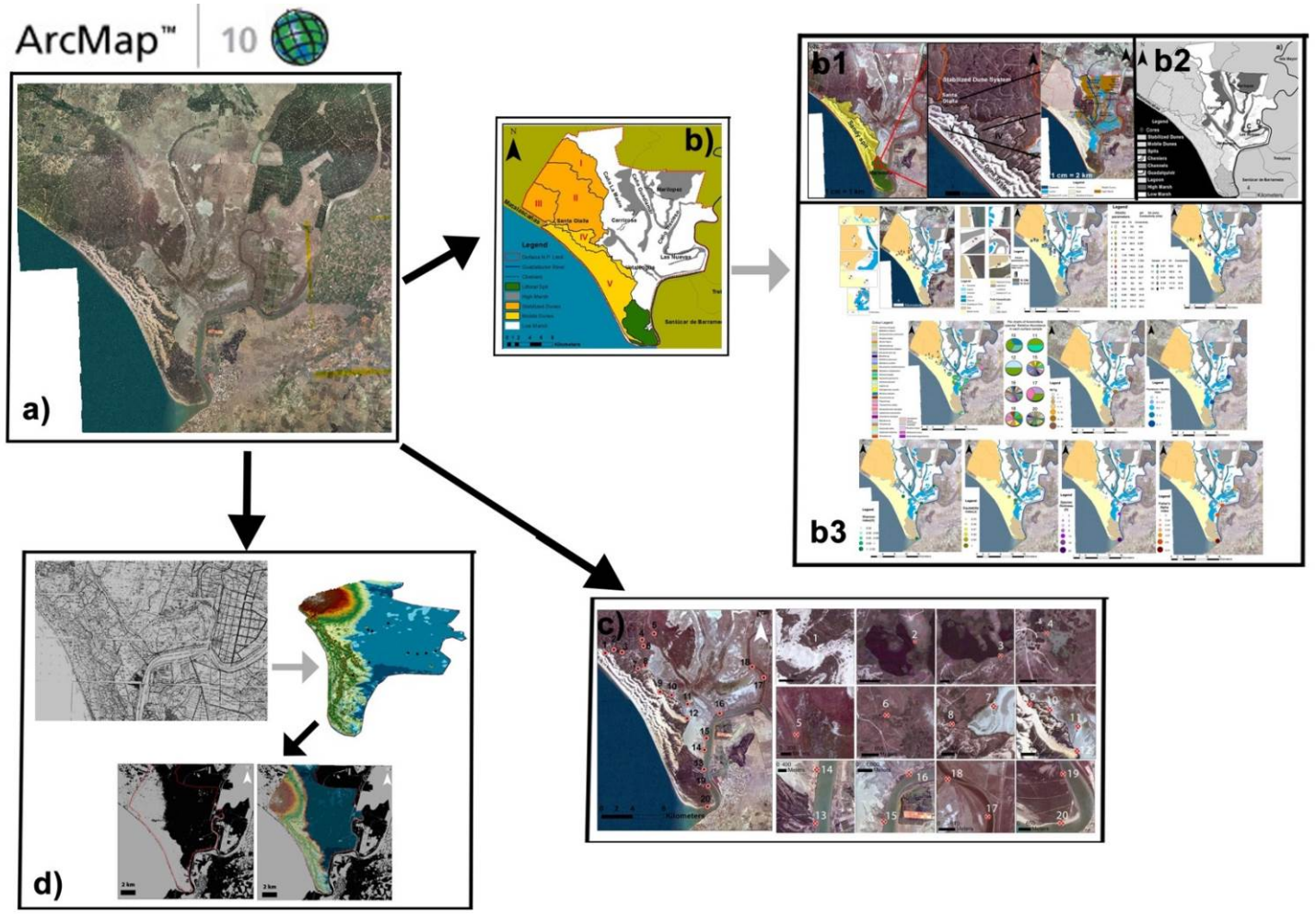

Figure 3.1 **-** Scheme representing the final maps created using ArcGIS 10 software. a) ortophoto map (1998-1999) used as a basis ; b) geomorphology map (b1) main geomorphology areas, b2) location of cores C and D, b3) surface samples grain size, abiotic parameters, foraminifera relative abundance and diversity indexes); c) surface samples location; d) Topography map, DMT created from this and floodable areas analysis

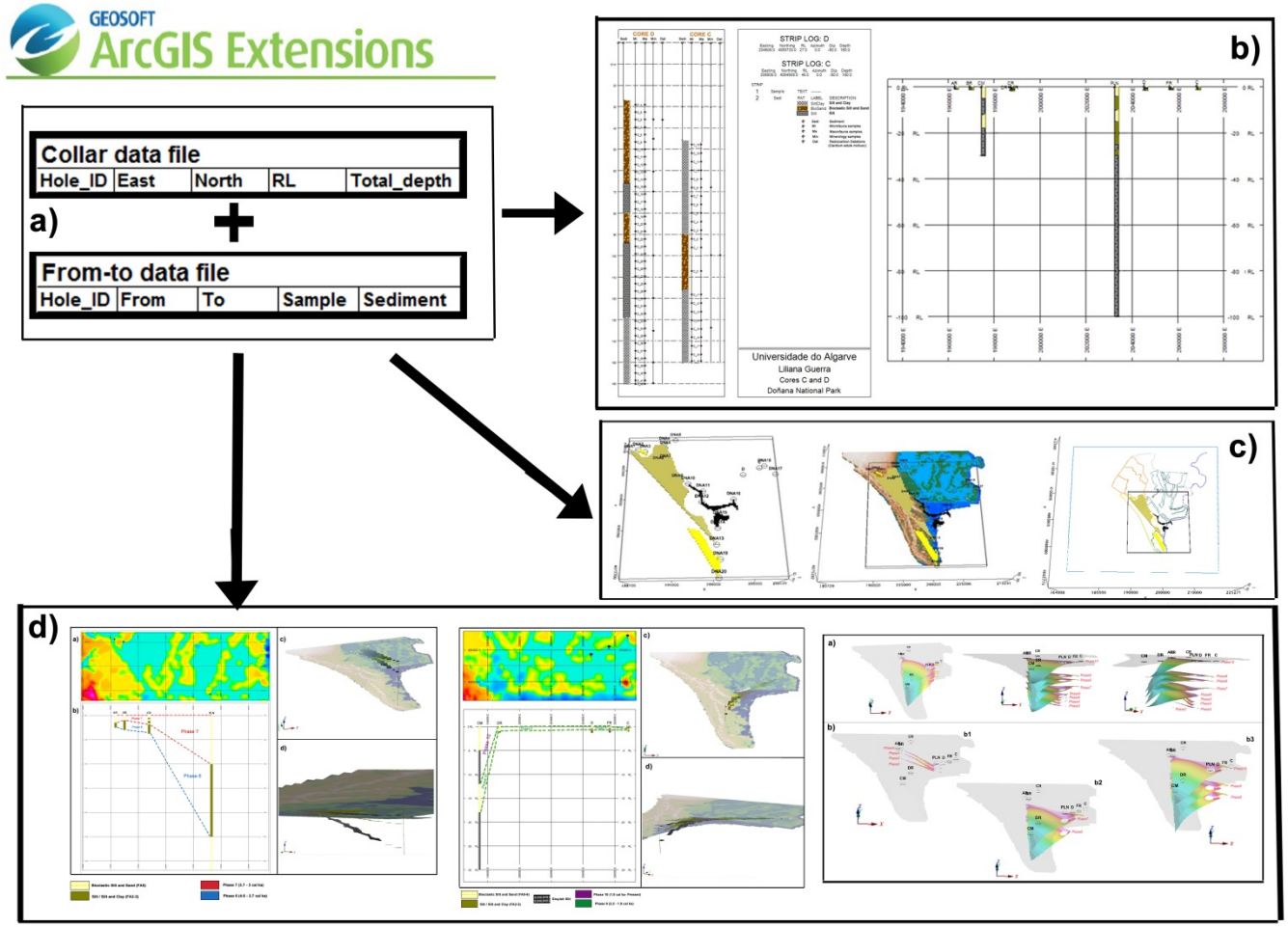

Figure 3.2 - Scheme representing the final maps created using Geosoft Target extension. a) Collar and From-to data files main tables; b) section maps for cores C, D and all nine cores (Ruiz et al., 2010); c) lithology voxels for surface samples; d) group of plan, sections and 3D voxels maps for all nine cores

2 – Coring and Sampling

2.1 – Cores

The short cores analyzed in the present work were selected and collected by Ruiz and co-workers, in 2004. In the area of Vetalengua-Las Nuevas, containing the main geomorphological features of the estuary (Figure 3.3).

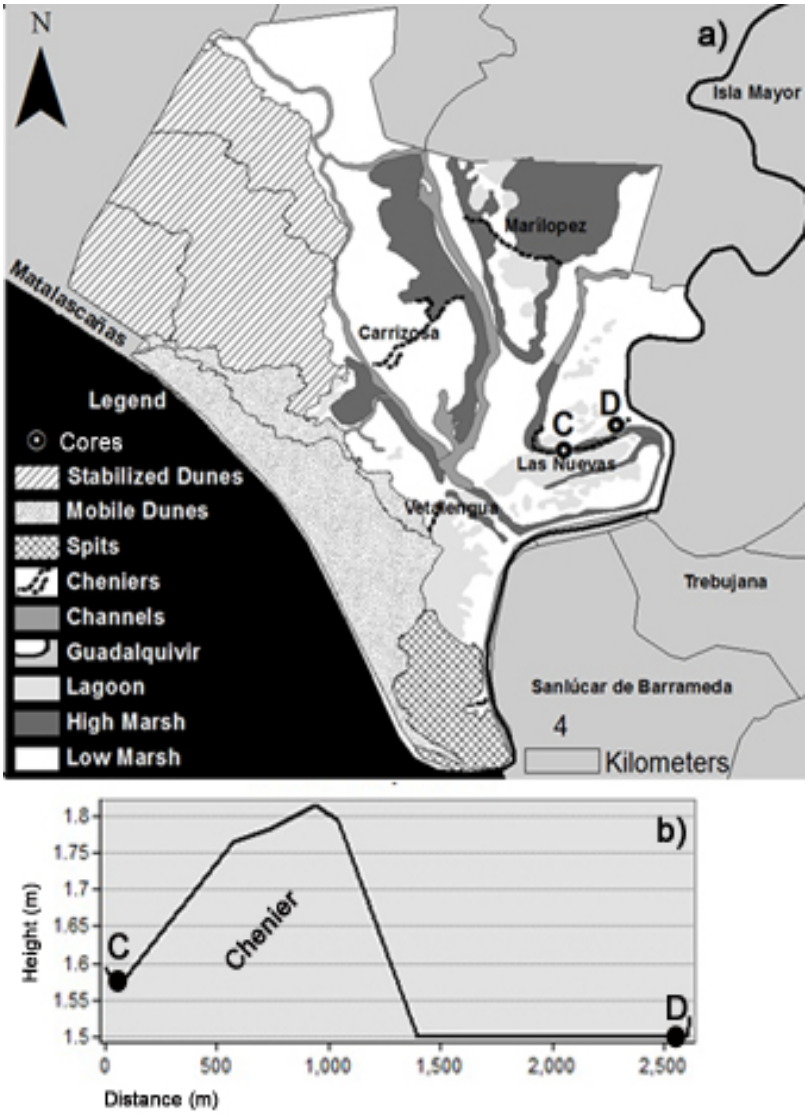

Figure 3.3 - a) Doñana National Park main geomorphology and core sites
b) Topographic profile between sampled cores C-D

The cores were collected with a 20 mm diameter vibracore reaching up to 1.5 and 1.6 m in depth below surface for cores C and D respectively (Fig. 4.1, chapter IV).

Sixty-two samples of approximately 15 g were taken for microfossil analysis, which were selected according to the main sedimentary changes observed in the cores (Fig. 4.1, chapter IV).

2.2 - Surface samples

On the 26th of November 2013, 20 surface samples (Figure 3.4) were taken at Doñana National Park, according to changes in the halophytic vegetation and sediment type, trying to sample the main distinct zones, from non-vegetated mud-flats to the higher levels of the marshlands. The coordinates of the sampling sites were registered with a GPS, for later positioning in GIS software (Table 3.1).

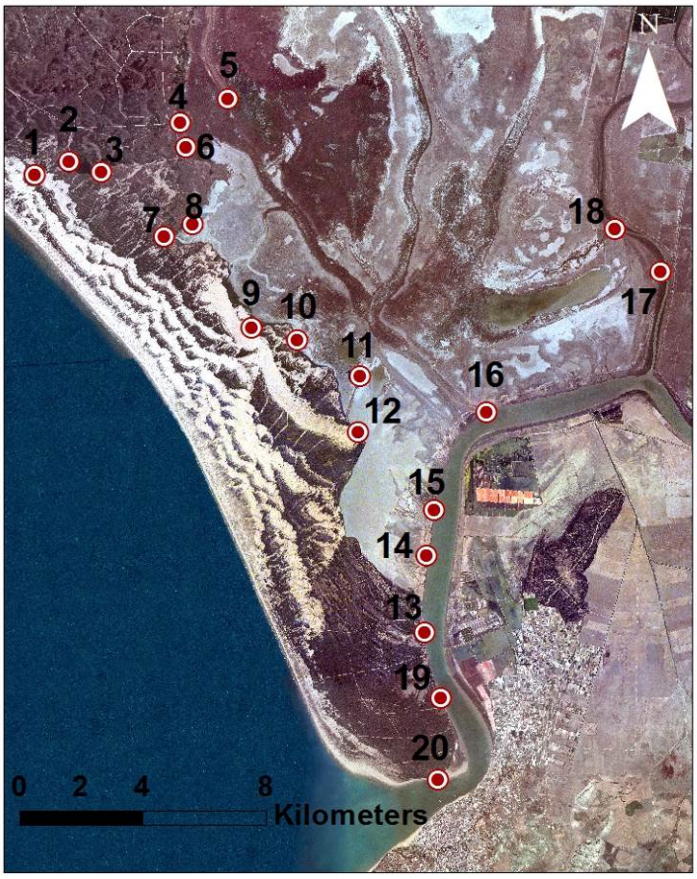

Figure 3.4 - Surface sampling sites at Doñana National Park

Table 3.1 - Surface sampling sites' coordinates in ED50 UTM 29N coordinate system

Sample number	Longitude	Latitude
1	722931	4095222
2	723984	4095566
3	725059	4095330
4	727925	4096887
5	729096	4097649
6	727749	4096067
7	727888	4093609
8	727106	4093207
9	729895	4090215
10	731377	4089838
11	733420	4088634
12	733601	4086937
13	735430	4080385
14	735527	4082834
15	735803	4084347
16	737502	4087502
17	743200	4092037
18	741694	4093427
19	735979	4078306
20	736035	4075514

The floodable areas (Fig. 3.5) and the mean tide level (Fig. 3.6) were also taken into account when planning sampling sites.

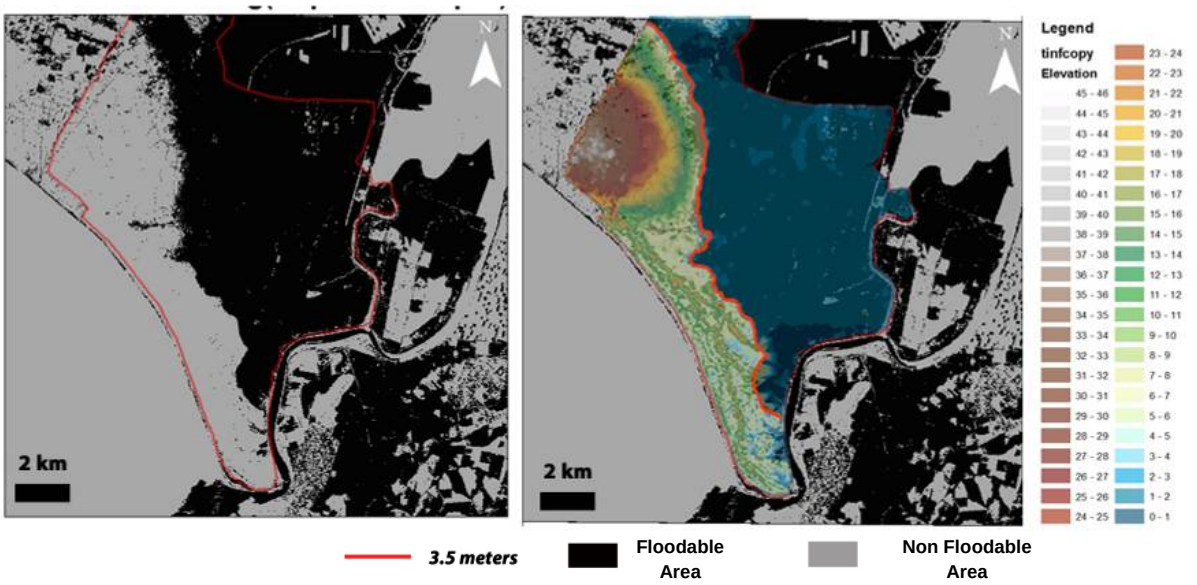

Figure 3.5 - Doñana National Park floodable areas. a) Resultant map from change detection analysis between April and September 2013, b) Map showing the elevation correspondent to the floodable area.

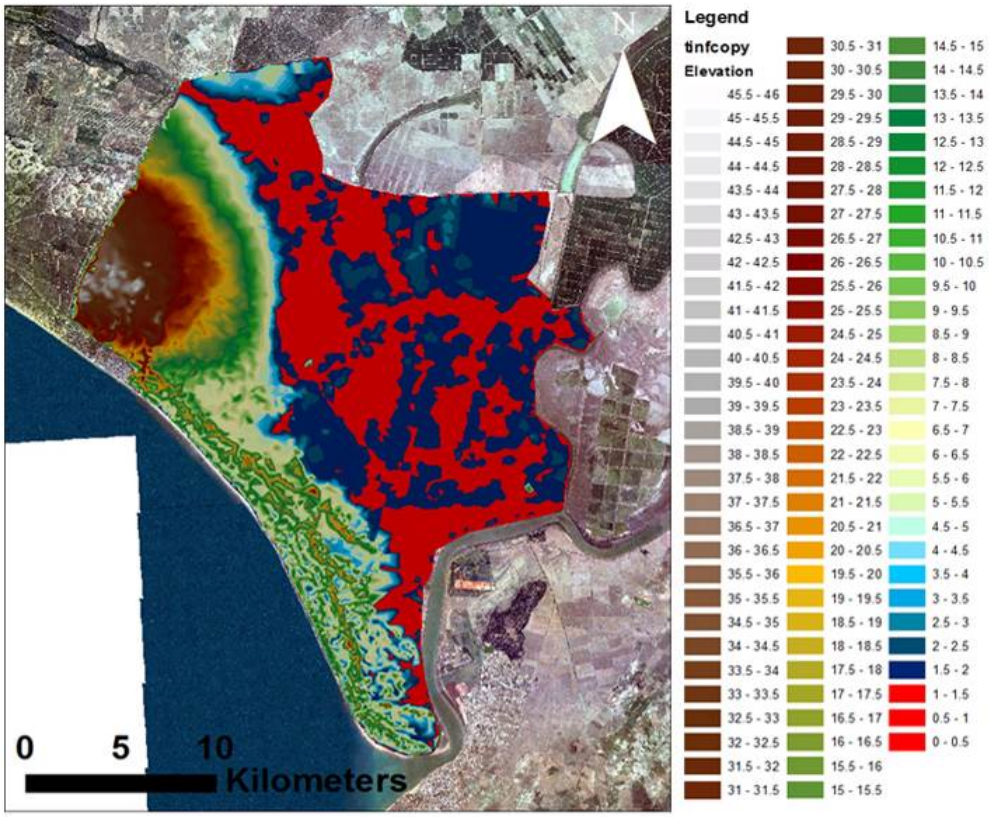

Figure 3.6 - Digital Terrain Model of Doñana National Park. Red sites correspond to the tide level during the sampling day, between 0.4 – 1.4 meters.

2.2.1 - Sample sites' description

The sampling sites were chosen in order to encompass a variety of marginal environments in a continent-ocean and intertidal transect (Figs 3.7 and 3.8). This approach was designed to capture the maximum spatial variation among species and environmental variables. In order to assess the degree of confinement registered by the microfauna, some places with a more restricted location in relation to the sea front (like temporary ponds) were also sampled. Twenty different sites were selected (Figs 3.7 and 3.8) and samples were collected along 3 transects, with a SW-NE, NW-SE and N-S orientation.

The transects were placed in order to include the main distinct zones in Doñana N.P., from temporary ponds, fresh water lagoons and marshlands to channel margins (Figs 3.7 and 3.8).

The first transect (with a SW-NE orientation) began nearby the "corrales", next to the mobile dune system, where the first sample (Fig 3.7.1) was collected. There the vegetation was dominated by *Pinus pinea* and *Juncetum sp.* (Figs 3.7 and 3.8.1).

The second sampling site was at the margin of "Laguna Dolce" (Figs 3.7 and 3.8.2), a fresh water lagoon that shared a physical connection with the third sampling site (Figs 3.7 and 3.8.3), another fresh water lagoon called "Laguna Sta. Eulália", both surrounded by a vegetation of *Juncentum* sp.

Further northeast ward, a temporary pond near the "Palacio de Doñana", where *Juncetum acuti* represented the main vegetation, was chosen for sampling site four (Figs 3.7 and 3.8.4).

The fifth sample was taken in a very dry area of the low marsh area, called "Marisma de los Hinojos" (Figs 3.7 and 3.8.5) and the sixth sample was taken in a temporary pond near a channel known as "Caño del Preal" (Figs 3.7 and 3.8.6), surrounded by vegetation.

The seventh sampling site was the first of the second transect (with a NW-SE orientation), at a temporary pond in "Lucio del Cavallero" (Figs 3.7 and 3.8.7), surrounded mainly by a vegetation of *Juncentum* sp.

Not further away, but closer to the dune system, the eighth sample was taken at a temporary lagoon (Figs 3.7 and 3.8.8), called "Laguna Saperón", where a varied vegetation of *Pinus pinea, Juncentum* sp. , *Scirpus* sp., and others were present.

In a more SE location, but also near the dune system, the ninth sample was collected, at the margins of a very eutrophicated temporary lagoon (Figs 3.7 and 3.8.9).

The tenth sampling site was in a temporary pond of a very dry marsh, in the boundary between the dune system and the marsh system, with a vegetation composed by S*arcocornia* sp (Figs 3.7 and 3.8.10).

The eleventh sampling site was taken next to the Ventalengua's chenier (Figs 3.7 and 3.8.11), one of the ancients cheniers in Doñana N.P.

Next to the boundary between the dune system and the marshland, there was a deserted marsh plain with several bubbling waterholes. Sample number twelve was taken at the margin of one of these waterholes (Figs 3.7 and 3.8.12). Although it was not planned to sample this area, it was thought to be an interesting site for sampling, once the waterholes had a sulfur smell and colour, great depth, and were located in a non-vegetated place, considered as an extreme environment.

The third transect (with a S-N orientation) was along the right margin of Guadalquivir River. The thirteenth sample was collected at a small beach, which was once an ancient marsh, posteriorly covered by sand (Figs 3.7 and 3.8.13).

The fourteenth sampling site was taken in a small pond near a *Spartina* sp. channel (Figs 3.7 and 3.8.14). Further North, the fifteenth sample was taken at the borders of Guadalquivir River (Figs 3.7 and 3.8.15), near an abandoned house.

The sixteenth sample was collected by the channel "Caño de Brenes", in the inter/infra tidal zone of Guadalquivir river (Figs 3.7 and 3.8.16).

The seventeenth sample was taken in a temporary pond, near the lagoon "Lucio del Tio Oreha" (Figs 3.7 and 3.8.17) and the eighteenth sample was taken at the margin of the channel "Caño del Buen Tiro" (Figs 3.7 and 3.8.18). These samples were probably the most important ones, since they are the nearest samples of the cores C and D, and will represent the fauna living there at the present.

The last two samples, nineteenth and twentieth (Figs 3.7, 3.8.19 and 3.8.20) were taken at the mouth of Guadalquivir river and at the Punta Malandar beach, respectively.

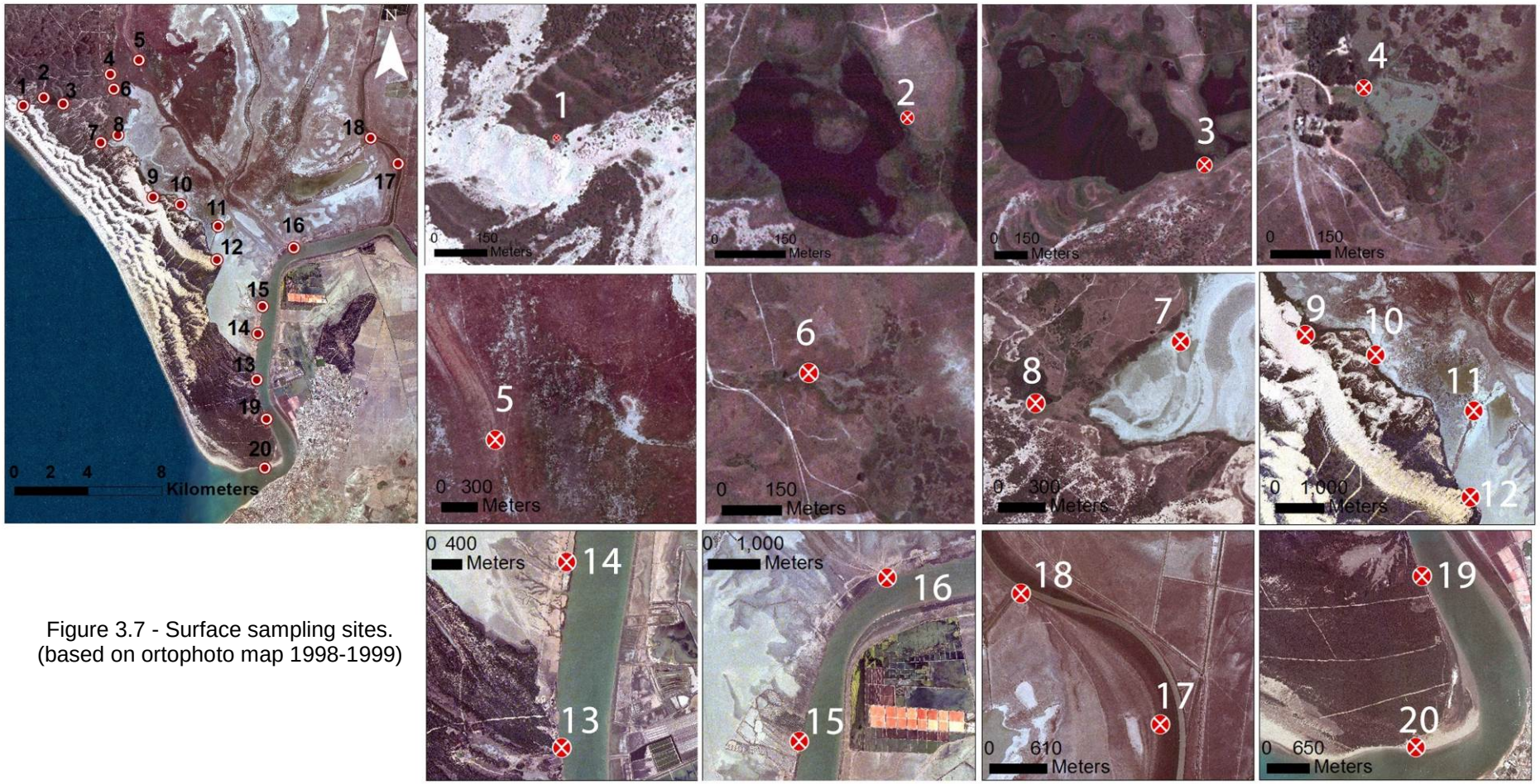

Figure 3.7 - Surface sampling sites.
(based on ortophoto map 1998-1999)

Figure 3.8 - Sampling sites' pictures . 1-temporary pond, with surrounding vegetation composed by *Pinus pinea* (above) and *Juncentum* sp. (below); 2- margins of the lagoon "Laguna Dolce; 3- margins of the lagoon "Laguna Sta. Eulália"; 4- temporary pound near Palacio de Doñana; 5- temporary pond at "Marisma de los Hinojos"; 6- "Caño del Preal"; 7- temporary pond near the "Lucio del Caballero"; 8– temporary lagoon, "Laguna Saperón"; 9- very eutrophicated temporary lagoon; 10- temporary pond of a very dry marsh (above), with a vegetation composed by S*arcocornia* sp (below); 11- next to the Ventalengua's chenier; 12- bubbling waterhole in marsh plain; 13- ancient marsh covered by sand; 14- small pond near a *Spartina* sp. channel; 15- borders of Guadalquivir River; 16- "Caño de Brenes" channel; 17- temporary pond, near the lagoon "Lucio del Tio Oreha"; 18- margin of the channel "Caño del Buen Tiro"; 19- mouth of Guadalquivir river; 20- Punta Malandar beach

2.2.2 - Subsampling sedimentological and microfaunal analysis

Approximately 200g of sediment were taken next to each microfauna sampling site, from 0 to 5 cm depth and stored in labeled plastic bags, for sedimentological analysis (Fig. 4.1, chapter IV).

Twenty surface samples of about $10cm^3$ were taken using marked syringes, and kept in vials with a Rose Bengal in Ethanol solution (1g/1L) for staining and preserving the live foraminifera. This solution was added because Rose Bengal adheres to proteins in the protoplasm of the foraminifera, giving it a fuchsia color which enables living tests to be distinguished from dead tests. This method was pioneered by Walton (1952) and is favoured by the majority of benthic marine ecologists and paleoceanographers because it is simple, fast and inexpensive (Bernhard et al., 2006).

The microfauna samples were kept in a coolbox, for better preservation until reaching the laboratory.

3 - Laboratory methods

3.1 - Cores

3.1.1 - Sedimentological and mineralogy analysis

The mineralogy of thirteen samples was studied by X-ray diffraction applied to three samples of core C and ten samples of core D (Fig. 4.1, chapter IV). The equipment used was a Philips PW 1130/90, with an automatic slit, using KK radiation of Cu and a Ni fillter at 20 mA and 40 kV (see Ruiz et al.,2004) .

The 62 µm fraction was separated by a standard sedimentation method (Barahona, 1974). Before the separation, carbonates were eliminated using 0.6 N acetic acid.

3.1.2 - Micro and macrofauna analysis

Sixty-two samples were obtained for macrofossil analysis (Fig. 4.1, chapter IV)(Ruiz et al., 2004). Samples were collected and prepared by washing the bulk sediment (12 cm^3) through a 1 mm sieve. Bivalves and gastropods were identified to the species

level and counted to study the semi-quantitative distribution in each core (see Ruiz et al., 2004).

Sixty-two samples of approximately 15 g were taken for microfossil analysis. These samples were washed through a 63 microns sieve to remove the mud fraction and then dried. If possible, more than 300 foraminifera from each sample were picked and placed faunal microscope slides.

All 33 samples of Core C had at least 300 individuals or more, whereas in Core D 4 of the 39 samples had less than 100 individuals and 3 had ~100 individuals.

Only species with abundance greater than 5% and 1%, in at least one sample, were considered for statistical analysis and species distribution.

Benthic foraminifers were classified according to the proposed generic classification of Loeblich and Tappan (1987), and identified by using Murray (1971), Milker and Schmiedl (2012), Martins and Gomes (2004), and studies therein. Further details about the taxonomic classification are given in Chapter VII. The best preserved foraminifera were documented using scanning electron microscope (SEM) photographs, taken with a JEOL, JSM-5410 LV microscope at the Departamento de Microscopía Electrónica y Rayos X of Universidad de Huelva and by microscope photographs taken with a Panasonic Lumix DMC-7Z28 camera, from Universidade do Algarve.

3.1.3 - Dating

Two ages, one on each core C and D, were carried out at the Beta Analytic Laboratory (Miami, FL, USA) and the Centro di Studio per il Quaternario e l'Evoluzione Ambientale del CNR (Rome, Italy) by radiocarbon methods applied to *Cardium edule* mollusc shells (see Table 1 Ruiz et al., 2004). Data were calibrated using CALIB version 4.3 (Stuiver and Reimer, 1993) and the Stuiver et al. (1998) calibration dataset. The final results correspond to calibrated ages (cal.) using 2sigma intervals, with a reservoir correction (3440 ± 85 yr) as suggested in Lario (1996) and Dabrio et al. (1999, 2000) for this area.

As the determination of a single mean ΔR value is not appropriate for this time interval (Soares & Martins, 2010), and the calibration curve is constantly changing, the calibration of all radiocarbon age obtained from cores in Doñana National Park (Table 3.2), were also carried out using the OxCal V.4.2.2 Bronk Ramsey (2013),

calibrated by the Atmospheric data from Reimer et al., 2004 (Figs. 4.2 to 4.5, chapter IV).

Table 3.2 - Radiocarbon dating for all cores in Doñana National Park, obtained by Ruiz and co-authors (2010).

Sample	Age (yrs BP)	Error	Maximum calibrated age (yr BP)	Most probable calibrated age	Minimum calibrated age (yr BP)
AR - 10	4548	59	5569	5309	5036
BR - 14	3380	40	4047	3763	3534
CR - 17	3460	40	4138	3862	3624
CR - 12	3679	48	4428	4153	3893
CR - 4	3694	61	4138	4182	3624
DR - 14	2230	60	2680	2336	2121
DR - 10	2171	36	2585	3204	2045
GR - 10	2140	70	2583	2288	1969
FR - 22	1940	60	2292	1992	1780
FR - 10	1960	40	2288	2020	1825
HR - 30	2284	39	2709	2373	2185
CM - 6	1750	40	2011	1800	1548
CM - 1	2430	40	2809	2710	2346
PLN - 28	3160	40	3750	3490	3283
PLN - 22	3680	40	4421	4160	3925
PLN - 18	3820	40	4634	4400	4083
PLN - 11	5690	40	6779	6580	6339
PLN - 8	43370	960	43610 +/- 960 yrs BP		

3.2 - Surface samples

3.2.1 - Sedimentological and mineralogy analysis

In the laboratory, each sample was dried in an oven and then passed through a 250-Wm sieve, to separate the coarse and fine fractions. The coarse fraction of the samples was then washed through >4 – 250 µm sieves for grainsize analysis. The fine fraction went through a H_2O_2 reaction for removing the organic matter, and was analysed in MALVERN mastersize for grainsize.

GRADISTAT 14.0 program was used to calculate the different grain size distribution of the samples and the sediment type, according to Folk & Ward (1957)(Appendix 1, Samples DNA1 to 20). The different grain size distribution results were then imported to ArcGIS software, where the USGS Sediment Tool was used to calculate the sediment type and to represent it in the sample's map (Fig. 4.6, chapter IV).

A lithology voxel (3D grid) was also performed, using the Geosoft Target extension for ArcGIS software, to see the relation among the sedimentological results from the surface samples (Fig. 4.7, chapter IV).

For mineralogy analysis, samples were dried in an oven at about 40°C and grinded in a mortar. They were then mixed with alcohol and grinded in Micronising Mill for ten minutes, and dried in an oven at 40°C. Once dried, the samples were grinded once more and read in X'Pert Pro PANalytical and analyzed in XPowder 2004 Version 0.4.0.2 Pro.

The percentage of water and organic matter in each sample was also calculated (Table 4.1 and Fig. 4.9, chapter IV) by loss of ignition after drying the samples and burning the organic matter respectively at 40ºC and 500ºC.

During the sampling of surface sediments, a multiparameter probe was also used to measure abiotic parameters like pH, temperature, conductivity and Eh, at each site (Fig. 4.10, chapter IV)(Table 4.1).

3.2.2 - Microfauna analysis

Surface samples remained untouched in the laboratory during 14 days, as it is the minimum time necessary for staining with Rose Bengal solution, as described by Schönfeld et al.(2012).

After, the samples were washed with water, through a 63 µm sieve, which had previously been placed in a tube of Methylene Blue. Fractions greater than 63 µm were then dried at 50°C.

A microsplitter was used to divide the samples in equally parts, and, if possible, more than 300 benthic foraminifera from each sample were collected, mounted on lightly glued cardboard slides, identified and counted.

The presence of Charophyta's seeds and ostracods in each sample was also recorded.

From the surface 20 samples studied, only 3 had ~300 individuals and 12 samples had no live or dead individuals at all. Only one sample yield living benthic foraminifera, but once the number of individuals was very low (less than 10 individuals), the distinction between the live and dead foraminifera was not made, neither the live/dead foraminifera and agglutinated/calcareous foraminifera ratios were calculated.

Only species with abundance greater than 1%, in at least in one sample, were considered for statistical analyses and species distribution.

As for core samples, benthic foraminifers were classified according to the proposed generic classification of Loeblich and Tappan (1987), and identified by using Murray (1971), Milker and Schmiedl (2012), Martins and Gomes (2004), and studies therein. Further detail about the taxonomic classification is given in Chapter VII. The best preserved foraminifera were documented using scanning electron microscope (SEM) photographs, taken with a JEOL, JSM-5410 LV microscope at the Departamento de Microscopía Electrónica y Rayos X of Universidad de Huelva and by microscope photographs taken with a Panasonic Lumix DMC-7Z28 camera.

4 - Microfauna population data analysis

4.1 - Abundance

The absolute abundance of a species is the total number of individuals of the same species in a sample. It is the first data resulting from the sorting and counting of a sample, providing the basis for calculation of relative abundance. The latter expresses the importance of each species in the whole sample and is calculated according to the following equation:

$$Aspi = xspi * 100 / Ni$$

Where *Aspi* is the relative abundance of species *i, xspi* is the number of individuals of species *i* in the sample and *Ni* is the total number of individuals in the sample.

4.2 - Faunistic density

In the present work, faunistic density expresses the number of individuals from a species I (Ni) per gram of sediment. This value was determined for total fossil assemblages of benthic foraminifera. The ration between Planktonic and Benthic foraminifera was also calculated based on faunistic density.

4.3 - Diversity

One method of analyzing taxonomic diversity is the application of indexes, which may be ratios or other mathematical expressions that quantify relations and importance between (Odum, 1997). Diversity has two components: the number of

species or ‘richness’ and the homogeneity of species distribution or ‘evenness’, described by the species’ relative abundances (Lin, 1992; Magurren, 1991).

The diversity indexes were calculated in the software for multivariate analysis Past, (PAleontological STatistics) version 2.17 for Windows.

4.3.1 - Shannon Index of Diversity (Hs)

The Shannon Index of Diversity (Hs), also called Shannon-Weaver information function (Buzas, 1979), is the diversity index adopted in the present study. It has the advantage of considering the relative abundances of species. It is not dependent on a mathematical model and allows the comparison of diversity between samples of different sizes (Odum, 1997). The Hs value is essentially determined by the relative abundances of common species and is little affected by the contribution of rare species (Gibson and Buzas, 1973). The Shannon index assumes that all the individuals are randomly sampled from an indefinitely large population and that all species are represented in the sample (Pielou, 1975 in Magurren, 1991). Its formula is:

$$Hs = - \Sigma\, pi * lnpi$$

Where $pi = ni/N$ is the proportion of the different species i in the sample, N is the total number of individuals in the sample, Hs is the diversity and s is the total number of species i (Magurren, 1991). Shannon diversity is highest when all the species in an assemblage present the same relative abundance: $Hs = lnS$. Hs usually varies between 1.5 and 3.5 and rarely exceeds 4.5 (Margalef, 1972 in Magurren 1991).

4.3.2 - Evenness, equitability (J)

Several authors, as for example Margalef (1974), prefer to directly interpret species diversity, as a function of physical, geographical, biological, or temporal variables, whereas others consider that species diversity is made of two components that should be interpreted separately. These two components are the *number of species* and the *evenness* of their frequency distribution. Although Margalef introduced the concept of evenness (1958), it was formally proposed in 1964 by Lloyd & Ghelardi for characterizing the *shape* of distributions, where the component “number of species”

corresponds to the length of the abscissa. In the literature “evenness” and “equitability” are synonym terms (Lloyd & Ghelardi, 1964; see also the review of Peet, 1974).

The simplest approach to evenness consists in comparing the measured diversity to the corresponding maximum value. When using *H*, diversity takes its maximum value when all species are equally represented. In such a case:

$$H_{max} = -\sum_{i=1}^{q} \frac{1}{q} \log \frac{1}{q} = \log q$$

where *q is* the number of species. Evenness (*J*) is computed as (Pielou, 1966):

$$J = H/H_{max} = \left(-\sum_{i=1}^{q} p_i \log p_i \right) / \log q$$

which is a ratio, whose value is independent of the base of logarithms used for the calculation.

4.3.3 - Fisher’s alpha

Fisher deduced his index of diversity based on the assumption that the abundances of species fit a log-series distribution (Fisher et al., 1943). That is, if the total number of individuals is *N*, and *p* is a constant proportion, then the most common species has *pN* individuals; the next most common, $p(1 - p)N$; the next, $p(1 - p)^2N$; etc. If abundances fit that distribution and samples are taken from one set of species, then the number of species you observe will obey this equation:

$$\mathbf{S = -\alpha} \ln(1 - x)$$

Where α is a constant that depends on diversity alone, and *x* is a variable that depends on sample size. The variable *x* satisfies:

$$\mathbf{S/N = \{(x - 1)/x\}} \ln(1 - x)$$

Fisher’s alpha can be used even though the abundances of the species do not fit a log-series distribution. Small, incomplete samples of other distributions almost fit the log-series (Boswell and Patil, 1971).

4.3.4 - Species' richness

This is the oldest and the simplest concept of species diversity - the number of species in the community or the region. McIntosh (1967) coined the name *species richness* to describe this concept.

5 - Multivariate analysis

Cluster analysis (CA) is one of the most widely used and commonly understood multivariate analytical techniques in the foraminiferal literature. It aggregates entities (samples, species, measurements) into 'naturally occurring' groups and quantifies the between-group relationships. In the present work, Cluster Analyses (CA) was also performed using PAST software (Hammer et al., 2008) on a data matrix of species with abundances > 5% in at least in one sample for Q-Mode and higher than 1% in at least one sample for R-Mode for the Cores, whereas for the surface samples the data matrix of species was based on abundances >1% for both Q and R modes. Although most authors agree on using only species with abundances >5% in at least one sample, in the present work it was thought that slight appearances of certain species could be important for the recognition of a paleo-tsunami. Hierarchical clustering produced four dendrograms indicating relationships between individual data point. Species for R-mode cluster analyses and samples for Q-mode cluster analyses were grouped according to their similarity using Bray-Curtis index for distance assessment.

To study the relation between biotic and abiotic features, a Canonical Correspondence Analysis (CCA) was made. Canonical Correspondence Analysis (CCA) is an ordination method that uses a multivariate direct gradient analysis, which is an advanced form of Correspondence Analysis (CA). CCA shows both patterns of assemblage composition and relationship between species and each of the environmental variables (Kent and Coker 1992). Thus it should display the extent to which organic matter, pH, Eh, conductivity, temperature and sediment type are controlling the distribution of the foraminifera. This multivariate analysis is preferred rather than other ordination methods such as CA and Detrended Correspondence Analysis (DCA) because it has been tailored to specifically include environmental data (Maddy and Brew 1995). The relative strength and direction each of

environmental variables is correlated to the length and direction of its line on the CCA plot.

The Canonical Correspondence Analysis was performed in R software using the Vegan library among abiotic parameters; between abiotic parameters and diversity indexes for the surface samples where foraminifera were present; and between diversity indexes and biotic parameters for the cores' samples.

IV. Results

1- ArcGIS

The first map (Fig.1.1, presented in chapter I) shows the three possible epicenter sites that may have generated the 1755' Lisbon Tsunami, based on Campos (1991). This map includes several bathymetric lines (downloaded from NOOA's site, World data service for geophysics, National Geophysical Data Center, National Oceanic and Atmospheric Administration), tectonic plate lines (downloaded from USGS (United States Geological Survey) site), as well as a shapefile (type multi point) created in ArcGIS software indicating the three main epicenter sites for the tsunami (Gorringe Bank, Gulf of Cadiz Accretionary Wedge and the Mid-Atlantic Ridge).

The second map (Fig.2.1, presented in chapter II) shows the location and geomorphological scheme of Doñana National Park. In this, Fig.2.1a and 2.1b, Autonomous Communities of Spain and Andalucia provinces respectively, are composed by polygon shapefiles downloaded from de Ministry of Agriculture, Alimentation and Environment of the Government of Spain (Ministerio de Agricultura, Alimentacion y Medio Ambiente, Gobierno de España) website (http://servicios2.marn.es/sia/visualizacion/descargas/mapas.jsp). Figure 2.1c, the geomorphological scheme of the park, was based on Rodríguez-Ramírez (2008) work. At the base of this map is an ortophoto, obtained during the flight made between July 1998 and July 1999 at a 1:60.000 scale, with a focal distance of 150 mm, flight height of ~9000 m and 1 m resolution, arising from a collaboration agreement between the Departments of Public Works and Transport, Agriculture and Fisheries, and Environment (Consejerías de Obras Públicas y Transportes, Agricultura y Pesca, y Medio Ambiente) of Spain. To this ortophoto several shapefiles were created and overlapped, corresponding to Doñana National Park limit, Guadalquivir River, Chenier areas (multipolyline shapfiles), Spits, High Marsh, Low

Marsh, Stabilized Dunes and Mobile Dunes (polygon shapefiles) in ED50 UTM zone 29N reference system.

The third, fourth and fifth maps (Figures 2.2, 2.4 and 2.5 respectively) all had map number two as a basis, and which purpose was only to approximate and show with more detail the geomorphological zones contained in it, namely the mobile dunes and spit systems (Fig. 2.2), the Aeolian system (Fig. 2.4) and the marsh areas (Fig. 2.5).

The sixth map (Fig. 2.6 present in chapter II) shows the Palaeogeographical evolution phases of Doñana National Park from the Atlantic Climatic Period (~6000 B.P.) to the SubAtlantic Climatic Period until present. For the creation of this map a bibliographical revision about the occurrence of tsunamis in the Iberian Peninsula was made, and the final result was the combination of the analysis of four main works: Ruiz et al., 2010; Schutt, 2005; Rodríguez-Ramírez, 2008; and Rodríguez-Ramírez et al., 1996. The final map has in fact 5 maps (Fig. 2.6a Atlantic Climatic Period, Fig. 2.6b SubBoreal Climatic Period, and Figs. 2.6c-e SubAtlantic Climatic period until present), each one with six main shapefiles, created and edited along the process, corresponding to Chenier areas, the Littoral spit, High Marsh, Low Marsh, Aeolian dunes and Mio-Plio sediment formations. The gradient background indicating a more or less marine influence (dark to light greenish blue) was achieved by choosing a gradient fill symbol in the symbology properties tab for the shapefile containing the work area limits. The arrows indicating the type of marine or/and fluvial influence were added latter on the layout view of the map. These maps are all at a 1:12.000 scale.

The seventh map (Fig. 3.1a presented in chapter III) is the same as the second map (Fig. 2.1, chapter II), where a multipoint shapefile was added with the location of the sampled cores C and D (in ED50 UTM zone 29N). The topographical profile between the cores (Fig. 3.1b) was accomplished with the 3D Analyst toolbar by the creation of a profile graph based on the digital model terrain (DMT) of the park. The creation of the DMT is later described in this section under map number nine.

The eighth map (Fig. 3.2 of chapter III) corresponds to the location of the surface samples, with the ortophoto as a base, and the addition of the coordinates of these (adquired with a GPS device at sampling day) in a new multipoint shapefile in ED50 UTM 29N reference system (see Table 3.1, in chapter III).

The ninth map (Figs. 3.3 and 3.4 of chapter III) was made in two phases. The first phase was the creation of the Doñana National Park DMT, throughout the

vectorization of altimetry points present at a topographical map provided by Professor Manuel Abad, with a 1:10.000 scale, which were then converted to a TIN file in Arctoolbox, 3D Analyst tools, TIN management, Create TIN option. The second phase implied to check what were the inundable areas by the tide and precipitation within the park. To do this I went to the Spanish Meteorological Institute (www.aemet.es/portada) to see the highest and lowest precipitation months for the Andalucia area, which were April and September 2013 respectively. The next step was to download ortophoto images from USGS Earth Explorer web site (http://earthexplorer.usgs.gov) for these months. The ortophoto images were then georeferenced in ArcGIS and a change detection process was made with Raster Calculator tool, through subtraction and quotient methods between the images (where the quotient show a better result) to check the areas within the park that suffered alteration, meaning that where inundable (black areas correspond to change and white to no change)(Fig. 3.3a). The DMT was then superimposed to the resultant change detection image to check the altimetry line that corresponds to the boundary between inundable and non-inundable areas (Fig. 3.3b). The last phase was to see the mean tide level for the sampling day and coloring the DMT altimetry zones that correspond to this (red areas at Fig. 3.4), representing the areas worth sampling.

The tenth map (Fig. 3.5, chapter III) is actually the same as the eighth map, but it the sampling areas approximated for better visualization.

The eleventh map (Fig. 4.1 presented in chapter IV) was the first map made in Geosoft Target extension for ArcGIS, which is a very complex extension and implies a variety of steps. The first step, when using this extension, is the creation of a new project, where the maximum and minimum number of holes as to be specified. Then the creation and importation of three types of data is obligatory, corresponding to:

- Collar data file (containing the hole ID, Easting, Northing and Elevation/Depth)
- From-To data file (data acquired over specific depth intervals down the hole, e.g. type of sediment)
- Point data file (data acquired in discrete measurements made at a specific depth, e.g. Planktonic/Benthic ratio at 27, 32, …, X cm depth).

Once these files are correctly imported, the extension allows you to make Plan Maps, Section Maps, Striplog Maps, and others. For this map, a Striplog Map was created, that enables the display of up to 16 data/graph type selections in each plot. Together to this plot, a legend was specified, the two holes (Cores C and D) were

chosen to be plotted, as well as their depth intervals and the data included on From-to and Point data files (sediment type, micro and macrofauna sampling depths, mineralogy samples and radiocarbon datation samples), resulting in Striplog Map shown in Fig. 4.1 of chapter IV.

The twelfth map (Fig. 4.6, chapter IV) shows the Sedimentological analysis of the surface samples. This map arose from the combination of granulometry data made for the samples along with the analysis of these by the USGS Sediment Tool for ArcGIS (downloaded from http://woodshole.er.usgs.gov/pubs/of2007-1186). The main objective of the creation of this map was to ckeck if the sediment analysis using GRADISTAT 14.0 software (largely used worldwide for this type of analysis) corresponds to the one made by the mentioned tool in ArcGIS.

The USGS Sediment tool is quite intuitive, in which attributes correspondent to the sediment type percentages are added to the sampling sites shapefile (gravel, sand, mud, clay %). There is the need of creating a new attribute named Silt, that results from the subtraction of Mud – Clay values for the analysis to be made, as well as an attribute LatLong that is the summarization of the latitude and longitude values of each sample, so one can average the sediment values where there are multiple points. Once these are created, the Folk Sediment Classification analysis option is chosen. Although the objective and final result of this analysis is the creation of a raster surface data with the sediment types, this interpolation had a lousy result due to the large distance between sampling sites. In order to overpass this problem, and since the sediment analysis ended up corresponding to the one made by GRADISTAT software, polygon shapefiles were created around the perimeter of each sample. Then, the attributes with the sediment type results were added and symbology schemes were chosen to represent the resulting Silt, Sand and Silty Sand sediment types (Fig. 4.6, chapter IV).

The thirteenth map (Fig. 4.7 chapter IV) was the second map performed with Geosoft Target extension for ArcGIS and shows the lithology voxel for the surface samples. For the creation of this map, the same steps as for the eleventh map had to be performed, including the creation of a new project, a Collar data and From-to data files. There was no need for the creation of the Point data file, once surface samples had only one depth, as opposed to the Cores. The Doñana National Park DMT was also added. This was transformed into a Geosoft GRID type file, with a cell size of 15.

The creation of voxels in this extension is made in the Target Toolbar in the option Generate 3D hole plot. A new window in then opened where it is possible to add the DMT Grid file and the base data files for the creation of a lithology voxel (sediment type of each sample, included in From-to data file). The lithology voxel for each sediment type is then created, throughout an Inverse Distance Weighted Gridding method, also with a cell size of 15 (Fig. 4.7, chapter IV). The colour scheme and transparency percentage are one of the many options that can be modified within this tool.

The fourteenth, fifteenth, sixteenth, seventeenth, eighteenth, nineteenth and twentieth maps (Figs. 4.9, 4.10, 4.13, 4.15, 4.18, 4.19 of chapter IV) correspond to the abiotic parameters, relative abundances of foraminifera and diversity indexes of the surface samples. For these, the basis was always the ortophoto map and geomorphological features of the park (Fig. 2.1, chapter II), to which shapfiles where added corresponding to the values of organic matter and water percentages (Fig. 4.9), pH, Eh and Conductivity measurements (Fig. 4.10), species relative abundances (Fig. 4.13), Faunistic density (ind/g) and Planktonic/Benthic ration (Fig. 4.18), Shannon H and Equitability indexes (Fig. 4.19), Species richness and Fisher Alpha indexes (Fig. 34), all with different symbologies.

The twenty-first map (Fig. 5.1 of chapter V) is the same as the thirteenth map, where the geomorphological shapefiles of the park where superimposed, in order to check the relation between the sediment type and the latter.

The twenty-second map (Fig. 5.6, chapter V) shows the location of nine cores present at Doñana National Park (AR, BR, CR, DR, FR, CM, PLN, C (GR) and D (HR) from Ruiz et al., 2010) superimposed to a DMT performed in ArcScene (Fig. 5.6a), aswell as a section map (Fig. 5.6b) showing the sediment types described for these, made in Geosoft Target extension, with similar description than that made for the eleventh map, but with altered Collar and From-to data files.

The twenty-third, twenty-forth and twenty- fift maps (Figs. 5.7, 5.8 and 5.9 respectively) where also performed with the Geosoft Target extension for ArcGIS, for Cores AR,CR, CR, PLN and C,D, FR, DR, CM respectively. Figure 5.7 is a section plan map in which the *y* axis corresponds to radiocarbon datings made by a linear interpolation method between the datings made by Ruiz and coworkers in each core, allowing to see the corresponding phases between them. Figures 5.8a and 5.9a are plan maps and Figures 5.8b and 5.9b are section maps performed between cores

that presented the same radiocarbon datation ages. Based on the description and analysis of sedimentary facies and radiocarbon datings made by Ruiz and coworkers (2010), the use of the Wireframing tool from Geosoft Target extension allowed to create a geological interpretation, which was added to the section. Figures 5.8c and Fig. 5.9c show the resultant lithology voxels from the interpolation of the facies present among the cores, with the DMT superimposed for easier interpretation.

At last the twenty-fifth map is a 3D plot Graph created in the Geosoft extension, representing the connection between phases among the cores, where Fig. 5.10a shows a general view of the phases (described in Ruiz et al., 2010) in sequence and Fig. 5.10b the plotted phases in groups, for better viewer perception.

2 – Cores

2.1 - Subsampling for sedimentological, mineralogical, micro and macrofaunal analysis

The cores description together with the identification of samples analyzed for micro and macrofauna, datitions and mineralogy are represented in the StripLog figure below (Figure 4.1), made with the Geosoft extension Target for ArcGIS software. The sedimentological and compositional analyses of the core samples collected and dated in the Doñana marshlands enable the differentiation of three main facies (Silt and Clay, Silt, and Sand).

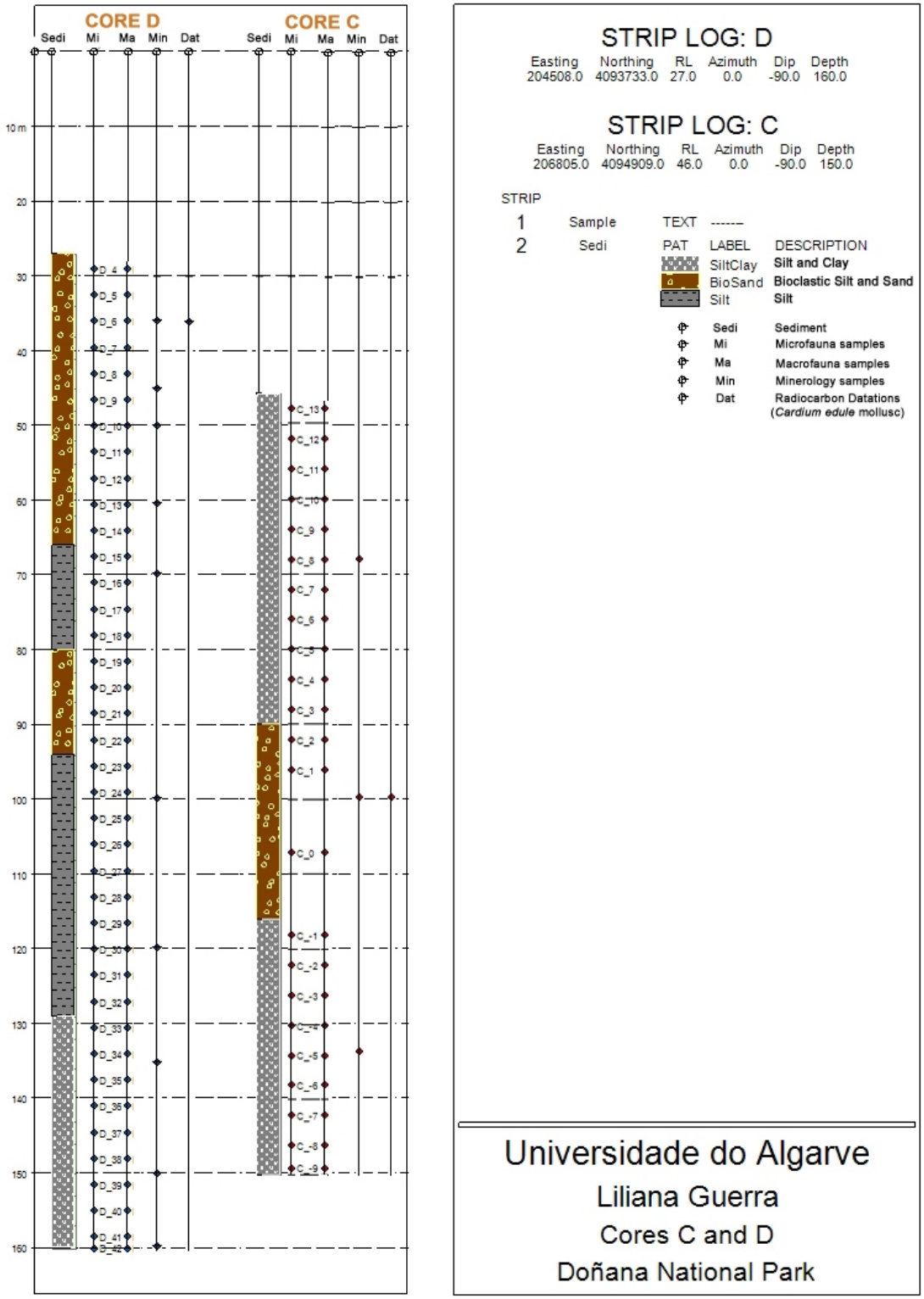

Figure 4.1 - Cores C and D sediment type's, micro and macrofauna samples, mineralogy samples and datation samples made in Geosoft Target Extension (ArcGIS)

2.2 Datations

Results of radiocarbon calibrated ages in OxCal V.4.2.2 software of all cores from Ruiz et al work (2004) are presented in the Figure 4.2.

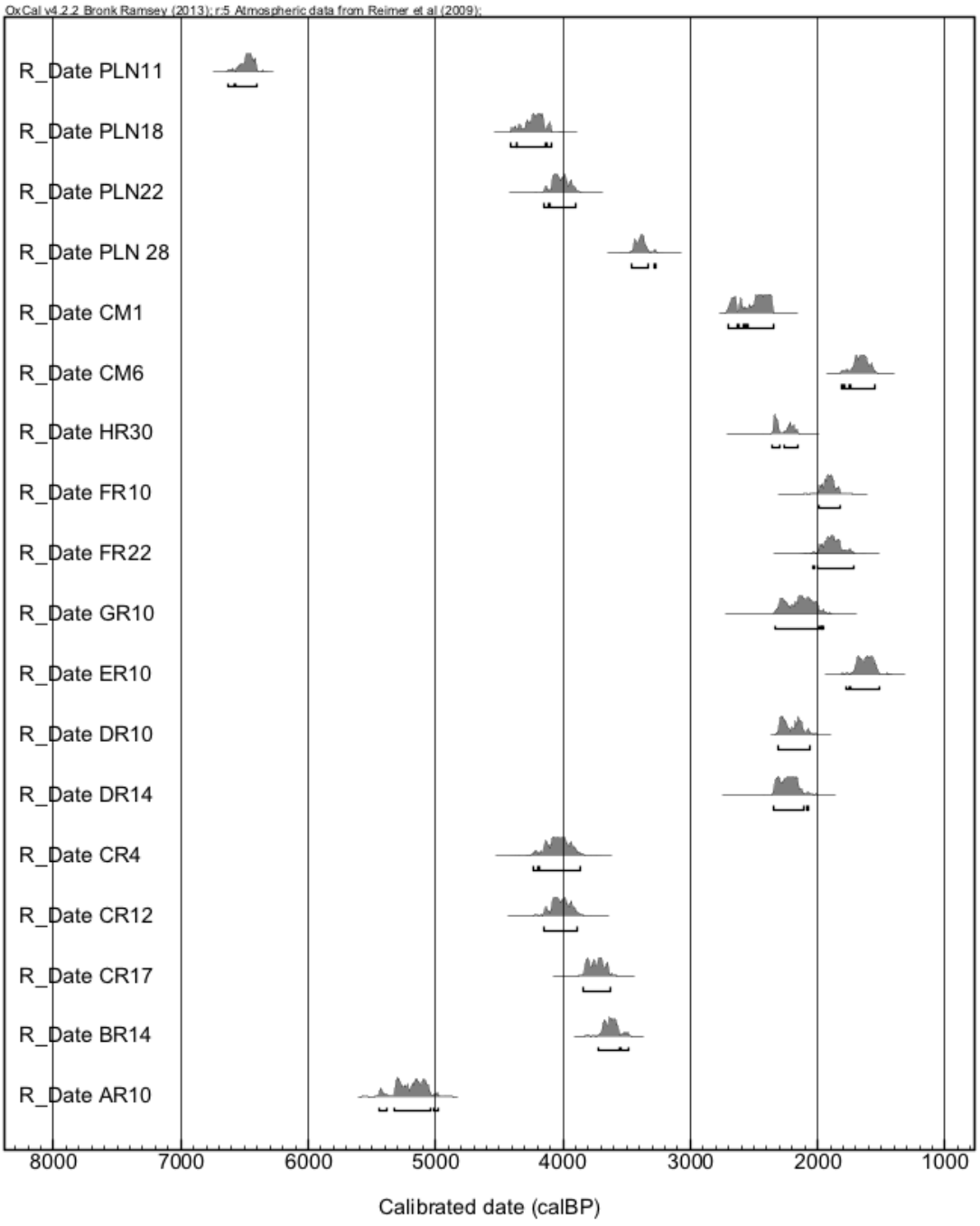

Figure 4.2 - Results of radiocarbon ages calibrated of all cores using OxCal V.4.2.2 (Bronk Ramsey 2013)

The results show more clearly the overlap between ages registered in the cores. Cores PLN22, CR4 and CR12 have registered radiocarbon ages of ~4000 cal BP; Cores GR10, DR10 and DR14 of ~2500 cal BP; FR10 and FR22 of ~2000 cal BP; and CM6 and ER10 of ~1500 cal. BP.

This process was also made only for Cores C and D, so that instead of simply using an average age, the time interval and overlapping could also be visualized and interpreted (Fig. 4.3).

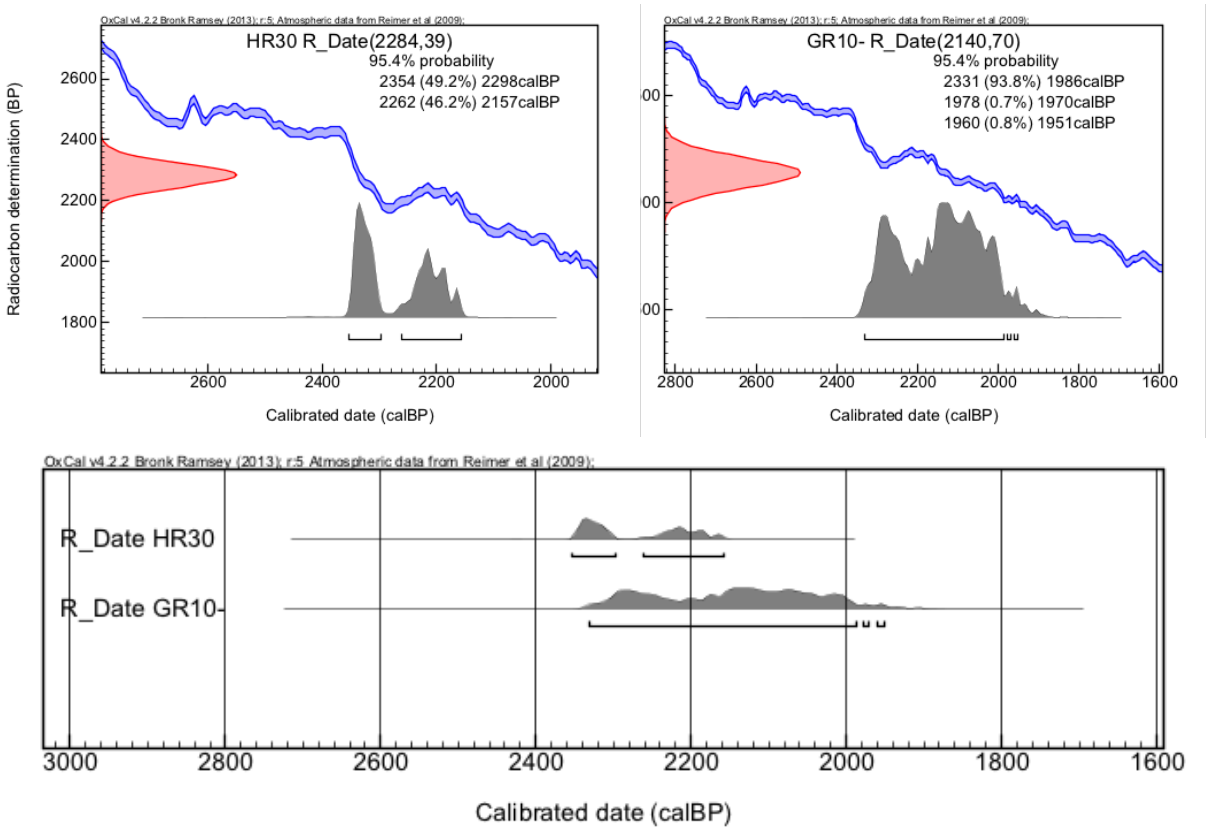

Figure 4.3 - Results of radiocarbon ages calibrated of cores C and D, and its overlap, using OxCal V.4.2.2 (Bronk Ramsey 2013)

Some imprecision in the dated ages is noted (Figs. 4.4 and 4.5), once these are comprehended within a time period where there is a plateau effect (an inversion of carbon in the atmosphere), making it difficult to say if the dated samples in the two cores have the same age, or if one is older or younger than the other.

Nevertheless, it is also important to underpin the apparent age inversion relatively to the depth in both cores, which is also important in part due to the difference of elevation of each core.

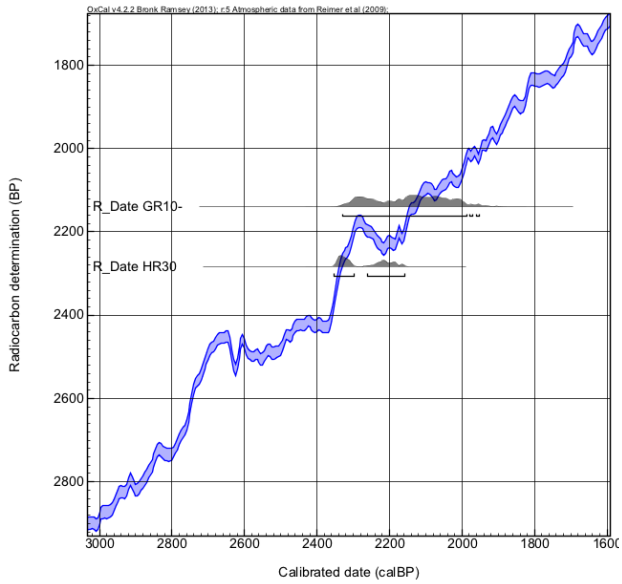

Figure 4.4 - Results of radiocarbon ages calibrated of cores C and D, its overlap, and the C14 curve using OxCal V.4.2.2 (Bronk Ramsey 2013)

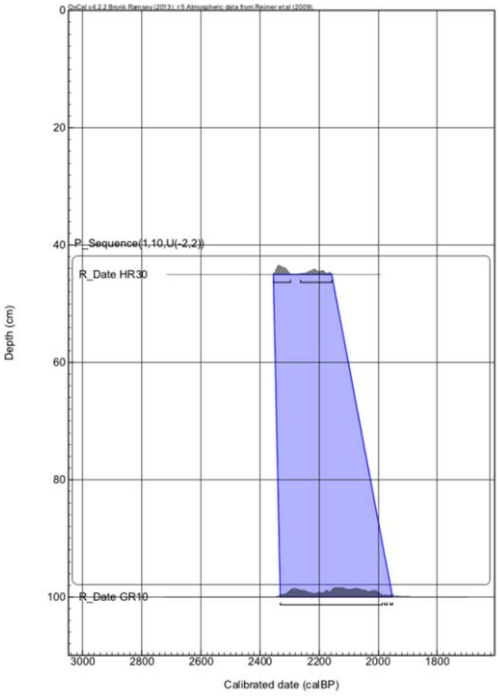

Figure 4.5 - Calibrated ages in relation to the sample depths in each core showing an inversion

3 - Sedimentological and mineralogical analysis of surface samples

The results of the type of sediment, according to Folk & Ward (1957), calculated in GRADISTAT 14.0 program were the same as those calculated with the USGS Sediment Tool in ArcGIS, resulting in three main textural types of sediment: Sand, Silt and Silty Sand (Fig. 4.6 and Appendix 1).

Surface samples 1, 4, 6, 7, 8, 9 and 13 belong to the sediment textural group of silty sand; samples 5, 10, 11, 12, 14, 15, 16, 17 and 18 to the textural group of silt; and samples 2, 3, 19 and 20 to the textural group of sand (Fig. 4.6).

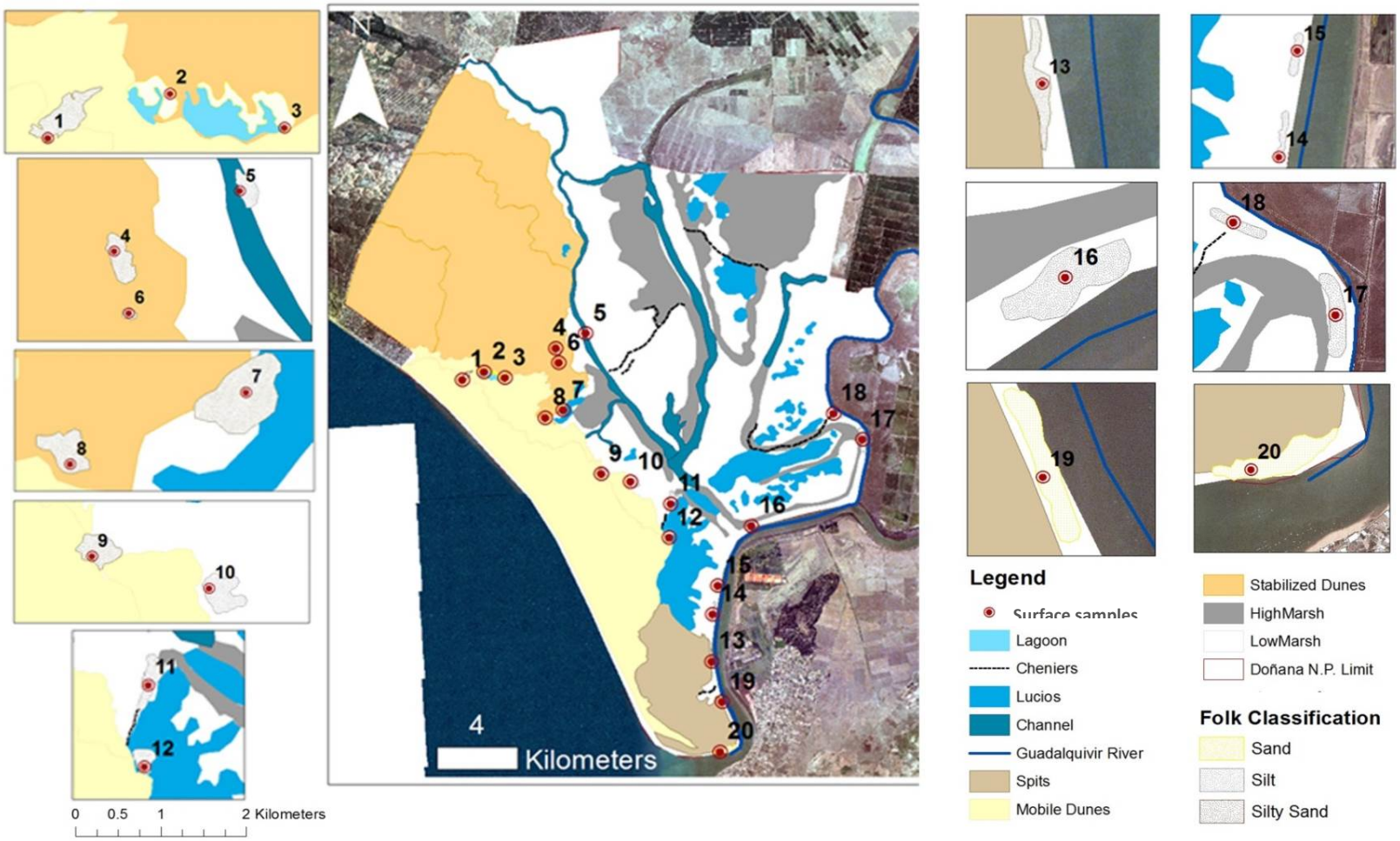

Figure 4.6 - Sedimentological analyses (Folk & Ward (1957) classification) for surface samples made in the USGS Sediment Tool (ArcGIS), resulted in three main sediment textural groups: Sand, Silt and Silty Sand, as shown for each surface sample in the small boxes around the main frame representing the general actual morphology of the Natural Park

The lithology voxel created based on the sediment type resulted in Figure 4.7 below, showing three main connected Sedimentological features. Surface samples 2, 3, 19 and 20 resulted in a lithology voxel composed by sand; samples 1, 4, 6, 7, 8, 9 and 13 in a lithology voxel composed by silty sand; and samples 10, 11, 12, 14, 15 and 16 in a voxel composed by silt. Due to the large distance between samples 5, 17 and 18 in relation to the other samples, a triangulation could not be performed, and no lithology voxel appears.

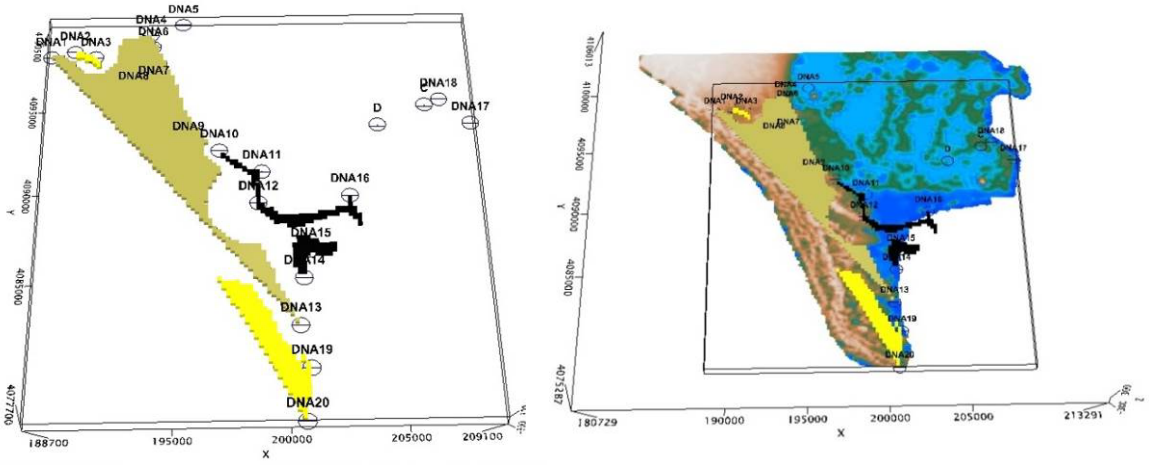

Figure 4.7 - Lithology voxels created in Geosoft Target extension for ArcGIS software, based on the sediment type of the surface samples. Left: Sedimentology only and Right: Sedimentology on top of the actual morphology

The mineralogy results analysed on XPowder 2004 Version 0.4.0.2 are show in Appendix 2 and in Figure 4.8 below.

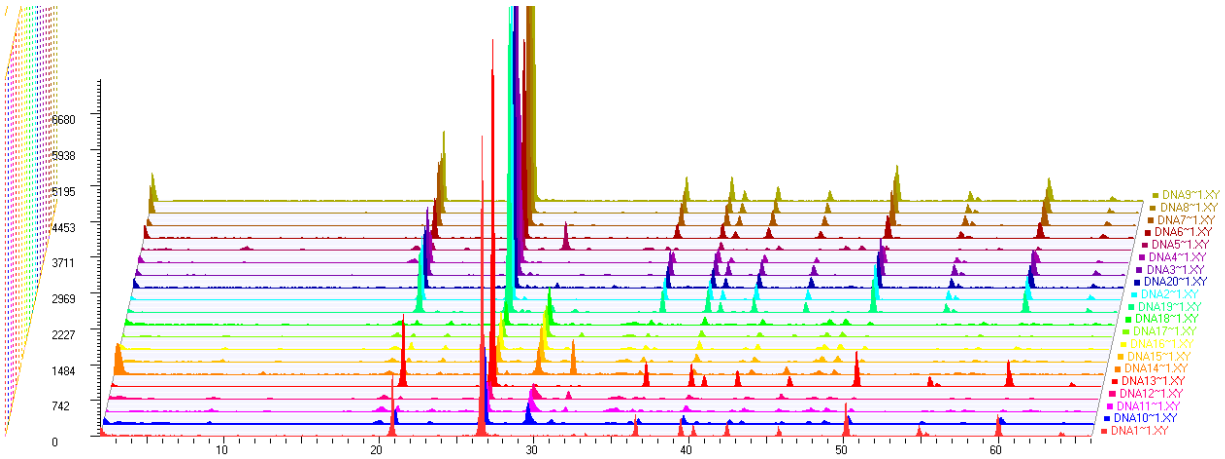

Figure 4.8 - Surface samples' mineralogy results, analysed in XPowder 2004 software Version 0.4.0.2. Axis X correspondes to 2θ values, Axis Y corresponds to the number of Counts.

Samples show two main groups one dominated by detritical minerals such as quartz and other, less abundant, dominated by precipitated minerals such as calcite.

The results of abiotic parameters such as the percentage of organic matter and water content, pH, temperature, conductivity and Eh in each sample are shown in Table 4.1 below and represented in Figs. 4.9 and 4.10.

Table 4.1 - Results of abiotic parameters measured at each sampling site and calculated by loss of ignition. NA means that no measure was made

Sample site	Organic Matter %	Water %	Temperature (C°)	Conductivity (m/s)	pH	Eh (mv)
1	1.41	14.21	NA	NA	NA	NA
2	0.53	18.52	5	2.69	NA	22.1
3	0.81	17.29	5.6	4.81	7.12	115.4
4	8.08	52.96	5.6	0.267	6.48	68.9
5	7.13	33.29	NA	NA	NA	NA
6	3.92	21.75	8.2	2.26	7.26	108.9
7	2.08	20.67	8.6	1.253	2.29	78.7
8	1.64	23.41	12.5	2.95	6.04	115.9
9	9.93	44.50	11.6	0.22	6.58	70.2
10	4.30	28.81	11.2	33.7	8.29	80.9
11	12.72	25.15	NA	NA	NA	NA
12	26.34	32.69	14.7	8.83	9.04	36.6
13	NA	19.13	15.1	31.9	8.08	108.9
14	13.70	48.22	16.3	143.1	8.41	118.4
15	4.89	34.57	18.1	24.3	8.42	101.5
16	6.32	35.39	14.8	20.5	8.81	95.6
17	12.77	42.76	17.4	44	8.35	106.3
18	4.93	40.48	11.5	8.72	8.06	106.4
19	0.91	19.80	13.6	24.6	8.18	111.8
20	0.51	18.27	13.6	31.5	8.3	108.1

The organic matter content varies from as low as 0.5 % in sample 2 and 26 % in sample 12.

The sediment water content is also highly variable from 14 to ~53 % in samples 1 and 4 respectively, which is mainly due to the sampling sites.

Temperature in ºCelsius has its lowest value in sample 2 and highest in sample 15, with 5 and 18ºC, respectively.

Conductivity values vary from 0.22 to 143 m/s in samples 9 and 14, respectively.

The pH values show large variation ranging from ~2 to 9 at samples 7 and 12, respectively. The lowest value found in sample 7, with pH value of ~2 is common of acid rains. Sample 8 also had a relatively low pH value (6 pH), corresponding to the normal range values of precipitation. The majority of the samples showed pH values

of normal range stream (values from ~6.5/7 – 8 pH), namely samples 3, 4, 9, 10, 13, 14, 15, 17, 18, 19 and 20. Sample 12 had a more alkaline pH value similar to that found at sea water (~9 pH).

As for Eh the lowest and highest values are present in samples 2 and 14, with 22 and 118 mv. In general the sampled soils had values correspondent to moderately reduced soils (with values > 0 mv), although samples 2, 4, 7, 9, 10, and 12 where lower than 100 mv, whereas the remaining ones where higher 100 mv.

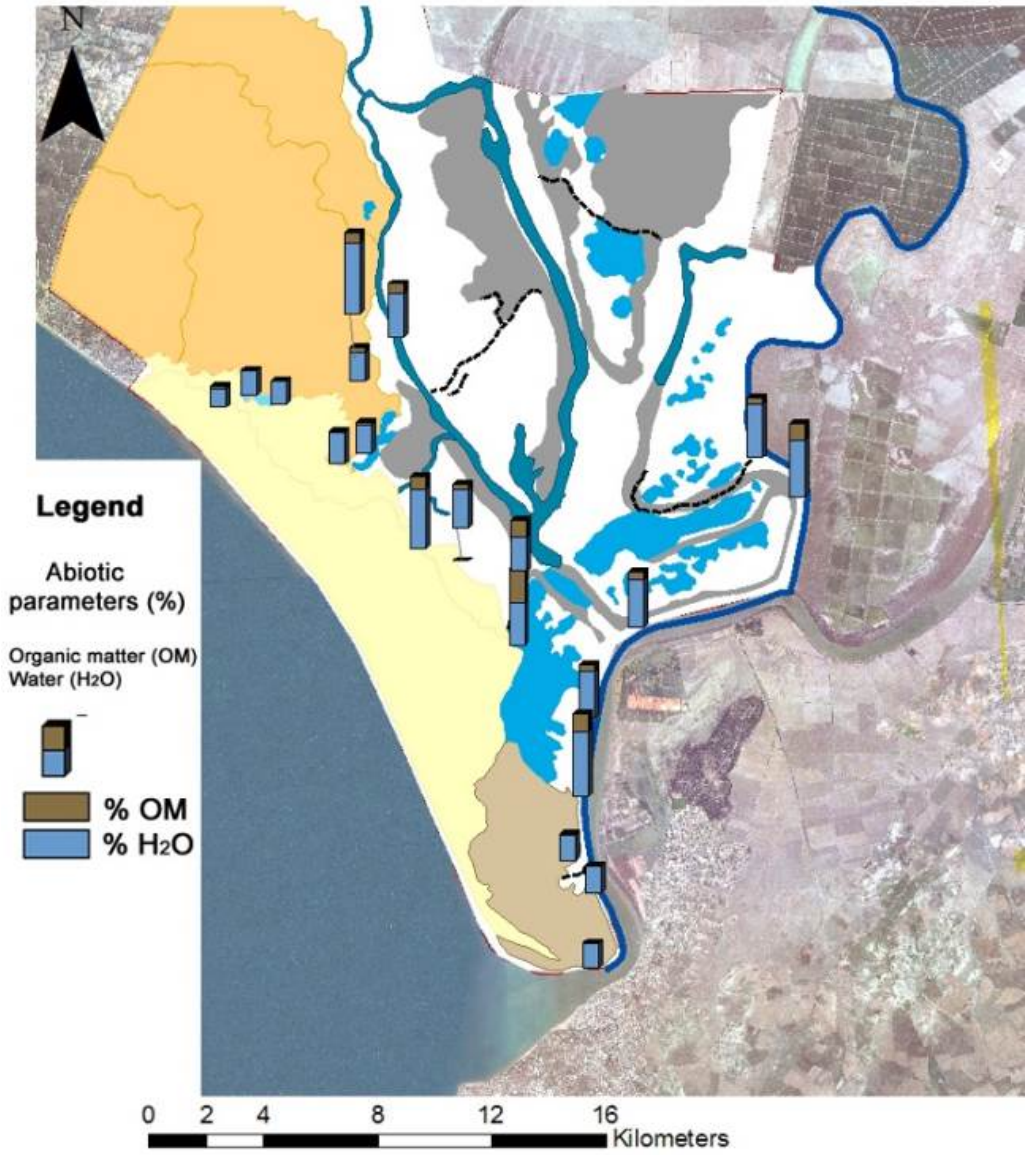

Figure 4.9 - Results of the percentage of organic matter and water, calculated for each sampling site. Made in ArcGIS software

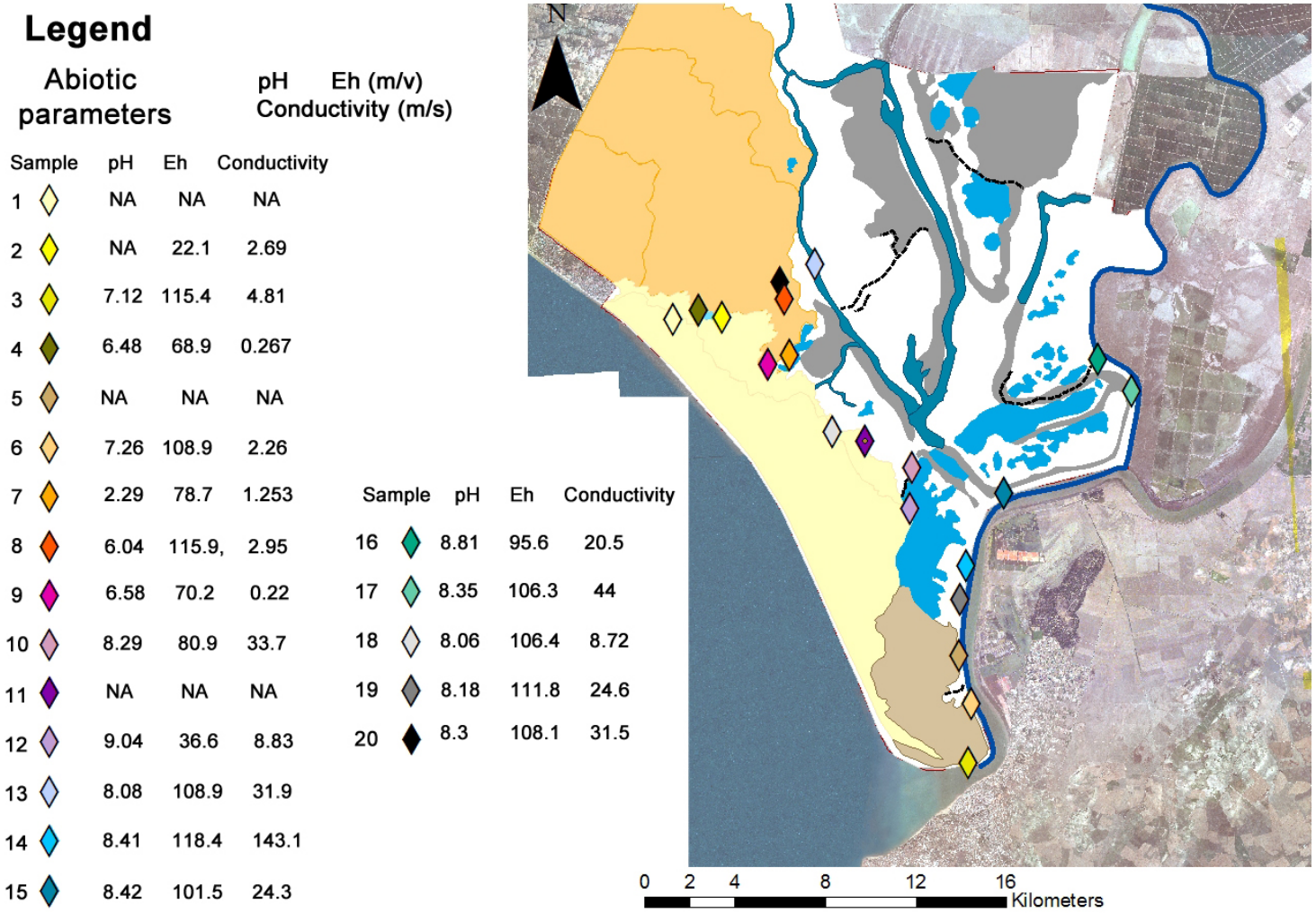

Figure 4.10 - Results of abiotic parameters, pH, Eh (m/v) and conductivity (m/s), measured at each sampling site. NA means that no measure was made. Made in ArcGIS software

4 - Microfauna population data analysis

4.1 - Abundance

A total of 50 benthic foraminiferal species were determined. Fourteen species were assigned to genera only and were left in open nomenclature due to difficulties in their identification, as a result of reworked or bad preserved individuals (*Ammotium, Textularia, Cornuloculina, Adelosina, Lagena, Fissurina, Stilostomella, Rectuvigerina, Elphidium, Quinqueloculina, Brizalina*).

In Core C, four of thirty-one species showed relative abundances > 5% in at least one analysed sample and twenty of thirty-one species showed relative abundances between 5% and 1% (Fig. 4.11 and Appendix 6).

Between 150 – 98 cm deep, *Haynesina germanica* and *Ammonia tepida* are the main species with relative abundance ranging from 62.5 – 76.7% at 120 and 132 cm respectively and with 15.7 – 25.9 % at 128 cm and 120 cm correspondently, with average values of 70 and 19.2 % respectively. Species *Quinqueloculina stelligera, Bolivina ordinaria, Elphidium cuvillieri, Elphidium granosum, Elphidium oceanensis* and *Elphidium* sp. show relative abundances from 2.528 % at 148-150 cm (average value of 0.28%), 0.22 – 2.8% (132 and 148-150 cm respectively, with an average value of 1.1%), 0.33 – 3.06% (144 and 116 cm respectively, mean average of 1.5%), 0.37 – 5.6% (136 and 116 cm respectively, with an average value of 2.2%), 1.02 – 4.6% (124 and 120 cm depth, mean value of 2.2%) and 0.99 – 3.65% (120 and 148-150 cm in depth, with an average value of 0.7%) correspondingly.

Fissurina sp showed abundances ranging from 1.345 – 3.745% (132 and 128 cm, with an average mean of 1.3%); *Quinqueloculina laevigata* from 0.329 – 1.859% (120 and 136 cm depth, mean of 0.2%); *Quinqueloculina* sp. from 0.372 – 3.8% (136 and 140 cm depth, with a mean value of 0.5%) and *Brizalina* sp. ranging from 0.28 – 1.04% (148-150 cm and 140 cm respectively, with an average of 0.2%).

Subsidiary species as *Buliminella elegantissima* (0.28 – 0.372% at 148-150 cm and 136 cm depth, with an average of 0.1%), *Bulimina elongata* (0.372 – 0.375% at 136 and 128 cm, with an average of 0.1%), *Asterigerinata mamilla* (0.224% at 132 cm, with an average value of 0.025%), *Spirillina vivipara* (0.28 – 0.67% at 148-150 cm and 144 cm depth, with an average of 0.1%), *Textularia* sp. (0.28 – 0.375% at 148-150 cm and 128 cm depth, average value of 0.1%), *Stilostomella* sp. (0.342 –

0.448% at 124 and 132 cm deep, with a mean of 0.1%), *Brizalina striatula* (0.342% at 124 cm, average of 0.038%), *Triloculina trigonula* (0.372% at 136 cm, with an average of 0.041%), *Cornuloculina* sp. and *Cornuspira involvens* (both with 0.348% at 140 cm, average of 0.039%) and *Nonionella stella* (0.281% at the depth of 148-150 cm, with a mean value of 0.031%) also occur between these depths.

Between 98 – 86 cm depth *Haynesina germanica* and *Ammonia tepida* remain the principal species, with relative abundances from 67.5 – 75.5% (94 and 90 cm, with an average of 72.4 and 21.8 respectively).

Quinqueloculina stelligera no longer occurs, whereas *Bolivina ordinaria* shows relative abundances ranging from 0.29 – 0.314% (94 and 98 cm deep, with an average of 0.2%), *Elphidium cuvillieri* from 0.2 – 1.57% (90 and 98 cm, with a mean of 1.1%), *Elphidium granosum* from 0.8 – 2.8% (90 and 98 cm, with an average of 1.6%), *Elphidium oceanensis* from 0.4 – 0.59% (90 and 94 cm, with a mean value of 0.3%) and *Elphidium* sp. from 0.4 – 3.77% (90 and 98 cm depth, with a mean value of 2.2%).

Subsidiary species like *Elphidium complanatum, Planorbulina mediterranensis*, *Spirillina* sp., and *Stainforthia complanata* were present with relative abundances of 0.4 % at 90 cm (mean value of 0.134%), 0.20 – 0.297% at 90 and 94 cm (mean value of 0.2%), 0.2% at 90 cm (mean of 0.067%) and 0.314% at 98 cm deep (mean value of 0.105%) respectively).

Between 86 – 66 cm deep, *Haynesina germanica* relative abundance ranges from 69.7 – 77.4% at 66 and 74 cm respectively and it's followed by *Ammonia tepida* with 19.5 – 23.7 % at 74 and 82 cm correspondently, and present mean averages of 73 and 22.4 % respectively.

Bolivina ordinaria, Elphidium cuvillieri, Elphidium granosum, Elphidium oceanensis and *Elphidium* sp. show relative abundances between 0.35 – 1.04% (82 and 70 cm, with mean average of 0.4%), 0.5 – 1.75% (74 and 66 cm, with average of 1%), 0.7 – 1.9% (82 and 86 cm depth, with a mean value of 0.9%), 0.58 – 3.5% (86 and 66 cm, with an average of 1.5%) and 0.78 % (at 74 cm with an average value of 0.13%).

Brizalina sp. shows a relative abundance of 0.145% at 86 cm and a mean average value of 0.024%.

Subsidiary species *Bulimina elongata* (0.44% at 66 cm, with a mean of 0.073%), *Asterigerinata mamilla* (0.26 – 0.44% at 74 and 66 cm, with an average of 0.12%), *Spirillina vivipara* (0.35% at 70 cm, with an average value of 0.058%), *Textularia* sp. (0.145 – 0.35% at 86 and 82 cm, with a mean value of 0.1%), *Spirillina* sp. and *Lagena sulcata* (both with 0.26% at 74 cm with an average of 0.043%), *Stainforthia complanata, Rosalina bradyi, Bulimina marginata* (with 0.145% at 86 cm and an average value of 0.024%) and *Uvigerina peregrina* (0.35% at 82 cm with an average of 0.058%) also occur between these depths.

In the 66 – 46 cm interval of this core *Haynesina germanica* and *Ammonia tepida* are still the dominant species, whose relative abundances range from 69.2 – 76.4% (58 and 54 cm deep respectively) and 19.5 – 25.2% (46 – 58 cm deep respectively) correspondingly, and a mean average of 72.8 and 22.4% respectively.

Species *Bolivina ordinaria, Elphidium cuvillieri, Elphidium granosum, Elphidium oceanensis* and *Elphidium* sp. occur with relative abundances 0.4 – 0.8% (66 and 46 cm deep), 0.3 – 1.8% (62 and 66 cm deep), 0.3 – 2.5% (46 and 62 cm deep), 0.9 – 3.5% (62 and 66 cm deep) and 1.2% (50 cm deep) respectively, and mean average of 0.6, 1, 1.4, 2.2 and 1.2% correpondingly.

Brizalina sp occurs, with relative abundance 0.5 – 0.6 % at 46 and 62 cm deep correspondingly, with an average value of 0.6% and subsidiary species with low relative abundance (<1%) like *Buliminella elegantissima* are also present at 46 cm deep with 0.26%, with an average of 0.052%.

In Core D, nine of thirty-two species showed relative abundances > 5% in at least one analysed sample and twenty of thirty-two species showed relative abundances between 5% and 1% (Fig. 4.12 and Appendix 7).

Between 160 – 132 cm deep, species *Haynesina germanica* and *Ammonia tepida*, are the main species, with relative abundances 40.8 – 69.1 % (150 and 157 cm deep) and 19.7 – 42.2 % (160 and 150 cm deep), with average values of 57.4 and 29.4% correspondingly.

Quinqueloculina sp., *Rosalina bradyi, Planorbulina mediterranensis, Uvigerina peregrina*, and *Asterigerinata mamilla* are present, with low relative abundances of 0.3% (at 153 cm deep, with an average value of 0.03%), 0.4% (at 139 cm deep, mean value of 0.04%), 1.14 % (146 cm deep, average value of 0.1%), 0.31 % (at 143

cm deep, with an average of 0.03%), and 0.34 – 0.91 % (at 160, 132, cm and 157 cm deep correspondingly, mean value of 0.34%).

The *Elphidium* group is present with *Elphidium* sp. with relative abundance of 3 % (at 153 cm deep, with an average value of 0.3%), *Elphidium granosum* from 1 – 1.85 % (160 and 157 cm deep, with a mean value of 0.5%), *Elphidium oceanensis* from 1 – 3 % (160 and 146 cm deep, mean of 1.2%) and *Elphidium cuvillieri* from 0.3 – 2.66 % (160 and 146 cm deep, with an average of 1.2%).

Cassidulina laevigata, Textularia sp., *Fissurina* sp., *Bolivina ordinaria* and *Brizalina* sp. show relative abundances of 0.3 – 1,05 % (153 and 132 cm deep, average of 0.23%), 0.3 – 1.74 % (157 and 132 cm deep, mean value of 0.81%), 0.3 – 7% (157 and 136 cm deep, average value of 2.46%), 0.6 – 8.9 % (153 cm and 150 cm deep, with an average of 3.6%) and 0.6 – 4.4 % (143 and 139 cm deep, with as mean value of 1.6%) respectively.

Some accessory species like *Buliminella elegantissima* (0.31 – 0.73% at 157, 143 cm and 139 cm respectively, average of 0.2%), *Bulimina elongata* (0.3 – 0.6% at 153 and 136 cm deep, with an average of 0.1%), *Nonionella stella* (0.38 – 0.61% at 146 and 143 cm, with a mean value of 0.11%), *Quinqueloculina stelligera* (0.38 – 0.61% at 146 and 143 cm deep, with an average of 0.11%), *Spirillina vivipara* (0.31 – 0.6% at 143 and 143 cm deep, mean of 0.2%), *Stillostomella* sp.(0.3 – 0.35% at 153 and 132 cm deep, with an average of 0.07%) and *Cassidulina minuta* (0.31% at 157 cm deep, with a mean value of 0.03%) also occur between these depth, although with relative abundances <1%.

At 132 – 94 cm deep *Haynesina germanica* is the principal species with relative abundances ranging from 38 – 90% (118 and 104 cm depth, with an average of 77.5%), followed by *Ammonia tepida* (4.4 – 46.7% at 104 and 118 cm, with a mean value of 17%).

Quinqueloculina sp. (0.37 – 0.39% at 108 and 115 cm deep, with an average of 0.07%), *Quinqueloculina seminulum* (0.36% at 118 cm, with an average of 0.03%), *Rosalina bradyi* (0.36% at 118 cm, with a mean value of 0.03%) and *Asterigerinata mamilla* (0.37 – 0.46% at 108 and 94 cm deep, with an average of 0.11%) are also present.

Species *Elphidium* sp., *Elphidium granosum*, *Elphidium oceanensis* and *Elphidium cuvillieri* also occur among these depths, with relative abundances ranging

from 0.4 – 4% (115 and 101 cm deep, with an average of 0.5%), 0.45 – 2.5% (97 and 118 cm deep, with mean value of 0.4%), 0.45 – 4.35% (97 and 118 cm deep, with an average value of 0.8%) and 0.37 – 3% (108 and 118 cm, mean of 0.4%), respectively.

Bolivina ordinaria ranges from 0.37 – 3.24% at 129 and 94 cm deep (average of 0.7%), *Fissurina* sp. from 1.4 – 6% at 94 and 108 cm deep (average of 2.8%), *Adelosina* sp. with 0.36% at 118 cm (average of 0.03%) and *Oolina squamosa* with 0.45% at 97 cm (average value of 0.04%).

Between 90 – 98 cm depth *Haynesina germanica* and *Ammonia tepida* show relative abundances from 35 – 54 % (80 and 83 cm deep) and 31 – 51 % (90 and 80 cm deep) and average values of 45 and 39% respectively.

Species *Quinqueloculina* sp., *Rosalina bradyi*, *Planorbulina mediterranensis* show relative abundances ranging of 0.35% (at 80 cm, with an average value of 0.1%), and *Elphidium crispum* and *Asterigerinata mamilla* with 2.08% (at 83 cm deep and a mean value of 0.5%) and 0.35 – 2.08% (80 and 83 cm deep, with an average of 0.61%), respectively.

The *Elphidium* group is represented by *Elphidium* sp., *Elphidium granosum* and *Elphidium oceanensis* with relative abundances of 2.83% (at 80 cm deep, average of 0.7%), 4.24 – 8% (80 and 87 cm deep, with a mean value of 4.6%) and 4 – 13% (87 and 90 cm deep, mean of 4.7%) correspondingly.

Quinqueloculina seminulum and *Triloculina trigonula* show relative abundances ranging from 0.71 – 6.25% (80 and 90 cm deep, with an average of 1.74%) and 0.35% (at 80 cm deep, mean of 0.1%) respectively.

Fissurina sp., *Bolivina ordinaria* and *Brizalina* sp. are also present, with relative abundances of 8% (87 cm, mean of 2%), 1.06% (80 cm deep, average of 0.3%) and 0.35% (80 cm, average value of 0.1%), respectively.

At 80 – 69 cm deep *Ammonia tepida* and *Haynesina germanica* alter in dominance, once the first one has now higher relative abundances than the latter with 46 – 53.4% (69 and 76 cm deep) and 30 – 43.5 % (76 and 69 cm deep), with an average of 49 and 37 % respectively.

Species *Quinqueloculina* sp., *Rosalina bradyi, Planorbulina mediterranensis* and *Asterigerinata mamilla* show relative abundances of 1.7% (at 76 cm deep with an average of 0.57%), 0.65 – 1.37% (69 and 76 cm, with a mean value of 0.67%),

0.65% (at 69 cm deep, with an average of 0.2%) and 0.34 – 0.65% (76 and 69 cm deep, mean of 0.33%) respectively.

Quinqueloculina seminulum and *Triloculina trigonula* both show relative abundances of 1.7% at 73 cm deep (with an average value of 0.6).

Elphidium sp., *Elphidium granosum, Elphidium oceanensis* and *Elphidium cuvillieri* have relative abundances of 2% (76 cm deep, with an average of 0.7%), 1.7 – 2.7% (73 and 76 cm deep, mean value of 1.5%), 4.6 – 6.16% (69 and 76 cm deep, with an average of 5.2%) and 1.37 – 2.6% (76 and 69 cm deep, mean of 2%) correspondingly.

Fissurina sp. occurs with relative abundance of 0.65% at 69 cm deep (average value of 0.22%) and subsidiary species *Buliminella elegantissima* (0.34 – 0.41% at 76 and 73 cm deep, average of 0.3%), *Bulimina elongata* (0.65% at 69 cm deep, mean value of 0.2%), *Spirillina vivipara* (0.34% at 76 cm deep, average of 0.1%), *Lagena sulcata* (0.41% at 73 cm, mean value of 0.14%) and *Adelosina* sp. (0.41% at 73 cm deep, average of 0.14%) also occur between these depths.

In the depth interval of 69 – 27 cm species *Ammonia tepida* and *Haynesina germanica* remain the main ones, with relative abundances from 16.4 – 64% (62 and 55 cm deep, average value of 51.3%) and 15.3 – 82% (41 and 62 cm deep, mean of 34%) respectively.

Species *Quinqueloculina* sp. ranges from 0.3 – 1.7 % (38 and 27 cm deep, with an average of 0.4%), *Nonion fabum* from 0.3 – 1.2 (31 and 27 cm deep, with an average of 0.36%), *Rosalina bradyi* from 0.3 – 1.4% (34 and 38 cm deep, average of 0.34%), *Planorbulina mediterranensis* from 0.3 – 0.6% (38 and 41 cm deep, average of 0.2%), *Uvigerina peregrina* from 0.3 – 1.3% (34 and 48 cm deep, mean value of 0.26%), *Elphidium crispum* from 0.2 – 0.9% (45 and 34 cm deep, average of 0.22%), and *Asterigerinata mamilla* from 0.2 – 1% (45 and 52 cm deep, mean value of 0.24%).

Quinqueloculina seminulum and *Triloculina trigonula* show relative abundances from 0.2 -1.2% (45 and 41 cm deep, mean of 0.31%) and 0.3 % (31 cm deep, average value of 0.03%) correspondingly.

Elphidium sp. shows relative abundances between 0.7 – 4.7% (52 and 45 cm deep with an average of 1.4%), *Elphidium granosum* from 0.7 – 3.9% (55 and 48 cm deep, mean of 2%), *Elphidium oceanensis* from 0.5 – 9.5% (59 and 38 cm deep, average

value of 5%) and *Elphidium cuvillieri* from 0.3 – 9.8 % (48 and 55 cm deep, mean of 3%).

Species *Fissurina* sp., *Bolivina ordinaria* and *Brizalina* sp. show relative abundances of 2.8% (66 cm deep with an average of 0.24%), 0.3 – 1.5% (41 and 62 cm deep, mean value of 0.2%) and 0.3 – 1% (31 and 38 cm with an average of 0.2%) respectively.

Within these depths subsidiary species like *Cornuloculina* sp., *Quinqueloculina stelligera, Buliminella elegantissima, Bulimina elongata, Adelosina* sp, *Lagena sulcata, Elphidium complanatum* and *Stilostomella* sp. are also present, with relative abundances of 0.3% (41 cm deep, average of 0.02%), 0.34 – 0.6% (38 and 41 cm deep, mean value of 0.11%), 0.34 – 0.9% (38 and 59 cm deep, mean value of 0.1%), 0.36 – 0.47% (55 and 45 cm deep, average of 0.1%), 0.34 – 0.58% (38 and 27 cm deep, average value of 0.16%), 0.31% (34 cm depth with an average of 0.03%), 0.35 – 0.98% (52 and 48 cm deep, mean of 0.3%) and 0.34% (38 cm deep with an average of 0.1%) respectively).

For the surface samples, twelve samples had no foraminifera alive or dead, whereas for the remaining eight, twelve of thirty-five species showed relative abundances > 5% in at least one analyzed sample and thirty-one of thirty-five species showed relative abundances between 5% and 1% (Fig. 4.13 and Appendix 8).

In sample 10, collected at a temporary pond of a very dry marsh, in the boundary between the dune system and the marsh system, only species *Ammonia tepida* (50%), *Bolivina ordinaria* (25%) and *Haynesina germanica* (25%), were present.

Sample 11, taken next to Ventalengua's chenier, had *Haynesina germanica* and *Ammonia tepida* with equal relative abundance of 50%.

In Sample 12 , collected at a bubbling waterhole in a deserted marsh plain, had only two species, where *Elphidium* sp. was dominant (67%), followed by *Haynesina germanica* (33%).

Near the borders of Guadalquivir River, sample 15 show a more diverse assemblage, composed by *Haynesina germanica* (53%), *Ammonia tepida* (23.5%), *Bolivina ordinaria* (1.4%), *Quinqueloculina stelligera* (4.7%), *Asterigerinata mamilla* (2.3%), *Fissurina* sp. (1.2%), *Brizalina* sp. and *Miliammina fusca* (both with 1.2%), *Planorbulina mediterranensis, Nonion fabum, Elphidium cuvillieri, Elphidium*

granosum, and *Cassidulina minuta* from, all with relative abundances of 1.2%; and *Quinqueloculina* sp. with 4.7%.

Sample 16, collected by the channel “Caño de Brenes”, in the inter/infra tidal zone of Guadalquivir river had relative abundances of 2.3% for *Trochammina inflata* and 65%, 5.6% and 5% for *Ammonia tepida, Bolivina ordinaria* and *Haynesia germanica*, respectively. Species *Quinqueloculina stelligera* and *Fissurina* sp. also occur, with 2.3 and 0.75% correspondingly; as well as *Miliammina fusca* (5.7%), *Textularia* sp., *Hopkinsina atlantica* and *Brizalina* sp. with 2.3%, *Nonionella stella* (1.5%), *Ammotium* sp. and *Stilostomella* sp. both with 0.75%. Rosalina bradyi and Q*uinqueloculina* sp. are also present with 0.4% of relative abundance, along with subsidiary species *Elphidium* sp. (2%), and *Buliminella elegantissima*, *Cassidulina laevigata* and *Cornuspira involvens* with 0.4%.

In sample 17, at a temporary pond, species *Trochammina inflata* and *Jadammina macrescens* are dominant, with 68 and 18% respectively, along with *Haynesina germanica* (1.3%).

At the margin of the channel “Caño del Buen Tiro”, sample 18 presented *Trochammina inflata* with relative abundance of 9%; *Haynesina germanica, Ammonia tepida* and *Bolivina ordinaria* with 24, 21 and 6% respectively, as well as *Fissurina* sp. (12%), *Quinqueloculina stelligera* and *Quinqueloculina laevigata* (both with 9%), *Cornuloculina* sp. (6%) and *Asterigerinata mamilla* (3%).

At the beach, sample 20 were collected, with species *Ammonia beccarii* being the most dominant form with 33.2%. Ammonia tepida, *Haynesina germanica* and *Bolivina ordinaria* showed relative abundances of 25.6, 6.2 and 0.4% respectively; *Quinqueloculina* sp. of 12%, *Quinqueloculina stelligera of* 4.4%, *Asterigerinata mamilla* of 0.4%, *Brizalina* sp. of 1%, *Elphidium crispum* of 4.4%, *Rosalina bradyi* of 3%, *Quinqueloculina seminulum* of 2.6%, *Elphidium complanatum* of 1.3%, *Bulimina elongata*, *Elphidium cuvillieri* and *Planorbulina mediterranensis* all with 1%, *Elphidium granosum* and *Nonion fabum* both with 0.4%. Species *Lagena* sp. and *Stilostomella* sp. also appear in this sample, as a subsidiary species (both with 0.4%).

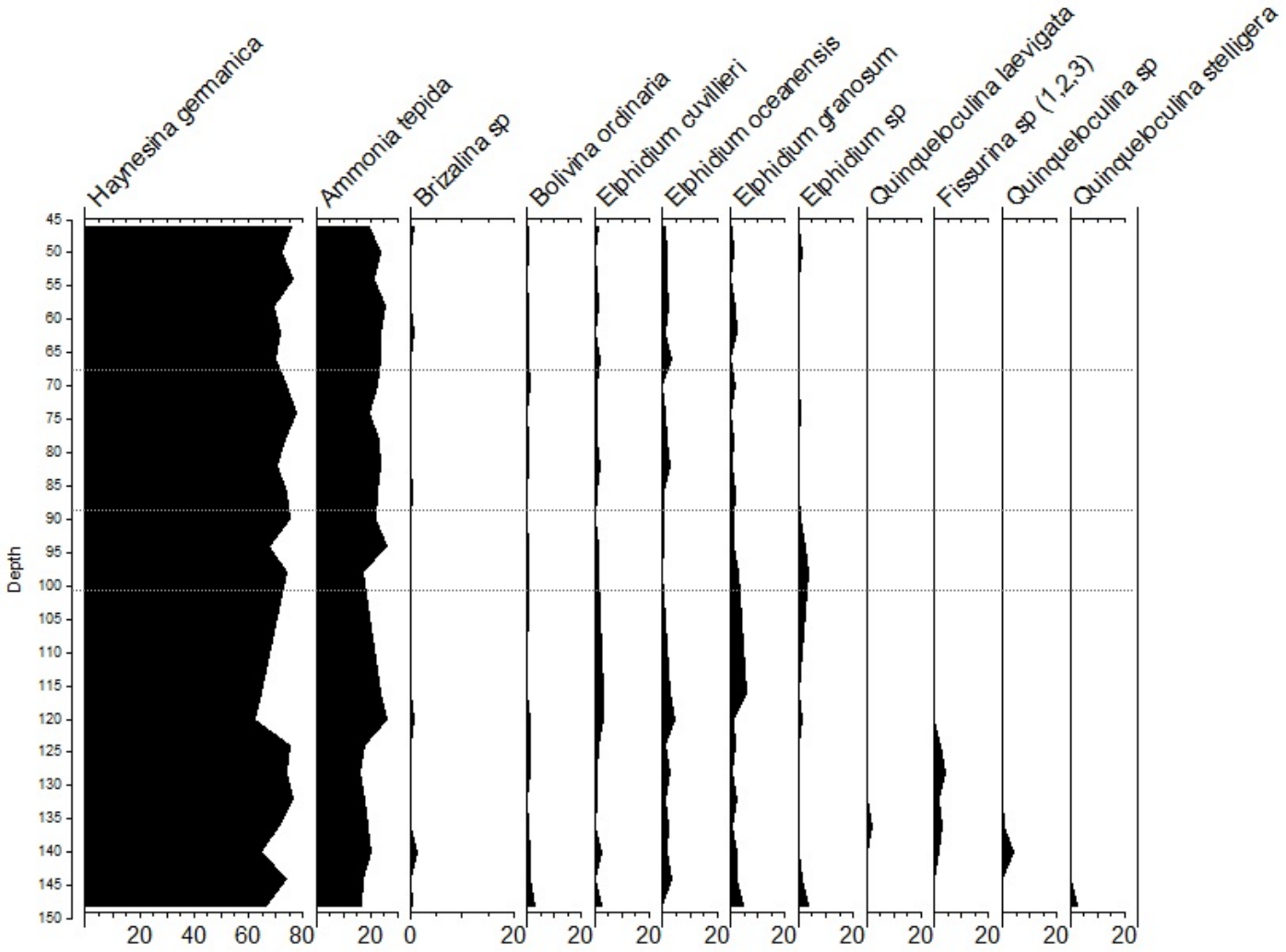

Figure 4.11 - Relative abundances of species with abundance >1% in Core C, depth in cm, made in Tilia software. See description in text for horizontal dashed lines

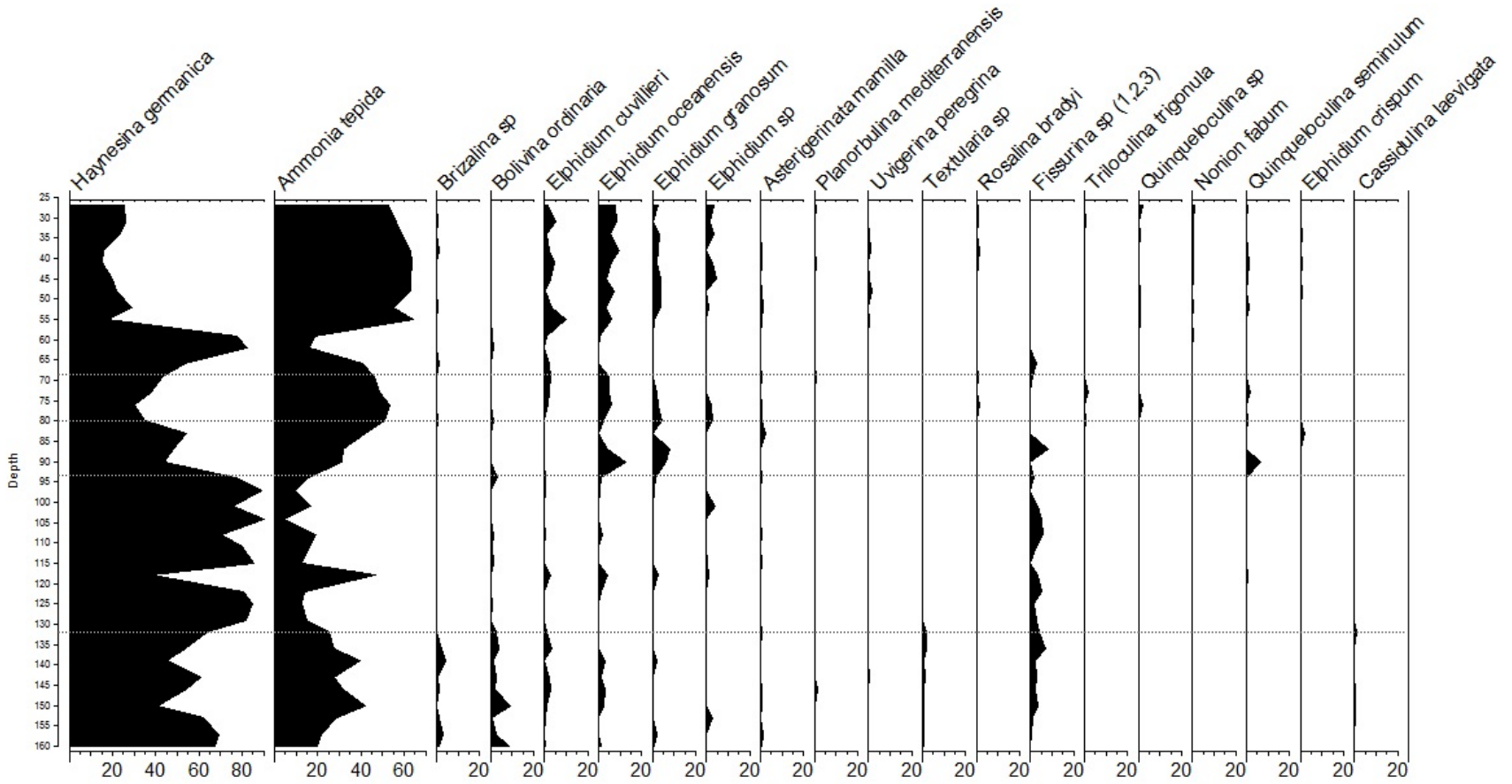

Figure 4.12 - Relative abundances of species with abundance >1% in Core D, depth in cm, made in Tilia software. See description in text for horizontal dashed lines

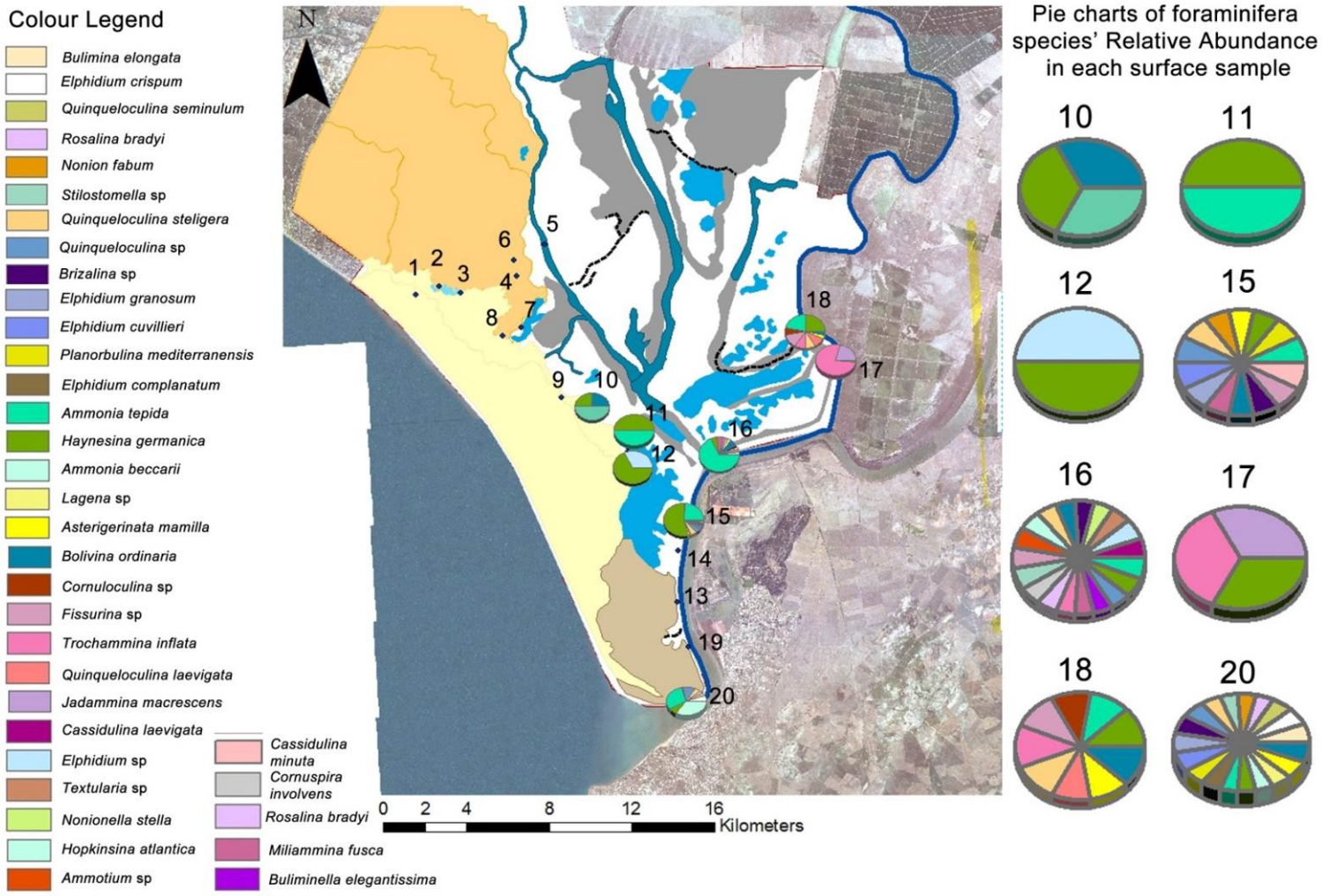

Figure 4.13 - Relative abundances of species with abundance >1% in surface samples, made in ArcGIS

4.2 - Faunistic density

The highest and lowest values obtained in Core C were 738 and 122 specimens/g, both in silty clayey sediments and at 86 cm depth, respectively (Fig. 4.14). For Core D the highest value obtained was 879 specimens/g at 31 cm depth in bioclastic sediments, whereas the lowest was 1 specimens/1 g at 90 m depth, in bioclastic sediments (Fig. 4.14).

Population density averaged 345 specimens/g in Core C and 244 specimens/g in Core D.

For the surface samples, the highest value (87 specimens/g) was obtained in sample 17 and the lowest value (3 specimens/g) in sample 18, both in silty clayey sediments.

The Faunistic density values are presented in Appendixes 3, 4 and 5 for Core C, D and surface samples, respectively.

The planktonic/benthic foraminifera ratio showed its highest value (2.2) at 150 cm depth in Core D, with values near 1 from 132 cm to the base of the core, with a sediment composition of bioclastic sediments. The lowest value of this ratio for Core D (0.03) was obtained at 104 cm depth in silty sediments.

Core C had lower values of this ratio than Core D, where the highest value (0.71) was obtained at 144 cm depth and the lowest (0.05) at 46 cm depth, both in silty clayey sediments.

Only six of the twenty surface samples had data to calculate the planktonic/benthic ratio, having the highest values, namely 6, 5 and 2.25, in samples 18, 15 and 16 respectively. Samples 11, 17 and 20 showed low values of this ratio, with 0.25, 0.01 and 0.6 respectively (Fig. 4.15).

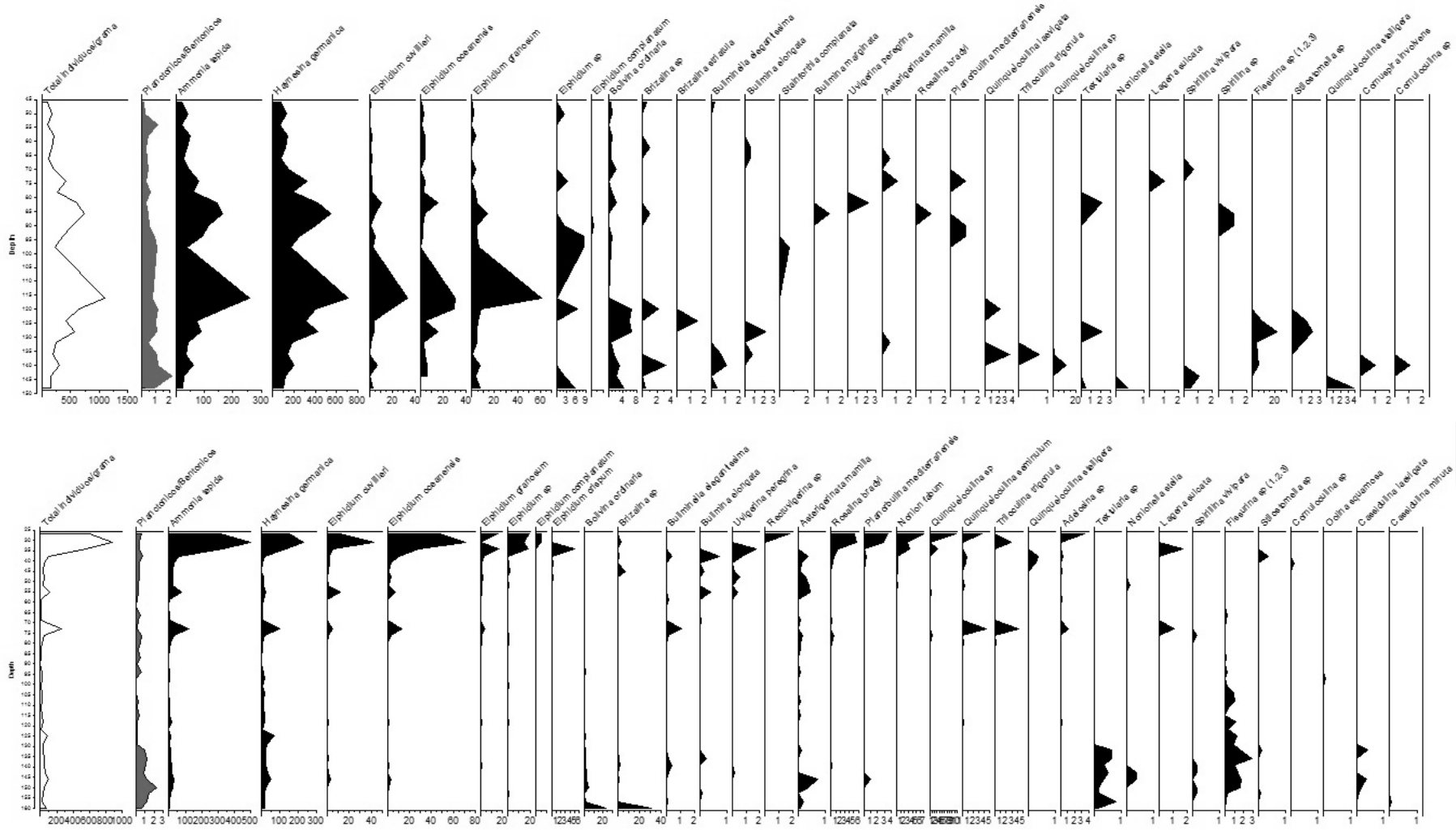

Figure 4.14 - Total individuals per gram found in each sample, planktonic/benthic ratio and faunistic Density (Ni/1g) for all species in Cores C (above) and D (below), depth in cm. Made in Tilia software

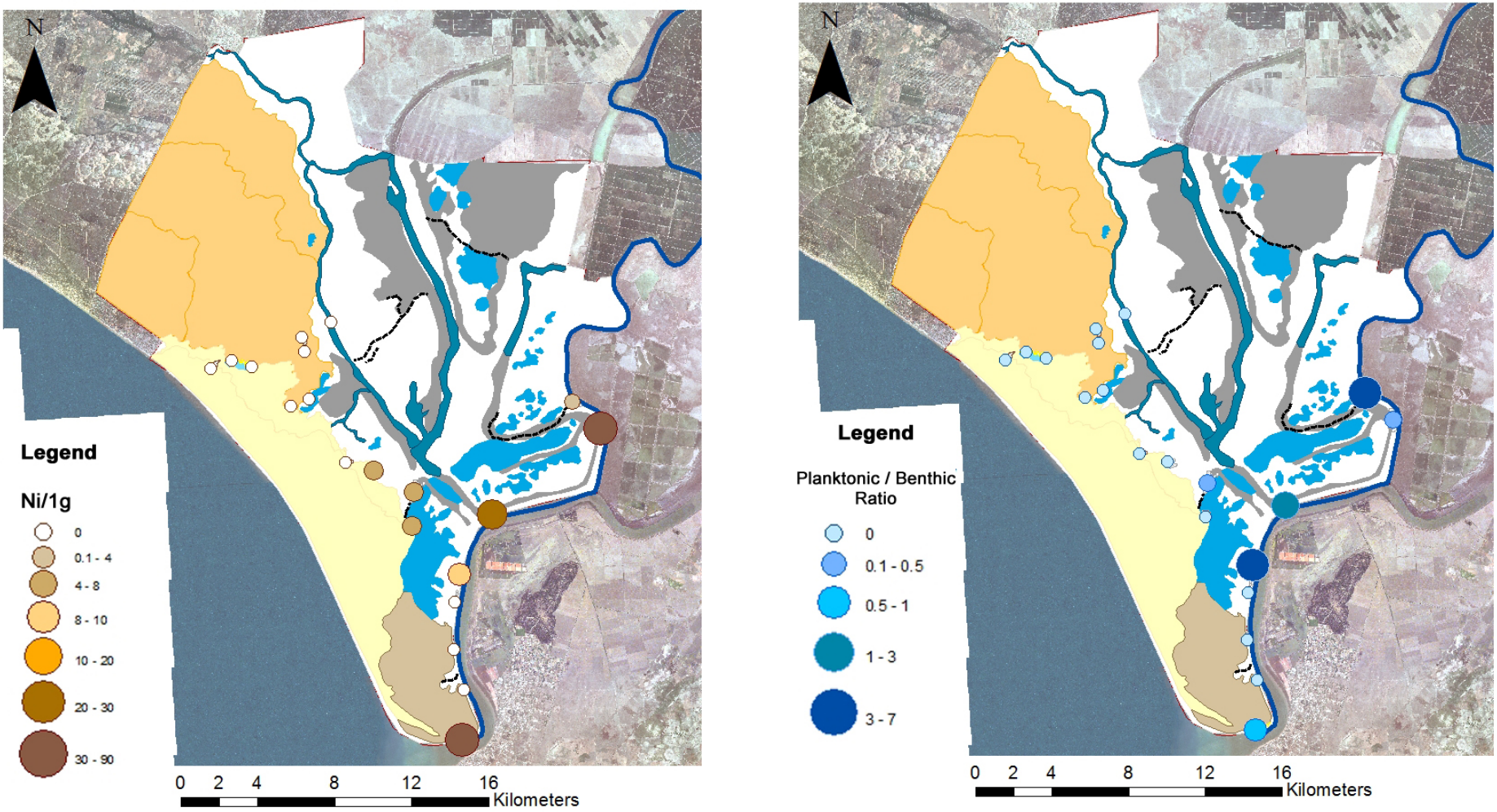

Figure 4.15 - Faunistic Density of total individuals per sample (Ni/1g) for surface samples (left) and planktonic/benthic ratio (right). Made in ArcGIS software

4.3 - Diversity

The Shannon index (H) ranges between 0.65 (54 cm depth) and 1.24 (148 - 150 cm depth), with an average value of 8.86 in Core C (Fig. 4.16) and between 0.41 (104 cm depth) and 1.48 (27 cm depth), with an average value of 1 in Core D (Fig. 4.17). For surface samples the highest values of the Shannon index are obtained in samples 18 and 20 (2.02 and 2.01, respectively), whereas the lowest value is found in sample 17 (0.58) (Fig. 4.18). Surface samples 10, 11, 12, 15 and 16 had values of this index of 1.04, 0.69, 0.64, 1.53 and 1.55 respectively (Fig. 4.18).

The Equitability (J) index ranges from 0.31 (90 cm depth) and 0.49 (120 cm depth), with an average value of 0.42 in Core C (Fig. 4.16) and between 0.24 (97 cm depth) and 0.83 (90 cm depth), with an average value of 0.49 in Core D (Fig. 4.17). For surface samples this index had values higher than 0.5 in all samples, where sample 11 has the highest value (1) and samples 16 and 17 the lowest value (0.53) (Fig. 4.18). Samples 10, 12, 15, 18 and 20 had values of this index of 0.95, 0.92, 0.58, 0.92 and 0.67 respectively (Fig. 4.18).

As for Species richness (S), the maximum and minimum values obtained were 12 and 5 species, respectively for Core C and 18 and 3 for Core D (Figs. 4.16 and 4.17 respectively). The average value was 8 species for Core C and 9 for Core D. The highest values of species richness are obtained in surface samples 20 and 16, with 20 and 19 species respectively (Fig. 4.19). Surface sample 18 had 14 species, samples 10 and 17 had 3 species and samples 11 and 12 had 2 species (Fig. 4.19).

The Alpha-Fisher index ranges from 0.81 (116 cm depth) and 2.64 (148 cm depth), with an average value of 1.5 in Core C (Fig. 4.16) and between 0.65 (62 cm depth) and 4.2 (38 cm depth), with an average value of 2 in Core D (Fig. 4.17). The highest values of this index is obtained in surface sample 20 (5.31), followed by samples 15, 16 and 18 (4.8, 4.65 and 4.07 respectively). The remaining surface samples showed lower values of the Alpha-Fisher index with values of 0.65, 0.47, 0.42 and 0.39 for samples 10, 17, 12 and 11 respectively (Fig. 4.19).

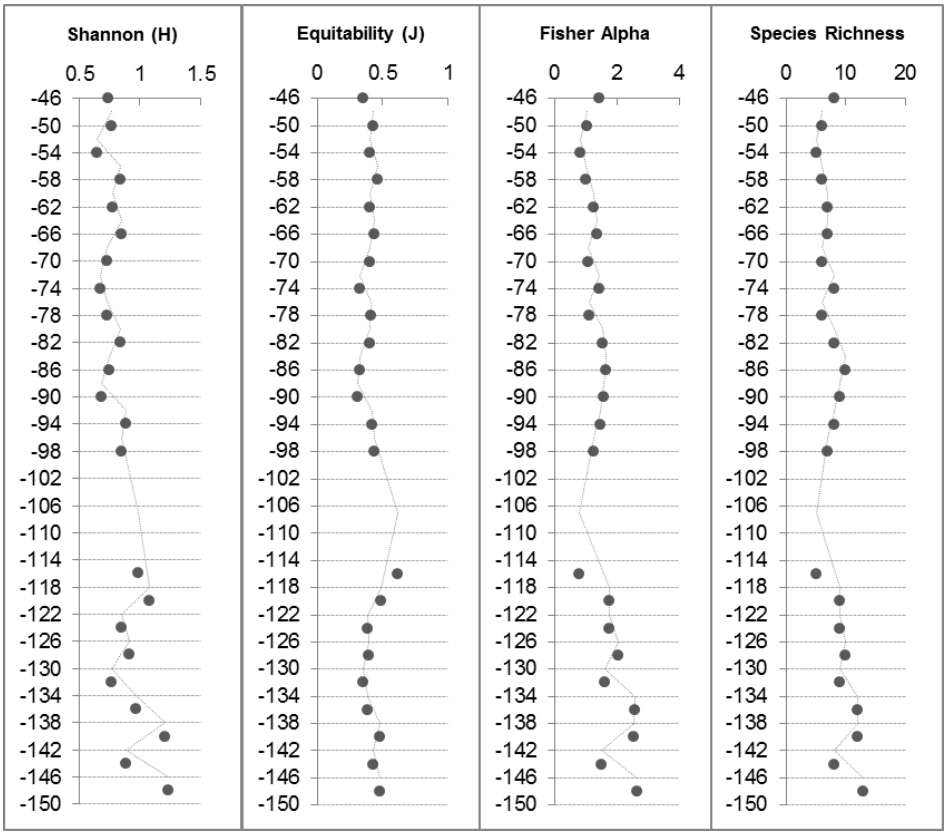

Figure 4.16 - Diversity indexes (Shannon Weaver, Equitability, Fisher alpha and Species richness) results for core C, depth in cm. Calculated in Past software and represented in Microsoft Exel

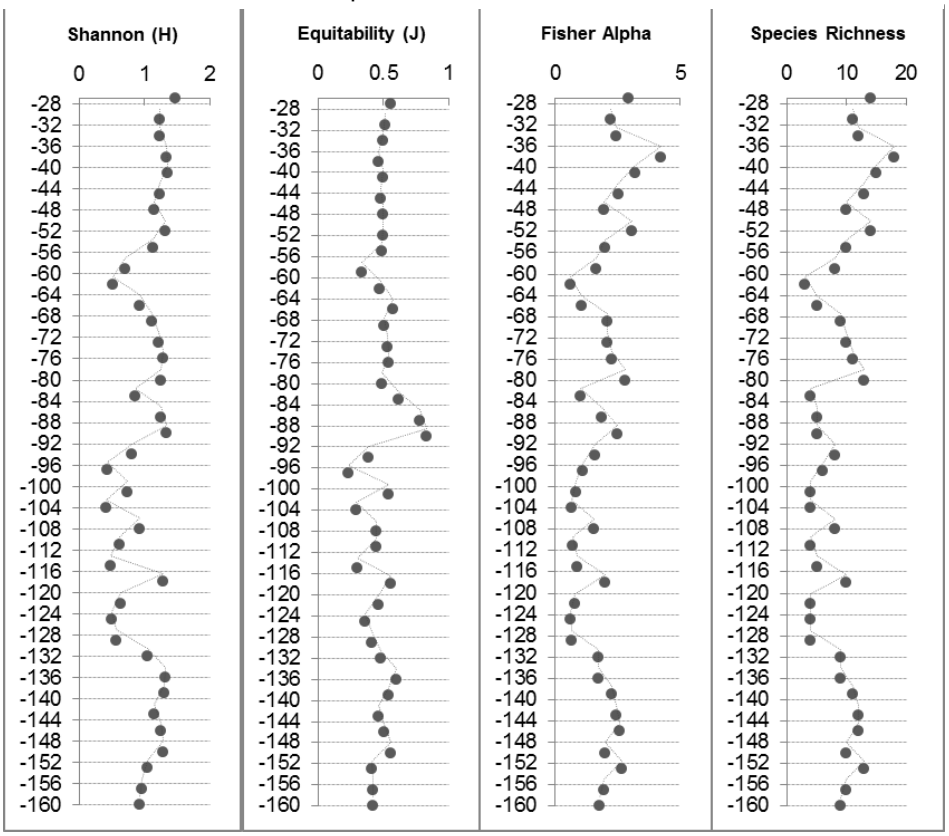

Figure 4.17 - Diversity indexes (Shannon Weaver, Equitability, Fisher alpha and Species richness) results for core D, depth in cm. Calculated in Past software and represented in Microsoft Exel

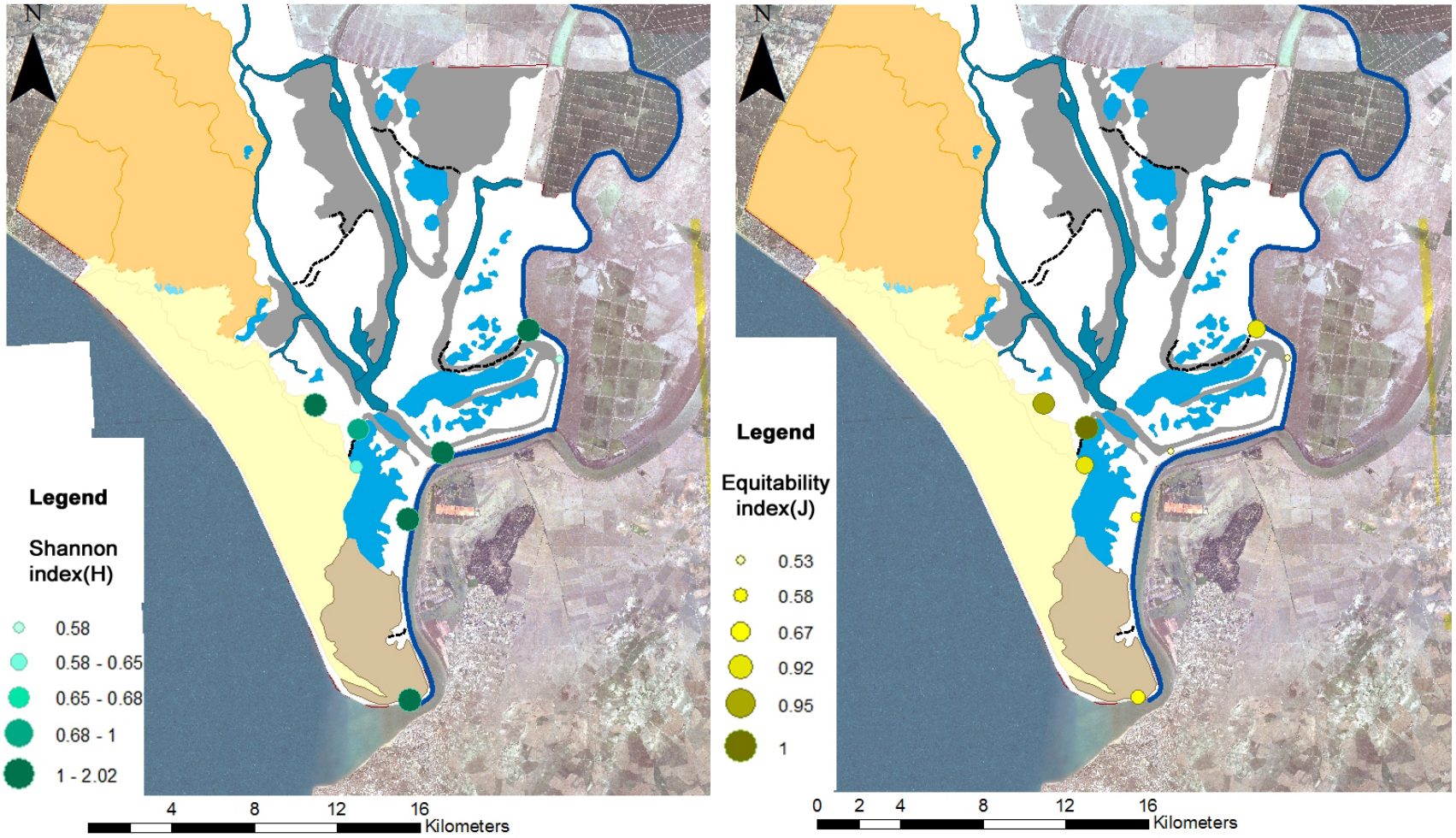

Figure 4.18 - Shannon Weaver (left) and Equitability (right) indexes results for surface samples. Made in ArcGIS software

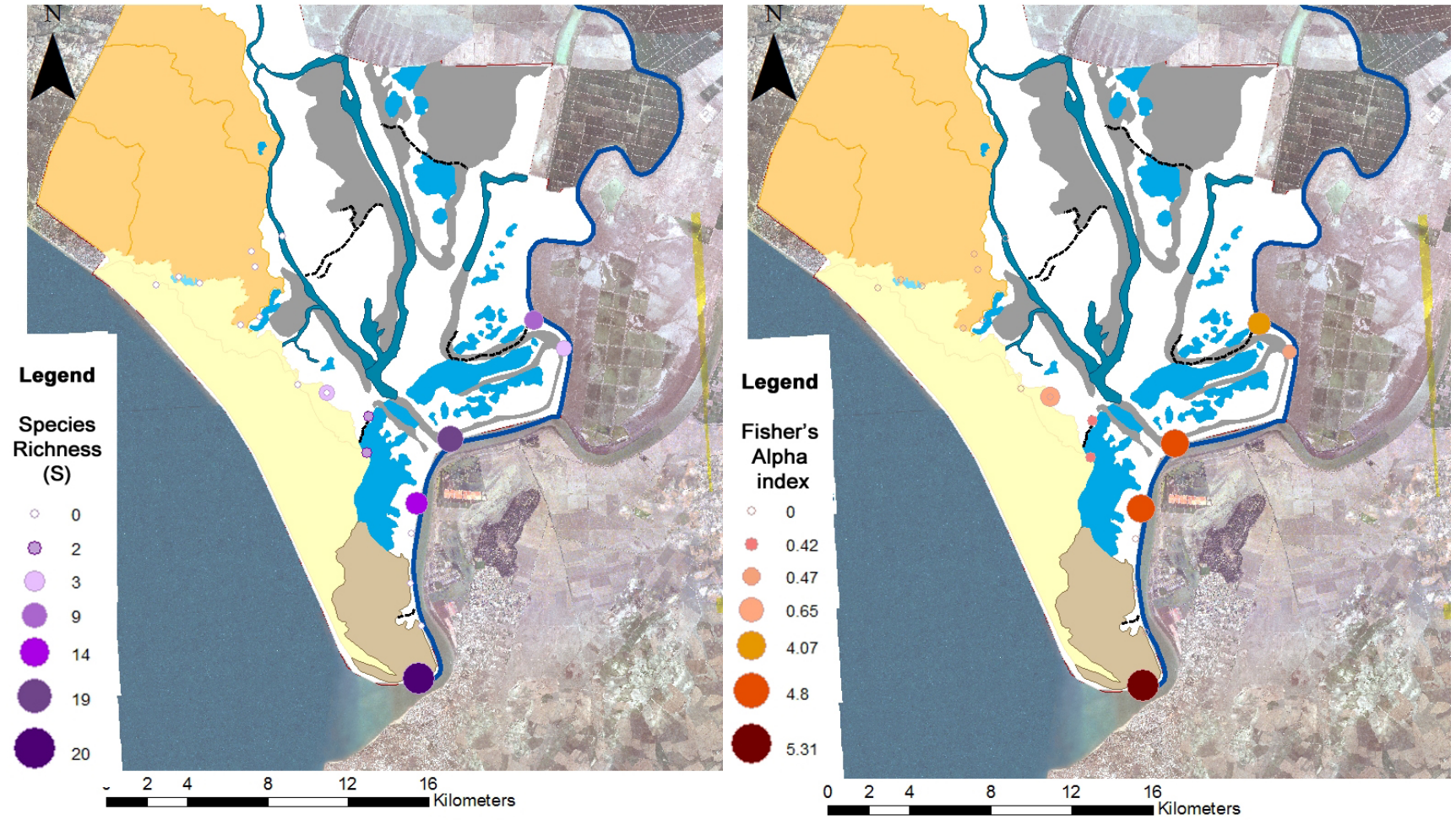

Figure 4.19 - Species richness (left) and Fisher's Alpha (right) indexes results for surface samples. Made in ArcGIS software

5. Multivariate Analysis

The multivariate analyses were undergone considering 4 species for Core C and 9 species for Core D, with relative abundances higher than 5% in at least one sample for Q-Mode and 12 species for Core C and 20 species for Core D with relative abundances higher than 1% in at least one sample for R-Mode. As for surface samples, due to the low number of individuals in almost every sample, the multivariate analyses considered 2 species for samples 11 and 12, 3 species for samples 10 and 17, 9 species for sample 18, 14 species for sample 15, 16 species for sample 16 and 18 species for sample 20, with relative abundances higher than 1% for both Q and R-Modes (Appendixes 6, 7 and 8 for Core C, D and surface samples, respectively)

The Q-mode cluster analysis for Core C, using a paired group algorithm, Bray-Curtis similarity measure and cophenetic correlation of 0.94, with a cut-off at a similarity of 0.92, resulted on a dendogram where two main clusters or assemblages can be recognized (Fig. 4.20a). Cluster I comprises eight samples, where *Haynesina germanica* (63 – 70 %) and *Ammonia tepida* (17 – 26%) are the most abundant species, accompanied by an *Elphidium* spp association (*Elphidium granosum, Elphidium cuvillieri and Elphidium oceanensis*) (1 – 5 %), *Bolivina ordinaria* (1 – 2 %) and 1 to 7 accessory species (~1%). Cluster II comprises fourteen samples, where again Haynesina germanica and Ammonia tepida are the main species, although with higher abundance values for the first one than in Cluster I, with 71 – 77 % and 16 – 23 % respectively. The *Elphidium* spp association (*Elphidium granosum, Elphidium cuvillieri and Elphidium oceanensis*) (1 – 2 %), *Bolivina ordinaria* and some accessory species are also present (~1%). The sample at 62 cm depth resulted as an outlier, although species *Haynesina germanica* (72%) and *Ammonia tepida* (22%) are the most abundant species, and *Bolivina ordinaria* with some accessory species also present.

The R-mode cluster analysis for Core C, using a paired group algorithm, Bray-Curtis similarity measure and cophenetic correlation of 0.88, with a cut-off at a similarity of 0.13, produced a dendrogram that allowed the differentiation of three assemblages or clusters (Fig. 4.20b): Cluster I with the species *Haynesina germanica* and *Ammonia tepida*; Cluster II with *Quinqueloculina stelligera, Elphidium* sp, *Elphidium granosum, Elphidium oceanensis, Elphidium cuvillieri* and *Bolivina*

ordinaria; and Cluster III with *Fissurina* sp, *Quinqueloculina laevigata, Quinqueloculina* sp and *Brizalina* sp..

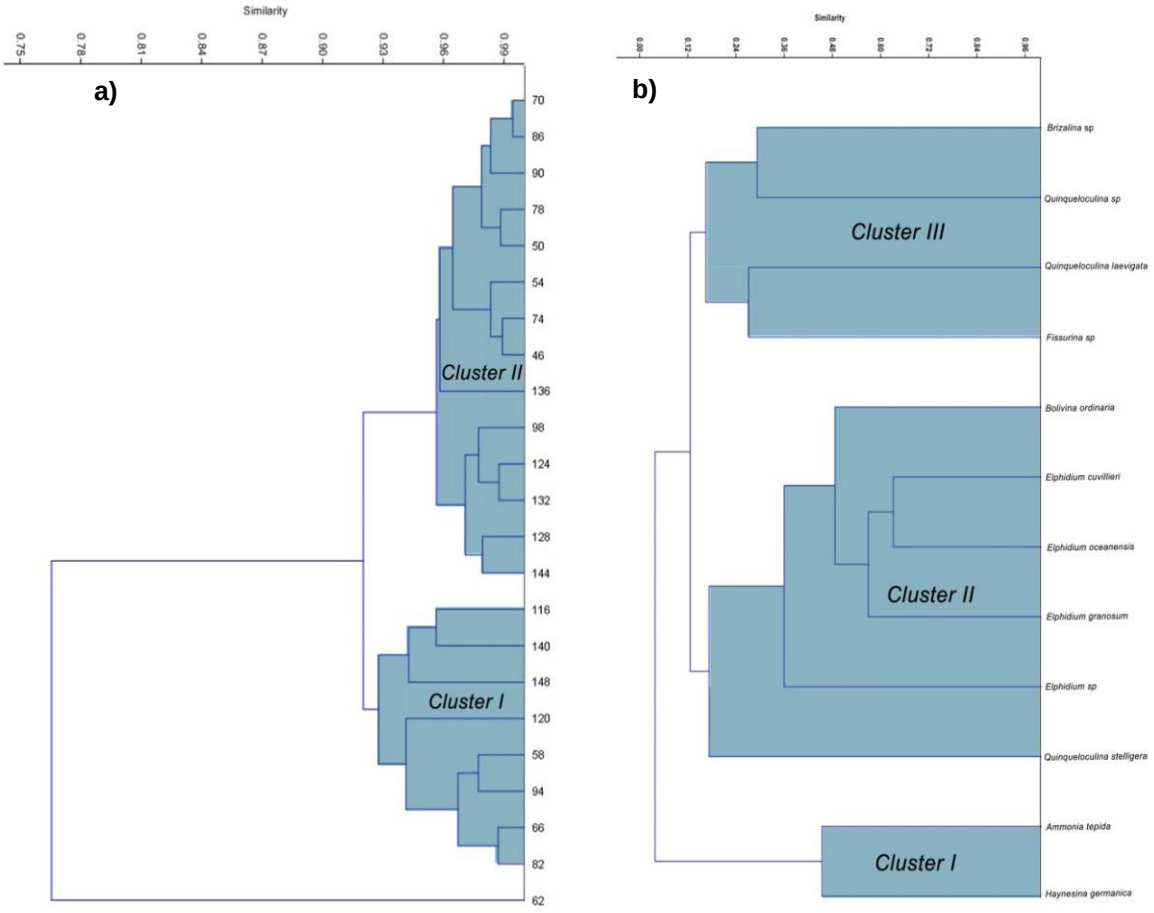

Figure 4.20 - Core C's Cluster analyses. a) Dendogram resulting from Q-mode analyses (Bray Curtis similarity) based on 4 species with total abundance >5%; b) Dendogram resulting from R-mode analyses (Bray Curtis similarity) based on 12 species with total abundance >1%;

The Q-mode cluster analysis for Core D, using a paired group algorithm, Bray-Curtis similarity measure and cophenetic correlation of 0.78, with a cut-off at a similarity of 0.76, produced a dendrogram that allowed the differentiation of three assemblages or clusters (Fig. 4.21a): Cluster I comprises eighteen samples, divided in 2 sub-clusters a) and b), comprising 5 and 14 samples respectively; in sub-cluster a) *Haynesina germanica* (53 – 64%) and *Ammonia tepida* (28 – 32%) are the most abundant species, along with *Fissurina* sp (2 – 7%), whereas in sub-cluster b) there is an increase of the relative abundance of *Haynesina germanica* (67 – 90%) and a decrease of *Ammonia tepida* (9 – 20%), both still being the most abundant species. Cluster II comprises ten samples in which *Ammonia tepida* (52 – 63%) and

Haynesina germanica (15 - 30%) are the most abundant species, followed by the *Elphidium* spp group (*Elphidium oceanensis, Elphidium cuvillieri and Elphidium granosum*) (1 – 10%). As for Cluster III it also comprises ten samples, where *Haynesina germanica* and *Ammonia tepida* have very similar relative abundances (33 – 54% and 31 - 51%, respectively), along with the *Elphidium* spp group (*Elphidum oceanensis, Elphidiu granosum, Elphidium cuvillieri*) (1 – 13%).

The R-mode cluster analysis for Core D, using a paired group algorithm, Bray-Curtis similarity measure and cophenetic correlation of 0.83, with a cut-off at a similarity of 0.15, produced a dendrogram that allowed the differentiation of five assemblages or clusters (Fig. 4.21b): Cluster I with the species *Haynesina germanica* and *Ammonia tepida*; Cluster II with *Quinqueloculina* sp*, Nonion fabum, Rosalina bradyi, Planorbulina mediterranensis, Uvigerina peregrina, Elphidium crispum and Asterigerinata mamilla*; Cluster III with *Quinqueloculina seminulum* and *Triloculina trigonula*; Cluster IV with *Elphidium* sp, *Elphidium granosum, Elphidium oceanensis* and *Elphidium cuvillieri*; and Cluster V with *Cassidulina laevigata, Textularia* sp, *Fissurina* sp, *Bolivina ordinaria* and *Brizalina* sp..

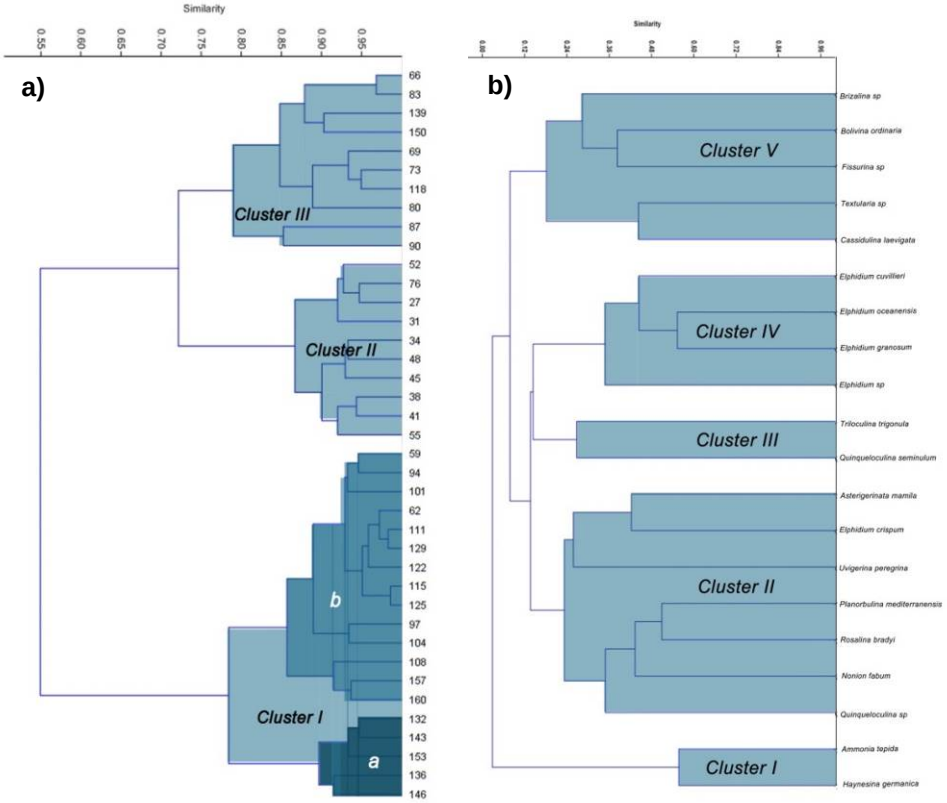

Figure 4.21 - Core D's Cluster analyses. a) Dendogram resulting from Q-mode analyses (Bray Curtis similarity) based on 9 species with total abundance >5%; b) Dendogram resulting from R-mode analyses (Bray Curtis similarity) based on 20 species with total abundance >1%;

The Q-mode cluster analysis for surface samples, using a paired group algorithm, Bray-Curtis similarity measure and cophenetic correlation of 0.89, with a cut-off at a similarity of 0.48, produced a dendrogram that allowed the differentiation of one assemblage or cluster (Fig. 4.22a): Cluster I comprises four surface samples (18, 10, 11 and 15) once these had the lowest values of the species' faunistic density (3.3, 6.4, 6.6 and 8.5 individuals/g respectively). In sample 18 *Haynesina germanica* (24%) and *Ammonia tepida* (21%) are the most abundant species, accompanied by *Fissurina sp* (11%), *Trochammina inflata* and *Quinqueloculina* spp (9%), *Bolivina ordinaria* (6%) and two accessory species. Sample 10 has *Ammonia tepida* (50%) as the main species, along with *Haynesina germanica* and *Bolivina ordinaria* (25%). Sample 11 is represented equally by *Haynesina germanica* and *Ammonia tepida*, both with 50% relative abundance. In sample 15, *Haynesina germanica* (53%) is the most abundant specie, followed by *Ammonia tepida* (24%), *Bolivina ordinaria* (2%) and eleven accessory species with very low relative abundances. Surface samples 20, 16 and 17 resulted as outliers, once these had the higher values of species' faunistic density (52, 88 and 27 individuals/g, respectively), although very different between them. In surface sample 20 *Ammonia beccarii* (33%) is the most abundant specie, along with *Ammonia tepida* (26%), *Quinqueloculina* spp (12%), *Haynesina germanica* (6%) and fifteen accessory species. Sample 16 had *Ammonia tepida* (65%) as the main species, accompanied by *Bolivina ordinaria* and *Miliammina fusca* (6%), *Haynesina germanica* (5%) and fifteen accessory species with low values of relative abundance. Sample 17 is dominated by *Trochammina inflata* (78%), *Jadammina macrescens* (21%) and *Haynesina germanica* (2%). Surface sample 12 is also considered an outlier, once although its value of faunistic density is low (4.8 individuals/g) along with samples 18, 10, 11 and 15, its benthic foraminifera assemblage is very distinct, with only two species, *Haynesina germanica* (67%) and *Elphidium* sp (33%).

The R-mode cluster analysis for surface samples, using a paired group algorithm, Bray-Curtis similarity measure and cophenetic correlation of 0.86, with a cut-off at a similarity of 0.24, produced a dendrogram that allowed the differentiation of six assemblages or clusters (Fig. 4.22b): Cluster I with the species *Jadammina macrescens* and *Trochammina inflata*; Cluster II with the species *Bolivina ordinaria*, Haynesina germanica and Ammonia tepida; Cluster III with Asterigerinata mamilla,

Fissurina sp, *Quinqueloculina laevigata*, *Cornuloculina* sp and *Quinqueloculina stelligera*; Cluster IV with *Milliamina fusca, Nonionella stella, Hopkinsina atlantica, Textularia* sp, *Brizalina* sp, *Ammotium* sp and *Stilostomella* sp; Cluster V with the species *Cassidulina minuta, Planorbulina mediterranensis, Elphidium cuvillieri, Elphidium granosum, Nonion fabum, Elphidium crispum, Rosalina bradyi, Quinqueloculina seminulum, Bulimina elongata* and *Elphidium complanatum*; Cluster VI with *Ammonia beccarii* and *Quinqueloculina* sp; and *Elphidium* sp as an outlier.

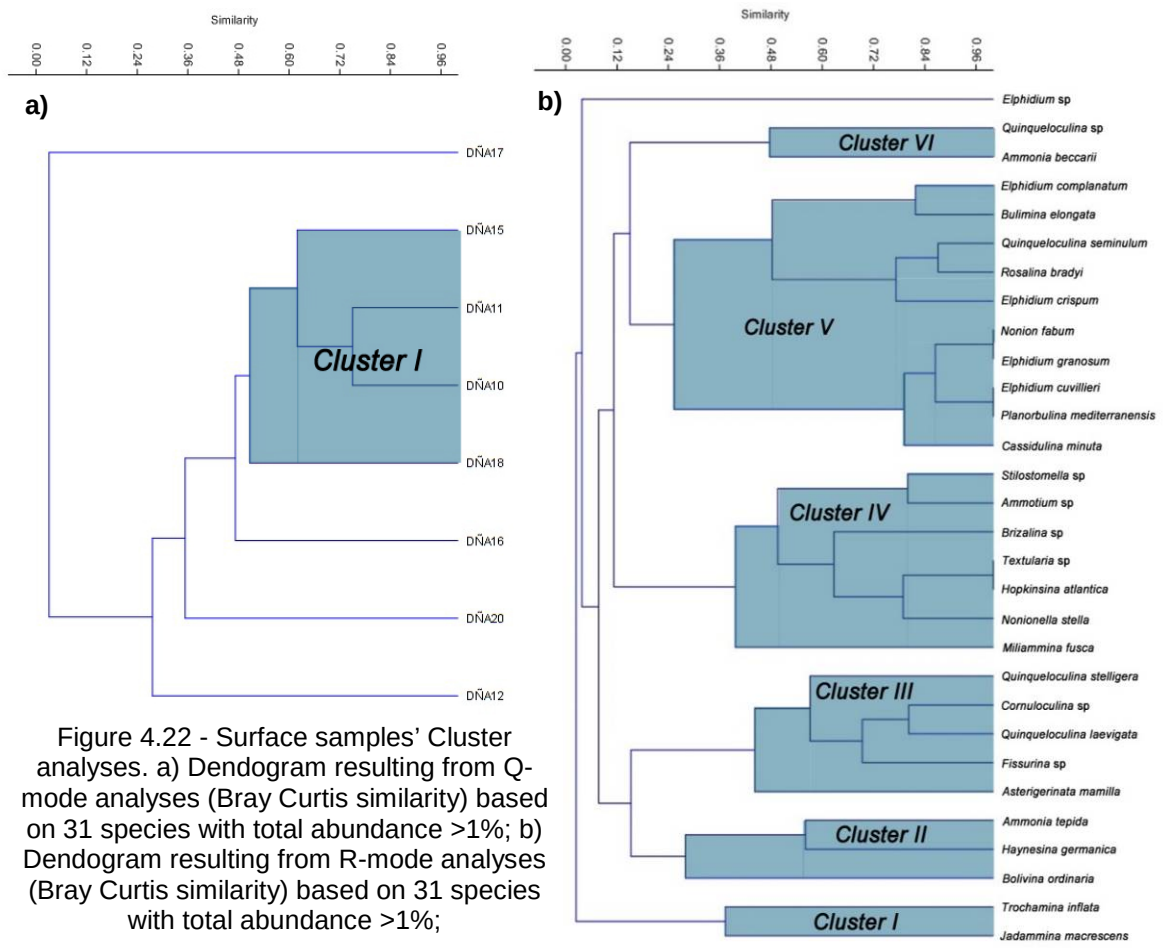

Figure 4.22 - Surface samples' Cluster analyses. a) Dendogram resulting from Q-mode analyses (Bray Curtis similarity) based on 31 species with total abundance >1%; b) Dendogram resulting from R-mode analyses (Bray Curtis similarity) based on 31 species with total abundance >1%;

The Canonical Correspondence Analysis (CCA) for abiotic parameters (Fig. 4.23) shows only a clear relation between organic matter (OM) and water percentage, and none between the others, probably due to an outlier, that could have hidden these relations.

As for the CCA between abiotic parameters and biotic parameters of the surface samples, the first two axes explain 91% of the relations, where Axis 1 is influenced positively by the abiotic parameters Eh, temperature, pH and organic matter (OM)

and negatively influenced by conductivity, whereas Axis 2 is positively influenced by Eh and negatively by temperature, pH, organic matter and water percentage (Fig. 4.24). Eh, organic matter and water percentage seem to be independent of temperature, pH and type of sediment.

This analysis shows that sample 12 is greatly influenced by water and organic matter percentage; sample 4 by water percentage; and samples 9, 17 and 12 by organic matter, with extreme values.

In general, samples show low variance between them, no clear relation between abiotic parameters and the presence of foraminifera is observed, and no factor was identified as responsible for the presence of individuals.

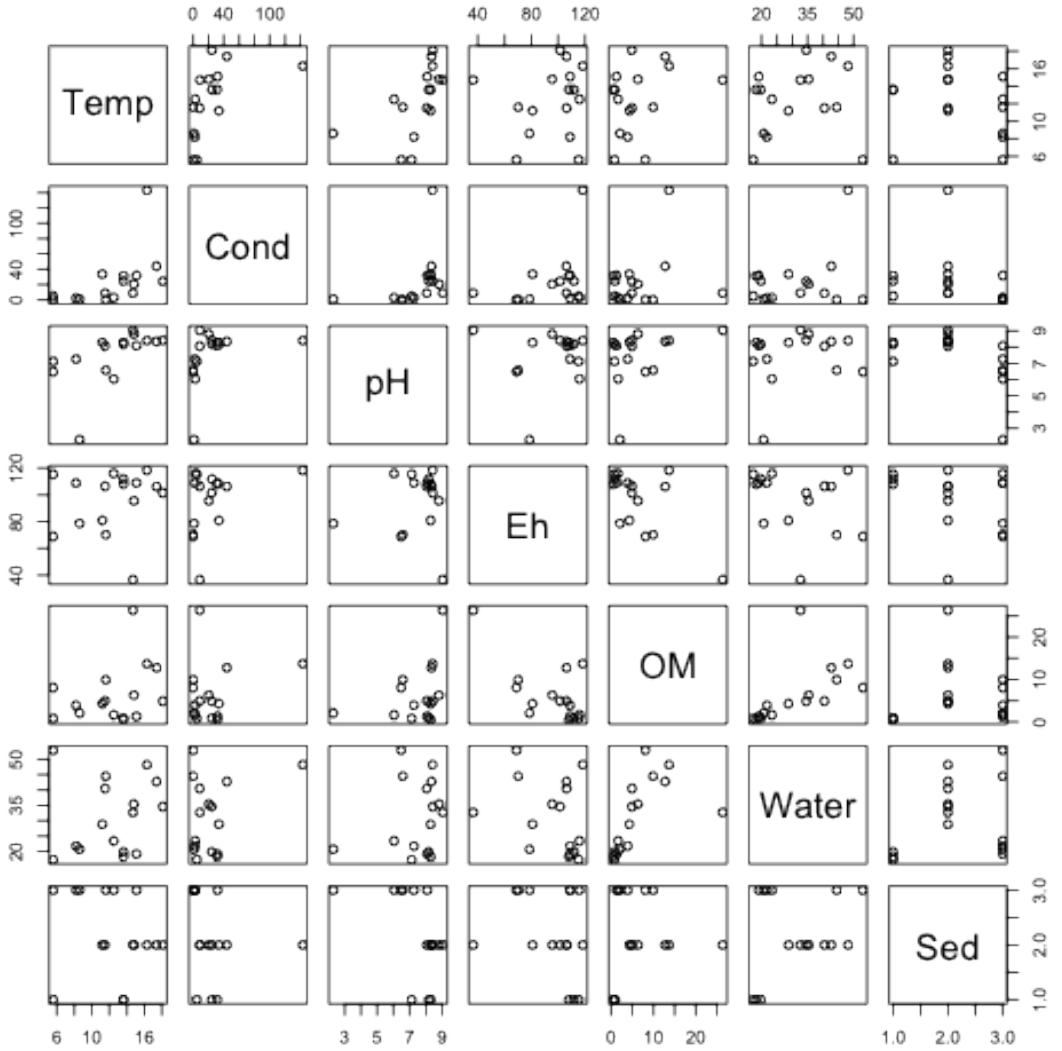

Figure 4.23 - CCA between surface samples' abiotic parameters. Made in Rexel

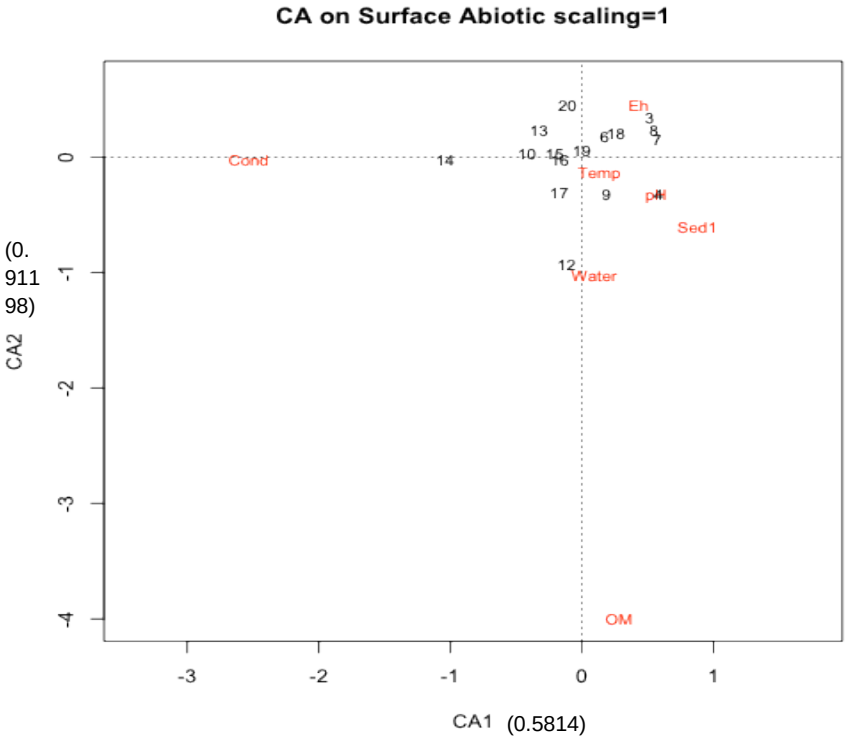

Figure 4.24 - CCA between surface samples' abiotic and biotic parameters, where Cond is conductivity, Temp is temperature, Sed1 is the type of sediment and OM the organic matter percentage. Made in Rexel.

To check if any abiotic parameters were influencing the diversity indexes, a CCA was also made (Fig. 4.25). Results show that water percentage has a positive relation with Shannon and Fisher's Alpha indexes and a negative relation with Species richness. The organic matter percentage shows a relation with Equitability index.

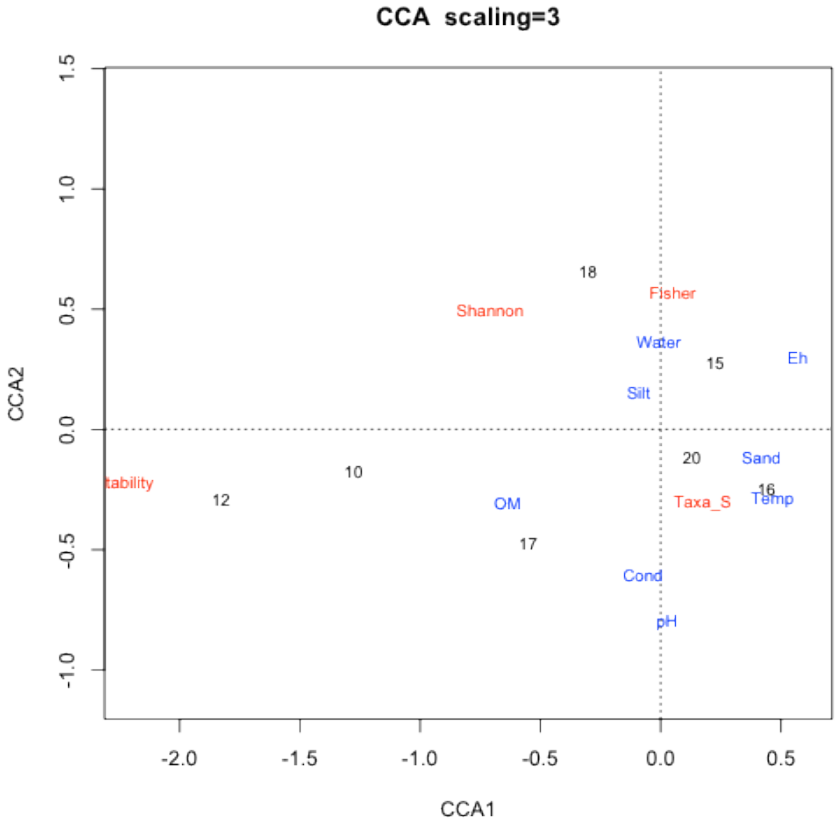

Figure 4.25 - CCA between surface samples' abiotic and biotic parameters, and diversity indexes. where Cond is conductivity, Temp is temperature, Sed1 is the type of sediment and OM the organic matter percentage. Made in Rexel.

As for the cores, the CCA shows a relation between Fisher's Alpha and Species richness indexes, and there seems to be a tendency between Equitability and Shannon indexes (two groups with two different relations) (Fig. 4.26).

The CCA between abiotic parameters and the Core's Samples show no evident relation, once these are very similar among them (Fig. 4.27).

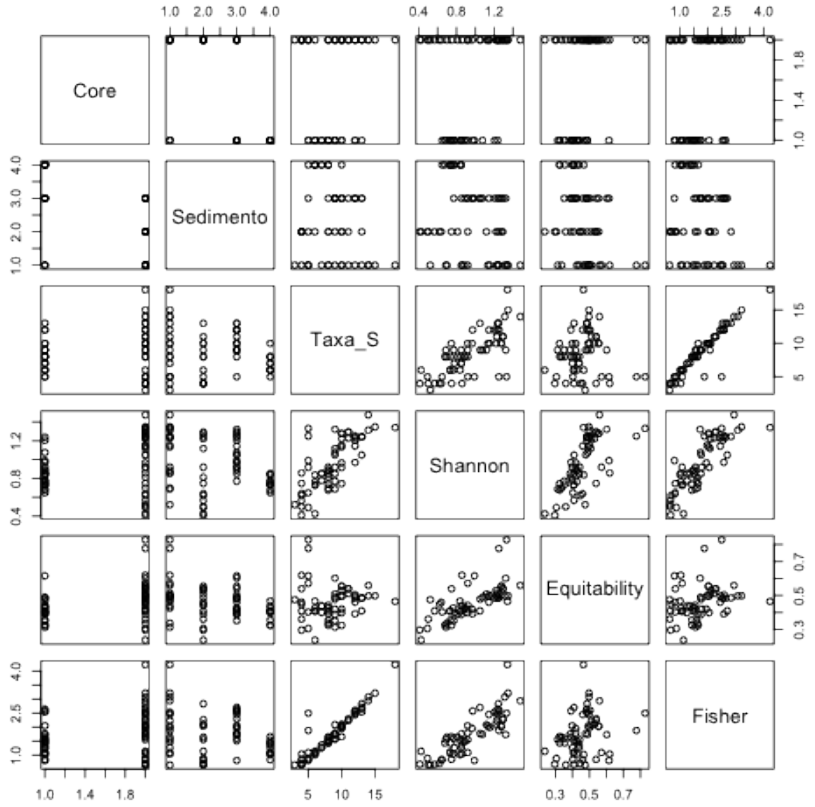

Figure 4.26 - CCA between Core samples' abiotic parameters (type of sediment) and diversity indexes. Made in Rexel.

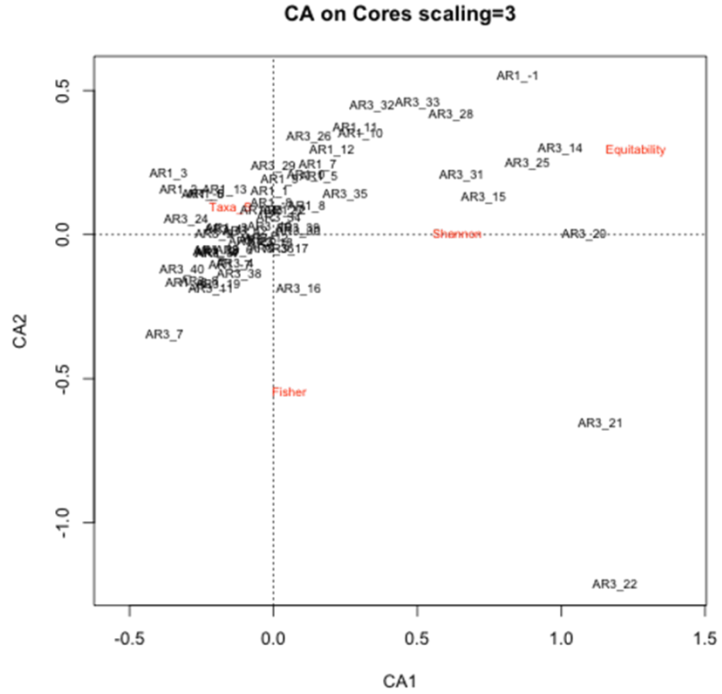

Figure 4.27 - CCA between Core samples' and diversity indexes. where Cond is conductivity, Temp is temperature, Sed1 is the type of sediment and OM the organic matter percentage. Made in Rexel.

V. Discussion

1 - ArcGIS

ArcGIS software showed itself to be extremely useful for the creation of maps referent to the location of the work area, delimitation of different geomorphological zones, as well as the position of the Cores and surface samples, and the representation of several parameters (abiotic parameters, diversity indexes, species relative abundances, etc).

The Editor tool allows the user to easily modify pre-created shapefiles for different purposes, instead of having to created several new shapefiles. The ArcTool box includes numerous tools that easily permit to create DMT models and raster analysis, very useful for the creation of topography profiles and floodable areas analysis.

The USGS Sediment Tool extension showed to be a very intuitive tool, easy to use and create grain size analysis, and could be a future alternative to GRADISTAT software.

The Geosoft Target extension is a very complex extension that works better when holes are previously planned. The obligatory creation of different data files is very thorough and has to be made with great attention so that errors are not committed. Plan and Section maps within the extension are relatively easy to be created, but attention must be taken with the selection of holes. Furthermore, there is a limitation between the distances between the holes, or else the user won't be able to have the expected result.

The creation of 3D plot graphs in this extension showed to result in original voxels easy to analyse. However, to make lithology voxels and contact surfaces from geological cgaracterization, care must be taken because at least three sediment types have to be the same within the holes so that the interpolation can be performed. This is one of the limitations of the extension, once in reality, sediment results from holes are not always coincident, and changes may have to be made for the extension to be able to create this type of analysis.

From a general point of view ArcGIS software and its extensions were very useful to the present work, and are a good complement for micropalaeontological studies.

2 - Cores

As mentioned in chapter one, tsunamis are major events in terms of sedimentary record, because they cause the deposition of sedimentary beds with characteristic textural and mineralogical features (Clague et al., 2000; Singarasubramanian et al., 2006; Babu et al., 2007), but identifying tsunami deposits is not easy.

Tsunami deposits in continental areas correspond to sediments that are at least partially of marine origin and deposited by a high-energy process (Papadopoulos, G. A. et al., 2014). Coastal lakes, lagoons and almost flat fluvial plains, characterized by low-energy environment, favor the investigation of tsunami deposits. The direct effects of coastal tsunami inundations, such as beach erosion, destruction of sand barriers and/or formation of landward washover fans, hummocky topography and large scars, are usually reflected in geomorphological features (e.g. Goff et al., 2009; Paris et al., 2009).

The southwestern Spanish, and Portuguese, estuaries are excellent geological archives of both prehistoric and historical tsunamis, with a wide set of sedimentological and geomorphological imprints. The most frequent features are beach erosion with shoreline retreat, breaking or overwash of sandy spits and deposition of bioclastic layers (Ruiz et al., 2013).

Ocean 2004 and Japan 2011 megatsunami events (e.g. Paris et al., 2010; Goto et al., 2011), confirmed that, during inundation of coastal areas, tsunamis are capable to transport a large amount of sediments inland, ranging from fine-medium sand to boulders and megaclasts. This material is eroded from both seafloor and shore by the waves approaching and flooding the coastal zone (Papadopoulos, G. A. et al., 2014).

Tsunami deposit thickness varies depending on the energy of waves and type of deposits involved as well as on the local topography. In general, tsunami deposits thickness does not exceed a few tens of cm (Morton et al., 2007). Usually, tsunami deposits do not display peculiar sedimentary structures apart from rare laminae, the number of layers being limited to a few and the basal contact being abrupt, i.e. ersional (Papadopoulos, G. A. et al., 2014).

Within the cores analysed in the present work, bioclastic silt and sand sediment layers with an erosive base are present between silt and clayey layers with pararel lamination (Fig. 4.1 chapter IV and Table 2.1 chapter II). The silt and clay layers with

fine lamination have been observed in temporary ponds and surrounding freshwater marshes of the Doñana N.P. They indicate a calm environment with a cyclic sedimentation suggested by the alternating color shades (greyish and blackish layers), probably due to alternating dry and wet periods, pulses from small tributaries or the vegetation distribution (Whittecar et al., 2001; Harter and Mitsch, 2003)(see Table 2.1, chapter II).

These silt and clay layers are interrupted by the bioclastic silt and sand layers, that show numerous features that have been described in tsunamigenic deposits (Bryant et al., 1992; Bryant, 2001; Costa et al., 2004; Dawson and Steward, 2007) such as: a) an erosional base; b) presence of intraclasts plant remains near the base; c) finer sediments toward the top; d) finer sediments landward; e) presence of higher sand percentages (near the Doñana spit) in relation to the underlying sediments; f) strong changes of fauna in relation to the underlying layers; g) presence of numerous marine species of both macrofauna and microfauna with evidence of reworking; and/or h) high-energy population structures of ostracodes. Consequently being attributed to a tsunamigenic origin (see Table 2.1, chapter II).

These tsunamigenic layers have a thickness between 8 and 26 cm in Core C (from 90 – 98/116 cm) (once the 98-116 cm sediment of the core has not been recovered, and so remains unknown) and 40 and 10 cm in Core D (between 27-66 cm and 80-90 cm respectively). The thickness of these layers agrees with the thickness described for tsunamigenic sandy deposits and storm deposits in both cores, once tsunamigenic sandy deposits are generally less than 25 cm thick while storm deposits usually exceed 30 cm in thickness (Lario et al., 2010).

These are also in accordance with the description of other reported sediments, that are usually interbedded in estuarine or spit barrier sedimentary units that act as effective sedimentary sinks, likely to preserve geomorphological features that witness the palaeoenvironmental changes (Lario et al., 2010).

Geomorphological and sedimentological features generated by extreme wave events (EWE) are common along the coasts of the Gulf of Cadiz, and have been assigned to either tsunami or storm surges. After many years of research some authors concluded that distinguishing coastal deposits generated by tsunamis and storm surges remains a major challenge and no single criterion can be inferred to identify conclusively the origin of deposits. Instead, a conjunction of features and criteria at various scales (trenches, transects, regional data) seems to be the most

reliable option for this purpose (summarized in Switzer 2008). Following this reasoning, the historical, geomorphological and sedimentological data gathered in the Gulf of Cadiz suggest the common occurrence of Extreme Wave Events in the area throughout the Holocene, but they are not always conclusive enough to decide unambiguously whether tsunamis or storms were the real cause.

The observed age discrepancies for the tsunami events of the SW Iberian Margin are probably due to flaws in the radiocarbon dating method, or even to the coincidence of a tsunami during a period of climatic instability and strong storms surges that increased the effects of the EWE (Papadopoulos, G. A. et al., 2014). In any case, correlation with published catalogues of historical earthquakes (Galbis 1932; Campos 1991) is very often imprecise because a single tsunami can produce separate features, vertically-superposed fining upward sequences or coarse-grained units, likely to be considered of different ages, assuming that they were deposited by separate events. On the other hand, it is also possible that a given event was assigned to different ages in separate localities (Galbis 1932). For instance, the events reported between 245 and 209 BC were compiled from diverse sources (Moreira De Mendoça 1758) and may perfectly well correspond to the same event but assigned erroneously to different ages in separate localities, depending on the dated material.

The radiocarbon dating results from the studied cores (C and D) and other mentioned cores in chapter IV will be discussed latter in the present chapter (section 6) together with the palaeogeographical evolution of Doñana N.P.

3 - Surface Samples

The grain size results of the surface samples represented in the litology voxel (Fig. 4.7, chapter IV) where overlapped with the geomorphological map (Fig. 2.1, chapter II) to check the relation between them (Fig. 5.1).

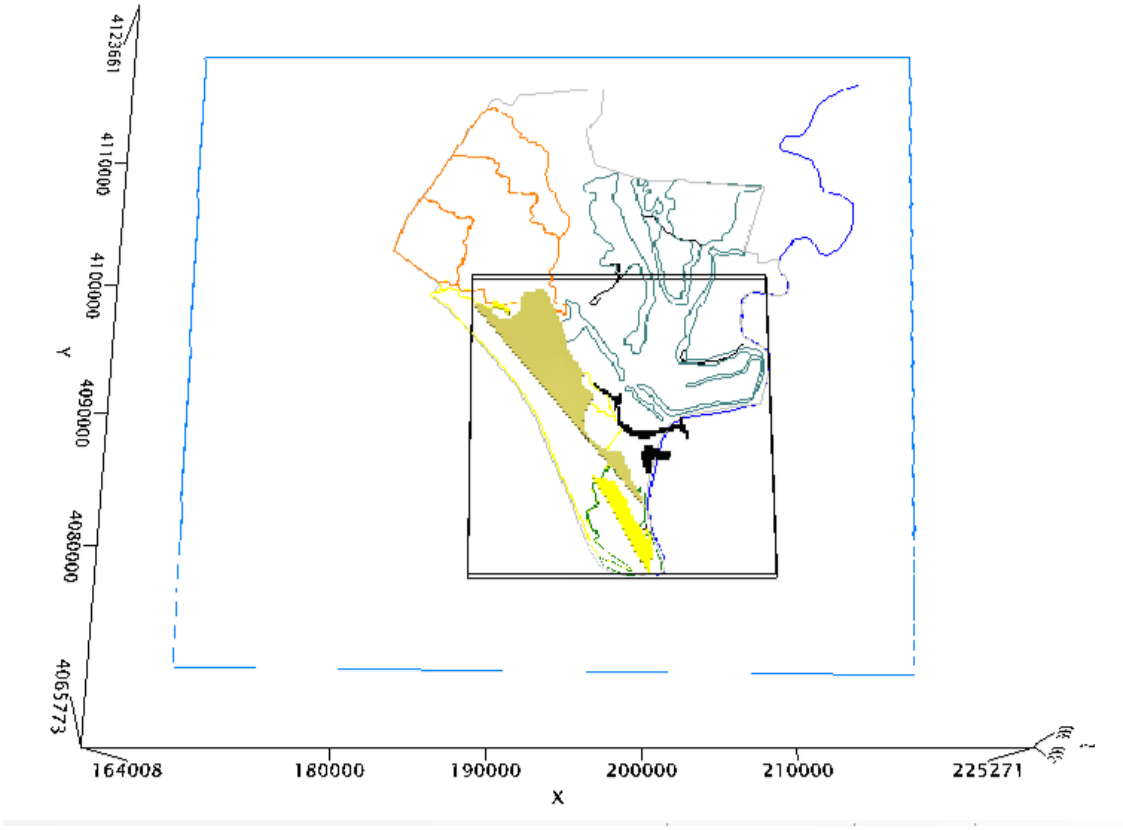

Figure 5.1 - Surface samples' Lithology voxel created in Geosoft Target extension for ArcGIS software, overlapped with geomorphological shapefiles of Doñana N.P

The resulting map shows that the sediment type is related to the geomorphological features found in the park. The mobilized dunes (see Fig. 2.1, chapter II) seem to be composed by silty sand, corresponding to surface samples 1, 4, 6, 7, 8, 9 and 13; whereas the Doñana spit and lower part of the stabilized dunes (see Fig. 2.1, chapter II) by sand, corresponding to samples 2, 3, 19 and 20. The inner part of the park, represented mainly by high and low marshes (see Fig. 2.1, chapter II), and corresponding to surface samples 10, 11, 12, 14, 15 and 16 are composed by silt sediments. Once again samples 5, 17 and 18 do not appear in the lithology voxel due to the large distance between samples in relation to the other samples, and therefore a triangulation could not be performed by the software, and no lithology voxel appears. Nevertheless samples 5, 17 and 18 are located in the margins of low and high marshes and are composed by silt as well.

As for the mineralogy results performed on XPowder 2004 Version 0.4.0.2, shown in Figure 4.8 (chapter IV), they show that, as expected from their environment, the

surface samples composed of silty sand (1, 4, 6, 7, 8, 9 and 13) are all composed by a mix of detritic and decantation minerals (Quartz, felspars, and plagioclase; where the first has the higher percentage (63-99%)). In these samples foraminifera, ostracods and carophytas are absent, with the exception of sample 8, where few ostracods were found.

The surface samples composed by sand (2, 3, 19 and 20) all shown mineral records of feldspars and quartz, the lattest being largely dominant (97-99%). The samples near the beach (19 and 20) also had minor contribution of calcite minerals (0.41 and 1.97% respectively). Foraminifera and carophytes were only found in surface sample 20 and ostracods only on sample 3. The higher percentage of calcite minerals found in sample 20 is probably due to the deposition and degradation of the foraminifera in it, although no organic matter have been found.

Surface samples 10, 15, 16, 17 and 18 composed by silt all had foraminifera and ostracods and no carophytas. These presented minerals of calcite, plagioclase, quartz and phylosilicates, which is in accordance with previous works.

Silty samples 11 and 12 had a more varied panoply of minerals such as halite, dolomite, calcite, plagioclase, quartz and anhydrite. Phylosilicates were also present in sample 12, with a 51%. These had record of foraminifera, ostracods and carophytas.

The remaining silt samples 5 and 14 have different mineral compositions, where the first one is composed by dolomite, calcite, plagioclase, quartz and phylosilicates and the second by dolomite, calcite, quartz, phylosilicates, halite, anhydrite and gypsum. These samples showed only records of ostracoda individuals.

The relation between the foraminifera species found in the samples and the mineral composition of these will be discussed latter in this chapter.

4 - Microfauna population data analysis

4.1 - Microfauna found in the Cores vs. palaeoenvironments description

4.1.1 - Core C

Based on sediment, mineral, as well as macrofauna and microfauna (ostracods) contents, Ruiz et al. (2004) distinguished three main palaeoenvironments within this Core. The lower 88 cm (from 66 – 150 cm deep) was described as an open lagoon environment, with the recognition of a tsunami layer between the depths of 90 – 98 cm. Above this interval, two more zones were distinguished and described as a restricted lagoon (32 – 66 cm in depth) and a temporary pond (32 cm to the top of the Core), although the second is not present in this work, once samples analyzed from Core C start at 46 cm depth.

Based on the description made by these authors, the benthic foraminifera assemblages, abundances and total number per gram of sediment found in the Core, will be discussed below. Two summarizing tables with some of these data are also presented below this description (Figs. 5.2 and 5.3).

In Core C, the most abundant species throughout the entire core are *Haynesina germanica* and *Ammonia tepida*. These species are common taxa present in entirely brackish to brackish-normal marine estuaries all around Europe and Africa, characteristic of shallow environments, with moderately restricted conditions (Murray, 1971; Scott, 1976; Hayward and Hollis, 1994; Hayward and others, 1999) and associated with mud/silt sediments (Murray 2006). *Ammonia tepida* tolerates a small marine influence that allows it to occur worldwide in paralic environments, where it is often associated with *Haynesina germanica* (review in Debenay and Guillou, 2002), as it is also the case in the present work. *Haynesina germanica* shows higher relative abundances than *Ammonia tepida*, which is normal since it is known as the most opportunistic brackish species (Murray, 2006).

The Elphidium sp. Species, Bolivina ordinaria and Brizalina sp. are also present thoughout the entire core, where the first are commonly found in normal marine and hypersaline marshes (Murray 2006) and the others were described as highly opportunistic species, highly adaptable and reaching their highest abundance in areas under the direct influence of rivers discharges (Mendes, 2010).

The assemblage of these combined species indicates a marginal marine environment, like lagoonal environments or marshes, present in all the interval depths of core C.

From a more detailed analyses of the lower part of Core C (150 – 98 cm), this assemblage is also combined with:

- *Quinqueloculina laevigata* and *Quinqueloculina stelligera* species, which are found in shallow waters and associated with muddy sand and sandy mud sediments (Mendes, 2010);
- *Quinqueloculina* sp., found in several lagoonal environments, and which is a dominant shallow neritic taxa (Murray, 2006);
- *Buliminella elegantissima,* a free living form at Ria de Vigo between 28 and 41 m water depths (Murray, 2006);
- *Bulimina elongata* found in temperate shelf seas with low energy and mud sediments as well in the Portuguese shelf and upper Guadiana shelf (Murray, 2006; Mendes, 2010);
- *Asterigerinata mamilla*, found at the inner shelf of the North Sea (Murray 2006);
- *Textularia* sp. which occurs in temperate sea shelves in high energy areas with coarse sediment (Murray, 2006);
- *Spirillina vivipara*, a subtidal epifaunal form at Ria de Vigo in exposed channels (Murray, 2006);
- *Nonionella stella*, a highly opportunistic species at Ria de Vigo, associated with upwelling events (Murray, 2006);
- *Fissurina* sp., *Cornuloculina* sp., *Cornuspira involvens* and *Stilostomella* sp..

This association indicates thus a more open environment than a simple marsh.

Furthermore, the higher values of faunistic density (1095 ind/g), Planktonic/Benthic ratio (0.71), Shannon H index (1.24), Species Richness (13 species), Fisher Alpha index (2.64) and Equitability index (0.62) concur with the description of an open lagoon environment (Ruiz et al., 2004). Indeed, it is considered that Fisher alpha values <2 correspond to extreme environments (brackish, hypersaline marshes, lagoons and estuaries) whereas slightly higher values are linked to normal marine lagoons. In the same way, Shannon H values <2.5 are from marginal marine environments and values between 1.51 and 3.50 from shelf and deep seas (Murray 2006).

The tsunamigenic layer between 98 – 86 cm has no evident signature in the foraminifera species analysed. Nevertheless, besides the interruption of the silt and clay sediment layers by a bioclastic silt and sand facies (see table 2.1 chapter II), there are also other small indicators that mark this layer such as i) the highest abundance of *Elphidium* sp. found in the Core (characteristic of shelf and littoral environments (Murray, 2006); ii) the presence of *Elphidium complanatum* (common at the outer bay of Cadiz Gulf (Villanueva-Guimerans & Canudo, 2008)) and iii) the presence of *Stainforthia complanata* (found in Galicia mud deposit and high organic sediments (Murray, 2006)). Diversity indexes registered between these depths show no evident differences that allow confirming the occurrence of a high-energy event (tsunami or storm). The fact that the 98-116 cm sediment interval of the core has not been recovered, and remains unknown does not help the interpretation of this layer.

The following layer (80 – 69 cm) is again described as an open lagoon environment and seems to be corroborated by the foraminifera species found in it. Indeed, together with the common ones along the entire core described above, there are several characteristic subsidiary species, namely:

- epifaunal species such as *Bulimina elongata, Asterigerinata mamilla, Spirillina vivipara, Textularia* sp., *Planorbulina mediterranenis*, *Rosalina bradyi* (Murray, 2006);
- *Bulimina marginata*, present at temperate shelf seas with low energy and mud substrates (Murray, 2006);
- *Uvigerina peregrina* and *Lagena sulcata*, common species at Cadiz Gulf's continental shelf and slope (Villanueva-Guimerans & Canudo, 2008).

Furthermore, between these depths the faunistic density, Planktonic/Benthic ratio, Shannon H, Species richness, Fisher Alpha and Equitability indexes values are similar to those registered in the tsunamigenic layer, with 392 ind/g, 0.14, 0.76, 8, 1.36, 0.4, respectively for this layer, and 374 ind/g, 0.28, 0.8, 8, 1.43, 0.38 for the tsunamigenic layer. These diversity indexes values are again commonly described for marginal marine environments, but relatively lower compared with those for the depths of 150 – 98 cm of this core.

The lowering of these values and the foraminifera assemblages found in the upper part of this core (66 – 46 cm), where only *Haynesina germanica*, *Ammonia tepida*, the *Elphidium* group, *Bolivina ordinaria, Brizalina* sp and *Buliminella eleganitssima* are present are in concordance with the description of a transition to a more restricted environment, with direct river discharge influence. The lowest values of

faunist density, plaktonic/benthic ratio and diversity indexes Shannon H, species richness, Fisher Alpha and Equitability indexes (87 ind/g at 147cm, 0.05 at 46 cm, 0.65 at 54 cm, 5 at 54 cm, 0.84 at 54 cm, 0.45, respectively) confirm this analysis, corresponding to a restricted lagoon environment as described by Ruiz et al. (2004).

.

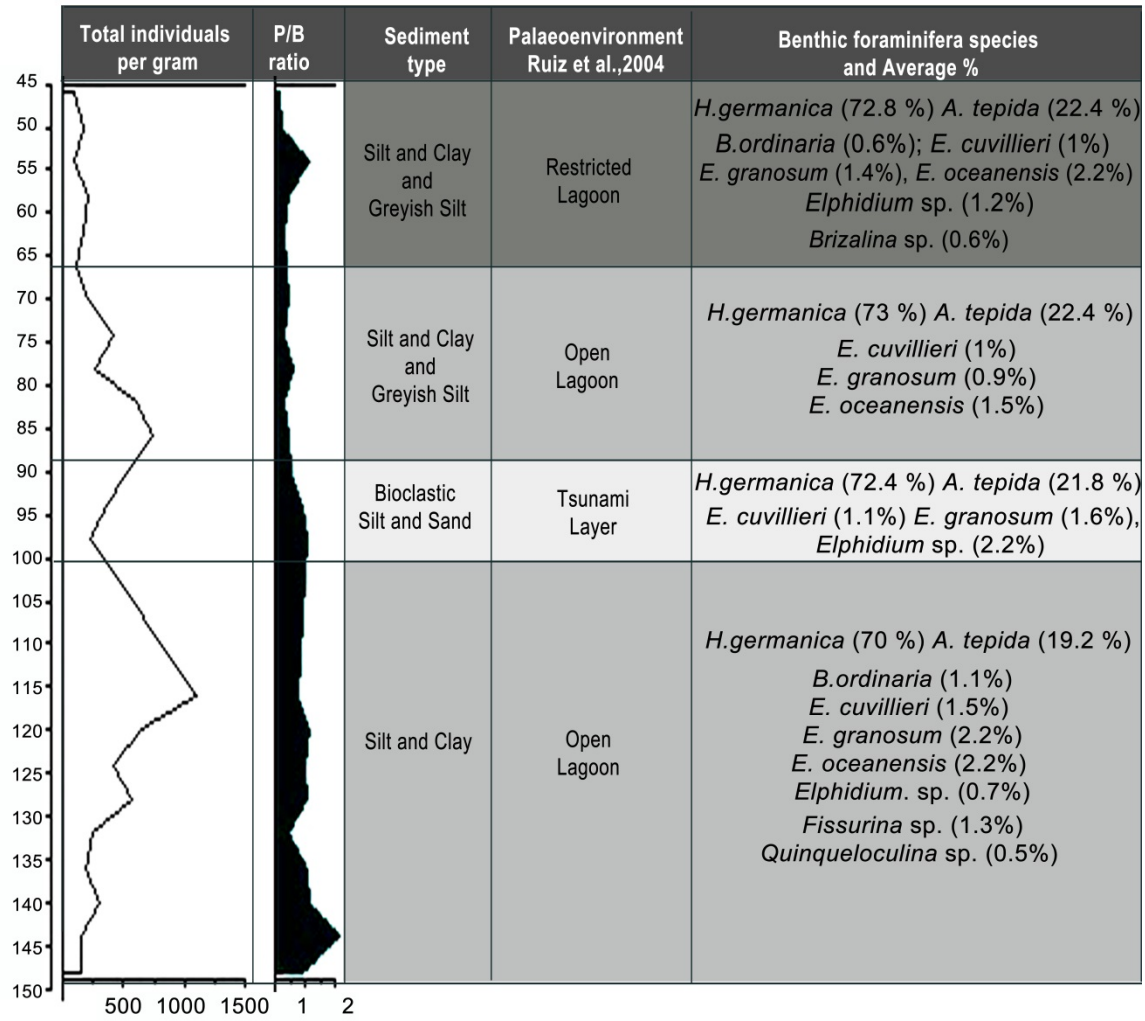

Figure 5.2 - Summarized image showing (from left to right) the nº of individuals/g, Planktonic/Benthic ratio, Sediment type and Palaeoenvironments described by Ruiz et al., 2004, Average values of benthic foraminifera species found for Core C with relative abundance >~1%.

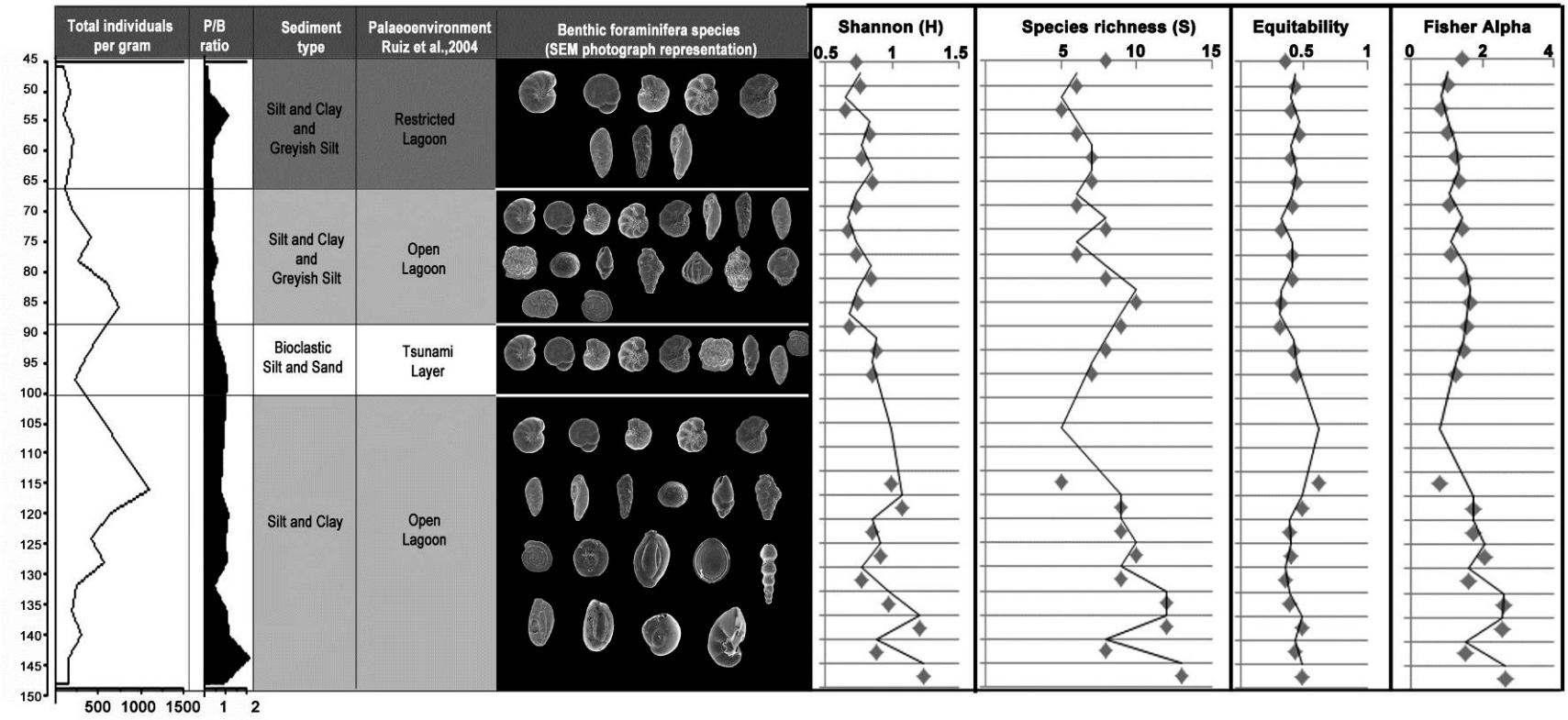

Figure 5.3 - Summarized image showing (from left to right) the nº of individuals/g, Planktonic/Benthic ratio, Sediment type and Palaeoenvironments described by Ruiz et al., 2004, Benthic foraminifera with SEM photographs, Shannon H, Species richness, Equitability and Fisher Alpha diversity indexes, for Core C

4.1.2 - Core D

Based again on sediment, mineral, macrofauna and microfauna (ostracods) analysis, Ruiz et al., 2004 distinguished three main palaeoenvironments within this Core. The lower part of Core D, from 160 – 132 cm in depth was described as a lagoon environment. From 132 – 69 cm in depth, a Mudflat-Saltmarsh environment was described, with an interruption between 90 – 80 cm where a tsunamigenic layer was distinguished. The upper part of this core (69 – 27 cm deep) was described as a chenier or tsunami layer as well.

Based on the description made by these authors, the benthic foraminifera assemblages, abundances and total number per gram of sediment found in the Core, will be discussed below. Two summarizing tables with some of these data are also present below this description (Figs. 5.4 and 5.5)

In Core D, as for core C, species *Haynesina germanica, Ammonia tepida* and the *Elphidium* group remain the common species in all depths, along with *Quinqueloculina* sp., *Asterigerinata mamilla*, *Rosalina bradyi* and *Fissurina* sp., indicating once more a marginal environment, though with a greater marine influence than in core C, due to the constant present of the latest.

At the lower part of Core D (160 – 132 cm), the previous species appear along with species *Uvigerina peregrina, Planorbulina mediterranensis, Textularia* sp., *Buliminella elegantissima, Bulimina elongata, Nonionella stella, Spirillina vivipara, Bolivina ordinaria* and *Brizalina* sp. (with higher values than those in Core C)(see description for these species made for Core C in the previous paragraphs). *Cassidulina laevigata* and *Cassidulina minuta* also occur at these depths. These two species have been described as dominant on the Portuguese continental shelf (130 m) (Levy et al., 1995) and on the Guadiana shelf (100m) (Mendes et al., 2004), as well as being the most opportunistic taxa in the Mediterranean, dependent on a pulsed supply of fresh organic matter with high nutrition value (de Rijk et al., 2000), preferentially marine organic detritus (Mojtahid et al., 2009)) and *Stilostomella* sp..

The highest Planktonic/benthic ratio is found at 150 cm in this core (value of 2.2). Fisher Alpha index is similar to that registered at the bottom of core C (2.64) with 2.14 as well as Shannon H index (1.14 here and 1.24 at 150 cm of Core C), indicating a similar environment of an open lagoon. Furthermore, Species richness

has a mean value of 11 species, Faunistic density of 51 ind/g and Equitability index of 0.5.

The layer above (129 – 94 cm) shows less diverse foraminifera assemblage, with presence of the common species throughout the whole core, along with miliolids *Quinqueloculina seminulum, Adelosina* sp., *Oolina squamosa* and *Bolivina ordinaria* with very low relative abundances (<1%). The lowest value of Shannon H and Equitability indexes (0.41 and 0.24 respectively), lower Placktonic/benthic ratio mean (0.17), species richness (mean of 6 species), Fisher Alpha (1.06) and faunistic density (mean of 24 ind/g) values, are in agreement with a transitional phase towards a more restricted environment, described as a mudflat-saltmarsh by Ruiz et al. (2004).

The interruption of this environment by a tsunamigenic event (layer above, between 90 – 80 cm depth) is not evident in the foraminifera fauna, where along with the common taxa, only *Bolivina ordinaria, Brizalina* sp, *Quinqueloculina seminulum*, *Triloculina* sp, *Planorbulina mediterranensis* and *Elphidium crispum* occur. Furthermore, even if these subsidiary species are common marine taxa (specially *Elphidium crispum* that never occurs in estuaries and appears to be stenohaline (Murray 2006)) and the layer presents the low faunistic density value (1 ind/g at 90 cm) as well as the highest Equitability index value (0.83 at 90 cm), this is not sufficient for the recognition of a tsunamigenic event. Indeed the planktonic/benthic ratio and species richness (with mean values of 0.35 and 7 species) are not very different from those found in the previous layer. Shannon H index and Fisher Alpha show higher values than those of the previous layer, with values of 1.17 and 2.06, being more similar to those described for marine or lagoonal environments (Murray, 2006, and description made for Core C). The absence of subsidiary species in this layer may be due to the non-adaption or remobilization of the species to this extreme environment.

Perhaps one of the most evident aspects of the occurrence of this high energy event is the switch between *Haynesina germanica* and *Ammonia tepida* dominance in the layer above this (76 – 69 cm), where the latter becomes the principal one. This species is probably more adapted and tolerates better more marine conditions than Haynesina germanica (review in Debenay and Guillou, 2002). In this layer, along with common species *Asterigerinata mamilla, Rosalina bradyi, Fissurina*

sp.,*Quinqueloculina* sp. and the *Elphidium* group, subsidiary species such as *Planorbulina mediterranensis, Quinqueloculina seminulum, Triloculina trigonula, Buliminella elegantissima, Bulimina elongata, Lagena sulcata, Spirillina vivipara* (see description for these species for Core C) and *Adelosina* sp. also occur in low percentages (<1%). The presence of these, as well as the faunistic density, planktonic/benthic ratio, Shannon H, species richness, Fisher Alpha and Equitability indexes mean values (106 ind/g, 0.34, 1.21, 10 species, 2.15 and 0.5 respectivelly) do not seem to correspond to the mudflat-saltmarsh environment described previously (Ruiz et al., 2004), but to a more marginal marine environment. However, one could argue that the foraminifera species could not have had the time to reestablish their normal population assemblages or this tsunamigenic event could have been the same as the high energy event described also for the upper layer of this Core (66 – 27 cm).

This next tsunamigenic layer is complex, once it has the highest values of faunistic density and Shannon H index (879 ind/g and 1.48), the lowest value of the planktonic/benthic ratio (0.04) and both the highest and lowest values for Species richness and Fisher Alpha index (3 species and 18 species; and 0.64 and 4.23), with Equitability index having a mean value of 0.5. The presence of the highest and lowest values of the diversity indexes are probably related to the occurrence of the abrupt event, that has an erosive base were the lowest values occur, and the deposition at the top of the foraminifera species including the common ones, along with *Nonion fabum, Uvigerina peregrina, Planorbulina mediterranensis, Elphidium crispum, Quinqueloculina seminulum, Triloculina trigonula, Bolivina ordinaria, Brizalina* sp., *Cornuloculina* sp., *Quinqueloculina stelligera, Buliminella elegantissima, Bulimina elongata, Adelosina* sp., *Lagena sulcata, Stilostomella* sp. and *Elphidium complanatum* (see species habitat description in previous paragraphs).

In conclusion, the diversity index that evidences the most the occurrence of a tsunami seems to be Fisher Alpha, which value is much higher than the other registered in both cores, and corresponds to those registered in shelf and deep sea assemblages (Fisher alpha 5-15 or 5-20 respectively)(Murray, 2006).

Nevertheless, all the other variables presented in the present work also concur with previous works on tsunamigenic layers found worldwide as for example Nagendra et al., (2005), Gadi & Rajashekhar (2007), Ricky Rositasari & Soedibjo (2008), Uchida

el al., (2010); Trog et al., (2013). These variables include the foraminifera species found in the tsunamigenic layer, the composition of sand beds (suggesting strong waves and currents), the presence of reworked molluscs, marine foraminifera taxa, high values for planktonic/benthic ratio, and high Shannon H, Fisher Alpha and Species richness diversity indexes.

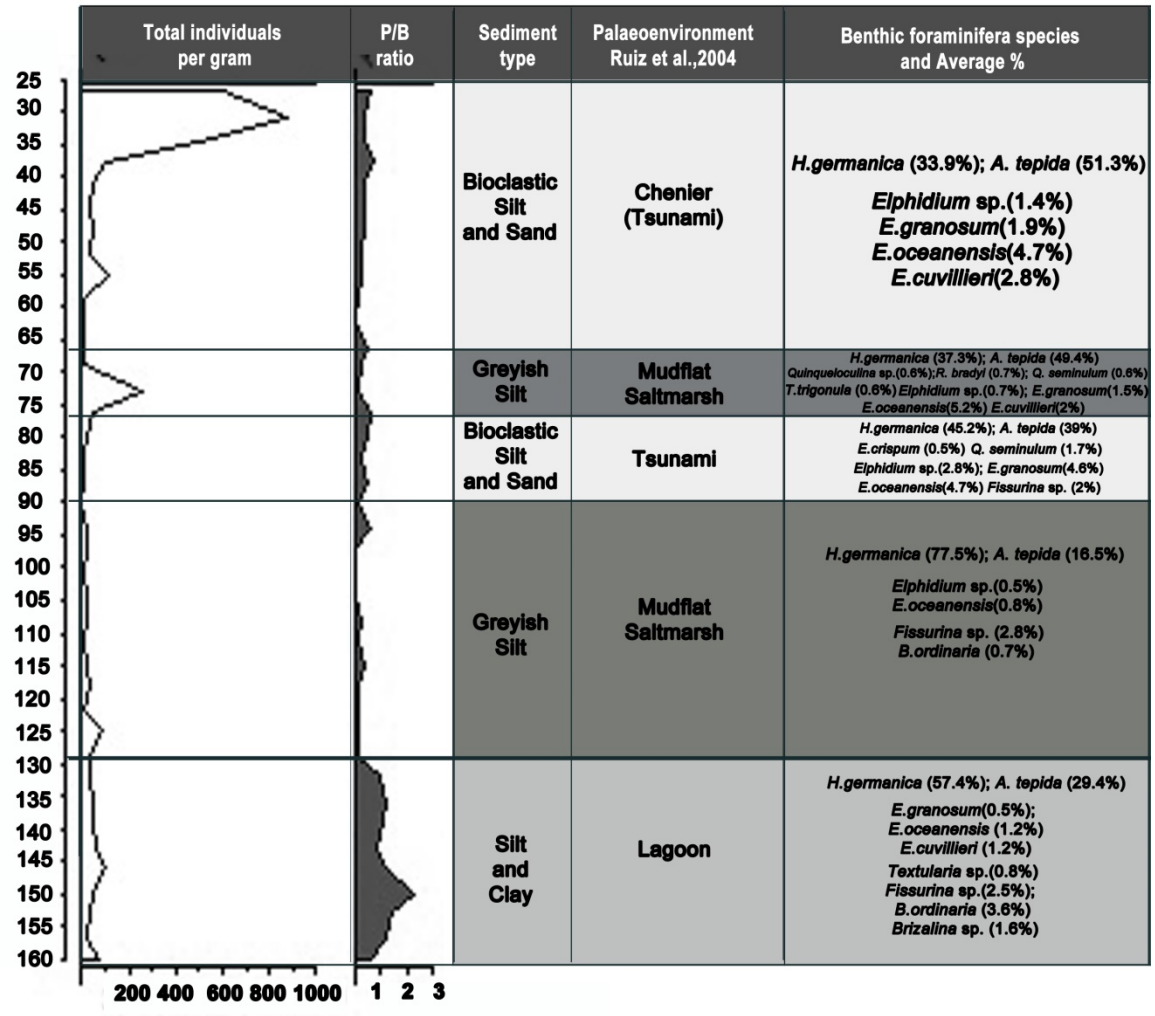

Figure 5.4 - Summarized image showing (from left to right) the nº of individuals/g, Planktonic/Benthic ratio, Sediment type and Palaeoenvironments described by Ruiz et al., 2004, Average values of benthic foraminifera species found, for Core D C with relative abundance >~1%.

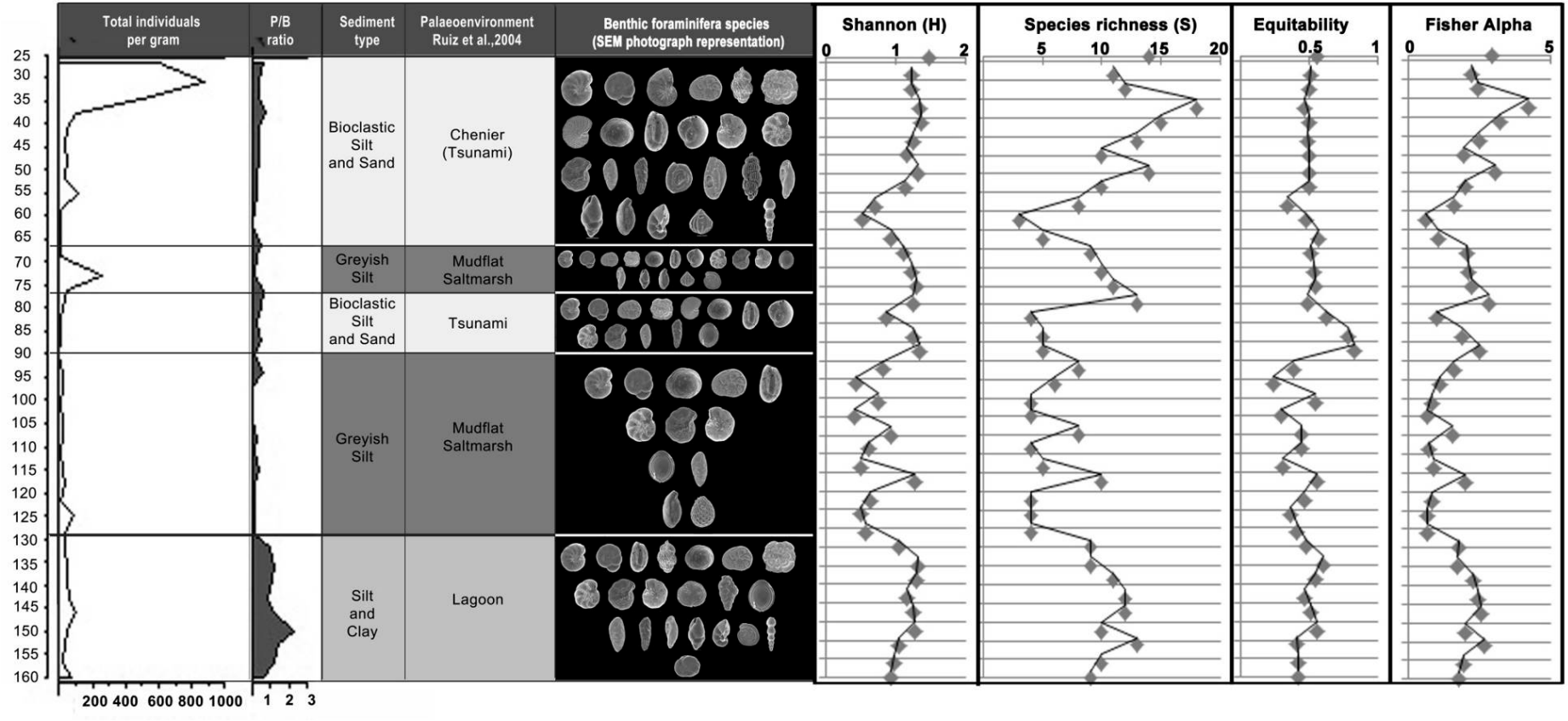

Figure 5.5 - Summarized image showing (from left to right) the nº of individuals/g, Planktonic/Benthic ratio, Sediment type and Palaeoenvironments described by Ruiz et al., 2004, Benthic foraminifera with SEM photographs, Shannon H, Species richness, Equitability and Fisher Alpha diversity indexes, for Core D

4.2 - Surface samples species relative abundance and diversity indexes

Regarding surface sediments, samples 1, 2, 3, 4, 6, 7, 8 and 9 had no foraminifera. This is probably due to the lack of marine influence at these locations, once all these samples were situated at the boundary between the dune and marsh systems. Although sample 10 was taken not further apart from sample 9, the latter was an euthrophicated lagoon and had higher organic matter content (10%) and lower pH (6.5) than the first (4% organic matter and pH of 8). These conditions could have dissolved the foraminifera present in there, or they simply do not support the existence of a foraminiferal population.

Most surface samples taken at SE margin of Doñana National Park (namely, samples 10, 11, 12, 13, 14, 15, 16, 17, 18, 19 and 20) do present foraminifera populations, except for samples 13, 14 and 19. No explanation was found for the absence of species at samples 13 and 19, once these correspond to small beach areas. Sample 14, taken at a small pond, had high organic matter content (14%), and the explanation for the absence of foraminifera could be the same as for sample 9, i.e. unadequate or dissolving conditions.

It is important to remind here that surface samples were collected in the winter season, when great precipitation had occurred in the previous weeks and months. In the great marshes of Massachusetts, De Rijk (1995) and De Rijk and Troelstra (1997) found that foraminifera distribution was not related to elevation, but with salinity variations, resulting from the balance between infiltration, precipitation and flood. Furthermore, the winter positive anomalies of precipitation, responsible for the increase of freshwater seepage and flooding in the upper part of intertidal zones, during longer periods, seem to control the high marsh foraminiferal assemblages: quantitatively reducing the number of individuals by cm^3 of sediment; and qualitatively increasing the dominance of low salinity species (Moreno et al., 2012).

Surface samples 10, 11 and 12 had only two to three calcareous species (namely *Ammonia tepida, Bolivina ordinaria*, *Haynesina germanica*, and Elphidium sp.) with similar faunistic density values (6, 6 and 5 respectively) and a planktonic/benthic ratio of ~0 (as it was expected). Fisher Alpha and Shannon H indexes values were the lowest in these samples (0.65, 0.39, 0.4 and 1, 0.7 and 0.6 respectivelly), typical of ponds or lagoons found in marshes. These values are similar to the annual species

diversity of Cowpen Marsh high marsh (α=0.63; H=0.92), typical of the most stressed environments (Murray, 2006).

Temporal changes in Fisher alpha and Shannon H indexes showed maximum values on the low marsh and tidal flats in late spring to early autumn and minimum values from late autumn to early winter. Similarly, Murray and Alve (2000) suggested that intertidal environments support only a limited number of species of taxa during environmentally harsh winter months, and that other species were able to temporarily colonize the intertidal zone when conditions improved.

Surface samples 15, 16 and 18 all showed similar diversity indexes values, with Shannon H of 1.5, 1.5 and 2, respectively; Fisher Alpha of 4.8, 4.6 and 4, respectively; and Equitability index of 0.57, 0.53 and 0.9 respectively. These values correspond to marginal marine environments (Murray, 2006). The foraminifera fauna found at these sites is in agreement with the index description once they are represented by a mixture of calcareous and agglutinated taxa (as *Haynesina germanica, Ammonia tepida, Bolivina ordinaria, Quinqueloculina stelligera*, *Asterigerinata mamilla, Fissurina* sp., *Brizalina* sp., *Miliammina fusca, Planorbulina mediterranensis, Nonion fabum, Elphidium cuvillieri, Elphidium granosum*, *Cassidulina minuta, Quinqueloculina* sp., *Trochammina inflata*, *Textularia* sp., *Hopkinsina atlantica*, *Nonionella stella*, *Ammotium* sp., *Stilostomella* sp., Rosalina bradyi, *Buliminella elegantissima*, *Cassidulina laevigata*, *Cornuspira involvens* (see foraminifera assemblages in previous section 5.2 of this chapter), common in marshes that experience some marine influence. The presence of planktonic individuals found at these samples corroborates the previous assumption, with ratio values of 6 (sample 18), 5 (sample 15) and 2.3 (sample 16), probably brought by and mixed in the Guadalquiver river – seawater flow connection.

Sample 17 is the only sample that presents a dominance of agglutinated foraminifera, where *Trochammina inflata* and *Jadammina macrescens* are dominant, along with subsidiary *Haynesina germanica* species. Shannon H index has the lowest value in this sample (0.58), and Fisher Alpha and Equitability indexes also present low values (0.47 and 0.52 respectively), corresponding to a typical brackish or hypersaline marginal marine environment (Murray 2006). These species are the dominant forms in hypersaline marshes from California, USA and Baja, California, the dominant forms (Murray, 2006). The organic matter content in this sample was 13% and the highest conductivity value was also found here (44 m/s), representing a

hypersaline environment. Here the planktonic/benthic ratio was ~0, showing again a restricted environment condition.

At last, sample 20 has the higher number of species (species richness = 20 species) and Fisher Alpha value (5.3), with Shannon H with 2 and Equitability index of 0.6. The presence of several subsidiary species described as present in the Cadiz Gulf, the dominance of Ammonia beccarii species, and the absent of agglutinated taxa, indicate an environment with great marine influence as well as with river discharge influence, in agreement with the beach environment sampling site.

5 - Sedimentary facies, radiocarbon dating, palaeogeographical evolution of Doñana National Park and relation with occurrence of tsunamis

In 2010, Ruiz and coworkers drawed a first palaeogeographical evolution scenario for Doñana National Park, where ten phases were delineated and described, such as reported hereafter. In this chapter a synthesis of the palaeogeographical evolution of the Park is complemented with a 3D analysis and representation of the connection between nine cores (Fig. 5.6). These cores are AR, BR, CR, FR, DR, CM, PLN, C, and D. The last two cores correspond respectively to core GR and core HR from Ruiz et al. (2010).

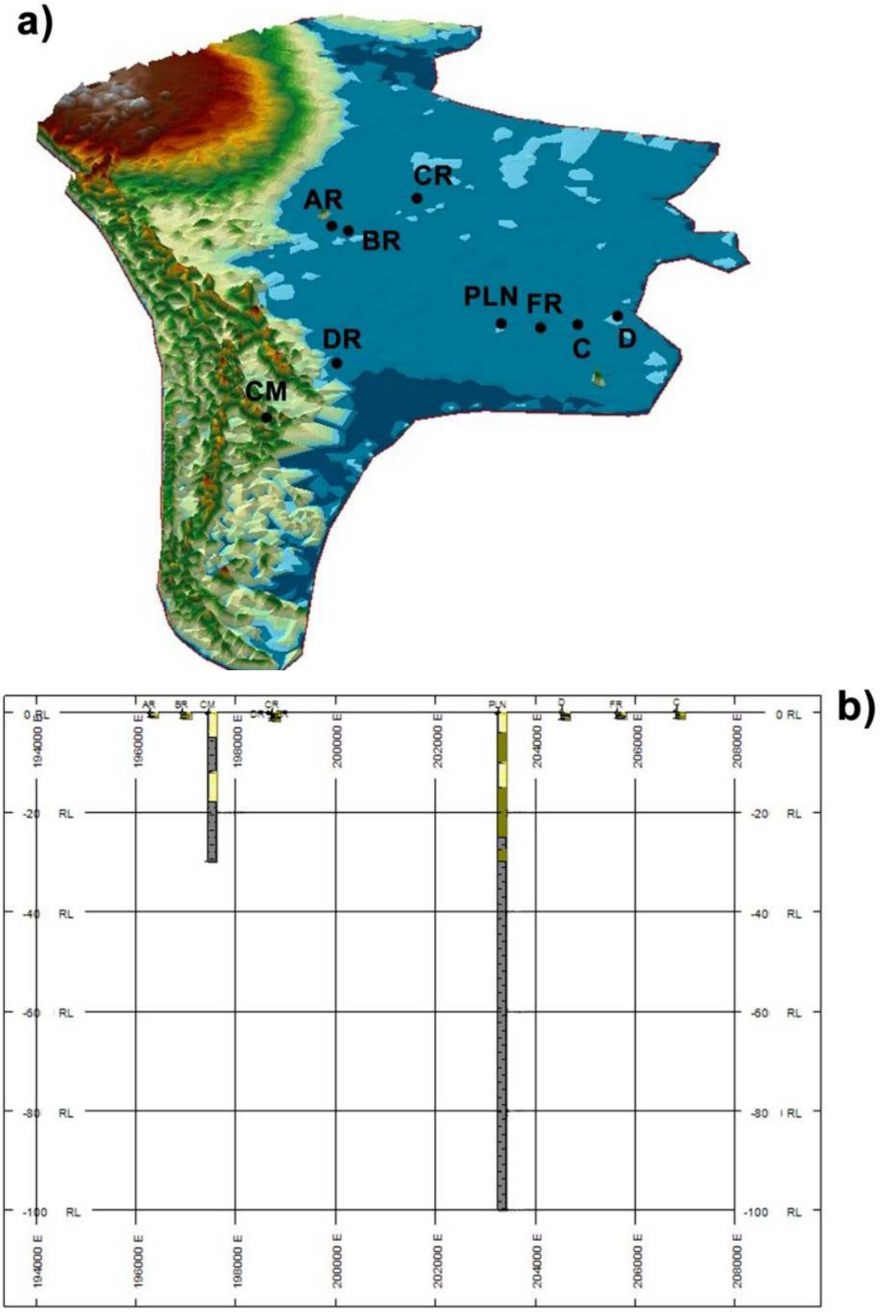

Figure 5.6 - Location (a) and section map with sediment facies (b) for Cores AR, BR, CR, DR, FR, C, D, CM and PLN, described in Ruiz et al., 2010

The analysis made with Geosoft Target extension enabled the interpretation between radiocarbon ages registred in the Cores and the generation of section plots (Figs. 5.7, 5.8 and 5.9) and 3D voxels (Figs. 5.8, 5.9 and 5.10) in order to see the connection between the facies and correspondent phases of the nine cores and to have a wider vision of palaeoenvironments present at the park. In the following paragraphs, the phases will then be described together with the information obtained from i) the linear interpolation made between radiocarbon datations of the Cores and correspondent phases (Fig. 5.7); ii) the interpolation between sets of cores that present the same type of facies and radiocarbon datings/phases (Fig. 5.8 and 5.9; futher information found in Ruiz et al., 2010); and iii) the voxel analysis made between phases, resulting from interpolations of these, plotted in sequence and with diferent XYZ orientations (Fig. 5.10).

The first phase (Phase 1) described by Ruiz and coworkers (2010) correspond to OIS 3 stage, when Doñana N.P. was at its eastermost part composed by freshwater marshes. This phase is only present at the bottom of Core PLN, therefore not being included in the present analysis.

During the Late Glacial Maximum (OIS 2, Phase 2), the eastern part of the park was occupied by freshwater and brackish marshes, partially enclosed by aeolian units (Zazo et al., 2005). This phase appears to be present at the bottom of cores AR, BR and PLN, all composed by Silt and Clay sediments, confirming a marsh environment (Fig. 5.7).

Phases 3, 4 and 5 of Ruiz et al., (2010) are included in the Early Holocene, and more precisely during the Atlantic Climatic Period (8000 yrs B.P. to 6000-5000 yrs B.P.) and the end of the transgression, when the Doñana National Park was occupied by an open lagoon, partially protected in its westernmost part by aeolian units (Zazo et al., 2008) due to the beginning of the growth of Doñana spit (Goy et al., 1996). In this period there is a record of a tsunami causing the erosion of this spit and the deposition of aeolian sand over the new salt marsh, registered mainly at cores PLN, AR and BR (Fig. 5.7 e Fig. 5.10b1) (see chapter II for further information).

Phases 6 and 7 of Ruiz et al. (2010) are coincident with the Sub-Boreal period (5000 – 3000 yrs B.P.) during which the central part of Doñana National Park was still occupied

by an open lagoon, whereas the sandy spit grew towards the southeast. During this time interval, there is record of one or two tsunami-like events (or very strong storms) that caused the erosion of the Doñana spit and the deposition of bioclastic, sandy-clayey silt over the lagoon bottom. These phases and correspondent palaeoenvironments are indeed very visible in Cores CR, AR, BR, PLN (Fig. 5.8) and CM (Fig. 5.7), so are the occurrence of the tsunamis that caused the deposition of new sediments over the lagoon (Fig. 5.10b2).

Phases 8, 9 and 10 of Ruiz et al. (2010) occurred during the Sub-Atlantic period (3000-1500 B.P.) in which the southwestern part of the Doñana National area remained emerged and the central and southern ones were occupied by a very shallow lagoon. The continuous growth of the Doñana spit and the progressive infilling induced the creation of new brackish marshes (Zazo et al., 1999) or the transition from marine conditions to more restricted scenarios (Ruiz et al.,2010).

During this period several tsunamis eroded the Doñana spit inducing the creation of small washover fans constituted by aeolian sediments and the accumulation of bioclastic ridges over the lagoon borders. These tsunamis may be assimilated to the historical tsunamis that devastated the southwestern Iberian coasts between 2168-2159 cal B.P. and 2010 cal B.P. (218-209 yrs BC and 60 yrs BC) (Campos, 1991).

From 1900 yrs B.P. to present times (Phase 10), there was an increasing infilling of the lagoon, with a progressive transition towards intertidal-supratidal conditions, but this tendency was again interrupted by a new introduction of marine sediments owing to new high-energy events. The more recent palaeoenvironmental evolution of the Doñana National Park (1500 yrs B.P. untill present) is marked by the creation of new wetlands with temporary ponds and the growing of the Doñana and La Algaida spits, with aeolian sands covering intertidal sediments.

These phases are well represented in Fig. 5.10b3 and Fig. 5.7, where cores CM, DR, C and D show an intercalation between tsunamigenic sediments (Bioclastic) and typical marsh sediments (Silt and Clay) (Fig. 5.9); and cores AR and BR continue to be protected by the Aeolian dune system.

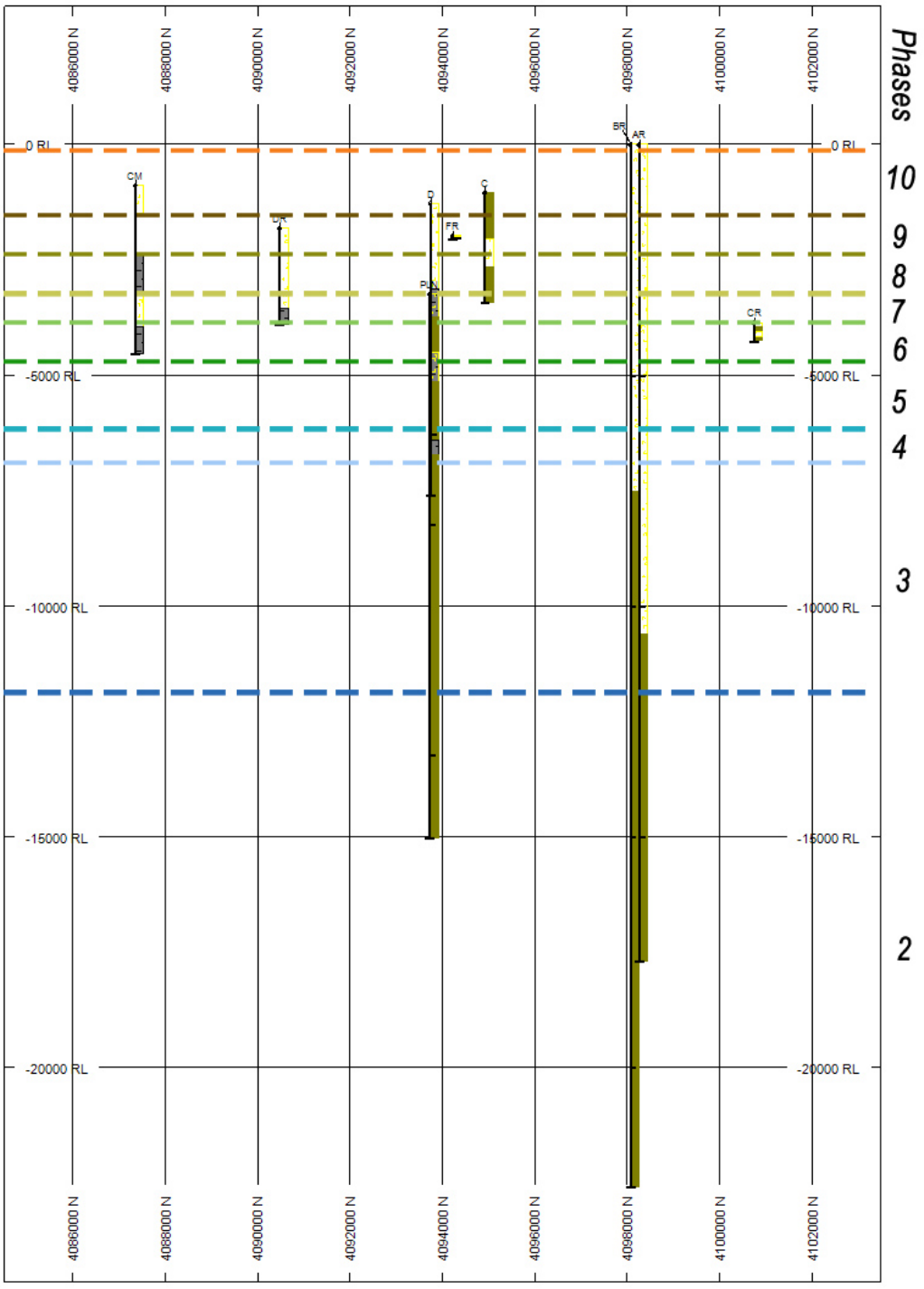

Figure 5.7 – Section map plot of all cores resultant of the linear interpolation between radiocarbon datations, where RL values correspond to cal BP ages, and correspondent phases

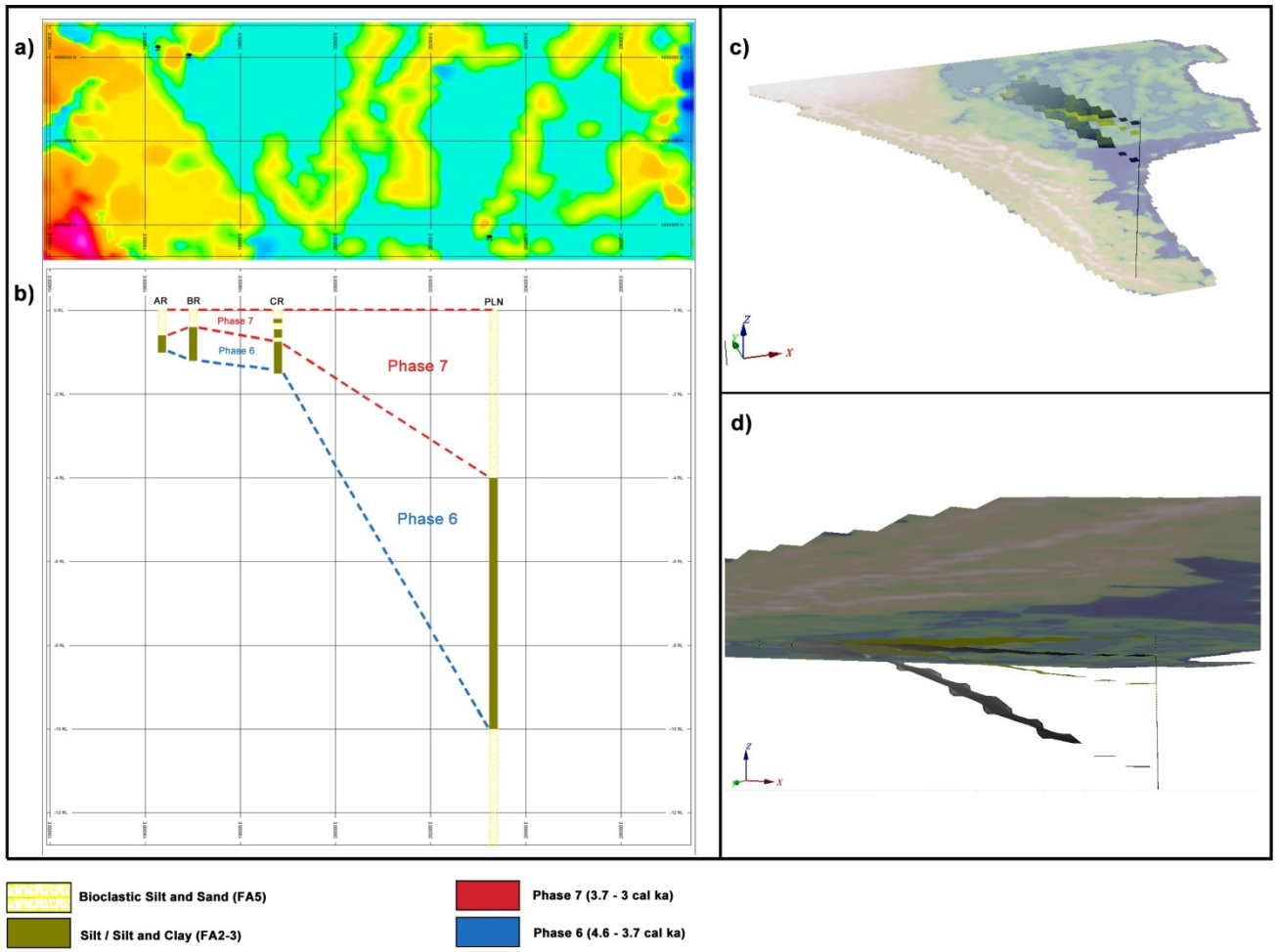

Figure 5.8 - Analysis between cores AR, CR, BR and PLN made in Geosoft Target extension for ArcGIS. a) plan map, b) section map with sediment facies and geological interpretations, c) 3D lithology voxel and superimposed DMT from a sky view d) 3D lithology voxel and superimposed DMT from a below ground view. Green/yellowish voxels correspond to Bioclastic Silt and Sand interpolation layers, Grey voxels to Silt/Silt and Clay interpolation layers

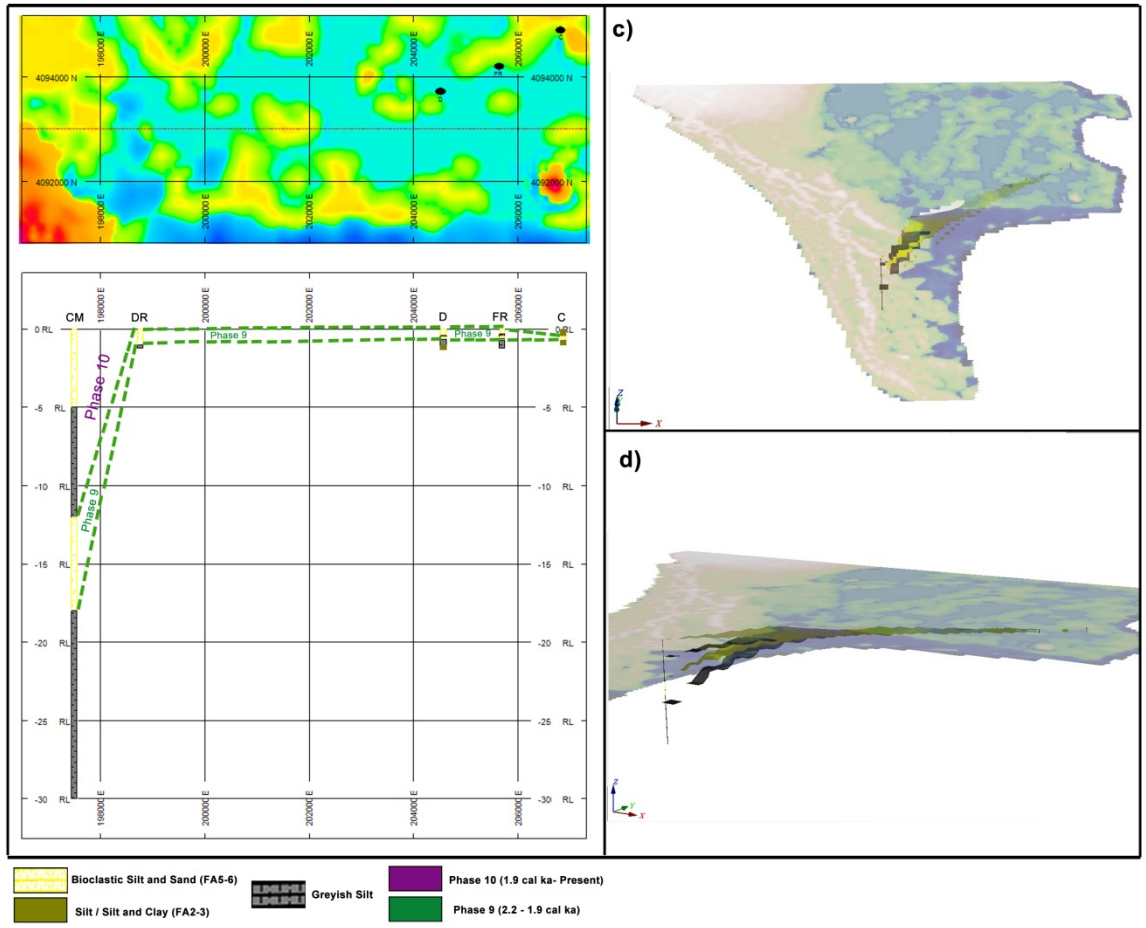

Figure 5.9 - Analysis between cores CM, DR, FR, C and D made in Geosoft Target extension for ArcGIS. a) plan map, b) section map with sediment facies and geological interpretations, c) 3D lithology voxel and superimposed DMT from a sky view d) 3D lithology voxel and superimposed DMT from a ground view. Green/yellowish voxels correspond to Bioclastic Silt and Sand interpolation layers, Grey voxels to Silt/Silt and Clay interpolation layers

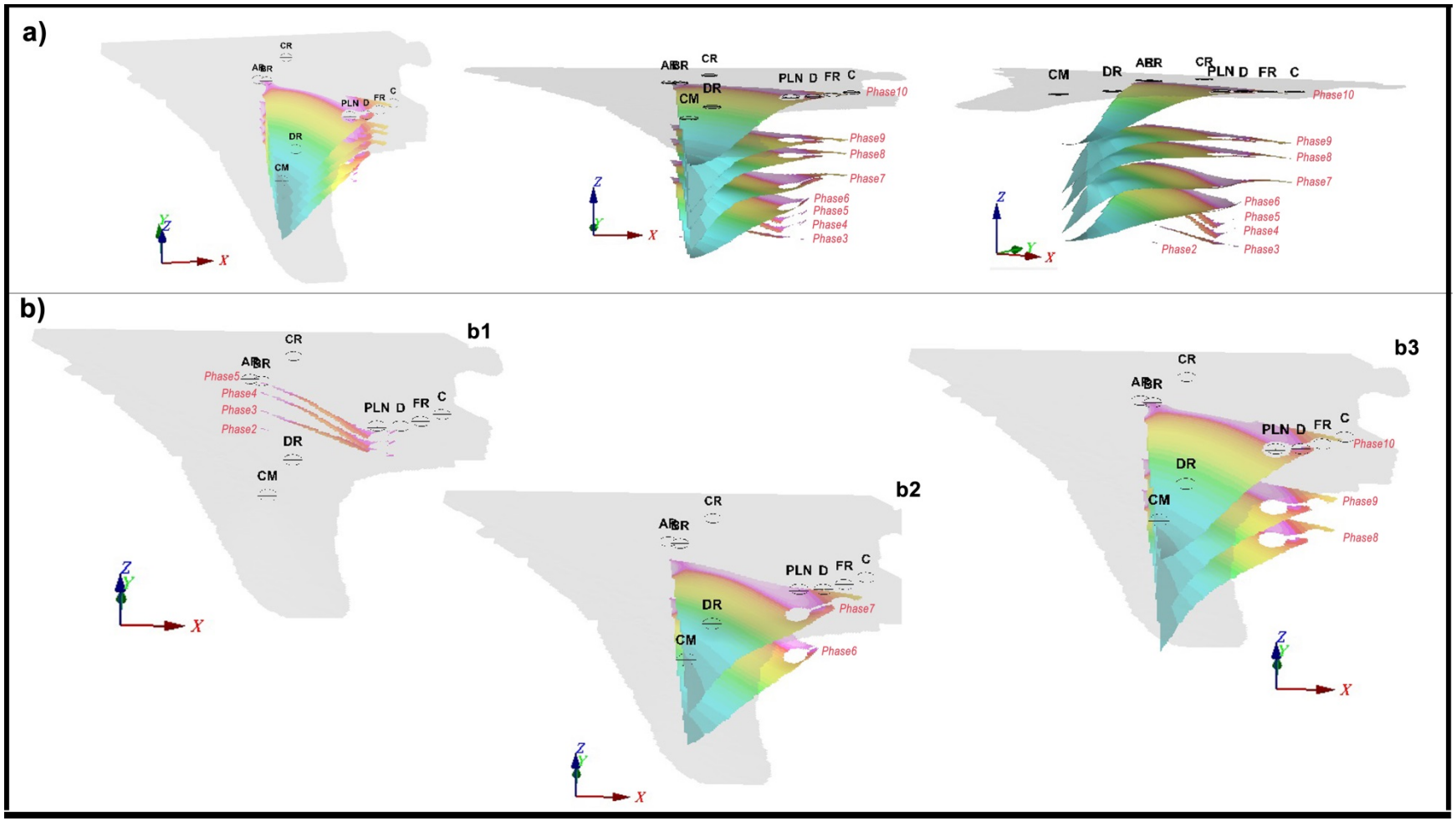

Figure 5.10 - 3D plots generated in Geosoft Target extension, showing the connection between the phases present at the nine cores: a) stacked Voxels resulting from the interpolation between sets of phases, showing different orientations; b) Group of phases and connection of these between the cores; b1 shows phases 2 to 5, b2 shows phases 6 and 7 and b3 phases 8 to 10.

Finally at presents days, and based on studied surface samples, the Doñana National Park is, at its most northeastern site, composed by silt and clay sediments, typical of marsh environments, protected from the marine influence. The western and central parts of the park are composed by Silt and Sandy layers, corresponding to marsh systems protected and influenced by aeolian units with several bioclastic ridges still remaining intact since the occurrence of the past tsunamigenic events. The margins of Doñana National Park are composed by silty to sandy sediments, mirroring the Guadalquivir River and marine influences.

VI. Conclusion

The southwestern Spanish estuaries are excellent geological archives of both prehistoric and historical tsunamis, with a wide set of sedimentological and geomorphological imprints.

Accordingly, the present work aimed to characterize the actual and past environments at Doñana National Park (SW Spain) throughout the study of benthic foraminifera assemblages at two drill holes (cores C and D, from Ruiz et al., 2004) and twenty surface samples, as well as to recognize and confirm the occurrence of an extreme energy events (storms/tsunamis) around 2165 yrs B.P. (215 yrs BC).

Foraminifera are unsurpassed stratigraphical, palaeoecological and palaeoenvironmental tools for statistical and systematic analysis in environmental reconstruction (Loeblich and Tappan, 1987; Hayward et al., 1999; Sen Gupta, 1999). However, one of the main conclusions of the present work is that in environments such as Doñana National Park, they cannot be used as a strong proxy for identifying high energy events (tsunami/storms).

Indeed, within the cores analyzed for the present work, bioclastic silt and sand sediment layers with an erosive base are present between silt and clayey layers with pararel lamination (Fig. 16 chapter IV and Table 3 chapter II). The silt and clay layers with fine lamination have been observed in temporary ponds and surrounding freshwater marshes of the Doñana N.P, and indicate a calm environment with a cyclic sedimentation suggested by the alternating color shades (greyish and blackish layers), probably due to alternating dry or wet periods, pulses from small tributaries or the vegetation distribution (Whittecar et al., 2001; Harter and Mitsch, 2003)(see Table 2.1, chapter II).

The bioclastic silt and sand layers further show numerous features that have been described in tsunamigenic deposits (Bryant et al., 1992; Bryant, 2001; Costa et al., 2004; Dawson and Steward, 2007) such as: a) an erosional base; b) the presence of intraclasts plant remains near the base; c) finer sediments toward the top and or landward; d) the presence of higher sand percentages (near the Doñana spit) in relation to the underlying sediments; e) strong changes of fauna in relation to the underlying layers; f) the presence of numerous marine species of both macrofauna and microfauna with evidence of reworking; and even g) high-energy population structures of ostracodes.

These tsunamigenic beds have between 8 to 26 cm in Core C and between 40 to 10 cm in Core D. The thickness of these layers concurs with the thickness described for tsunamigenic sandy deposits and storm deposits in both cores, once tsunamigenic sandy deposits are generally less than 25 cm thick while storm deposits usually exceed 30 cm in thickness (Lario et al., 2010).

These also concur with the description of other reported sediments, that are usually interbedded in estuarine or spit barrier sedimentary units that act as effective sedimentary sinks, likely to preserve geomorphological features and witness the palaeoenvironmental changes (Lario et al., 2010).

Other variables studied in the present work also concur with previous works on tsunamigenic layers found worldwide as for example Nagendra et al., (2005), Gadi & Rajashekhar (2007), Ricky Rositasari & Soedibjo (2008), Uchida el al., (2010); Trog et al., (2013). These variables include the foraminifera species found in the tsunamigenic layer, the composition of sand beds (suggesting strong waves and currents), the presence of reworked molluscs, marine foraminifera taxa, high values of planktonic/benthic ratio, high Shannon H, Fisher Alpha and Species richness diversity indexes.

Regarding foraminifera species, results with relative abundance >1% were considered in the present work, rather than abundances >5% as used by many authors. These results show the presence of marine foraminifera at the tsunamigenic layers, and their absence in the remaining records, which appeared extremely important for the recognition of the occurrence of these high energy events.

Based on studied surface samples, the Doñana National Park is, at its most northeastern site, composed by silt and clay sediments, typical of marsh environments, protected from the marine influence. The western and central parts of

the park are composed by Silt and Sandy layers, corresponding to marsh systems protected and influenced by aeolian units with several bioclastic ridges still remaining intact since the occurrence of the past tsunamigenic events. The margins of Doñana National Park are composed by silty to sandy sediments, mirroring the Guadalquivir River and marine influences.

The analysis made with Geosoft Target extension enabled the interpretation between radiocarbon ages Cores and the generation of section plots as well as 3D voxels in order to see the connection between the facies and correspondent phases. The use of the nine cores from Ruiz et al. (2004) for this 3D visualization enabled to achieve a wider vision of palaeoenvironments sucession at the park.

This analysis confirms the palaeoenvironments described for each core within the phases described by Ruiz and coworkers (2010).

Finally ArcGIS software and its extensions were very useful to the present work, and are a good complement for micropalaeontological studies. This GIS analysis together with the microfauna analysis enabled to confirm the palaeoenvironments description made for Doñana National Park by other authors, as well as the occurrence of palaeotsunamis in this area.

VII. References

Allen, S. (2010). Environmental controls and distributions of surface foraminifera from the Otter estuary salt marsh, UK: their potential use as sea level indicators. *The Plymouth Student Scientist* **4** (1), 293-324

Alvarez-Zarikian, C.A.; Soter, S.; Katsonopoulou, D. (2008). Recurrent submergence and uplift in the area of ancient Helike, Gulf of Corinth, Greece: microfaunal and archaeological evidence. *Journal of Coastal Research* **24** (1), 110–125

Alve, E., & Murray, J. W. (2001). Temporal variability in vertical distributions of live (stained) intertidal foraminifera, Southern England. *Journal of Foraminiferal Research* **31**, 12-24

Andrade, C.; Hidson, R.; Freitas, C.; Dawson, A. (1994). Sedimentary evidence of tsunami flooding in Algarve coastal lowlands. *Proceedings of the Symposium Littoral* , Lisbon, **2**, 26-29

Andrade, C.; Andrade, A.; Kortekaas, S.; Dawson, A. (1997). Sedimentological traces of tsunamigenic overwash of the Martinhal lowland (Western Algarve-Portugal). *Proceedings Seminário da Zona Costeira do Algarve*, Faro, *Eurocoast-Portugal*, 11-18

Andrade, C.; Munhá, J. M.; Paulino, J. (1998). Geochemical signature of extreme marine flooding in the Boca do Rio lowland (Algarve, Port ugal). *V Congresso Nacional de Geologia Lisboa*, IGN, SGP, **84**(1), C-51/C-54

Atwater, B. F. & Moore, A.L. (1992). A tsunami about 1000 years ago in Puget Sound, Washington. *Science* **258**, 1614-1617

Atwater, B. F. (1986). Evidence for Great Holocene earthquakes along the outer coast of Washington State. *Science* **236**, 942-944

Atwater, B. F.; Nelson, A. R.; Clague, J. J.; Carver, G. A.; Yamaguchi, D. K.; Bobrowsky, P. T.; Bourgeois, J.; Darienzo, M. E.; Grant, W. C.; Hemphill-Haley, E.; Kesley, H. M.; Jacoby, G. C.; Nishenko, S. P.; Palmer, S. P.; Peterson, C. D.; Reinhart, M. A. (1995). Summary of coastal geologic evidence for past great earthquakes at the Cascadia subduction zone. *Earthquake Spectra* **11**, 1-18

Babu, N.; Suresh Babu, D.S.; Mohan Das, P.N. (2007). Impact of tsunami on texture and mineralogy of a major placer deposit in southwest coast of India. *Environmental Geology* **52**, 71-80

Borrego, J.; López González, N.; Carro, B. (2004). Geochemical signature as palaeoenvironmental markers in Holocene sediments of the Tinto River estuary (Southwestern Spain*). Estuar. Coast. Shelf Sci*. **61**, 631-641

Borrego, J.; Morales, J.A.; Pendón, J.G. (1993). Elementos morfodina micos responsables de la evolucion reciente del estuario bajo del rio Guadiana (Huelva). *Geogaceta* **11**, 86-89

Borrego, J.; Ruiz, F.; González-Regalado, M. L.; Pendón, J. G.; Morales, J. A. (1999). The Holocene transgression into the estuarine central basin of the Odiel River mouth (Cádiz Gulf, SW Spain): lithology and faunal assemblages. *Quat. Sci. Rev*. **18**, 769- 788

Boswell, M.T. & Patil, G.P. (1971). Change mechanisms generating the logarithmic series distribution used in the analysis of number of species and individuals. In Statistical Ecology, Vol. 3. Ed. G.P. Patil, E.C. Pielou and W.E. Waters, 99-130. University Park, PA: Pennsylvania State University Press

Bronk Ramsey, C.; Dee, M.; Lee, S.; Nakagawa, T.; Staff, R. (2010). Developments in the calibration and modelling of radiocarbon dates. *Radiocarbon,* **52** (3), 953-961.

Bruzzi C. & Prone A. (2000). A method of sedimentological identification of storm and tsunami deposits: Exoscopic analysis, preliminary results. *Quaternaire* **11**, 167-177

Bryant, E.A. (2001). Natural Hazards. Cambridge University Press, Hong Kong

Bryant, E.A.; Young, R.W.; Price, D.M. (1992). Evidence of tsunami sedimentation on the southeastern coast of Australia. *Journal of Geology* **100**, 753-765

Buzas, M. A. (1979). The measurement of species diversity. In: Lipps, J.H.,Berger, W. H., Buzas, M. A., Douglas, R. G. and Ross, C. A., Foraminiferal ecology and paleoecology. *Society of Economic Paleontologists and Mineralogists, Houston, Short Course* **6**, 3-10.

C.E.E.P.Y.C. (1979). Plan de estudio de la dinamica litoral de la provincia de Huelva. Informe Direccion General de Puertos y Costas, Ministerio Obras Publicas, Madrid.

Campos, M.L. (1991). Tsunami hazard on the Spanish coasts of the Iberian Peninsula. *Science of Tsunami Hazards* 9, 83-90.

Campos, M.L., (1992). El riesgo de tsunamis en España. Análisis y valoración geográfica. *Monografías Instituto Geográfico Nacional* **9**, Madrid.

Casas, J. & Urdiales, C. (1995). "Introducción a la Gestión Hidráulica de las Marismas del Parque Nacional de Doñana" en *Bases ecológicas para la restauración de humedales en la cuenca Mediterránea*. Montes, C. (ed.) Consejería de Medio Ambiente, Junta de Andalucía. Sevilla.

Cearreta, A. (1988). Population dynamics of benthic foraminifera in the Santoña estuary, Spain. *Revue de paléobiologie*, *volume special **2***, 721 – 4.

Cita, M.B. & Rimoldi, B. (1997). Geological and geophysical evidence for a Holocene tsunami deposit in the eastern Mediterranean deep-sea record. *Journal of Geodynamics* 24, 293-304.

Clague, J.J.; Bobrowsky, P.T.; Hutchinson, I. (2000). A review of geological records of large tsunami at Vancouver Island, British Columbia. *Quaternary Science Reviews* **19**, 849-863.

Costa, P. J. M.; Leroy, S. A. G.; Kershaw, S.; Dinis, J. (2005). Tsunamis: causes, behaviour and sedimentary signature. Studies on the AD 1755 (Portugal)

Cuena, G.J. (1991). Proyecto de regeneracion de las playas de Isla Cristina. Memoria M.O.P.T., Madrid

Cundy, A.B., et al., (2000). Coastal wetlands as recorders of earthquake subsidence in the Aegean: a case study of the 1894 Gulf of Atalanti earthquakes, central Greece. *Marine Geology* **170** (1–2), 3–26.

Dabrio, C. J.; Zazo, C.; Lario, J.; Goy, J. L.; Sierro, F. J.; Borja, F.; González, J. A.; Flores, J. A. (2000). Depositional history of estuarine infill during the last

postglacial transgression (Gulf of Cadiz, southern Spain). *Mar. Geol.* **162**, 381-404.

Dansgaard, W.; Johnsen, S.J.; Møller, J. (1969). One thousand Centuries of Climatic Record from Camp Century on the Greenland Ice Sheet. *Science* **166**, 377-381

Dawson A. G.; Foster, I. D. L.; Shi, S.; Smith, D.E. & Long D. (1991). The identification of tsunami deposits in coastal sediment sequences. *Science of Tsunami Hazards* **9**, 73-82.

Dawson A.G.; Hindson R.; Andrade C.; Freitas C.; Parish R.; Bateman M. (1995). Tsunami sedimentation associated with the Lisbon earthquake of November 1755 AD: Boca do Rio, Algarve, Portugal. *The Holocene* **5**, 209-215

de Rijk, S.; Jorissem, F. J.; Rohling, E. J.; Troelstra, S. R. (2000). Organic flux control on bathymetric zonation of Mediterranean benthic foraminifera. *Marine Micropaleontology* **40**, 151-166.

Debenay, J.P. & Guillou, J.J. (2002). Ecological transitions indicated by foraminiferal assemglages in paralic environments. *Estuaries*, **25**, 1107 – 20.

Debenay, J.P.; Tsakiridis, E.; Soulard, R.; Grossel, H. (2001). Factors determining the distribution of foraminiferal assemblages in Port Joinville Harbor (Ile d'Yeu, France): the influence of pollution. *Marine Micropaleontology* **43**, 75-118.

Diz, P. & Francés, G. (2008). Distribution of live benthic foraminifera in the Ría de Vigo (NW Spain). *Marine Micropaleontology* **66**, 165-191.

Diz, P.; Francés, G.; Rosón, G. (2006). Effects of contrasting upwelling-downwelling on benthic foraminiferal distribution in the Ría de Vigo (NW Spain). *Journal of Marine Systems* **60**, 1-18

Dominey-Howes, D.; Dawson, A.; Smith, D. (1998). Late Holocene coastal tectonics at Falasarna, western Crete: a sedimentary study. In: Stewart, I., Vita-Finzi, C. (Eds.), Coastal Tectonics. Special Publications. *Geological Society*, London, 343–352

Donnici, S. & Barbero, R. S. (2002). The benthic foraminiferal communities of the northern Adriatic continental shelf. *Marine Micropaleontology* **44**, 93-123

Einsele, G.; Chough, S. K.; Shiki, T. (1996). Depositional events and their records - an introduction. *Sedimentary Geology* **104**, 1-9.

Ernst, S.; Bours, R.; Duijnstee, I.; Van Der Zwaan, B. (2005). Experimental effects of an organic matter pulse and oxygen depletion on a benthic foraminiferal shelf community. *Journal of Foraminiferal Research* **35**, 177-197.

Ernst, S.; Duijnstee, I.; Van der Zwaan, B. (2002). The dynamics of the benthic foraminiferal microhabitat: recovery after experimental disturbance. *Marine Micropaleontology* **46**, 343-361.

Fatela, F., & Taborda, R. (2002). Confidence limits of species proportions in microfossil assemblages. *Marine Micropaleontology* **45**, 169-174.

Fisher, R.A.; Corbet, A.S.; Williams, C.B. (1943). The relation between the number of species and the number of individuals in a random sample of an animal population. *Journal Animal Ecology* **12**, 42 – 58.

Foster, I.D.L.; Albon, A . J.; Bardell, K.M.; Fletcher, J.C.; Jardine, T.C.; Mothers, R.J.; Pritchard, M.A.; Tu rner, S.E. (1991). High energy coastal sedimentary deposits; an evaluation of depositional processes in southwest England. *Earth Surface Processes and Landforms* **16**, 341-356.

Frezza, V. & Carboni, M. G. (2009). Distribution of recent foraminiferal assemblages near the Ombrone River mouth (Northern Tyrrhenian). *Micropaléontologie* **52**, 43-66

Gadi, S.D. & Rajashekhar, K.P. (2007). Changes in inter-tidal foraminifera following tsunami inundation of Indian coast Subhadra. *Indian Journal of Marine Sciences* 36 (1), 35-42

Galbis, J., 1940. Catálogo sísmico de la zona comprendida entre los meridianos 5ºE y 20ºW de Greenwich y los paralelos 45º y 25ºN. Madrid, *Dirección General del Instituto Geogr á fi c o Catastral*, 277.

García Novo, F. & Marín, C. (2005). Doñana: Agua y Biosfera. Ed. Ministerio de Medio Ambiente. Confederación Hidrográfica del Guadalquivir. Madrid. ISBN: 84-609-6326-8.

García Viñas, J. I.; Mintegui, J.A.; Robredo, J.C. (2005). La vegetación en la marisma del Parque Nacional de Doñana en relación a su régimen hidráulico. Serie Técnica Naturaleza y Parques Nacionales. Ed. Organismo Autónomo Parques Nacionales.

Gibson, T. G. & Buzas, M. A. (1973) Species diversity: patterns in modern and Miocene Foraminifera of the Eastern Margin of North America. *Geol. Soc. America Bull*. **84**, 217-238.

Goff, J.; Lane, E.M.; Arnold, J. (2009). The tsunami geomorphology of coastal dunes. *Natural Hazards and Earth SystemSciences* **9**, 847–854.

Gómez-Rodríguez, C.; Díaz-Paniagua, C.; Bustamante,J. (2011). Cartografia de lagunas temporales del Parque Nacional de Doñana. Agencia Andaluza del Agua, Consejeria de medio ambiente.

Gonzalez, R.; Dias, J. A.; Lobo, F.; Mendes, I. (2004). Sedimentological and paleoenvironmental characterisation of transgressive sediments on the Guadiana Shelf (Northern Gulf of Cadiz, SW Iberia). *Quaternary International* **120**, 133-144

Goof, J.R.; Crozier, M.; Sutherland, V.; Cochran, U. & Shane, P. (1998). Possible tsunami deposits from the 1855 earthquake, North Island. In: Stewart I.S. and Vita-Finzi C. (eds). *Coastal Tectonics*. Geological Society, London, Special Publications, 146, 353-374.

Goto, K.; Chagué-Goff, C.; Fujino, S.; Goff, J.; Jaffe, B.; Nishimura, Y.; Richmond, B.; Suguwara, D.; Szczuciński,W.; Tappin, D.R.; Witter, R.; Yulianto, E. (2011).Newinsights into tsunami risk from the 2011 Tohokuoki event. *Marine Geology* **290**, 46–50.

Goudie, A.S. (1996). The Geomorphology of the Seasonal Tropics. – In: Adams, W.M., A.S. Goudie and A.R. Orme (eds.): The Physical Geography of Africa. – Oxford: 148-160

Goy, J. L.; Zazo, C.; Dabrio, C. J.; Lario, J.; Borja, F.; Sierro, F. J.; Flores, J. A. (1996). Global and regional factors controlling changes of coastlines in southern Iberia (Spain) during the Holocene. *Quat. Sci. Rev*. **15**, 773-780.

Gràcia, E., et al., (2010). Holocene earthquake record offshore Portugal (SW Iberia): testing turbidite paleoseismology in a slow-convergence margin. *Quaternary Science Reviews* **29**, 1156–1172

Groves, J.R.; Rettori, R.; Payne, J.L.; Boyce, M.D.; Altiner, D.E.M. (2007). End-Permian mass extinction of Lagenide Foraminifers in the Southern Alps (Northern Italy). *Journal of of Paleontology* **81** (3), 415–434.

Guilbault, J.; Clague, J.J.; Lapointe, M. (1996). Foraminiferal evidence for the amount of coseismic subsidence during a late Holocene earthquake on Vancouver Island,West Coast of Canada. *Quaternary Science Reviews* **15** (8–9), 913–937

Gutiérrez Elorza, M. & J.L. Peña Monné (1992). Evolución climática y geomorfológica del Holo- ceno Superior (Cordillera Ibérica, Depresión del Ebro y Pre-Pirineo). – In: Cearreta, A. and F.M. Ugarte (eds.): The Late Quaternary in the Western Pyrenean Region. – Bilbao, 109-124

Harter, S.K. & Mitsch, W.J. (2003). Patterns of short-term sedimentation in a fresh-water created marsh. *Journal of Environmental Quality* **32**, 325-334

Hawkes, A. (2007). 2004 Indian Ocean tsunami sediment characteristics along the Malaysia-Thailand Peninsula, EOS Transactions. American Geophysical Union. Jt. Assem. Suppl., Acapulco, Mexico, Abstract#T43B-02.

Hawkes, A.D., et al., (2007). Sediments deposited by the 2004 Indian Ocean Tsunami along the Malaysia–Thailand Peninsula. *Marine Geology* **242**, 169–190.

Haynes, J.R. (1981). Foraminifera. Macmillan Publishers Ltd, London, 433.

Hayward, B.W., & Hollis, C. J. (1994). Brackish foraminifera in New Zealand: A taxonomic and ecologic review. *Micropaleontology* 40, 185–222

Hayward, B.W.; Grenfell,H.R.; Reid, C.M.; Hayward,K.A. (1999).Recent New Zealand shallow- water benthic foraminifera: taxonomy, ecologic distribution,

biogeography and use in paleoenvironmental assessment. *Institute of Geological & Nuclear Sciences monograph (New Zealand Geological Survey paleontological bulletin*, **21** (75),14–249.

Herguera, J.C. & Berger, W.H. (1991). Palaeoproductivity from benthic foraminifera abundance: glacial to postglacial change in the west-equatorial Pacific. *Geology* **19**, 1173–1176

Hindson, R.; Andrade, C.; Dawson, A. (1996). Sedimentary processes associated with the tsunami generated by the 1755 Lisbon earthquake on the Algarve Coast, Portugal. *Physics and Chemistry of the Earth* **21** (12), 57–63.

Hindson, R.; Andrade, C.; Parish, R. (1999). A microfaunal and sedimentary record of environmental change within the late Holocene sediments of Boca do Rio (Algarve, Portugal). *Geologie en Mijnbouw* **77** (3), 311–321

Hindson, R.A. & Andrade, C. (1999). Sedimentation and hydrodynamic processes associated with the tsunami generated by the 1755 Lisbon earthquake. *Quaternary International* **56**, 27-38.

Horton, B.P. & Edwards, R.J. (2005). The application of local and regional transfer functions to the reconstruction of Holocene sea levels, north Norfolk, England. *The Holocene*, **15**, 216 – 28

ICONA (1994). “Desarrollo Sectorial del Plan Rector de Uso y Gestión del Parque Nacional de Doñana en Materia de Manejo de los Recursos Hídricos”. Ministerio de Agricultura, Pesca y Alimentación. Madrid.

Jiménez, C.C. (2011). Mapa Guia Digital de Espacios Naturales: La guia interectiva más completa y actualizada del Espacio Natural de Doñana. Junta de Andalucia. Consejeria de Medio Ambiente.

Kent, M., & Coker, P. (1992). Vegetation description and analysis: a practical approach. Belhaven Press, London

Kortekaas S. (2002). Tsunamis, storms and earthquakes: distinguishing coastal flooding events. PhD Tesis. Coventry University.

Kortekaas, S. & Dawson, A. (2007). Distinguishing tsunami and storm deposits: an example from Martinhal, SW Portugal. *Sedimentary Geology* **200**, 208–221.

Kortekaas, S.; Andrade, C.; Andrade, A.M.(1998ª). Litoestratigrafia e foraminiferos do enchimento sedimentar da baixa do Martinhal - Algarve (Portugal)-dados preliminares. *V Congresso Nacional de Geologia*, Lisboa, IGN, SGP, **84**(1), C-55/C-58.

Kortekaas, S.; Andrade, C.; Dawson, A. (1998b). Palaeotsunami deposits at Martinhal, South West Portugal, associated with the earthquake of November 1st, 1755 A D. In S. C. Stiros, P.A. Pirazzoli, (conv.), *Meeting on Rapid Coastal Changes in the Late Quaternary* INQUA, Greece, **29**.

Lamb, H.H. (1971). Climates and Circulation Regimes Developed over the Northern Hemisphere during and since the Last Ice Age. *Palaeogeography, Palaeoclimatology, Palaeoecology* **10**, 125-162

Lapidus D. F. (1990). Collins Dictionary of Geology. *Harper Collins*, London **519**, 460-464.

Lario, J. (1996). Último y Presente Interglacial en el área de conexión Atlántico-Mediterráneo: variaciones del nivel del mar, paleoclima y paleoambientes. Ph. D. Thesis, Universidad Complutense de Madrid, Madrid.

Lario, J.; Luque, L.; Zazo,C.; Goy,J.L.; Spencer,C.; Cabero,A.; Bardají, T.; Borja, F.; Dario, C.J.; Civis,J.; González-Delgado, J.A.; Borja, C.; Alonso-Azcárate, J. (2010).Tsunami vs. Storm surge deposits: a review of the sedimentological and geomorphological records of extreme wave events (EWE) during the Holocene in the Gulf of Cadiz, Spain. *Zeitschrift fur Geomorphologie* **54** (3), 301-316

Lario, J.; Luque,L.; Zazo,C.; Goy, J.L.; Spencer,C.; Cabero, A.; Bardají, T.; Borja, F.; Dabrio, C.J.; Civis, J.; González-Delgado, J.A.; Borja, C.; and Alonso-Azcárate, J. (2010). Tsunami vs. storm surge deposits: a review of the sedimentological and geomorphological records of extreme wave events (EWE) during the Holocene in the Gulf of Cadiz, Spain. *Zeitschrift für Geomorphologie* **54**, (3), 301-316

Lario, J.; Zazo, C.; Goy, J.L.; Silva, P.G.; Bardaji, T.; Cabero, A.; Dabrio, C.J. (2011). Holocene palaeotsunami catalogue of SW Iberia. *Quaternary International* **242**, 196–200.

Lee, J.J. & Anderson, O.R. (1991). Cytology and fine structure. In: Lee, J.J., Anderson, O.R. (Eds.), *Biology of Foraminifera*. *Academic Press Inc*., San Diego, 7–40.

Legendre, P. & Legendre, P. (1998). Numerical Ecology.

Leroy, S. (2006). From natural hazards to environmental catastrophe, past and present. *Quaternary Internation*.

Levy, A., (1991). Peuplements actuels et thanatocénoses á Soritidae et Peneroplidae des keys de Floride (USA). *Oceanologia acta*, **14**, 515 – 24

Levy, A.; Mathieu, R.; Poignant, A.; Rosset-Moulinier, M.; Ubaldo, M.; Lebreiro, S. (1995). Foraminiferes actuels de la Marge Continentale Portugaise - Inventaire et Distribuition. Memórias do Instituto Geológico e Mineiro, Lisboa.

Lin, J. (1992) – "Paleoecology, paleoclimate and paleogeography of Quaternary foraminiferal faunas in China. Ph. D. Thesis, Free Uniersity of Brussels, 152.

Linke, P. & Lutze, G.F. (1993). Microhabitat preferences of benthic foraminifera — a static concept or a dynamic adaptation to optimize food acquisition. *Marine Micropaleontology* **20**, 215–234.

Liu, K. B. & Fearn, M. L. (1993). Lake-sediment record of late Holocene hurricane activities from coastal Alabama. *Geology* **21**, 793-796.

Liu, K-B. & Fearn, M.L. (2000b). Holocene history of catastrophic hurricane landfalls along the Gulf of Mexico coast reconstructed from coastal lake and marsh sediments. *Current Stresses and Potential Vulnerabilities: Implications of Global Change for the Gulf Coast Region of the United States*, ed. Z.H. Ning and K. Abdollahi, 38-47.

Liu, K-B. & Fearn, M.L.(2000a). Reconstruction of prehistoric landfall frequencies of catastrophic hurricanes in NW Florida from lake sediment records. *Quaternary Research* **54**., 238-245.

Lloyd, M. & Ghelardi, R. J. (1964). A table for calculating the «equitability» component of species diversity. *J. Anim. Ecol.* **33**, 217-225

Lobo, F. J.; Hernández-Molina, F. J.; Somoza, L.; Díaz del Río, V. (2001). The sedimentary record of the post-glacial transgression on the Gulf of Cádiz continental shelf. *Mar. Geol.* **178**, 171-195.

Lobo, F. J.; Hernández-Molina, F. J.; Somoza, L.; Díaz del Río, V.; Dias, J. A. (2002). Stratigraphic evidence of an Upper Pleistocene TST to HST complex on the Cádiz Gulf continental shelf (southwest Iberian Peninsula*). Geo-Mar. Let*. **22**, 95-107.

Loeblich, A.R. & Tappan, H. (1987). Foraminiferal Genera and their Classification. Van Nostrand Reinhold, London.

Loeblich, A.R. & Tappan, H. (1992). Present status of foraminiferal classification. In: Takayanagi, Y., Saito, T. (Eds.), *Studies in Benthic Foraminifera*, Proceedings of the 4th International Symposium on Benthic Foraminifera, Sendai 1990 (BENTHOS '90). Tokai University Press, Tokai University, Tokyo, 93–102.

Luque, L.; Lario, J.; Civis, J.; Silva, P. G.; Zazo, C.; Goy, J. L.; Dabrio, C. J. (2002). Sedimentary record of a tsunami during Roman times, Bay of Cadiz, Spain*. J. Quat. Sci.* **17**, 623-631

Luque, L.; Lario, J; Zazo, C.; Goy, J.L.; Dabrio, C.J.; Silva, P.G. (2001). Tsunami deposits as paleoseismic indicators: examples from the Spanish coast. *Acta Geologica Hispanica* **36**, 197-211

Luque, L.; Zazo, C.; Goy, J.L.; Dabrio, C.J.; Civis, J.; Lario, J.; Gómez - Ponce, C. (1999). Los depósitos del tsunami de Lisboa de 1755. Su registro en la Bahía de Cádiz: Flecha de Valdela grana (Spain). In L. Pallí Buxó, C. Roqué Pau (eds.), *Avances en el estudio del Cuaternario Español*, Girona, 63-66.

Lynts, J.W. (1971). Distribution and model studies on foraminifera living in Buttonwood Sound, Florida Bay. *Miami Geological Society* **1**, 73–245

Maddy, D. & Brew, J.S. (1995). Statistical modelling of Quaternary science data.Technical Guide 5. Quaternary Research Association, Cambridge

Magurren, A. (1991) – "Ecological Diversity and its Measurement". Chapman and Hall, *Princeton University Press*, 179 .

Mamoa, B.; Strotz, L; Dominey-Howes, D. (2009) .Tsunami sediments and their foraminiferal assemblages Briony. *Earth-Science Reviews* **96**, 263–278

Margalef, R. (1958). Information theory in ecology. *General Systems* **3**: 36-71

Margalef, R. (1974). *Ecologia.* Ediciones Omega, Barcelona, 31, 237, 239, 243

Martins, V., & Gomes, V. (2004). "Foraminíferos da Margem Continental NW Ibérica, Sistemática, Ecologia e Distribuição." Agenda Comum - Comunicação Lda

Martins, V.; Dubert, J.; Jouanneau, J.-M.; Weber, O.; da Silva, E. F.; Patinha, C.; Alveirinho Dias, J. M.; Rocha, F. (2007). A multiproxy approach of the Holocene evolution of shelf-slope circulation on the NW Iberian Continental Shelf. *Marine Geology* **239**, 1-18

Martins, V.; Jouanneau, J.-M.; Weber, O.;Rocha, F. (2006a). Tracing the late Holocene evolution of the NW Iberian upwelling system. *Marine Micropaleontology* **59**, 35-55.

McIntosh, R.P. (1967). An Index of Diversity and the Relation of Certain Concepts to Diversity. *Ecology* **48**, 392–404

McMurty, G., et al. (2007). Elevated marine deposits in Bermuda record a late Quaternary megatsunami. *Sedimentary Geology* **200**, 155–165

Menanteau, L. (1979). Les Marismas du Guadalquivir. Exemple de transformation d'un paysage alluvial au cours du Quaternaire récent. Thése 3er Cycle, Paris-Sorbonne University, Paris.

Mendes, I. (2010). Benthic foraminifera as palaeoenvironmental indicators in the Northern Gulf of Cadiz. Doctoral Thesis at University of Algarve.

Miao, Q. & Thunell, R.C. (1993). Recent deep-sea benthic foraminiferal distributions in the South China and Sulu Seas. *Marine Micropaleontology* **22** (1–2), 1–32.

Milker, Y. & Schmiedl ,G. (2012). A taxonomic guide to modern benthic shelf foraminifera of the western Mediterranean Sea. *Palaeontologia Electronica* **15** (2),134

Ministerio de Medio Ambiente (MMA) (2001). “Documento Marco para el Desarrollo del Proyecto Doñana 2005”. Regeneración hídrica de las cuencas y cauces vertientes a las marismas del Parque Nacional de Doñana. Informe técnico. Madrid.

Mojtahid, M.; Jorissen, F.; Lansard, B.; Fontanier, C.; Bombled, B.; Rabouille, C. (2009). Spatial distribution of live benthic foraminifera in the Rhône prodelta: Faunal response to a continental-marine organic matter gradient. *Marine Micropaleontology* **70**, 177-200

Moodley, L. (1990b). Southern North Sea seafloor and subsurface distribution of living benthic foraminifera. *Netherlands Journal of Sea Research*, **27**, 51 – 71.

Moreira de Mendoça, J.J. (1758): Historia universal dos terremotos, que tem havido no mundo. – Off . Antonio Vicente da Silva, Lisboa, 272.

Morton, R.A.; Gelfenbaum, G.; Jaffe, B.E. (2007). Physical criteria for distinguishing sandy tsunami and storm deposits using modern examples. *Sedimentary Geology* **200**, 184–207.

Murray, A. E. (2006). Ecology and Applications of Benthic Foraminifera. Cambrige University Press.

Murray, J. W. (1971). "An Atlas of British Recent Foraminiferids." Heinemann Educational Books, London

Murray, J. W. (1971). "An Atlas of British Tecent Foraminiferids." Heinemann Educational Books, London

Murray, J.W. (1963). Ecological experiments on Foraminiferida. *Journal of Marine Biological Association*, UK, **43**, 621 – 42

Myers, E.H. (1943). Life activities of foraminifera in relation to marine ecology. *Proceedings of the American Philosophical Society*, **86**, 439 – 58

Nagendra, R.; Kamalak-Kannan, B.V.; Sajith, C; Sen, G.; Reddy, A.N.; Srinivasalu, S. (2005). A record of foraminiferal assemblage in tsunami sediments along Nagappattinam coast, Tamil Nadu. *Current Science 89*, **11**.

Nanayama, F. & Shigeno, K. (2006). Inflow and outflow facies from the 1993 tsunami in southwest Hokkaido. *Sedimentary Geology* **1287**, 139–158.

Nanayama, F.; Shigeno, K.; Satake, K.; Shimokawa, K.; Koitabashi, S.; Miyasaka, S. & Ishii, M. (2000). Sedimentary differences between the 1993 Hokkaido-nansei-oki tsunami and the 1959 Miyakojima typhoon at Taisei, south-western Hokkaido, northern Japan. *Sedimentary Geology* **135**, 255-264.

Narayan, Y.R.; Barnes, C.R.; Johns, M.J. (2005). Taxonomy and biostratigraphy of Cenozoic foraminifers from Shell Canada Wells, Tolfino Basin, offshore Vancouver Island, British Columbia. *Micropaleontology* **51** (2), 101–167

Navarro, R.S. (2009). Environmental flows in the marsh of the National Park of Doñana and its area of influence .*Synthesis report,* Madrid, Spain.

Odum, E. P. (1997), Ecology: A bridge between Science and Society.Sinauer Associates Publishers, Sunderland, Mass., USA.

Palma, R.M.; López-Gómez, J.; Piethé, R.D. (2007). Oxfordian ramp system (La Manga Formation) in the Bardas Blancas area(Mendoza Province)Neuquén Basin, Argentina: Facies and depositional sequences. *Sedimentary Geology* **195** (3–4), 113–134

Papadopoulos, G.A.; Gràcia, E.; Urgeles, R.; Sallares, V.; DeMartini, P.M.; Pantosti, D.; González, M.; Yalciner, A.C.; Mascle, J.; Sakellariou, D.; Salamon, A.; Tinti, S.; Karastathis, V.; Fokaefs, A.; Camerlenghi, A.; Novikova, J.T.; Papageorgiou, A. (2014). Historical and pre-historical tsunamis in the Mediterranean and its connected seas: Geological signatures, generation mechanisms and coastal impacts. *Marine Geology* **354**, 81–109

Paris, R.; Fournier, J.; Poizot, E.; Etienne, S.; Mortin, J.; Lavigne, F.; Wassmer, P. (2010). Boulder and fine sediment transport and deposition by the 2004 tsunami in Lhok Nga (western Banda Aceh, Sumatra, Indonesia): a coupled offshore–onshore model. *Marine Geology* **268**, 43–54.

Peet, R. K. (1974). The measurement of species diversity. *Annu. Rev. Ecol. Syst.* **5,** 285-307

Pereira de Sousa, F. L. (1919). O Terramoto do 1 de Novembro de 1755, Um estudo demográfico. *Servicos Geologicos de Portugal* **1, 2**.

Petit-Maire, N.; Beaufort, L.; Page, N. (1997). Holocene Climatic Change and Man in the Present- Day Sahara Desert. – In: Dalfes, H.N., G. Kukla and H. Weiss (eds.): Third Millenium BC Climate Change and Old World Collapse. Advanced Research Work- shop held at Kemer, Turkey, Sept. 19-24, 1994. – *NATO ASI Series I* **49**. – Berlin et al., 297-308

Pielou, E. C. (1966). The measurement of diversity in different types of biological collections. *J. Theor. Biol.* **13**, 131-144.

Pielou, E. C. (1975). *Ecological diversity.* John Wiley & Sons, New York., 209, 215, 238, 239, 239, 244, 245

Pinegina, T. K.; Bourgeois, J.; Bazanova, L. I. (2003). A millennial-scale record of Holocene tsunamis on the Kronotskiy bay coast, Kamchatka, Russia. *Quaternary Research* **59**, 36-47.

Pinegina, T.K.; Bourgeois, J.; Bazanova, L.I.; Melekestsev & Brait-Seva, O.A. (2003). A millennial-scale record of Holocene tsunamis on the Kronotskiy Bay coast, Kamchatka, Russia. *Quaternary Research* **59**, 36-47.

Piper, D. J.W. & Panagos, A. G. (1979). Recent salt marsh and intertidal mudflat foraminifera from the western coast of Greece. *Rivista Italiana di Paleontologia e Stratigrafia* **85**, 243–266.

Ramirez-Herrera, M.T., et al., (2007). Sedimentary record of late-Holocene relative sea-level change and tectonic deformation from the Guerrero Seismic Gap, Mexican Pacific Coast. *The Holocene* **17** (8), 1211–1220

Reicherter, K. (2001). Paleoseismological advances in the Granada Basin (Betic Cordilleras, southern Spain). *Acta Geol. Hispan* **36**, 267-281.

Reimer, P. J.; Brown, T. A.; Reimer, R. W. (2004). Discussion: Reporting and calibration of post-bomb C-14 data. *Radiocarbon,* **46** (3), 1299-1304.

Rodríguez Ramírez, A.; Siljeström, P.; Clemente, L.; Rodríguez Vidal, J.; Moreno, A. (1995). Caracterización de las pautas geomorfológicas de la flecha litoral de Doñana. *Rev. Teled* **5**, 28-32.

Rodríguez Ramírez,A.; Rodríguez Vidal,J.; Cáceres, L.M. ; Clemente, L.; Belluomini, G. ; Manfra, L. ; Improta, S. ; de Andrés, J.R. (1996). Evolución costera de la desembocadura del Gualdalquivir en los últimos 6.000 años (SW España). *Geogaceta* **20** (5), 1996

Rositasari, R. & Soedibjo, B.S. (2008). Post mortem foraminifera distribution in Aceh Water post-tsunami. *Journal of Coastal Development* **12** (1), 30-40

Ruiz, F.; González-Regalado, M. L.; Pendón, J. G.; Abad, M.; Olías, M.; Muñoz, J. M. (2005). Correlation between foraminifera and sedimentary environments in recent estuaries of Southwestern Spain: Applications to Holocene reconstructions. *Quaternary International* **140-141**, 21-36

Ruiz, F.; Pozo, M. ;Carretero, M. I.; Abad, M.; González-Regalado, M. L.; Muñoz, J. M.; Rodríguez-Vidal, J.; Cáceres, L. M.; Pendón, J. G.; Prudêncio, M. I.; Dias, M. I. (2010). Birth, evolution and death of a lagoon: Late Pleistocene to Holocene palaeoenvironmental reconstruction of the Doñana National Park (SW Spain). *Lagoons: Biology, Management and Environmental Impac*t , 1-26

Ruiz, F.; Rodríguez-Vidal, J.; Abad, M.; Cáceres, L.M.; Carretero, M.I.; Pozo, M.; Rodríguez-Llanes, J.M.; Gómez-Toscano, F.; Izquierdo, T.; Font, E.; Toscano, A. (2013). Sedimentological and geomorphological imprints of Holocene tsunamis in southwestern Spain: An approach to establish the recurrence period. *Geomorphology* **203**, 97–104

Salvany, J. M.; Medialvilla, C.; Mantecón, R.; Manzano, M. (2001). Geología del Valle del Guadiamar y áreas colindantes. *Bol. Geol. y Min.* **spec. vol.,** 57-68

Satyanarayana, K., et al., (2007). A note on foraminifera, grain size and clay mineralogy of tsunami sediments from Karaikal–Nagore–Nagapattiuam Beaches, Southeast Coast of India. *Journal Geological Society of India* **69** (1), 70–74.

Scheffers, F. & Kelletat, D. (2005). Boulder deposits on the southern Spanish Atlantic coast: possible evidence for the 1755 AD Lisbon Tsunami. *Sci.Tsunami Haz*. **23**, 25- 38.

Schönfeld, J.; Alve, E.; Geslin ,E.; Jorissen, F.; Korsun, S.; Spezzaferri ,S. (2012). The FOBIMO (FOraminiferal BIo-MOnitoring) initiative—Towards a standardised protocol for soft-bottom benthic foraminiferal monitoring studies. *Marine Micropaleontology* **94–95**, 1–13

Schönwiese, C. (1995). Klimaänderungen – Daten, Analysen, Prognosen. – Berlin

Schutt, B. (2005). Late Quaternary Environmental Change on the Iberian Peninsula. *DIE ERDE* **136**, 3–14.

Scott, D.B. (1976). Brackish-water foraminifera from southern California and description of *Polysaccammina ipohalina* n. gen., n. sp.: Journal of Foraminiferal Research **6**, 312–321.

Selby, K. A. & Smith, D. E. (2007). Late Devensian and Holocene sea-level changes on the Isle of Skye, Scotland, UK. *J. Quat. Sci*. **22**, 119-139.

Sen Gupta, B.K. (1999). Systematics of modern foraminifera. In: Sen Gupta, B.K. (Ed.), *Modern Foraminifera*. Kluwer Academic, London, 7–36.

Singarasubramanian, S.R.; Mukesh, M.V.; Manoharan, K.; Murugan, S.; Bakkiaraj, D.; Meter, A.J.; Seralathan, P. (2006). Sediment characteristics of the M-9 tsunami event between Rameswaram and Thoothukudi, Gulf of Mannar, southeast coast of India. *Science of Tsunami Hazards* **25**, 160-172

Soares, A.M.M. &, Martins, J.M.M. (2010). Radiocarbon dating of marine samples from Gulf of Cadiz: The reservoir effect. *Quaternary International* **221**, 9–12

Strotz, L. (2003). Holocene foraminifera from Tuross Estuary and Coila Lake, south coast, New SouthWales: a preliminary study. *Proceedings of the Linnean Society of New SouthWales* **124**, 163–182

Sturrock, s. & Murray, J. W. (1981). Comparison of low energy middle shelf foraminiferal faunas: Celtic Sea and western English Channel. In Neale, J.W. and Brasier, M.D., eds. *Microfossil from Recent and Fossil Shelf Seas*. Chichester: Ellis Horwood, 250 – 60.

Sun, X.; Corliss, B.; Brown, C.; Showers,W. (2006). The effect of primary productivity and seasonality on the distribution of deep-sea benthic foraminifera in the North Atlantic. *Deep-Sea Research I* **53**, 28–47.

Switzer, A.D. (2008). 20 years of paleotsunami studies on coastal sandsheets: a review. *2nd International Tsunami Field Symposium*. IGCP Project 495. *GI2S Coast Res.* **6**, 163–165

Trog, C.; Höfera, D.; Frenzel, P.; Camacho, S.; Schneider, H.; Mäusbacher, R. (2013). A multi-proxy reconstruction and comparison of Holocene palaeoenvironmental changes in the Alvor and Alcantarilha estuaries (southern Portugal). *Revue de micropaléontologie* **56**, 131–158

Uchida, J.; Abe, K.; Hasegawa, S.; Fujiwara, O. (2007ª). Studies on the source of run-up tsunami deposits based on foraminiferal tests and their hydrodynamic verification. *Quaternary Research* (Daiyonki-Kenkyu) **46** (6), 533–540.

Uchida, J.; Abe, K.; Hasegawa, S.; Fujiwara, O.; Kamataki, T. (2004). The depositional processes of tsunami deposits based on sorting of foraminiferal tests—a case study of tsunami deposits at Tateyama, southern part of the Boso peninsula, central Japan. *Memoirs of Geological Society of Japan* **58**, 19–33

Uchida, J.; Fujiwara, O.; Hasegawa, S.; Kamataki, T. (2010). Sources and depositional processes of tsunami deposits: Analysis using foraminiferal tests and hydrodynamic verification. *Island Arc* **19**, 427–442

Udías, A.; López Arroyo, A.; Mezcua, J. (1976). Seismotectonic of the Azores-Alboran region. *Tectono physics* **31**, 259-289 .

Vanney, J.R. (1970). L'hydrologie du Bas Guadalquivir. *Publicaciones Departamento Geografia Aplicada* C.S.I.C., Madrid.

Vilanova, I.; Prieto, A. R.; Espinosa, M. (2006). Palaeoenvironmental evolution and sea-level fluctuations along the southeastern Pampa grasslands coast of Argentina during the Holocene. *J. Quat. Sci*. **21**, 227-242.

Vizcaino, A.; Gràcia, E.; Escutia, C.; Asioli, A.; García-Orellana, J.; Lebreiro, S.; Cacho, I.; Thouveny, N.; Larrasoaña, J. C.; Diez, S.; Dañobeitia, J. J. (2006a). Characterizing Holocene Paleoseismic Record in the SW Portuguese Margin. Geophys. *Res. Abstracts* **8**, 08469

Weiss, R. (2008). Sediment grains moved by passing tsunami waves: tsunami deposits in deep water. *Marine Geology* 250, 251–257

Wells, P.; Wells, G.; Cali, J.; Chivas, A. (1994). Response of deep-sea benthic foraminifera to Late Quaternary climate changes, southeast Indian Ocean, offshore Western Australia*. Marine Micropaleontology* **23**, 185–229.

Whittecar, G.R.; Megonigal, J.P.; Darke, A.K. (2001). Sedimentation patterns within tidal fresh-water marshes, Mattaponi River, Virginia. GSA Annual meeting, Boston, session 180, booth 69Yll, R.; Zazo, C.; Goy, J. L.; Pérez-Obiol, R.; Pantaleón-Cano, J.; Civis, J.; Dabrio, C.; González, A.; Borja, F.; Soler, V.; Lario, J.; Luque, L.; Sierro, F. J.; González- Hernández, F. M.; Lezine, A. M.; Denefle, M.; Roure, J. M. (2003). Quaternary palaeoenvironmental changes in south Spain. In: M. B., Ruiz Zapata, M., Dorado, A., Valdeolmillos, M. A., Gil, T., Bardají, I. Bustamante, & I. Martínez, (Eds.), *Quaternary climatic changes and environmental crises in the Mediterranean region.* Alcalá de Henares, 201-213.

Zazo, C.; Dabrio, C. J.; González, A.; Sierro, F. J.; Yll, E. I.; Goy, J. L.; Luque, L.; Pantaleón-Cano, J.; Soler, V.; Roure, J. M.; Hoyos, M.; Borja, F. (1999). The record of the later glacial and interglacial periods in the Guadalquivir marshlands (Mari López drilling, S. W. Spain). *Geogaceta* **26**, 119-122.

Zazo, C.; Dabrio, C. J.; Goy, J. L.; Lario, J.; Cabero, A.; Silva, P. G.; Bardají, T.; Mercier, N.; Borja, F.; Roquero, E. (2008). The coastal archives of the last 15 ka

in the Atlantic-Mediterranean Spanish linkage area: Sea level and climate changes. *Quat. Int*. **181**, 72-87.

Zazo, C.; Goy, J. L.; Hillaire-Marcel, C.; Dabrio, C. J.; Belloumini, G.; Improta, S.; Lario, J.; Bardají, T.; Silva, P. G. (1994). Holocene sequence of sea-level fluctuations in relation to climatic trends in the Atlantic-Mediterranean linkage coast. *J. Coast. Res*. **10**, 933-945.

IX. Appendix

Appendix 1 – Results of Grain size distribution of surface samples and sediment type, according to Folk & Ward (1957), calculated by GRADISTAT 14.0 program

VIII. Taxonomy and Plates

PHYLUM FORAMINIFERIDA Eichwald, 1830

ORDER LITUOLIDA

SUBORDER LITUOLINA

Superfamily LITUOLOIDEA

Family LITUOLIDAE de Blainville, 1827

Subfamily AMMOMARGINULININAE Podobina, 1978

Genus *Ammotium* Loeblich & Tappan, 1953

***Ammotium* sp.**

Plate 1, fig. 1a

SUBORDER RZEHAKININA

Superfamily RZEHAKINOIDEA

Family RZEHAKINIDAE Cushman, 1933

Genus *Miliammina* Heron-Allen and Earland, 1930

***Miliammina fusca* Brady, 1870**

Miliammina fusca (Brady 1870), Scott and Medioli, 1980, p. 38, pl. 2, figs. 1-3; Scott et al.,1991, p. 387, pl. 1, fig. 14: Javaux and Scott, 2003, p. 24, fig. 6, subfig. 7 and Camacho, D.S., 2012, p. 23, fig. 9.12

ORDER TEXTULARIIDA Delage & Hérouard, 1896

SUBORDER TEXTULARIINA Delage and Hérovard, 1896

Superfamily TEXTULARIOIDEA Ehrenberg, 1838

Family TEXTULARIIDAE Ehrenberg, 1838

Subfamily TEXTULARIINAE Ehrenberg, 1838

Genus *Textularia* Defrance, 1824

***Textularia* sp.**

Plate 1, fig. 2a

SUBORDER TROCHAMMINIDA

Superfamily TROCHAMMINOIDEA Schwager, 1877

Family TROCHAMMINIDAE Schwager, 1877

Subfamily TROCHAMMININAE Schwager, 1877

Genus *Trochammina* Parker & Jones, 1859

***Trochammina inflata* Montagu, 1808**

Plate 1, fig. 3 a-c

Trochammina inflata (Montagu), Scott and Medioli, 1980, p. 39, pl. 3, figs. 12-14 and pl. 4, figs. 1-3; Jones, 1994, p. 46, pl. 41, fig. 4; Debenay et al., 1998b, p. 75, pl. 2, figs. 16,17 and 20; and Camacho, D.S., 2012, vol.2, pg. 39, fig. 9.26

Subfamily JADAMMININAE Saidova, 1981

Genus *Jadammina* Bartenstein & Brand, 1938

***Jadammina macrescens* Brady, 1870**

Plate 1, fig. 4 a-d

Trochammina macrescens (Brady, 1870), Scott and Medioli (1980), p. 39, pl. 3, figs. 1-11; Javaux and Scott (2003), p. 24, fig. 6, subfigs. 14-19; Barbosa et al., 2005, p. 36, pl. 2, figs. 13-15

Jadammina macrescens (Brady, 1870), Debenay et al., 2001, p. 86, pl. 1, fig.

ORDER SPIRILLINIDA Hohenegger & Piller, 1975

SUBORDER SPIRILLININA Ehrenberg, 1843

Family SPIRILLINIDAE Reuss & Fritsch, 1861

Genus *Spirillina* Ehrenberg, 1843

Spirillina sp.

***Spirillina vivipara* Ehrenberg, 1843**

Plate 1, fig. 7a

Spirillina vivipara Ehrenberg, 1843, Abh. Akad. Wiss. Berlin (Jahrg. 1841), pt. I, pp. 323, 422, pl. 3, fig. 41

Spirillina vivipara (Ehrenberg), Murray 1971, p. 145, pl. 60, figs. 1-2

ORDER MILIOLIDA Delage & Hérouard, 1896

SUBORDER MILIOLINA Delage and Hérovard, 1896

Superfamily CORNUSPIRACEA Schultze, 2854

Family CORNUSPIRIDAE Schultze, 2854

Subfamily CORNUSPIRINAE Schultze, 2854

Genus *Cornuloculina* Burbach, 1886

***Cornuloculina* sp.**

Plate 1, fig. 6a

Genus *Cornuspira* Schultze, 2854

***Cornuspira involvens* Reuss, 1850**

Plate 1, fig. 7a

Cyclogyra involvens (Reuss), Murray, 1971, p.53, pl. 18, figs. 1-3

Cornuspira involvens (Reuss), Jones, 1994, p.26, pl. 11, figs. 1-3

Superfamily MILIOLOIDEA Ehrenberg, 1839

Family SPIROLOCULINIDAE Wiesner, 1920

Genus *Adelosina* d' Orbigny, 1826

***Adelosina* sp.**

Plate 1, fig. 8 a-c

Family HAUERINIDAE Wiesner, 1920

Subfamily HAUERININAE Schwager, 1876

Genus *Quinqueloculina* d'Orbigny, 1826

***Quinqueloculina laevigata* d' Orbigny 1839**

Plate 1, fig. 9a

Quinqueloculina laevigata d'Orbigny, 1839, Paris: Béthume, tome 2, pt. 2, Zool., p. 143, pl.3, figs 31-33

Quinqueloculina laevigata d'Orbigny, Mendes et al.,2004, pl.1, fig.7.

***Quinqueloculina seminulum* Linnaeus 1758**

Plate 1, fig. 10 a-d

Serpula seminulum Linnaeus, 1758, Holmiae, Sweden, impensis L. Salvii, tomus 1, p. 786

Quinqueloculina seminulum (Linnaeus), Murray, 1971, p. 65, pl.24, figs. 1-6; Jones, 1994, p.21. pl. 5, fig. 6; Levy et al., 1995, p. 23, pl. 4, fig. 3 and Martins and Gomes, 2004, p. 53-54, fig. 2.26.

***Quinqueloculina stelligera* Schlumberger 1893**

Plate 1, fig. 11 a-c

Quinqueloculina stelligera Schlumberger, 1893, Soc. Zool. France, Mém., Paris, tome 6, p. 68, pl. 2, figs. 58-59

Quinqueloculina stelligera Schlumberger, Debenay et al., 2001, pl. 2, figs. 3-4

Subfamily MILIOLINELLINAE Vella, 1957

Genus *Triloculina* d'Orbigny, 1826

***Triloculina trigonula* Lamarck 1804**

Plate 2, fig. 1 a-b

Miliolina trigonula Williamson, 1858, Recent Foram. Great Britain, p. 84, pl. 7, figs. 180-182

Miliolina trigonula Brady, 1884, Challenger Rept., vol. 9, p. 164, pl. 3, figs. 15-16

ORDER LAGENIDA Delage & Hérouard, 1896

SUBORDER LAGENINA Delage & Hérouard, 1896

Superfamily NODOSARIOIDEA Ehrenberg, 1838

Family LAGENIDAE Reuss, 1862

Genus *Lagena* Walker & Boys, 1784

***Lagena* sp.**

Plate 2, fig. 2a

***Lagena striata* d'Orbigny, 1839**

Plate 2, fig. 3a

Oolina striata d' Orbigny, 1839, Levrault, Stasbourg, France, tome 5, pt. 5, p. 21, pl. 5, fig. 12

Lagena striata (d'Orbigny), Jones, 1994, p. 64, pl. 57, figs. 22, 24 and Levy et la., 1995, p. 28, pl. 5, fig. 13.

***Lagena sulcata* Walker & Jacob, 1798**

Plate 2, fig. 4a

Serpula (Lagena) sulcata Walker & Jacob, 1798, Kanmacher, Adam's essays on the microscope, Ed. 2, p. 634, pl. 14, fig.5.

Lagena sulcata (Walker & Jacob), Murray, 1971, p. 87, pl. 34, figs. 5-8

Genus *Fissurina* Reuss, 1850

***Fissurina marginata* Montagu, 1803**

Plate 2, fig. 5a

Vermiculum marginatum Montagu, 1803, J.S. Hollis, Romsey, England, p. 524

Fissurina marginata (Montagu), Murray, 2003, p. 17, fig. 5.3-5.4 and Martins and Gomes, 2004, p. 76-77, fig. 2.44

***Fissurina* sp.1**

Plate 2, fig. 6a

***Fissurina* sp.2**

Plate 2, fig. 7a

***Fissurina* sp.3**

Plate 2, fig. 8a

Superfamily POLYMORPHINOIDEA

Family ELLIPSOLAGENIDAE A. Silvestri, 1923

Subfamily ELLIPSOLAGENINAE Silvestri, 1923

Subfamily OOLININAE Loeblich & Tappan, 1961

Genus *Oolina* d'Orbigny, 1839

***Oolina squamosa* Montagu, 1803**

Plate 2, fig. 9a

Vermiculum squamosum Montagu, 1803, *Testacea britannica*, p. 526, pl. 14, fig. 2

Oolina squamosa Montagu, Murray, 1971, pag. 95, pl. 38, figs. 1-3

Superfamily STILOSTOMELLOIDEA Finlay, 1947

Family STILOSTOMELLIDAE Finlay, 1947

Genus *Stilostomella* Guppy, 1894

***Stilostomella* sp.**

Plate 2, fig. 10 a-b

ORDER ROTALIIDA Delage and Hérouard, 1896

SUBORDER ROTALIINA Delage and Hérouard, 1896

Superfamily BOLIVINOIDEA Glaessner, 1937

Family BOLIVINIDAE Glaessner, 1937

Genus *Bolivina* d'Orbigny, 1839

***Bolivina ordinaria* Pheleger and Parker, 1952**

Plate 2, fig. 11 a-b

Bolivina ordinaria Pheleger and Parker, 1952, Cushman Found. Foram. Res., Contr., Washington, D.C., vol. 3, pt. 1, p. 14.

Bolivina ordinaria Pheleger and Parker; Boltovskoy et al., 1980, p. 18, pl. 3, figs. 1-3 and Martins and Gomes, 2004, p. 90-91, fig. 2.53

Bolivina ordinaria (Pheleger and Parker), Mendes, I.,2010, p.205, pl. 2, fig. 3

Genus Brizalina Costa, 1856

***Brizalina striatula* Cushman, 1922**

Plate 2, fig. 12a

Bolivina striatula Cushman, 1995a; Levy et al., p. 32, pl.7, fig. 11

Bolivina striatula, Cushman, Martins and Gomes, 2004, p. 100-101, fig. 2.57

Superfamily CASSIDULINOIDEA d' Orbigny, 1839

Family CASSIDULINIDAE d' Orbigny, 1839

Subfamily CASSIDULININAE d' Orbigny, 1839

Genus *Cassidulina* d' Orbigny, 1826

***Cassidulina laevigata* d' Orbigny, 1826**

Plate 2, fig. 13a

Cassidulina laevigata d' Orbigny, 1826, Ann. Sci. Nat., Paris, France, ser. 1, tome 7, p. 282, pl. 15, figs. 4-5

Cassidulina laevigata d' Orbigny, Murray, 2003, p. 21, fgis. 6.8-6.10; Debenay et al., 2001, pl. 4, fig. 19 and Mendes, I., 2010, pg. 206, pl. 2, fig. 8.

***Cassidulina minuta* Cushman 1933**

Plate 2, fig. 14a

Cassidulina minuta Cushman, 1933, Cushman Lab. Forams. Res., Sharon, Mass., U.S.A., vol. 9, pt. 4, no. 137, p. 92, pl. 10, fig. 3.

Cassidulina minuta Cushman, Martins and Gomes, 2004, p. 123, fig. 2.69 and Mendes, I., 2010, pg. 206, pl. 2, fig. 9.

Superfamily TURRILINACEA Cushman, 1927

Family STAINFORTHIIDAE Reiss, 1963

Genus *Hopkinsina* Howe & Wallace, 1933

***Hopkinsina atlantica* Cushman, 1944**

Plate 2, fig. 15a

Hopkinsina pacifica Cushman var. atlantica Cushman, 1944, Cushman Lab. Forams. Res., Sharon, Mass., U.S.A., no. 12, p. 30, pl. 4, fig. 1.

Hopkinsina atlantica Cushman, Debenay et al., 2001, pl. 4, fig. 14 and Mendes, I., 2010, pg. 210, pl. 3, fig.1.

Genus *Stainforthia* Hofker, 1956

***Stainforthia complanata* Egger, 1895**

Plate 2, fig. 16a

Stainforthia complanata Egger, 1995, Fatela, p. 144, pl. 2, fig. 2

Fursenkoina complanata Egger, 1995; Yassini & Jones, pg. 154, figs. 580-581, 646-648

Superfamily BULIMINOIDEA Jones, 1875

Family SIPHOGENERINOIDIDAE Saidova, 1981

Subfamily TUBULOGENERININAE Saidova, 1981

Genus *Rectuvigerina* Mathews, 1945

***Rectuvigerina* sp.**

Plate 2, fig. 17a

Family BULIMINIDAE Jones, 1875

Genus *Bulimina* d' Orbigny, 1826

***Bulimina elongata* d'Orbigny 1846**

Plate 2, fig. 18 a-b

Bulimina elongata d'Orbigny, 1846, Paris: Gide et Comp., p. 187, pl. 11, figs. 19-20

Bulimina elongata d'Orbigny, Jones, 1994, p. 54, pl. 50, figs. 3-4; Levy et al., 1995, p. 35, pl. 7, fig. 10 and Mendes, I, 2010, p. 210, pl. 3, fig.6

***Bulimina marginata* d' Orbigny 1826**

Plate 3, fig. 1a

Bulimina marginata d' Orbigny, Murray, 1971, p. 119, pl. 49, figs. 1-7; Jones, 1994, p. 55, pl. 51, figs. 3-5; Levy et al., 1995, p. 35, pl. 7, fig. 12; Martins and Gomes, 2004, p. 148-150, fig. 2.83 and Mendes, I., 2010, p. 210, pl.3, fig. 7

Family BULIMINELLIDAE Hofker, 1951

Genus *Buliminella* Cushman, 1911

***Buliminella elegantissima* d'Orbigny, 1839**

Plate 3, fig. 2 a-b

Buliminella elegantissima d' Orbigny, 1839, Strasbourg, France, Levrault, tome 5, pt. 5, p. 51, pl. 7, figs. 13-14

Buliminella elegantissima (d' Orbigny), Murray, 1971, p. 105, pl. 42, figs. 1-4; Jones, 1994, p. 55, pl. 50, figs. 20-22 and Martins and Gomes, 2004, p. 157-158, fig. 2.89

Family UVIGERINIDAE Haeckel, 1894

Subfamily UVIGERININAE Haeckel, 1894

Genus *Uvigerina* d'Orbigny, 1826

***Uvigerina peregrina* Cushman, 1923**

Plate 3, fig. 3 a-b

Uvigerina peregrina Cushman, 1923, U.S. Nat. Mus., Bull, Washington, D.C., U.S.A., no. 104, p. 166, pl. 42, figs. 7-10

Uvigerina peregrina Cushman, Murray, 1971, p. 121, pl. 50, figs. 1-7; Levy et al., 1995, p. 38, pl. 8, fig. 11; and Martins and Gomes, 2004, p. 162-163, fig. 2.93-2.94

Subfamily ANGULOGERININAE Galloway, 1933

Genus *Trifarina* Cushman, 1923

***Trifarina angulosa* Williamson, 1858**

Plate 3, fig. 4a

Uvigerina angulosa Williamson, 1858, Williamson, W. C., On the Recent foraminifera of Great Britain, Ray Society, London, England, p. 67, pl. 5, fig. 140

Trifarina angulosa (Williamson), 1995a, Levy et al., p. 38-39, pl. 9, fig. 1 and Martins and Gomes, 2004, pg. 166-168, fig. 2.96

Family ROSALINIDAE Reiss, 1963

Genus *Rosalina* d' Orbigny, 1826

***Rosalina bradyi* Cushman, 1915**

Plate 3, fig. 5 a-d

Discorbis globularis (d'Orbigny) var. *bradyi* Cushman, 1915, U.S. Nat. Mus., Bull., Washington, D.C., U.S.A., no. 71, p. 12, pl. 8, fig.1

Rosalina bradyi (Cushman), Jones, 1994, p. 93, pl. 86, fig.8 and Debenay and Redois, 1997, pl. 3, fig. 36

Superfamily PLANORBULINOIDEA Schwager, 1877

Family PLANORBULINIDAE Schwager, 1877

Subfamily PLANORBULININAE Schwager, 1877

Genus *Planorbulina* d'Orbigny, 1826

***Planorbulina mediterranensis* d'Orbigny, 1826**

Plate 3, fig. 6 a-d

Planorbulina mediterranensis d'Orbigny, 1826, Ann. Sci. Nat., Paris, France, ser. 1, tome 7, p. 280, pl. 14, figs. 4-6

Planorbulina mediterranensis d'Orbigny, Murray, 1971, p. 179, pl. 75, figs. 1-6; Jones, 1994, p. 96, pl. 92, fig. 1; Levy et al., 1995, p. 44-45, pl. 10, fig.6; Martins and Gomes, 2004, p. 214-215, fig. 2.127 and Mendes, I., 2010, pg. 214, pl. 4, fig. 1.

Superfamily ASTERIGERINOIDEA d'Orbigny, 1839

Family ASTERIGERINATIDAE Reiss, 1963

Genus *Asterigerinata* Bermúdez, 1949

***Asterigerinata mamilla* Williamson, 1858**

Plate 3, fig. 7 a-d

Rosalina mamilla Williamson, 1858, Ray Society, London, England, p. 54, pl. 4, fig. 109

Asterigerinata mamilla (Williamson), Murray, 1971, p. 141, pl. 59, figs. 1-6; Levy et al., 1995, p. 46, pl. 10, fig. 10; Martins and Gomes, 2004, p. 218-219, fig. 2.129 and Mendes, I, 2010, p. 214, pl.4, fig. 2.

Superfamily NONIONOIDEA Schultze, 1854

Family NONIONIDAE Schultze, 1854

Subfamily NONIONINAE Schultze, 1854

Genus *Haynesina* Banner and Culver, 1978

***Haynesina germanica* Ehrenberg, 1840**

Plate 3, fig. 8 a-b

Nonion germanica (Ehrenberg, 1840)

Haynesina germanica (Ehrenberg), Langer, 2000, pg. 643, fig. 1, subfigs. A-C and Leorri and Cearreta, 2004, p. 78, pl. 1, fig. 3

Genus *Nonion* de Montfort, 1808

***Nonion fabum* Fichtel and Moll, 1798**

Plate 3, fig. 9 a-c

Nonion commune (d'Orbigny); Levy et al., 1995, p. 46, pl. 11, fig. 1

Nonion fabum (Fichtel and Moll), Jones, 1994, p. 108, pl. 109, figs. 12-13; Martins and Gomes, 2004, p. 223-224, fig. 2.132 and Mendes, I., 2010, pg. 214, pl. 4, fig. 3.

Genus *Nonionella* Rhumbler, 1949

***Nonionella stella* Cushman & Moyer, 1930**

Plate 3, fig. 10 a-c

Nonionella miocenica Cushman var. stella Cushman and Moyer, 1930, Contr. Cushman Lab. Foram. Res., Sharon, Mass., U.S.A., vol. 6, pt.3, no. 93, p. 56, pl. 7, fig. 17

Nonionella stella (Cushman and Moyer); Martins and Gomes, 2004, p. 229-230, fig. 2.136 and Mendes, I., 2010, p. 214, pl. 4, fig. 5.

Superfamily ROTALIOIDEA Ehrenberg, 1839

Family ROTALIIDAE Ehrenberg, 1839

Subfamily AMMONIINAE Saidova, 1981

Genus *Ammonia* Brünnich, 1772

***Ammonia beccarii* Linnaeus, 1758**

Plate 4, fig. 1 a-b

Ammonia beccarii (Linnaeus), Colom, 1974, p. 132, fig. 24, a-e; Martins and Gomes, 2004, p. 254, fig. 2.150D and p. 256, fig. 2.151; Camacho, D.S., 2012, vol.2, pg. 73, fig. 9.49

***Ammonia tepida* Cushman, 1926**

Plate 4, fig. 2 a-d

Ammonia tepida (Cushman),Debenay et al., 1998, p.238, figs. 6-7

Family ELPHIDIIDAE Galloway, 1933

Subfamily ELPHIDIINAE Galloway, 1933

Genus *Elphidium* de Montfort, 1808

***Elphidium complanatum* d'Orbigny, 1839**

Polystomella complanata d' Orbigny, 1839, Paris: Béthune, tome 2, pt. 2, Zool., p. 129, pl. 2, figs. 35-36

Elphidium complanatum (d'Orbigny), Martins and Gomes, 2004, p. 259-260, fig.2.153

***Elphidium crispum* Linnaeus, 1758**

Plate 4, fig. 3 a-b

Nautilus crispus Linnaeus, 1758, Impensis L. Salvii, Holmiae, Sweden, tomus 1, p. 709

Elphidium crispum (Linnaeus), Murray, 1971, p. 155, pl. 64, figs. 1-6; Jones, 1994, p. 109, pl. 110, figs. 6-7; Martins and Gomes, 2004, p. 261-262, fig. 2.154 and Mendes, I., 2010, pg. 219, pl. 5, fig.2

***Elphidium cuvillieri* Levy, 1966**

Plate 4, fig. 4 a-b

Elphidium cuvillieri Levy, 1966, Vie et Milieu, Paris, t. 17, fasc. 1a, p. 5-6, pl. 1, fig. 6, pl.2

Elphidium cuvillieri (Levy 1966), Mendes, I., pag. 218, pl. 5, fig.3.

Cibroelphidium cuvillieri (Levy), Debenay et al., 2001, pl. 6, fig. 18 and Villanueva and Canudo, 1999, p. 213-214, pl. 2, fig. 4, a-b.

***Elphidium granosum* d'Orbigny, 1846**

Plate 4, fig. 5 a-b

Elphidium granosum (d'Orbigny), Jorissen, 1987, p. 47, pl. 2, figs. 1-2

Porosononion granosum (d'Orbigny), Poignant et al., 2000, p. 400, pl. 1, figs. 13-15

***Elphidium oceanensis* d'Orbigny, 1826**

Plate 4, fig. 6 a-b

Elphidium gunteri Cole, 1931, Debenay et al., 1998c, p. 80, pl. IV, fig. 17; Hayward and Hollis, 1994, p. 209, pl. 4, figs. 10-12

Elphidium oceanensis (d'Orbigny), Murray, 1971, p. 165, pl. 69, figs. 1-7; Cearreta, 1988, p. 36, pl. I, fig. 8; Leorri and Cearreta, 2004, p. 78, pl. 1, fig.5; Cearreta et al., 2007, p.128, pl. I, fig.3.

Plate 1

1- *Ammotium* sp, scale bar ~100 µm
   a - SEM photograph,side view

2- *Textularia* sp, scale bar ~100 µm
   a - SEM photograph, side view

3- *Trochammina inflata* Montagu 1808, scale bar ~100 µm
   a - SEM photograph, dorsal side
   b - BM photograph, dorsal side
   c - BM photograph, ventral side

4- *Jadammina macrescens* Brady 1870, scale bar ~100 µm
   a - SEM photograph, dorsal side
   b - BM photograph, dorsal side
   c - SEM photograph, ventral side
   d - BM photograph, ventral side

5- *Spirillina vivipara* Ehrenberg 1843, scale bar ~100 µm
   a - SEM photograph, side view

6- *Cornuloculina* sp, scale bar ~100 µm
   a - SEM photograph, dorsal side

7- *Cornuspira involvens* Reuss 1850, scale bar ~100 µm
   a - SEM photograph,side view

8- *Adelosina* sp, scale bar ~100 µm
   a - SEM photograph,side view

b - BM photograph, side view

c - SEM photograph,side view

9- *Quinqueloculina laevigata* d' Orbigny 1839, scale bar ~100 µm

a - SEM photograph,side view

10- *Quinqueloculina seminulum* Linnaeus 1758, scale bar ~100 µm

a - SEM photograph, side view

b - BM photograph, side view

c - SEM photograph, side view

d - BM photograph, side view

11- *Quinqueloculina stelligera* Schlumberger 1893, scale bar ~100 µm

a - SEM photograph, side view

b - BM photograph, side view

c - SEM photograph, side view

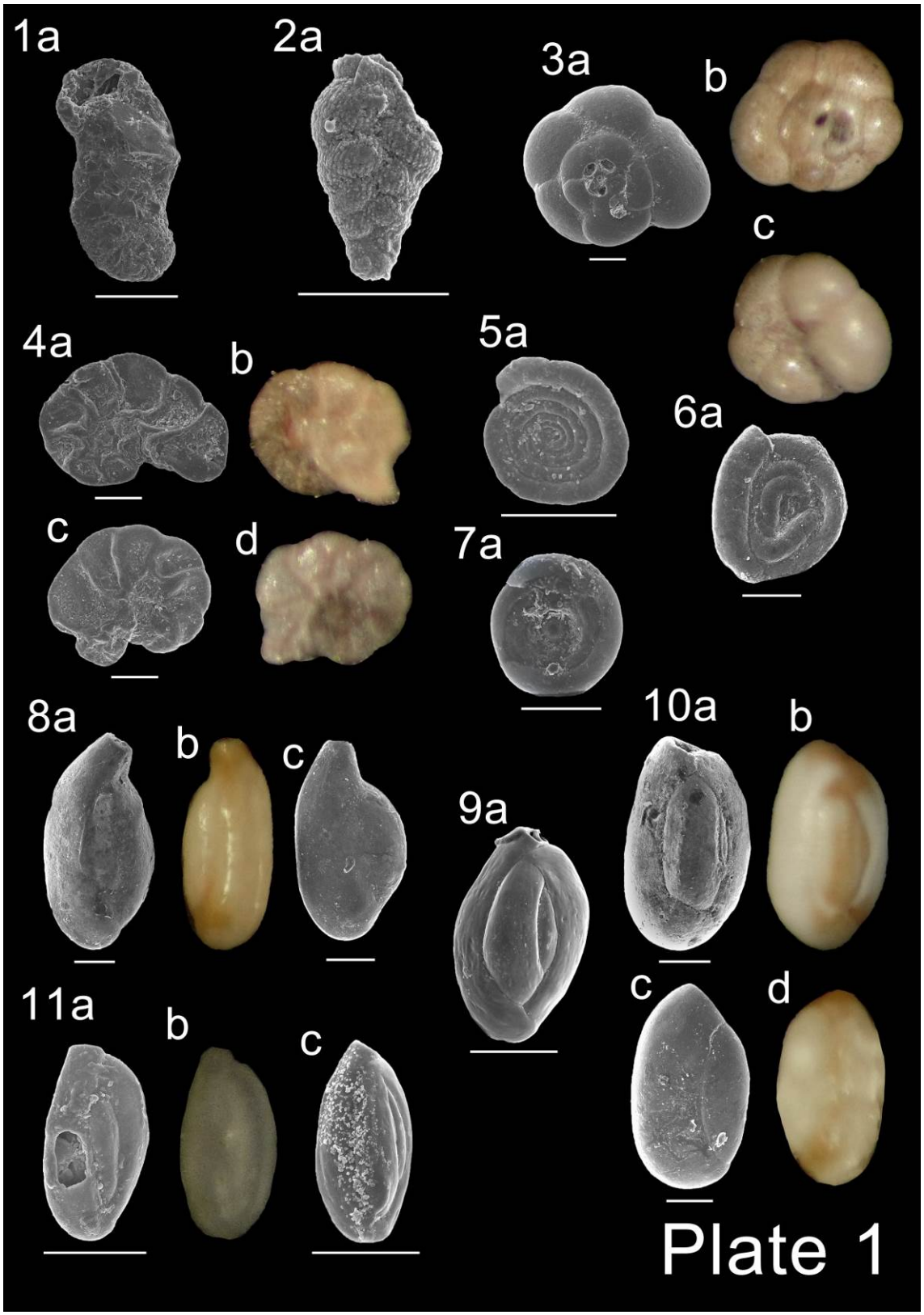
1a
2a
3a
b
c
4a
b
5a
6a
c
d
7a
8a
b
c
10a
b
9a
11a
b
c
c
d
Plate 1

Plate 2

1- *Triloculina trigonula* Lamarck 1804, scale bar ~100 µm
   a - SEM photograph,side view
   b - BM photograph, side view

2- *Lagena* sp, scale bar ~100 µm
   a - SEM photograph,side view

3- *Lagena striata* d'Orbigny 1839, scale bar ~100 µm
   a - SEM photograph,side view

4- *Lagena sulcata* Walker & Jacob 1798, scale bar ~100 µm
   a - SEM photograph,side view

5- *Fissurina marginata* Montagu 1803, scale bar ~100 µm
   a - scanning electron microscope (SEM) photograph,side view
   b - binocular microscope (BM) photograph, side view

6- *Fissurina* sp1, scale bar ~100 µm
   a - SEM photograph,side view
   b - BM photograph, side view

7- *Fissurina* sp2, scale bar ~100 µm
   a - SEM photograph,side view

8- *Fissurina* sp3, scale bar ~100 µm
   a - SEM photograph,side view

9- *Oolina squamosa* Montagu 1803, scale bar ~100 µm
   a - SEM photograph,side view

10- *Stilostomella* sp, scale bar ~100 µm
   a - SEM photograph,side view
   b - BM photograph, side view

11- *Bolivina ordinaria* Pheleger and Parker 1952, scale bar ~100 µm

a - SEM photograph, side view

b - BM photograph, side view

12- *Brizalina striatula* Cushman 1922, scale bar ~100 µm

a - SEM photograph, side view

13-*Cassidulina laevigata* d' Orbigny 1826, scale bar ~100 µm

a - SEM photograph, side view

14-*Cassidulina minuta* Cushman 1933, scale bar ~100 µm

a - SEM photograph, side view

15-*Hopkinsina atlantica* Cushman 1944, scale bar ~100 µm

a - SEM photograph, side view

16-*Stainforthia complanata* Egger 1895, scale bar ~100 µm

a - SEM photograph, side view

17-*Rectuvigerina* sp, scale bar ~100 µm

a - SEM photograph, side view

18- Bulimina elongata d'Orbigny 1846, scale bar ~100 µm

a - SEM photograph, side view

b - BM photograph, side view

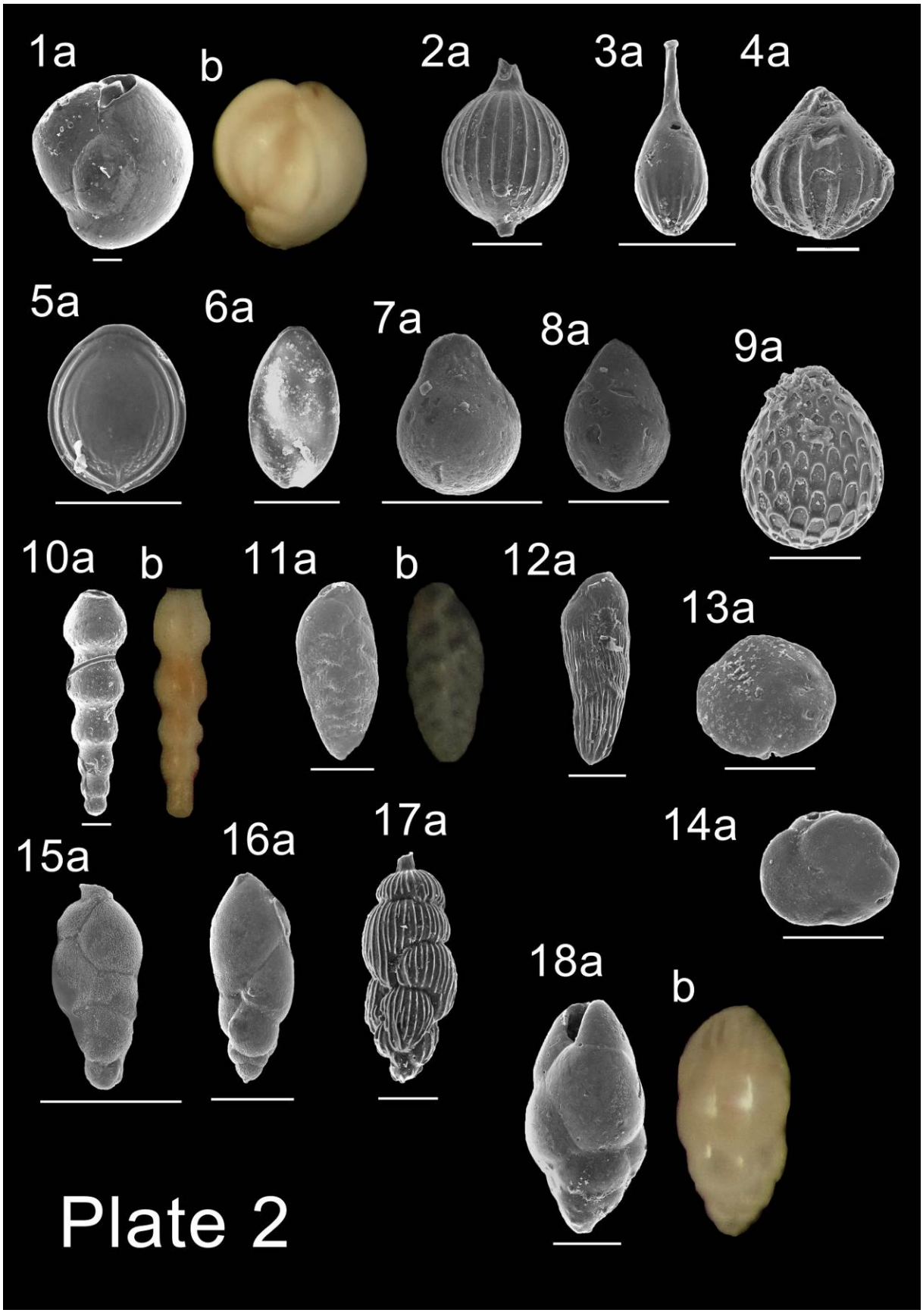
1a
b
2a
3a
4a
5a
6a
7a
8a
9a
10a
b
11a
b
12a
13a
15a
16a
17a
14a
18a
b
Plate 2

Plate 3

1- *Bulimina marginata* d' Orbigny 1826, scale bar ~100 µm
   a - SEM photograph, aperture view

2- *Buliminella elegantissima* d'Orbigny 1839, scale bar ~100 µm
   a - SEM photograph, side view
   b - BM photograph, side view

3- *Uvigerina peregrina* Cushman 1923, scale bar ~100 µm
   a - SEM photograph, side view
   b - BM photograph, side view

4- *Trifarina angulosa* Williamson 1858, scale bar ~100 µm
   a - SEM photograph, side view

5- *Rosalina bradyi* Cushman 1915, scale bar ~100 µm
   a - SEM photograph, dorsal side
   b - BM photograph, dorsal side
   c - SEM photograph, ventral side
   d - BM photograph, ventral side

6- *Planorbulina mediterranensis* d'Orbigny 1826, scale bar ~100 µm
   a - SEM photograph, ventral side
   b - BM photograph, ventral side
   c - SEM photograph, dorsal side
   d - BM photograph, dorsal side

7- *Asterigerinata mamilla* Williamson 1858, scale bar ~100 µm
   a - SEM photograph, dorsal side
   b - BM photograph, dorsal side
   c - SEM photograph, ventral side
   d - BM photograph, ventral side

8- *Haynesina germanica* Ehrenberg 1840, scale bar ~100 µm

a - SEM photograph, side view

b - BM photograph, side view

9- *Nonion fabum* Fichtel and Moll 1798, scale bar ~100 µm

a - SEM photograph, side view

b - BM photograph, side view

c - SEM photograph, aperture view

10-*Nonionella stella* Cushman & Moyer 1930, scale bar ~100 µm

a - SEM photograph, dorsal side

b - BM photograph, dorsal side

c - SEM photograph, ventral side

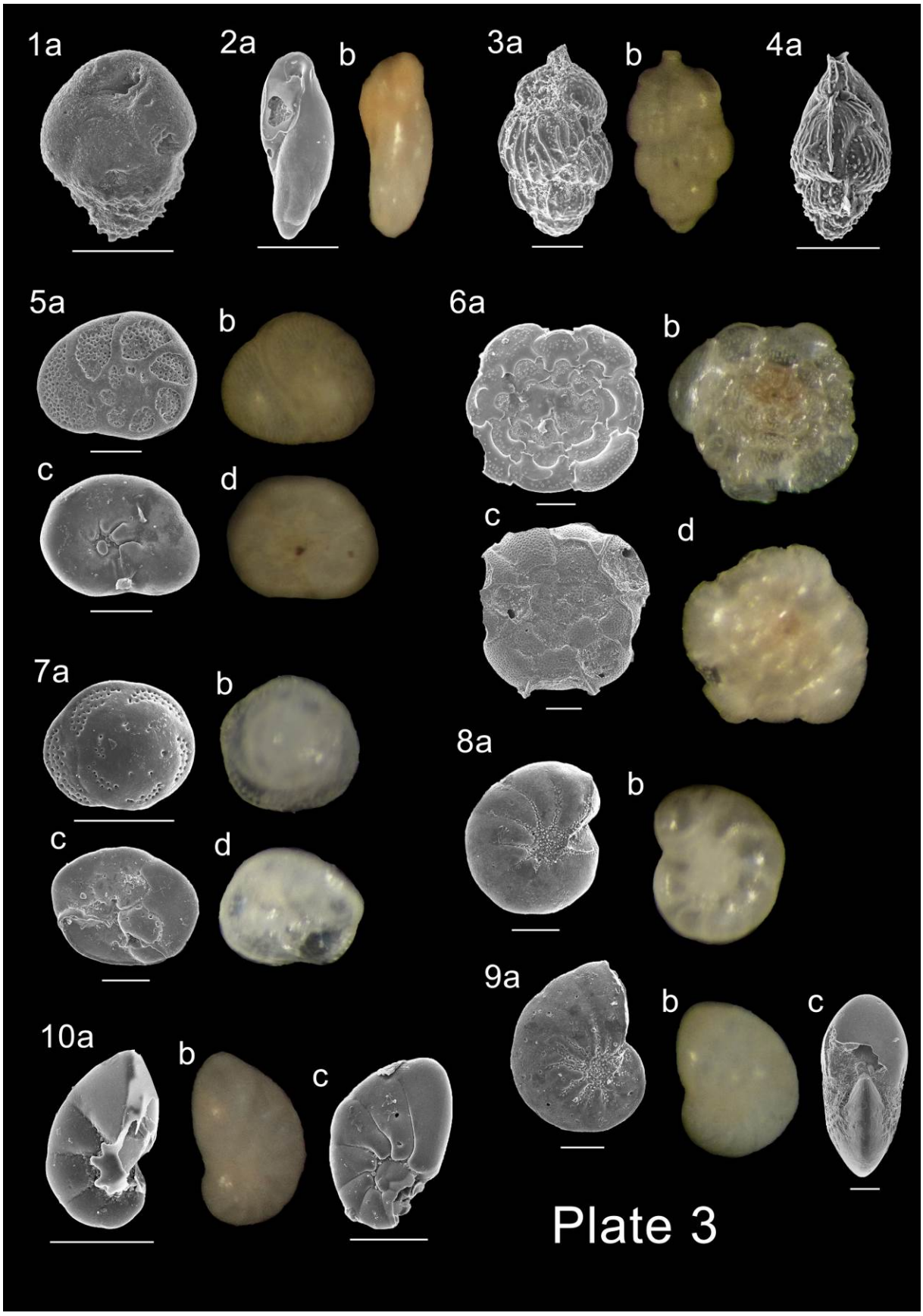
1a
2a
b
3a
b
4a
5a
b
c
d
6a
b
c
d
7a
b
c
d
8a
b
9a
b
c
10a
b
c
Plate 3

Plate 4

1- *Ammonia beccarii* Linnaeus 1758, scale bar ~100 µm
   a - SEM photograph, dorsal side
   b- SEM photograph, ventral side

2- *Ammonia tepida* Cushman 1926, scale bar ~100 µm
   a - SEM photograph, dorsal side
   b - BM photograph, dorsal side
   c- SEM photograph, ventral side
   d - BM photograph, ventral side

3- *Elphidium crispum* Linnaeus 1758, scale bar ~100 µm
   a - SEM photograph, side view
   d - BM photograph, side view

4- *Elphidium cuvillieri* Levy 1966, scale bar ~100 µm
   a - SEM photograph, side view
   d - BM photograph, side view

5- *Elphidium granosum* d'Orbigny 1846, scale bar ~100 µm
   a - SEM photograph, side view
   d - BM photograph, side view

6- *Elphidium oceanensis* d'Orbigny 1826, scale bar ~100 µm
   a - SEM photograph, side view
   b - BM photograph, side view

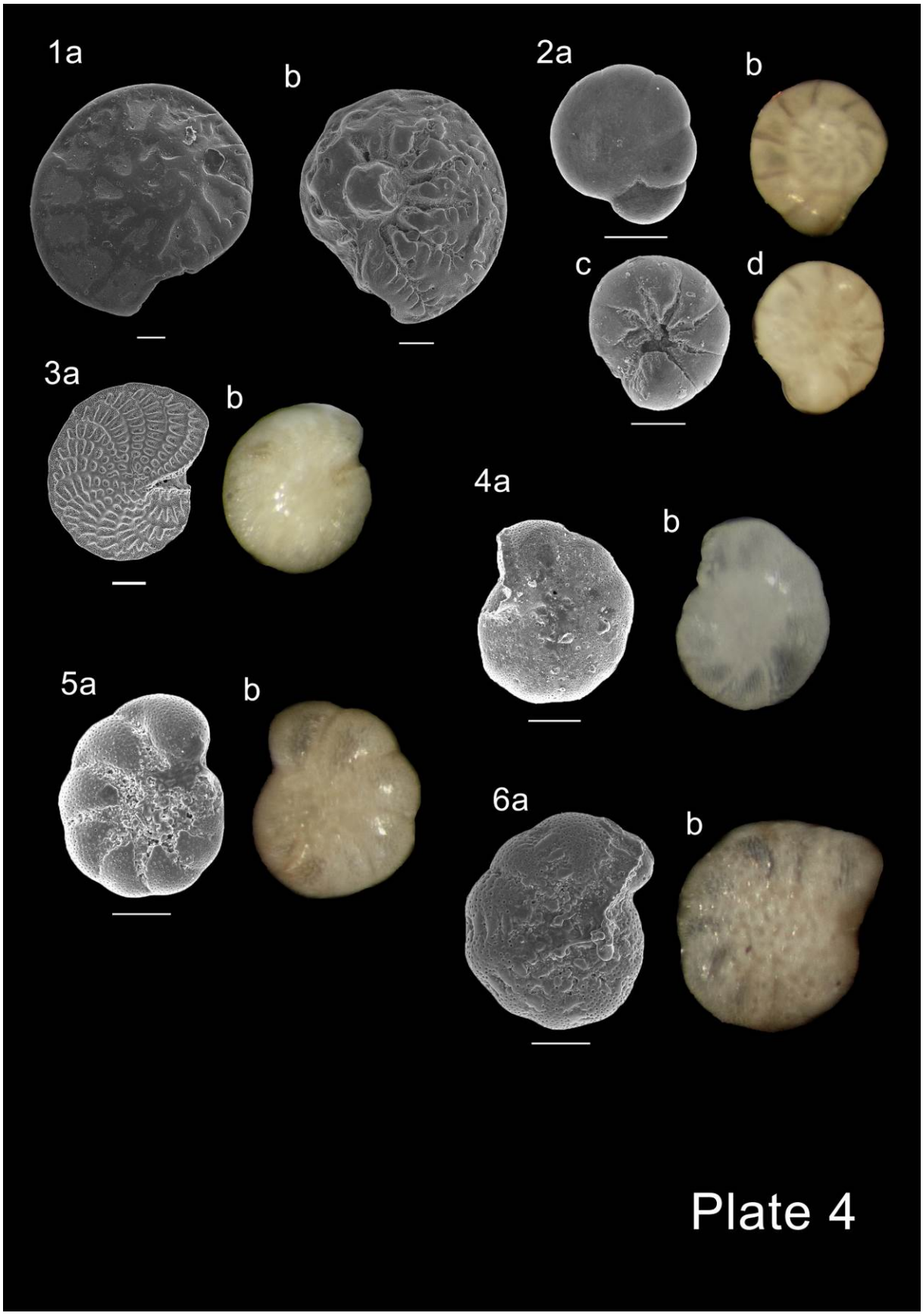
1a
b
2a
b
c
d
3a
b
4a
b
5a
b
6a
b
Plate 4

Appendix

Appendix 1 – Results of Grain size distribution of surface samples and sediment type, according to Folk & Ward (1957), calculated by GRADISTAT 14.0 program

DÑA1

SAMPLE STATISTICS

SAMPLE IDENTITY: **DNA1** ANALYST & DATE: ,

SAMPLE TYPE: Unimodal, Very Poorly Sorted TEXTURAL GROUP: Muddy Sand

SEDIMENT NAME: Fine Silty Fine Sand

	μm	ϕ
MODE 1:	240.6	2.059
MODE 2:		
MODE 3:		
D_{10}:	4.327	1.769
MEDIAN or D_{50}:	208.5	2.262
D_{90}:	293.3	7.852
(D_{90} / D_{10}):	67.78	4.438
(D_{90} - D_{10}):	289.0	6.083
(D_{75} / D_{25}):	1.948	1.493
(D_{75} - D_{25}):	125.8	0.962

GRAIN SIZE DISTRIBUTION

GRAVEL: 0.0%	COARSE SAND: 0.0%
SAND: 79.7%	MEDIUM SAND: 29.2%
MUD: 20.3%	FINE SAND: 47.2%
	V FINE SAND: 3.3%
V COARSE GRAVEL: 0.0%	V COARSE SILT: 1.6%
COARSE GRAVEL: 0.0%	COARSE SILT: 2.6%
MEDIUM GRAVEL: 0.0%	MEDIUM SILT: 2.6%
FINE GRAVEL: 0.0%	FINE SILT: 4.2%
V FINE GRAVEL: 0.0%	V FINE SILT: 4.0%
V COARSE SAND: 0.0%	CLAY: 5.3%

	METHOD OF MOMENTS			FOLK & WARD METHOD		
	Arithmetic	Geometric	Logarithmic	Geometric	Logarithmic	Description
	μm	μm	ϕ	μm	ϕ	
MEAN ($\bar{x}$):	161.5	68.15	3.210	96.23	3.377	Very Fine Sand
SORTING (σ):	103.2	7.302	2.512	4.689	2.229	Very Poorly Sorted
SKEWNESS (Sk):	-0.546	-1.306	1.561	-0.776	0.776	Very Fine Skewed
KURTOSIS (K):	1.781	3.057	4.495	3.327	3.327	Extremely Leptokurtic

GRAIN SIZE DISTRIBUTION

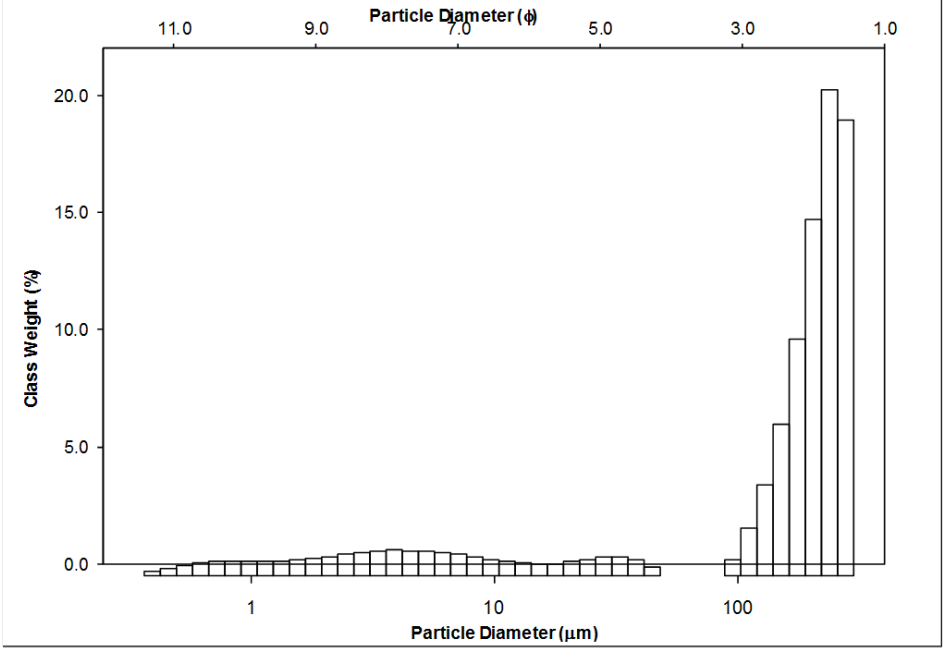

DÑA2

SAMPLE STATISTICS

SAMPLE IDENTITY:	**DNA5**		ANALYST & DATE:	,	
SAMPLE TYPE:	Unimodal, Moderately Well Sorted		TEXTURAL GROUP:	Sand	
SEDIMENT NAME:	Moderately Well Sorted Fine Sand				

	□m	□	GRAIN SIZE DISTRIBUTION			
MODE 1:	240.6	2.059	GRAVEL:	0.0%	COARSE SAND:	0.0%
MODE 2:			SAND:	96.2%	MEDIUM SAND:	38.7%
MODE 3:			MUD:	3.8%	FINE SAND:	53.7%
D_{10}:	138.0	1.708			V FINE SAND:	3.7%
AN or D_{50}:	231.6	2.111	V COARSE GRAVEL:	0.0%	V COARSE SILT:	0.5%
D_{90}:	306.2	2.857	COARSE GRAVEL:	0.0%	COARSE SILT:	1.0%
(D_{90} / D_{10}):	2.218	1.673	MEDIUM GRAVEL:	0.0%	MEDIUM SILT:	0.2%
(D_{90} - D_{10}):	168.2	1.150	FINE GRAVEL:	0.0%	FINE SILT:	0.6%
(D_{75} / D_{25}):	1.490	1.309	V FINE GRAVEL:	0.0%	V FINE SILT:	0.4%
(D_{75} - D_{25}):	90.37	0.576	V COARSE SAND:	0.0%	CLAY:	1.1%

	METHOD OF MOMENTS			FOLK & WARD METHOD		
	Arithmetic	Geometric	Logarithmic	Geometric	Logarithmic	Description
	□m	□m	□	□m	□	
MEAN (□):	187.6	101.4	2.174	221.5	2.175	Fine Sand
SORTING (□):	90.31	6.204	1.367	1.505	0.590	Moderately Well Sorted
SKEWNESS (Sk):	-1.040	-2.024	2.797	-0.066	0.066	Symmetrical
KURTOSIS (K):	2.957	5.320	17.87	1.756	1.756	Very Leptokurtic

GRAIN SIZE DISTRIBUTION

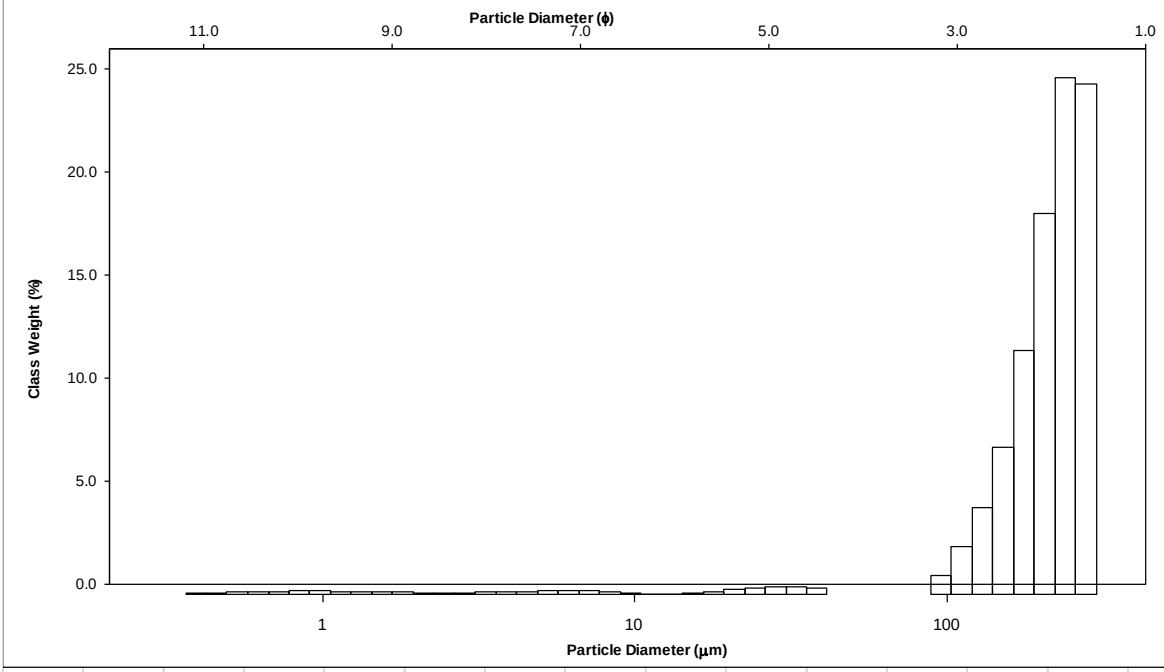

DÑA3

SAMPLE STATISTICS

SAMPLE IDENTITY:	**DNA3**		ANALYST & DATE:	,	
SAMPLE TYPE:	Unimodal, Well Sorted		TEXTURAL GROUP:	Sand	
SEDIMENT NAME:	Well Sorted Fine Sand				

	□m	□	GRAIN SIZE DISTRIBUTION			
MODE 1:	177.3	2.500	GRAVEL:	0.0%	COARSE SAND:	0.0%
MODE 2:			SAND:	100.0%	MEDIUM SAND:	17.3%
MODE 3:			MUD:	0.0%	FINE SAND:	66.8%
D_{10}:	113.1	1.854			V FINE SAND:	15.9%
AN or D_{50}:	181.1	2.465	V COARSE GRAVEL:	0.0%	V COARSE SILT:	0.0%
D_{90}:	276.6	3.145	COARSE GRAVEL:	0.0%	COARSE SILT:	0.0%
(D_{90} / D_{10}):	2.446	1.696	MEDIUM GRAVEL:	0.0%	MEDIUM SILT:	0.0%
(D_{90} - D_{10}):	163.5	1.291	FINE GRAVEL:	0.0%	FINE SILT:	0.0%
(D_{75} / D_{25}):	1.626	1.330	V FINE GRAVEL:	0.0%	V FINE SILT:	0.0%
(D_{75} - D_{25}):	88.39	0.701	V COARSE SAND:	0.0%	CLAY:	0.0%

	METHOD OF MOMENTS			FOLK & WARD METHOD		
	Arithmetic	Geometric	Logarithmic	Geometric	Logarithmic	Description
	□m	□m	□	□m	□	
MEAN (x̄):	173.9	137.2	2.411	179.2	2.481	Fine Sand
SORTING (□):	64.79	3.056	0.683	1.406	0.492	Well Sorted
SKEWNESS (*Sk*):	-0.506	-3.852	-1.720	-0.059	0.059	Symmetrical
KURTOSIS (*K*):	3.461	17.21	7.614	0.915	0.915	Mesokurtic

GRAIN SIZE DISTRIBUTION

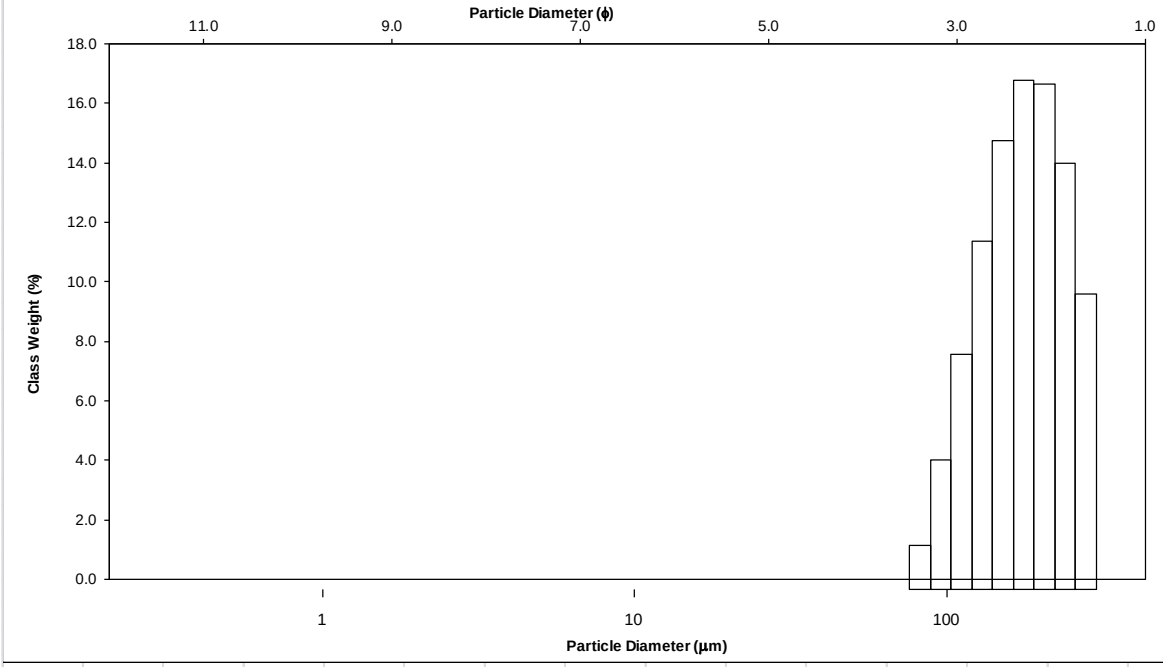

DÑA4

SAMPLE STATISTICS

SAMPLE IDENTITY:	**DNA4**			ANALYST & DATE:	,
SAMPLE TYPE:	Bimodal, Very Poorly Sorted			TEXTURAL GROUP:	Muddy Sand
SEDIMENT NAME:	Fine Silty Medium Sand				

	□m	□			GRAIN SIZE DISTRIBUTION			
MODE 1:	280.3	1.839		GRAVEL:	0.0%		COARSE SAND:	0.0%
MODE 2:	7.175	7.127		SAND:	57.3%		MEDIUM SAND:	29.2%
MODE 3:				MUD:	42.7%		FINE SAND:	24.7%
D_{10}:	2.187	1.453					V FINE SAND:	3.4%
AN or D_{50}:	153.4	2.705		V COARSE GRAVEL:	0.0%		V COARSE SILT:	3.0%
D_{90}:	365.3	8.837		COARSE GRAVEL:	0.0%		COARSE SILT:	5.6%
(D_{90} / D_{10}):	167.0	6.082		MEDIUM GRAVEL:	0.0%		MEDIUM SILT:	8.6%
(D_{90} - D_{10}):	363.1	7.384		FINE GRAVEL:	0.0%		FINE SILT:	9.4%
(D_{75} / D_{25}):	34.79	3.667		V FINE GRAVEL:	0.0%		V FINE SILT:	6.9%
(D_{75} - D_{25}):	256.6	5.121		V COARSE SAND:	0.0%		CLAY:	9.1%

	METHOD OF MOMENTS			FOLK & WARD METHOD		
	Arithmetic	Geometric	Logarithmic	Geometric	Logarithmic	Description
	□m	□m	□	□m	□	
MEAN (x̄):	102.1	22.25	4.217	55.92	4.160	Very Coarse Silt
SORTING (□):	112.0	9.326	3.170	7.758	2.956	Very Poorly Sorted
SKEWNESS (*Sk*):	0.488	-0.220	0.478	-0.632	0.632	Very Fine Skewed
KURTOSIS (*K*):	1.500	1.455	1.967	0.740	0.740	Platykurtic

GRAIN SIZE DISTRIBUTION

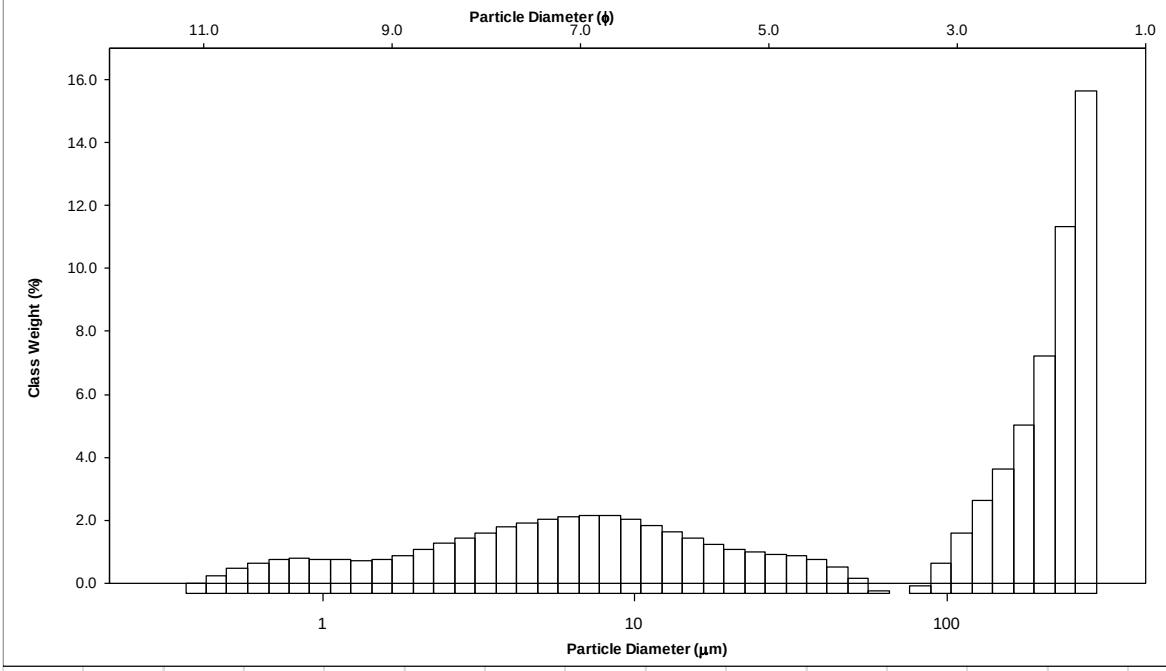

DÑA5

SAMPLE STATISTICS

SAMPLE IDENTITY:	**DNA5**		ANALYST & DATE:	,	
SAMPLE TYPE:	Bimodal, Poorly Sorted		TEXTURAL GROUP:	Mud	
SEDIMENT NAME:	Medium Silt				

	□m	□	GRAIN SIZE DISTRIBUTION			
MODE 1:	8.359	6.907	GRAVEL:	0.0%	COARSE SAND:	0.0%
MODE 2:	0.846	10.21	SAND:	1.2%	MEDIUM SAND:	0.0%
MODE 3:			MUD:	98.8%	FINE SAND:	0.1%
D_{10}:	0.770	5.465			V FINE SAND:	1.0%
AN or D_{50}:	5.376	7.539	V COARSE GRAVEL:	0.0%	V COARSE SILT:	4.0%
D_{90}:	22.64	10.34	COARSE GRAVEL:	0.0%	COARSE SILT:	13.3%
(D_{90} / D_{10}):	29.40	1.893	MEDIUM GRAVEL:	0.0%	MEDIUM SILT:	20.4%
(D_{90} - D_{10}):	21.87	4.878	FINE GRAVEL:	0.0%	FINE SILT:	19.6%
(D_{75} / D_{25}):	6.994	1.443	V FINE GRAVEL:	0.0%	V FINE SILT:	14.8%
(D_{75} - D_{25}):	10.61	2.806	V COARSE SAND:	0.0%	CLAY:	26.7%

	METHOD OF MOMENTS			FOLK & WARD METHOD		
	Arithmetic	Geometric	Logarithmic	Geometric	Logarithmic	Description
	□m	□m	□	□m	□	
MEAN (□):	9.713	4.774	7.711	4.599	7.764	Fine Silt
SORTING (□):	13.50	3.505	1.809	3.686	1.882	Poorly Sorted
SKEWNESS (*Sk*):	4.058	-0.096	0.096	-0.138	0.138	Fine Skewed
KURTOSIS (*K*):	28.17	2.222	2.222	0.841	0.841	Platykurtic

GRAIN SIZE DISTRIBUTION

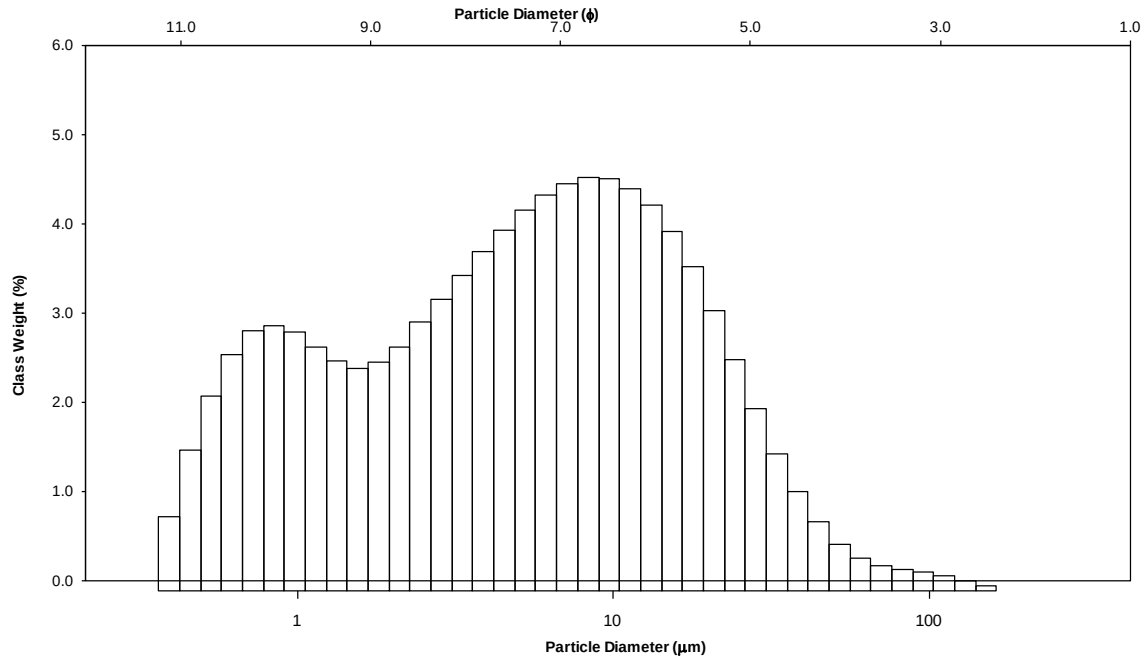

DÑA6

SAMPLE STATISTICS

SAMPLE IDENTITY:	**DNA6**			ANALYST & DATE:	,
SAMPLE TYPE:	Trimodal, Very Poorly Sorted			TEXTURAL GROUP:	Muddy Sand
SEDIMENT NAME:	Fine Silty Fine Sand				

	□m	□			GRAIN SIZE DISTRIBUTION	
MODE 1:	206.5	2.280	GRAVEL:	0.0%	COARSE SAND:	0.0%
MODE 2:	4.538	7.788	SAND:	54.2%	MEDIUM SAND:	9.7%
MODE 3:	20.90	5.585	MUD:	45.8%	FINE SAND:	32.9%
D_{10}:	2.112	2.009			V FINE SAND:	11.5%
AN or D_{50}:	93.11	3.425	V COARSE GRAVEL:	0.0%	V COARSE SILT:	5.6%
D_{90}:	248.5	8.887	COARSE GRAVEL:	0.0%	COARSE SILT:	7.5%
(D_{90} / D_{10}):	117.7	4.425	MEDIUM GRAVEL:	0.0%	MEDIUM SILT:	7.6%
(D_{90} - D_{10}):	246.4	6.879	FINE GRAVEL:	0.0%	FINE SILT:	8.3%
(D_{75} / D_{25}):	23.97	2.882	V FINE GRAVEL:	0.0%	V FINE SILT:	7.6%
(D_{75} - D_{25}):	177.1	4.583	V COARSE SAND:	0.0%	CLAY:	9.3%

	METHOD OF MOMENTS			FOLK & WARD METHOD		
	Arithmetic	Geometric	Logarithmic	Geometric	Logarithmic	Description
	□m	□m	□	□m	□	
MEAN (□):	96.69	32.26	4.681	42.05	4.572	Very Coarse Silt
SORTING (□):	93.12	6.898	2.770	6.434	2.686	Very Poorly Sorted
SKEWNESS (*Sk*):	0.482	-0.597	0.585	-0.590	0.590	Very Fine Skewed
KURTOSIS (*K*):	1.807	1.945	2.150	0.713	0.713	Platykurtic

GRAIN SIZE DISTRIBUTION

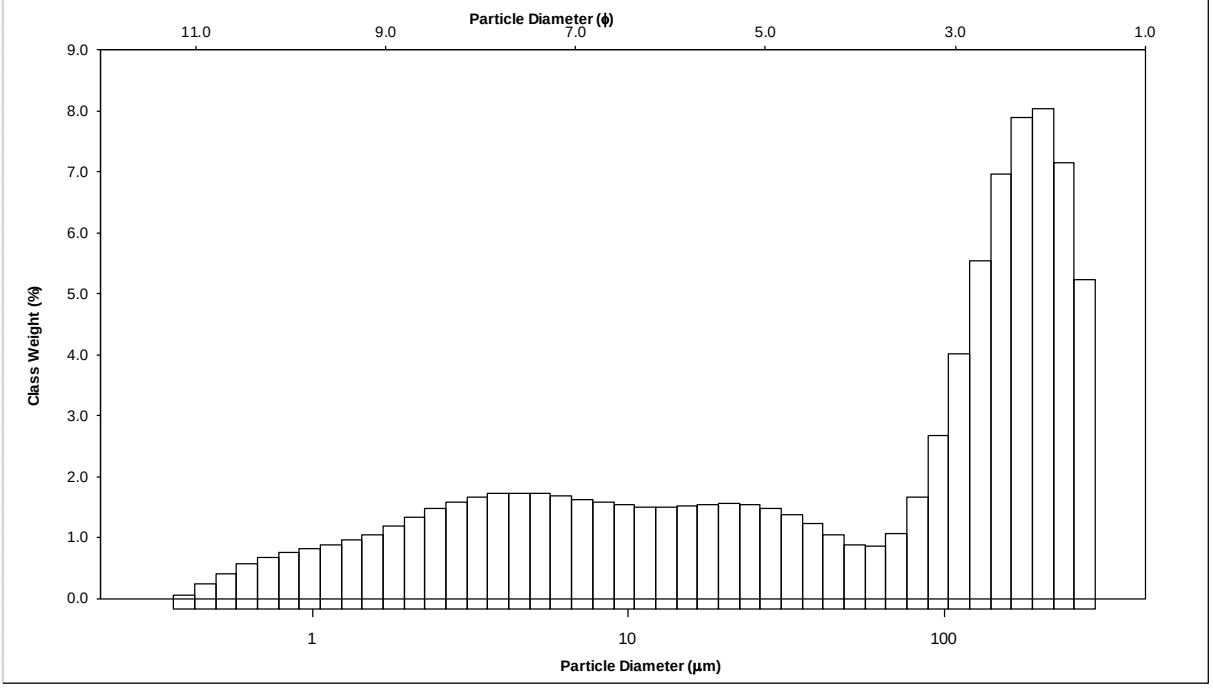

DÑA7

SAMPLE STATISTICS

SAMPLE IDENTITY: **DNA7** ANALYST & DATE: ,

SAMPLE TYPE: Unimodal, Very Poorly Sorted TEXTURAL GROUP: Muddy Sand

SEDIMENT NAME: Coarse Silty Fine Sand

	□m	□
MODE 1:	240.6	2.059
MODE 2:		
MODE 3:		
D_{10}:	5.114	1.806
MEDIAN or D_{50}:	183.0	2.450
D_{90}:	285.9	7.611
(D_{90} / D_{10}):	55.91	4.214
(D_{90} - D_{10}):	280.8	5.805
(D_{75} / D_{25}):	2.379	1.610
(D_{75} - D_{25}):	139.9	1.250

GRAIN SIZE DISTRIBUTION

GRAVEL: 0.0%	COARSE SAND: 0.0%
SAND: 77.2%	MEDIUM SAND: 21.6%
MUD: 22.8%	FINE SAND: 48.6%
	V FINE SAND: 7.1%
V COARSE GRAVEL: 0.0%	V COARSE SILT: 2.0%
COARSE GRAVEL: 0.0%	COARSE SILT: 4.5%
MEDIUM GRAVEL: 0.0%	MEDIUM SILT: 3.8%
FINE GRAVEL: 0.0%	FINE SILT: 3.9%
V FINE GRAVEL: 0.0%	V FINE SILT: 3.1%
V COARSE SAND: 0.0%	CLAY: 5.4%

	METHOD OF MOMENTS			FOLK & WARD METHOD		
	Arithmetic □m	Geometric □m	Logarithmic □	Geometric □m	Logarithmic □	Description
MEAN ($\bar{x}$)	147.1	64.60	3.392	89.67	3.479	Very Fine Sand
SORTING (□):	98.47	6.690	2.460	4.585	2.197	Very Poorly Sorted
SKEWNESS (Sk):	-0.333	-1.321	1.471	-0.751	0.751	Very Fine Skewed
KURTOSIS (K):	1.700	3.237	4.392	2.502	2.502	Very Leptokurtic

GRAIN SIZE DISTRIBUTION

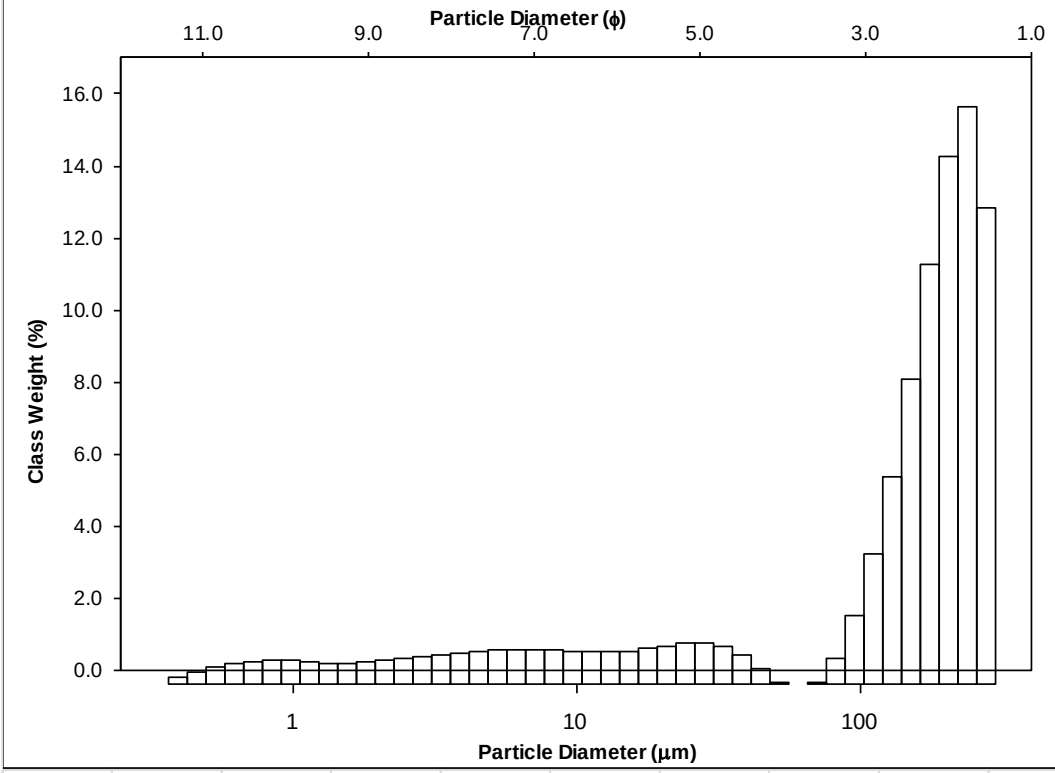

DÑA8

SAMPLE STATISTICS

SAMPLE IDENTITY:	**DNA20**		ANALYST & DATE:	,	
SAMPLE TYPE:	Trimodal, Very Poorly Sorted		TEXTURAL GROUP:	Muddy Sand	
SEDIMENT NAME:	Coarse Silty Fine Sand				

	□m	□	GRAIN SIZE DISTRIBUTION			
MODE 1:	177.3	2.500	GRAVEL:	0.0%	COARSE SAND:	0.0%
MODE 2:	20.90	5.585	SAND:	55.9%	MEDIUM SAND:	7.9%
MODE 3:	7.175	7.127	MUD:	44.1%	FINE SAND:	34.1%
D_{10}:	2.139	2.070			V FINE SAND:	13.9%
AN or D_{50}:	97.35	3.361	V COARSE GRAVEL:	0.0%	V COARSE SILT:	4.6%
D_{90}:	238.1	8.869	COARSE GRAVEL:	0.0%	COARSE SILT:	8.1%
(D_{90} / D_{10}):	111.3	4.284	MEDIUM GRAVEL:	0.0%	MEDIUM SILT:	8.1%
(D_{90} - D_{10}):	235.9	6.798	FINE GRAVEL:	0.0%	FINE SILT:	8.1%
(D_{75} / D_{25}):	19.38	2.710	V FINE GRAVEL:	0.0%	V FINE SILT:	5.7%
(D_{75} - D_{25}):	167.5	4.277	V COARSE SAND:	0.0%	CLAY:	9.4%

	METHOD OF MOMENTS			FOLK & WARD METHOD		
	Arithmetic	Geometric	Logarithmic	Geometric	Logarithmic	Description
	□m	□m	□	□m	□	
MEAN (□):	96.89	34.54	4.651	44.30	4.497	Very Coarse Silt
SORTING (□):	89.76	6.663	2.719	6.221	2.637	Very Poorly Sorted
SKEWNESS (*Sk*):	0.446	-0.718	0.705	-0.621	0.621	Very Fine Skewed
KURTOSIS (*K*):	1.850	2.176	2.362	0.780	0.780	Platykurtic

GRAIN SIZE DISTRIBUTION

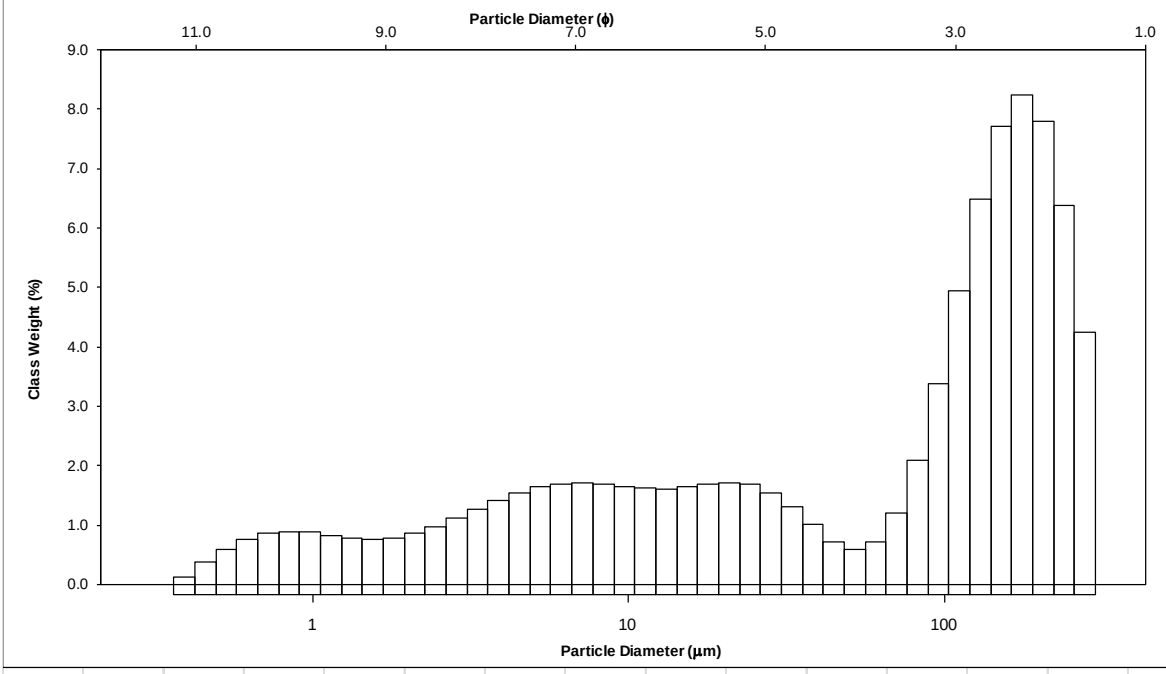

DÑA9

SAMPLE STATISTICS

SAMPLE IDENTITY:	**DNA9**		ANALYST & DATE:	,	
SAMPLE TYPE:	Unimodal, Poorly Sorted		TEXTURAL GROUP:	Muddy Sand	
SEDIMENT NAME:	Very Coarse Silty Medium Sand				

	□m	□			GRAIN SIZE DISTRIBUTION	
MODE 1:	280.3	1.839	GRAVEL:	0.0%	COARSE SAND:	0.0%
MODE 2:			SAND:	82.8%	MEDIUM SAND:	47.7%
MODE 3:			MUD:	17.2%	FINE SAND:	29.9%
D_{10}:	24.27	0.887			V FINE SAND:	5.2%
AN or D_{50}:	243.9	2.036	V COARSE GRAVEL:	0.0%	V COARSE SILT:	5.4%
D_{90}:	540.6	5.365	COARSE GRAVEL:	0.0%	COARSE SILT:	4.2%
(D_{90} / D_{10}):	22.27	6.046	MEDIUM GRAVEL:	0.0%	MEDIUM SILT:	2.6%
(D_{90} - D_{10}):	516.4	4.477	FINE GRAVEL:	0.0%	FINE SILT:	2.0%
(D_{75} / D_{25}):	2.070	1.596	V FINE GRAVEL:	0.0%	V FINE SILT:	1.2%
(D_{75} - D_{25}):	152.5	1.049	V COARSE SAND:	0.0%	CLAY:	1.9%

	METHOD OF MOMENTS			FOLK & WARD METHOD		
	Arithmetic	Geometric	Logarithmic	Geometric	Logarithmic	Description
	□m	□m	□	□m	□	
MEAN (□):	141.0	41.31	2.438	172.7	2.534	Fine Sand
SORTING (□):	114.5	9.836	2.133	3.381	1.758	Poorly Sorted
SKEWNESS (*Sk*):	-0.092	-0.814	1.460	-0.501	0.501	Very Fine Skewed
KURTOSIS (*K*):	1.312	1.914	5.636	2.589	2.589	Very Leptokurtic

GRAIN SIZE DISTRIBUTION

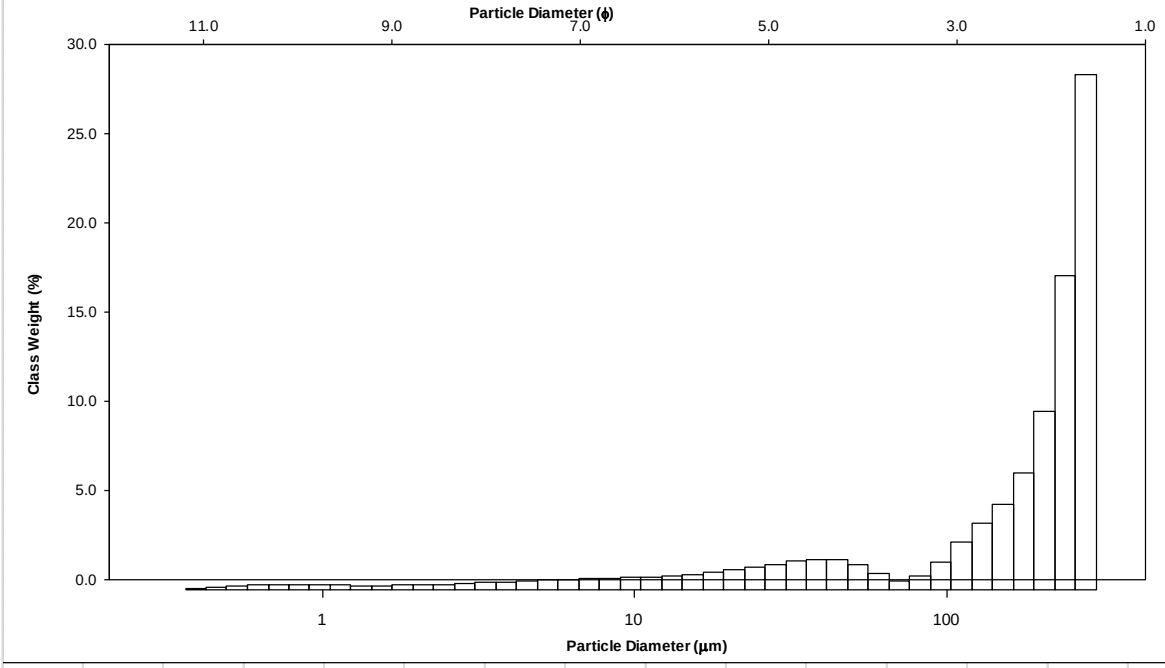

DÑA10

SAMPLE STATISTICS

SAMPLE IDENTITY:	**DNA10**			ANALYST & DATE:	,
SAMPLE TYPE:	Trimodal, Very Poorly Sorted			TEXTURAL GROUP:	Mud
SEDIMENT NAME:	Fine Silt				

	□m	□			GRAIN SIZE DISTRIBUTION	
MODE 1:	7.175	7.127	GRAVEL:	0.0%	COARSE SAND:	0.0%
MODE 2:	0.985	9.992	SAND:	6.9%	MEDIUM SAND:	1.6%
MODE 3:	240.6	2.059	MUD:	93.1%	FINE SAND:	3.2%
D_{10}:	0.820	4.577			V FINE SAND:	2.0%
AN or D_{50}:	5.479	7.512	V COARSE GRAVEL:	0.0%	V COARSE SILT:	6.5%
D_{90}:	41.91	10.25	COARSE GRAVEL:	0.0%	COARSE SILT:	11.9%
(D_{90} / D_{10}):	51.09	2.240	MEDIUM GRAVEL:	0.0%	MEDIUM SILT:	16.0%
(D_{90} - D_{10}):	41.09	5.675	FINE GRAVEL:	0.0%	FINE SILT:	16.9%
(D_{75} / D_{25}):	8.897	1.527	V FINE GRAVEL:	0.0%	V FINE SILT:	15.1%
(D_{75} - D_{25}):	14.03	3.153	V COARSE SAND:	0.0%	CLAY:	26.8%

	METHOD OF MOMENTS			FOLK & WARD METHOD		
	Arithmetic	Geometric	Logarithmic	Geometric	Logarithmic	Description
	□m	□m	□	□m	□	
MEAN (x̄):	19.89	5.713	7.400	5.406	7.531	Fine Silt
SORTING (□):	45.36	4.512	2.231	4.873	2.285	Very Poorly Sorted
SKEWNESS (*Sk*):	4.048	0.417	-0.517	0.078	-0.078	Symmetrical
KURTOSIS (*K*):	19.80	2.698	3.018	0.985	0.985	Mesokurtic

GRAIN SIZE DISTRIBUTION

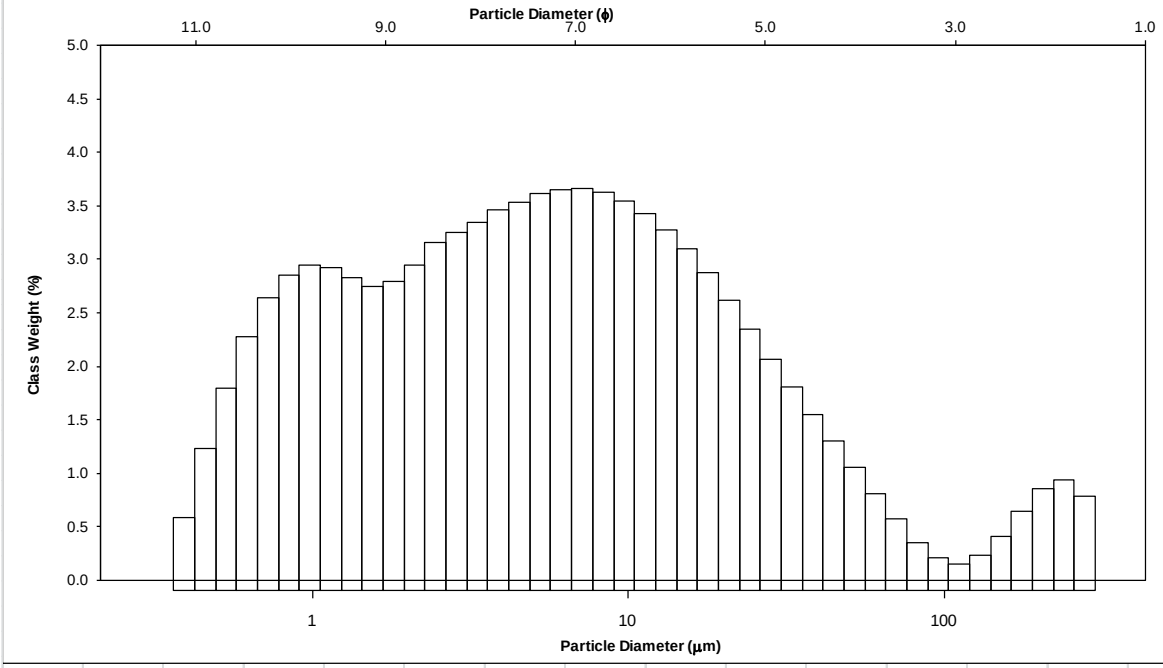

DÑA11

SAMPLE STATISTICS

SAMPLE IDENTITY:	**DNA11**				ANALYST & DATE:	,	
SAMPLE TYPE:	Bimodal, Very Poorly Sorted				TEXTURAL GROUP:	Mud	
SEDIMENT NAME:	Fine Silt						
	□m	□			GRAIN SIZE DISTRIBUTION		
MODE 1:	7.175	7.127		GRAVEL:	0.0%	COARSE SAND:	0.0%
MODE 2:	0.985	9.992		SAND:	3.2%	MEDIUM SAND:	0.0%
MODE 3:				MUD:	96.8%	FINE SAND:	0.8%
D_{10}:	0.751	5.247				V FINE SAND:	2.4%
AN or D_{50}:	4.750	7.718		V COARSE GRAVEL:	0.0%	V COARSE SILT:	4.6%
D_{90}:	26.34	10.38		COARSE GRAVEL:	0.0%	COARSE SILT:	12.1%
(D_{90} / D_{10}):	35.09	1.978		MEDIUM GRAVEL:	0.0%	MEDIUM SILT:	17.2%
(D_{90} - D_{10}):	25.59	5.133		FINE GRAVEL:	0.0%	FINE SILT:	17.7%
(D_{75} / D_{25}):	8.199	1.481		V FINE GRAVEL:	0.0%	V FINE SILT:	15.4%
(D_{75} - D_{25}):	11.04	3.035		V COARSE SAND:	0.0%	CLAY:	29.8%

	METHOD OF MOMENTS			FOLK & WARD METHOD		
	Arithmetic	Geometric	Logarithmic	Geometric	Logarithmic	Description
	□m	□m	□	□m	□	
MEAN (□):	11.57	4.669	7.743	4.451	7.812	Fine Silt
SORTING (□):	20.38	3.860	1.949	4.001	2.000	Very Poorly Sorted
SKEWNESS (*Sk*):	4.174	0.182	-0.182	-0.021	0.021	Symmetrical
KURTOSIS (*K*):	24.38	2.342	2.342	0.838	0.838	Platykurtic

GRAIN SIZE DISTRIBUTION

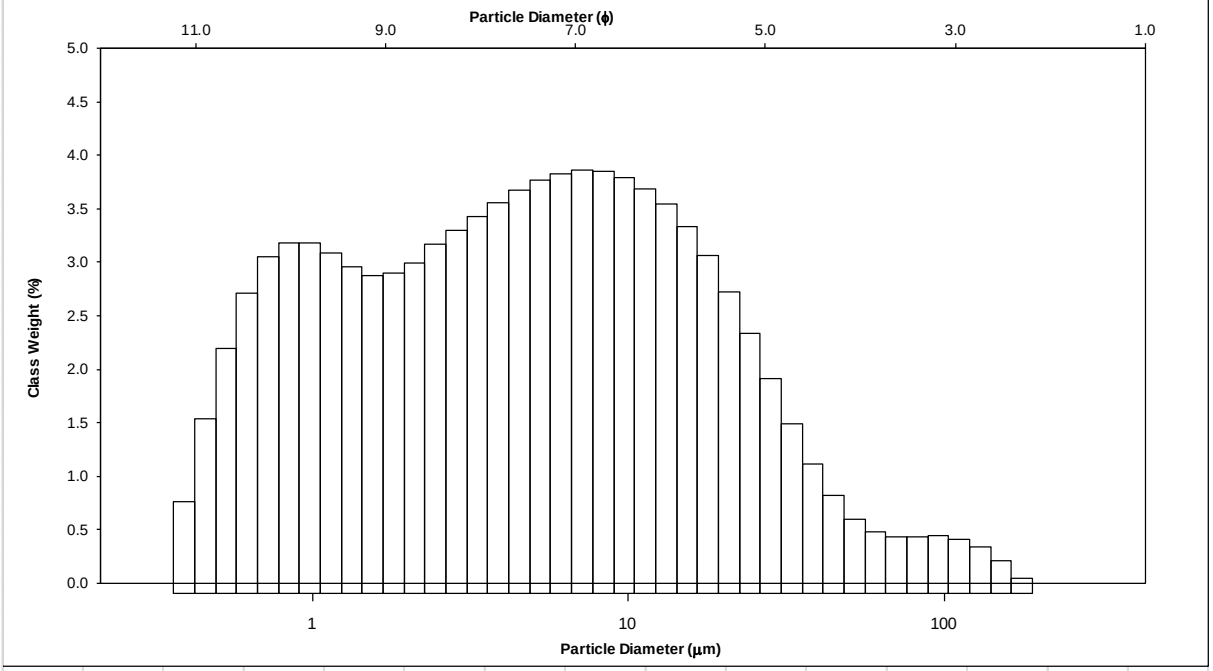

DÑA12

SAMPLE STATISTICS

SAMPLE IDENTITY:	**DNA12**				ANALYST & DATE:	,	
SAMPLE TYPE:	Trimodal, Very Poorly Sorted				TEXTURAL GROUP:	Mud	
SEDIMENT NAME:	Fine Silt						
	□m	□			GRAIN SIZE DISTRIBUTION		
MODE 1:	5.287	7.568		GRAVEL:	0.0%	COARSE SAND:	0.0%
MODE 2:	0.985	9.992		SAND:	7.1%	MEDIUM SAND:	0.7%
MODE 3:	152.2	2.720		MUD:	92.9%	FINE SAND:	3.1%
D_{10}:	0.765	4.634				V FINE SAND:	3.3%
AN or D_{50}:	4.623	7.757		V COARSE GRAVEL:	0.0%	V COARSE SILT:	5.1%
D_{90}:	40.28	10.35		COARSE GRAVEL:	0.0%	COARSE SILT:	9.7%
(D_{90} / D_{10}):	52.63	2.234		MEDIUM GRAVEL:	0.0%	MEDIUM SILT:	14.9%
(D_{90} - D_{10}):	39.51	5.718		FINE GRAVEL:	0.0%	FINE SILT:	17.5%
(D_{75} / D_{25}):	8.551	1.497		V FINE GRAVEL:	0.0%	V FINE SILT:	16.2%
(D_{75} - D_{25}):	11.74	3.096		V COARSE SAND:	0.0%	CLAY:	29.6%

	METHOD OF MOMENTS			FOLK & WARD METHOD		
	Arithmetic	Geometric	Logarithmic	Geometric	Logarithmic	Description
	□m	□m	□	□m	□	
MEAN (□):	17.62	5.090	7.600	4.733	7.723	Fine Silt
SORTING (□):	39.11	4.467	2.181	4.711	2.236	Very Poorly Sorted
SKEWNESS (*Sk*):	4.036	0.478	-0.518	0.107	-0.107	Coarse Skewed
KURTOSIS (*K*):	20.84	2.682	2.825	0.973	0.973	Mesokurtic

GRAIN SIZE DISTRIBUTION

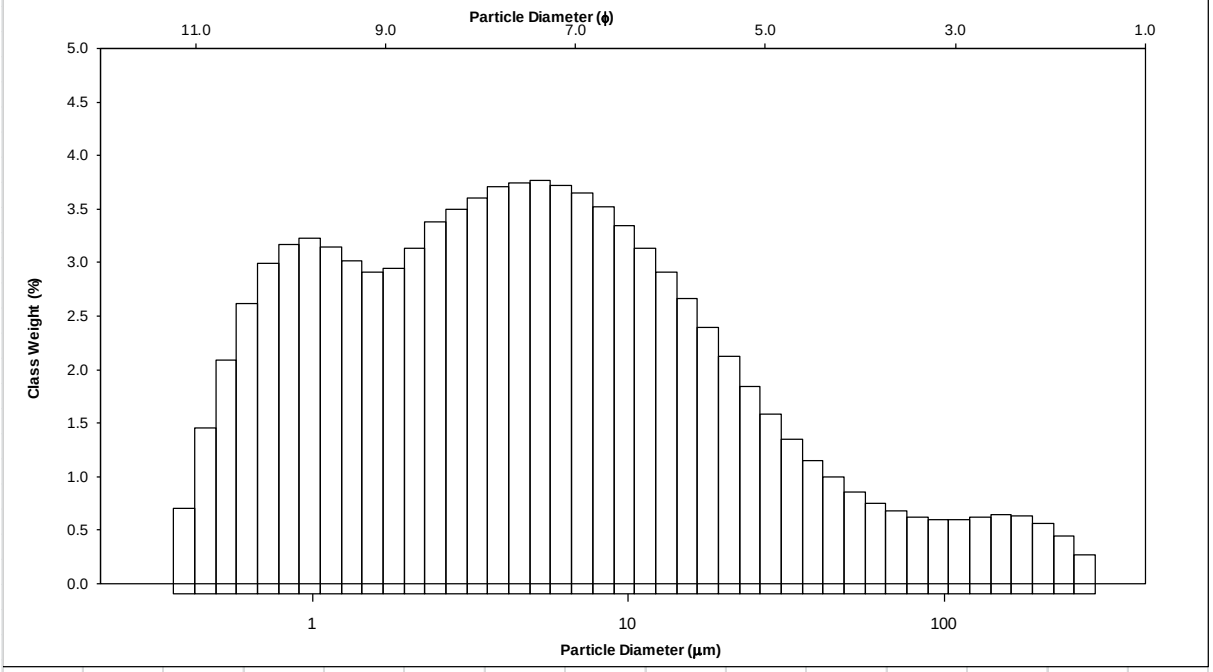

DÑA13

SAMPLE STATISTICS

SAMPLE IDENTITY:	**DNA13**			ANALYST & DATE:	,
SAMPLE TYPE:	Unimodal, Poorly Sorted			TEXTURAL GROUP:	Muddy Sand
SEDIMENT NAME:	Coarse Silty Fine Sand				

	□m	□			GRAIN SIZE DISTRIBUTION			
MODE 1:	206.5	2.280			GRAVEL:	0.0%	COARSE SAND:	0.0%
MODE 2:					SAND:	85.3%	MEDIUM SAND:	19.4%
MODE 3:					MUD:	14.7%	FINE SAND:	57.4%
D_{10}:	14.15	1.824					V FINE SAND:	8.5%
AN or D_{50}:	181.9	2.459			V COARSE GRAVEL:	0.0%	V COARSE SILT:	1.2%
D_{90}:	282.4	6.143			COARSE GRAVEL:	0.0%	COARSE SILT:	3.2%
(D_{90} / D_{10}):	19.95	3.368			MEDIUM GRAVEL:	0.0%	MEDIUM SILT:	1.9%
(D_{90} - D_{10}):	268.3	4.319			FINE GRAVEL:	0.0%	FINE SILT:	2.4%
(D_{75} / D_{25}):	1.818	1.413			V FINE GRAVEL:	0.0%	V FINE SILT:	1.9%
(D_{75} - D_{25}):	105.9	0.862			V COARSE SAND:	0.0%	CLAY:	4.1%

	METHOD OF MOMENTS			FOLK & WARD METHOD		
	Arithmetic	Geometric	Logarithmic	Geometric	Logarithmic	Description
	□m	□m	□	□m	□	
MEAN (X̄):	156.7	83.40	3.049	166.1	2.590	Fine Sand
SORTING (□):	88.12	5.667	2.117	2.629	1.395	Poorly Sorted
SKEWNESS (*Sk*):	-0.545	-1.806	2.027	-0.516	0.516	Very Fine Skewed
KURTOSIS (*K*):	2.230	4.793	7.032	3.264	3.264	Extremely Leptokurtic

GRAIN SIZE DISTRIBUTION

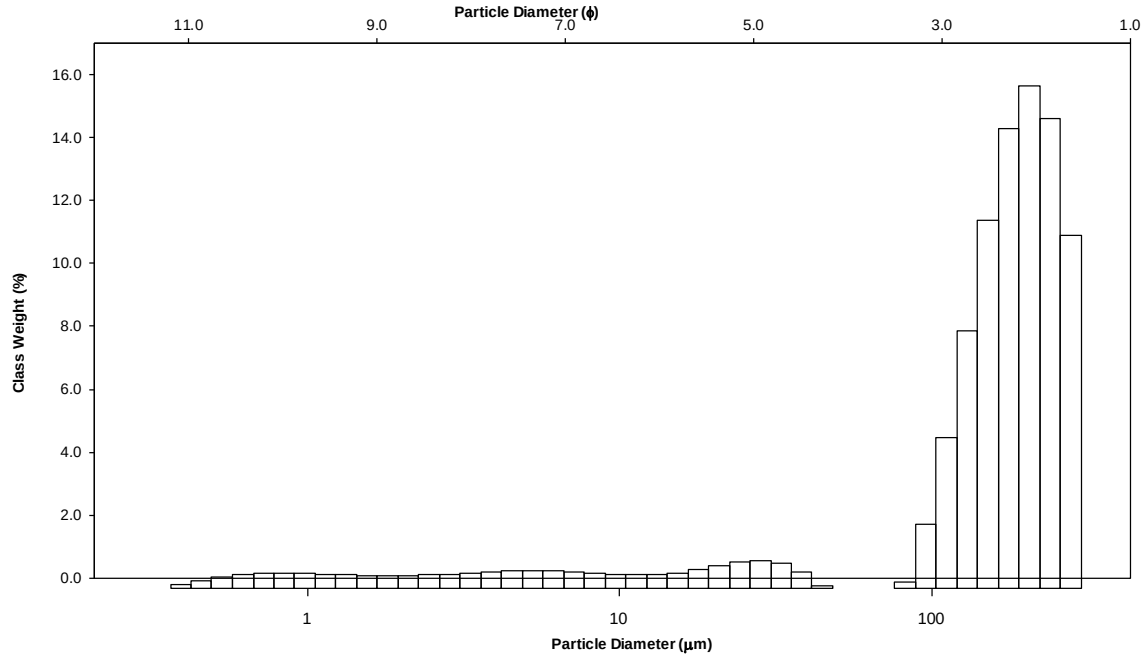

DÑA14

SAMPLE STATISTICS

SAMPLE IDENTITY:	**DNA14**			ANALYST & DATE:	,
SAMPLE TYPE:	Unimodal, Poorly Sorted			TEXTURAL GROUP:	Mud
SEDIMENT NAME:	Fine Silt				

	□m	□	GRAIN SIZE DISTRIBUTION			
MODE 1:	5.287	7.568	GRAVEL:	0.0%	COARSE SAND:	0.0%
MODE 2:			SAND:	4.8%	MEDIUM SAND:	0.3%
MODE 3:			MUD:	95.2%	FINE SAND:	1.7%
D_{10}:	0.802	5.256			V FINE SAND:	2.8%
AN or D_{50}:	4.292	7.864	V COARSE GRAVEL:	0.0%	V COARSE SILT:	3.8%
D_{90}:	26.17	10.28	COARSE GRAVEL:	0.0%	COARSE SILT:	7.7%
(D_{90} / D_{10}):	32.61	1.956	MEDIUM GRAVEL:	0.0%	MEDIUM SILT:	15.9%
(D_{90} - D_{10}):	25.36	5.027	FINE GRAVEL:	0.0%	FINE SILT:	20.6%
(D_{75} / D_{25}):	6.268	1.401	V FINE GRAVEL:	0.0%	V FINE SILT:	18.3%
(D_{75} - D_{25}):	8.602	2.648	V COARSE SAND:	0.0%	CLAY:	29.0%

	METHOD OF MOMENTS			FOLK & WARD METHOD		
	Arithmetic	Geometric	Logarithmic	Geometric	Logarithmic	Description
	□m	□m	□	□m	□	
MEAN (□):	13.07	4.528	7.780	4.185	7.901	Fine Silt
SORTING (□):	29.62	3.850	1.955	3.937	1.977	Poorly Sorted
SKEWNESS (*Sk*):	4.916	0.495	-0.522	0.060	-0.060	Symmetrical
KURTOSIS (*K*):	31.63	2.982	3.089	1.025	1.025	Mesokurtic

GRAIN SIZE DISTRIBUTION

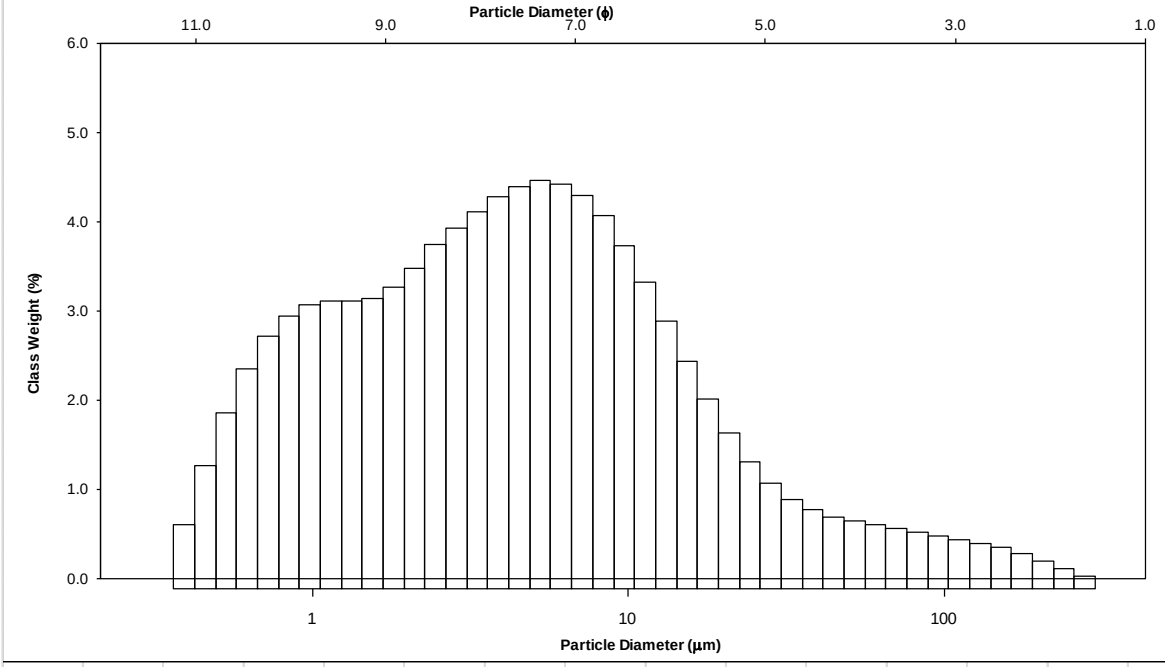

DÑA15

SAMPLE STATISTICS

SAMPLE IDENTITY:	**DNA15**			ANALYST & DATE:	,
SAMPLE TYPE:	Bimodal, Poorly Sorted			TEXTURAL GROUP:	Mud
SEDIMENT NAME:	Fine Silt				

	□m	□	GRAIN SIZE DISTRIBUTION			
MODE 1:	7.175	7.127	GRAVEL:	0.0%	COARSE SAND:	0.0%
MODE 2:	0.985	9.992	SAND:	3.3%	MEDIUM SAND:	0.0%
MODE 3:			MUD:	96.7%	FINE SAND:	0.8%
D_{10}:	0.840	5.147			V FINE SAND:	2.5%
AN or D_{50}:	5.415	7.529	V COARSE GRAVEL:	0.0%	V COARSE SILT:	5.4%
D_{90}:	28.23	10.22	COARSE GRAVEL:	0.0%	COARSE SILT:	12.0%
(D_{90} / D_{10}):	33.61	1.985	MEDIUM GRAVEL:	0.0%	MEDIUM SILT:	18.5%
(D_{90} - D_{10}):	27.39	5.071	FINE GRAVEL:	0.0%	FINE SILT:	19.9%
(D_{75} / D_{25}):	6.650	1.437	V FINE GRAVEL:	0.0%	V FINE SILT:	16.0%
(D_{75} - D_{25}):	11.12	2.733	V COARSE SAND:	0.0%	CLAY:	24.8%

	METHOD OF MOMENTS			FOLK & WARD METHOD		
	Arithmetic	Geometric	Logarithmic	Geometric	Logarithmic	Description
	□m	□m	□	□m	□	
MEAN (□):	12.25	5.245	7.575	5.001	7.644	Fine Silt
SORTING (□):	20.75	3.710	1.891	3.881	1.956	Poorly Sorted
SKEWNESS (*Sk*):	4.136	0.113	-0.113	-0.043	0.043	Symmetrical
KURTOSIS (*K*):	24.70	2.466	2.466	0.936	0.936	Mesokurtic

GRAIN SIZE DISTRIBUTION

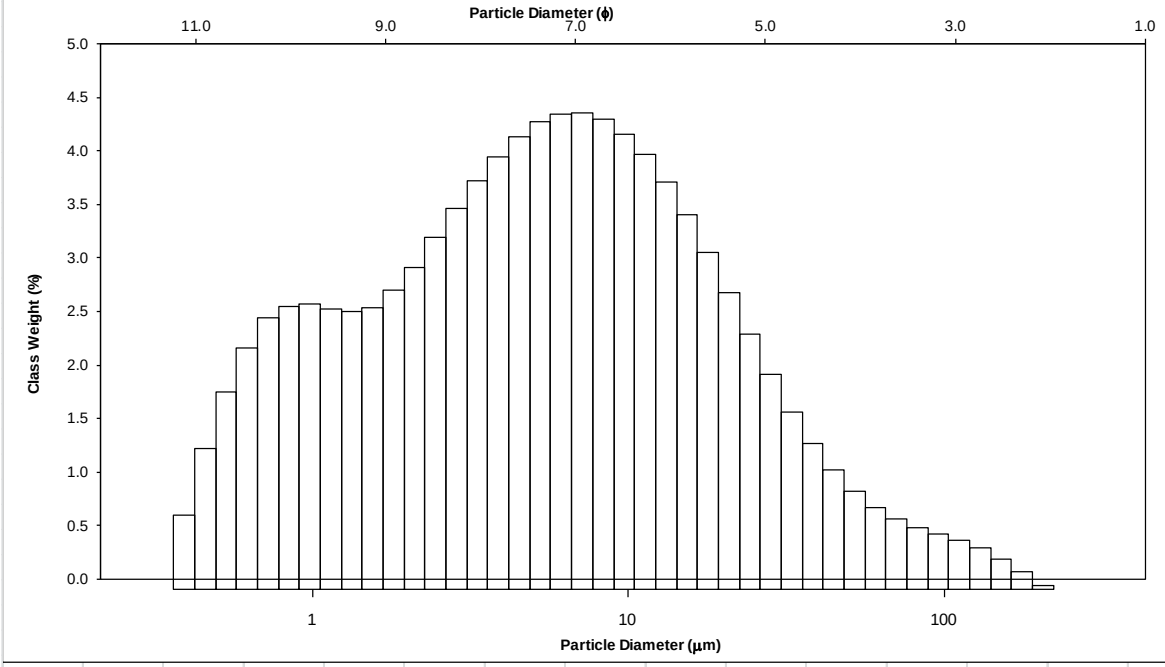

DÑA16

SAMPLE STATISTICS

SAMPLE IDENTITY:	**DNA16**				ANALYST & DATE:	,	
SAMPLE TYPE:	Bimodal, Very Poorly Sorted				TEXTURAL GROUP:	Mud	
SEDIMENT NAME:	Medium Silt						
	□m	□			GRAIN SIZE DISTRIBUTION		
MODE 1:	9.738	6.686		GRAVEL:	0.0%	COARSE SAND:	0.0%
MODE 2:	0.985	9.992		SAND:	6.0%	MEDIUM SAND:	0.0%
MODE 3:				MUD:	94.0%	FINE SAND:	1.1%
D_{10}:	0.892	4.441				V FINE SAND:	4.9%
AN or D_{50}:	7.497	7.060		V COARSE GRAVEL:	0.0%	V COARSE SILT:	10.7%
D_{90}:	46.04	10.13		COARSE GRAVEL:	0.0%	COARSE SILT:	15.4%
(D_{90} / D_{10}):	51.63	2.281		MEDIUM GRAVEL:	0.0%	MEDIUM SILT:	16.9%
(D_{90} - D_{10}):	45.15	5.690		FINE GRAVEL:	0.0%	FINE SILT:	16.0%
(D_{75} / D_{25}):	9.148	1.574		V FINE GRAVEL:	0.0%	V FINE SILT:	12.8%
(D_{75} - D_{25}):	18.87	3.194		V COARSE SAND:	0.0%	CLAY:	22.2%

	METHOD OF MOMENTS			FOLK & WARD METHOD		
	Arithmetic	Geometric	Logarithmic	Geometric	Logarithmic	Description
	□m	□m	□	□m	□	
MEAN (M):	17.44	7.019	7.155	6.819	7.196	Fine Silt
SORTING (□):	25.77	4.218	2.077	4.536	2.181	Very Poorly Sorted
SKEWNESS (*Sk*):	3.036	-0.055	0.055	-0.070	0.070	Symmetrical
KURTOSIS (*K*):	15.08	2.155	2.155	0.866	0.866	Platykurtic

GRAIN SIZE DISTRIBUTION

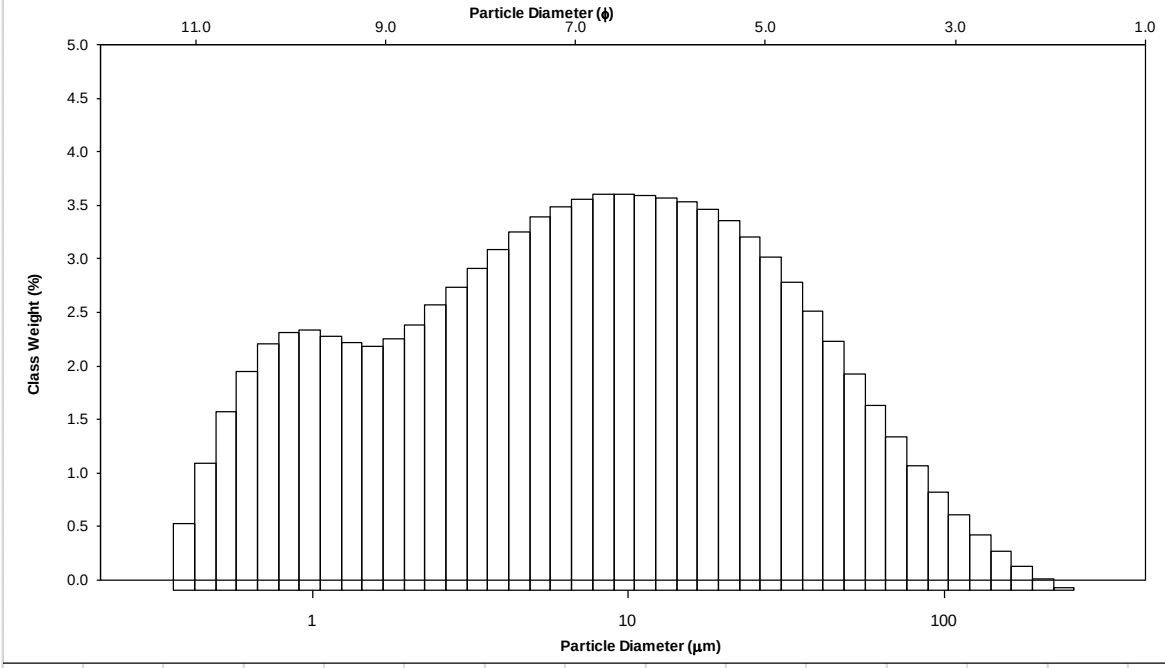

DÑA17

SAMPLE STATISTICS

SAMPLE IDENTITY:	**DNA17**				ANALYST & DATE:	,	
SAMPLE TYPE:	Bimodal, Poorly Sorted				TEXTURAL GROUP:	Mud	
SEDIMENT NAME:	Fine Silt						
	□m	□			GRAIN SIZE DISTRIBUTION		
MODE 1:	7.175	7.127		GRAVEL:	0.0%	COARSE SAND:	0.0%
MODE 2:	0.846	10.21		SAND:	1.8%	MEDIUM SAND:	0.0%
MODE 3:				MUD:	98.2%	FINE SAND:	0.3%
D_{10}:	0.744	5.667				V FINE SAND:	1.5%
AN or D_{50}:	4.430	7.818		V COARSE GRAVEL:	0.0%	V COARSE SILT:	2.9%
D_{90}:	19.68	10.39		COARSE GRAVEL:	0.0%	COARSE SILT:	9.7%
(D_{90} / D_{10}):	26.47	1.834		MEDIUM GRAVEL:	0.0%	MEDIUM SILT:	18.6%
(D_{90} - D_{10}):	18.94	4.726		FINE GRAVEL:	0.0%	FINE SILT:	20.6%
(D_{75} / D_{25}):	6.707	1.415		V FINE GRAVEL:	0.0%	V FINE SILT:	16.6%
(D_{75} - D_{25}):	8.694	2.746		V COARSE SAND:	0.0%	CLAY:	29.9%

	METHOD OF MOMENTS			FOLK & WARD METHOD		
	Arithmetic	Geometric	Logarithmic	Geometric	Logarithmic	Description
	□m	□m	□	□m	□	
MEAN ($\bar{x}$):	9.045	4.167	7.907	3.978	7.974	Fine Silt
SORTING (□):	15.33	3.470	1.795	3.564	1.833	Poorly Sorted
SKEWNESS (Sk):	4.848	0.124	-0.124	-0.076	0.076	Symmetrical
KURTOSIS (K):	33.38	2.443	2.443	0.850	0.850	Platykurtic

GRAIN SIZE DISTRIBUTION

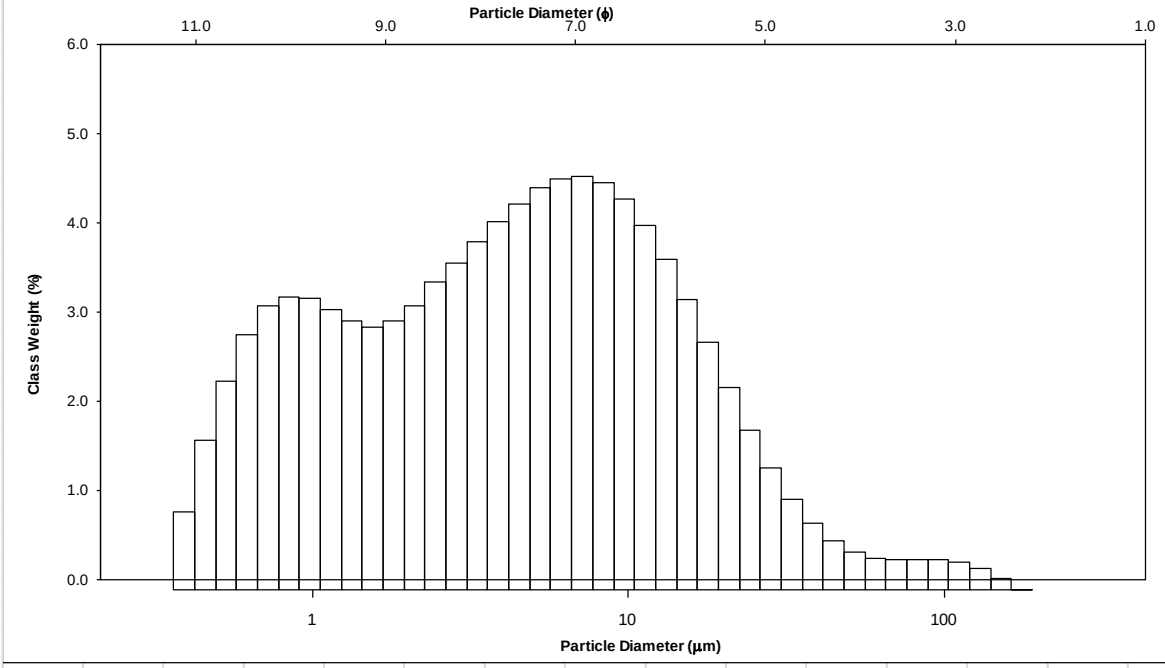

DÑA18

SAMPLE STATISTICS

SAMPLE IDENTITY:	**DNA18**			ANALYST & DATE:	,
SAMPLE TYPE:	Bimodal, Very Poorly Sorted			TEXTURAL GROUP:	Mud
SEDIMENT NAME:	Medium Silt				

	□m	□			GRAIN SIZE DISTRIBUTION			
MODE 1:	8.359	6.907		GRAVEL:	0.0%		COARSE SAND:	0.0%
MODE 2:	0.846	10.21		SAND:	2.1%		MEDIUM SAND:	0.0%
MODE 3:				MUD:	97.9%		FINE SAND:	0.1%
D_{10}:	0.744	5.091					V FINE SAND:	2.0%
AN or D_{50}:	5.362	7.543		V COARSE GRAVEL:	0.0%		V COARSE SILT:	6.9%
D_{90}:	29.34	10.39		COARSE GRAVEL:	0.0%		COARSE SILT:	13.9%
(D_{90} / D_{10}):	39.45	2.041		MEDIUM GRAVEL:	0.0%		MEDIUM SILT:	17.6%
(D_{90} - D_{10}):	28.59	5.302		FINE GRAVEL:	0.0%		FINE SILT:	17.0%
(D_{75} / D_{25}):	8.966	1.517		V FINE GRAVEL:	0.0%		V FINE SILT:	14.0%
(D_{75} - D_{25}):	12.75	3.164		V COARSE SAND:	0.0%		CLAY:	28.5%

	METHOD OF MOMENTS			FOLK & WARD METHOD		
	Arithmetic	Geometric	Logarithmic	Geometric	Logarithmic	Description
	□m	□m	□	□m	□	
MEAN (□):	11.41	4.994	7.646	4.833	7.693	Fine Silt
SORTING (□):	16.06	3.880	1.956	4.134	2.048	Very Poorly Sorted
SKEWNESS (*Sk*):	3.012	-0.004	0.004	-0.069	0.069	Symmetrical
KURTOSIS (*K*):	15.36	2.068	2.068	0.805	0.805	Platykurtic

GRAIN SIZE DISTRIBUTION

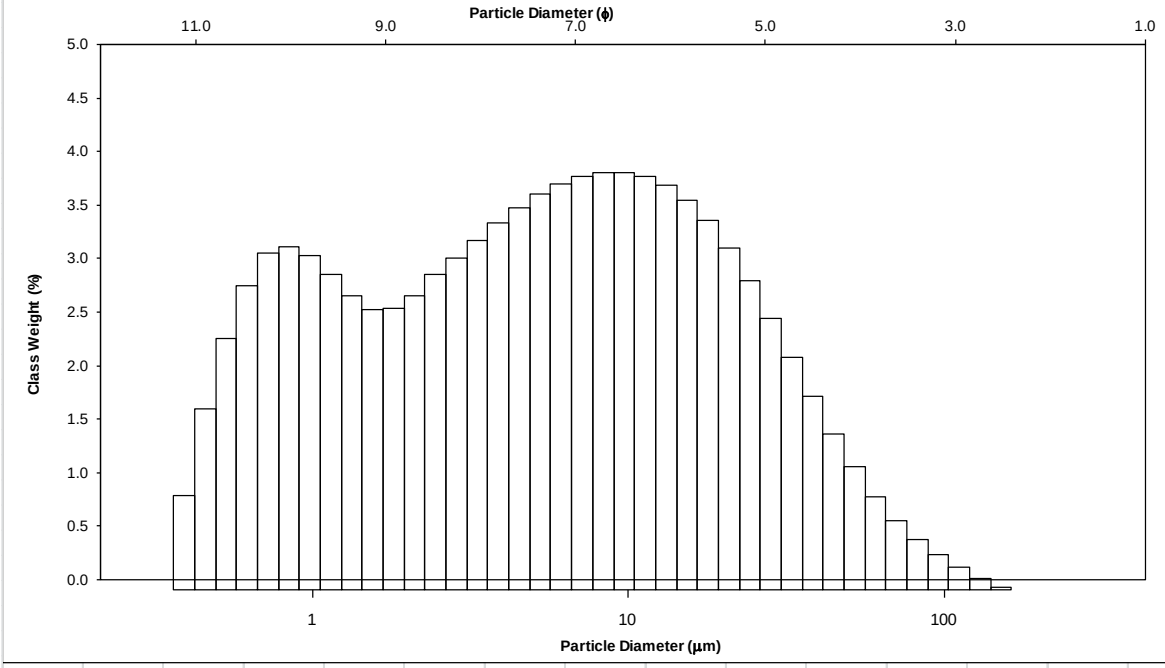

DÑA19

SAMPLE STATISTICS

SAMPLE IDENTITY:	**DNA19**		ANALYST & DATE:	,	
SAMPLE TYPE:	Unimodal, Moderately Sorted		TEXTURAL GROUP:	Sand	
SEDIMENT NAME:	Moderately Sorted Fine Sand				

	□m	□	GRAIN SIZE DISTRIBUTION			
MODE 1:	240.6	2.059	GRAVEL:	0.0%	COARSE SAND:	0.0%
MODE 2:			SAND:	94.1%	MEDIUM SAND:	24.5%
MODE 3:			MUD:	5.9%	FINE SAND:	64.4%
D_{10}:	121.6	1.801			V FINE SAND:	5.2%
AN or D_{50}:	206.3	2.277	V COARSE GRAVEL:	0.0%	V COARSE SILT:	1.0%
D_{90}:	287.0	3.040	COARSE GRAVEL:	0.0%	COARSE SILT:	1.6%
(D_{90} / D_{10}):	2.361	1.688	MEDIUM GRAVEL:	0.0%	MEDIUM SILT:	0.2%
(D_{90} - D_{10}):	165.5	1.239	FINE GRAVEL:	0.0%	FINE SILT:	0.8%
(D_{75} / D_{25}):	1.522	1.302	V FINE GRAVEL:	0.0%	V FINE SILT:	0.6%
(D_{75} - D_{25}):	85.43	0.606	V COARSE SAND:	0.0%	CLAY:	1.6%

	METHOD OF MOMENTS			FOLK & WARD METHOD		
	Arithmetic	Geometric	Logarithmic	Geometric	Logarithmic	Description
	□m	□m	□	□m	□	
MEAN (x̄):	184.5	123.8	2.490	199.1	2.328	Fine Sand
SORTING (□):	77.90	4.279	1.436	1.661	0.732	Moderately Sorted
SKEWNESS (*Sk*):	-1.027	-2.729	3.196	-0.391	0.391	Very Fine Skewed
KURTOSIS (*K*):	3.470	9.106	17.43	2.237	2.237	Very Leptokurtic

GRAIN SIZE DISTRIBUTION

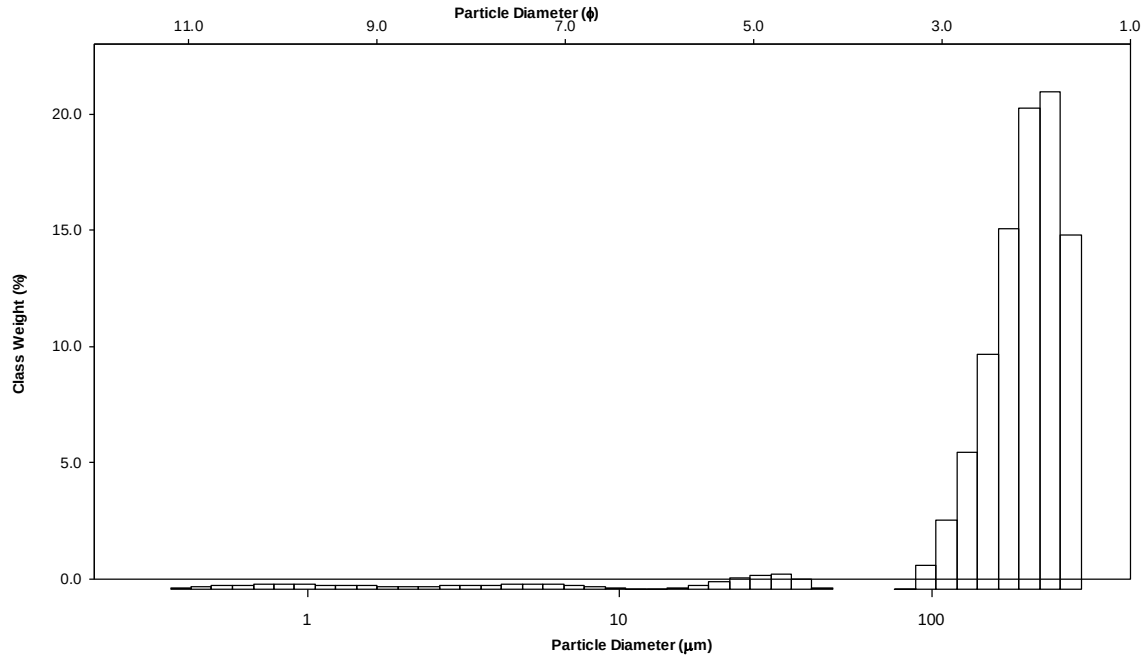

DÑA20

SAMPLE STATISTICS

SAMPLE IDENTITY:	**DNA20**			ANALYST & DATE:	,
SAMPLE TYPE:	Unimodal, Moderately Well Sorted			TEXTURAL GROUP:	Sand
SEDIMENT NAME:	Moderately Well Sorted Fine Sand				

	□m	□			GRAIN SIZE DISTRIBUTION			
MODE 1:	206.5	2.280		GRAVEL:	0.0%		COARSE SAND:	0.0%
MODE 2:				SAND:	96.2%		MEDIUM SAND:	17.1%
MODE 3:				MUD:	3.8%		FINE SAND:	66.7%
D_{10}:	108.4	1.862					V FINE SAND:	12.3%
AN or D_{50}:	183.8	2.444		V COARSE GRAVEL:	0.0%		V COARSE SILT:	0.2%
D_{90}:	275.0	3.205		COARSE GRAVEL:	0.0%		COARSE SILT:	1.6%
(D_{90} / D_{10}):	2.536	1.721		MEDIUM GRAVEL:	0.0%		MEDIUM SILT:	0.2%
(D_{90} - D_{10}):	166.6	1.343		FINE GRAVEL:	0.0%		FINE SILT:	0.5%
(D_{75} / D_{25}):	1.608	1.324		V FINE GRAVEL:	0.0%		V FINE SILT:	0.4%
(D_{75} - D_{25}):	87.08	0.686		V COARSE SAND:	0.0%		CLAY:	0.8%

	METHOD OF MOMENTS			FOLK & WARD METHOD		
	Arithmetic	Geometric	Logarithmic	Geometric	Logarithmic	Description
	□m	□m	□	□m	□	
MEAN (x̄):	172.5	127.7	2.553	179.7	2.477	Fine Sand
SORTING (□):	70.22	3.436	1.149	1.440	0.526	Moderately Well Sorte
SKEWNESS (*Sk*):	-0.694	-3.202	2.898	-0.159	0.159	Fine Skewed
KURTOSIS (*K*):	3.341	12.43	19.51	1.068	1.068	Mesokurtic

GRAIN SIZE DISTRIBUTION

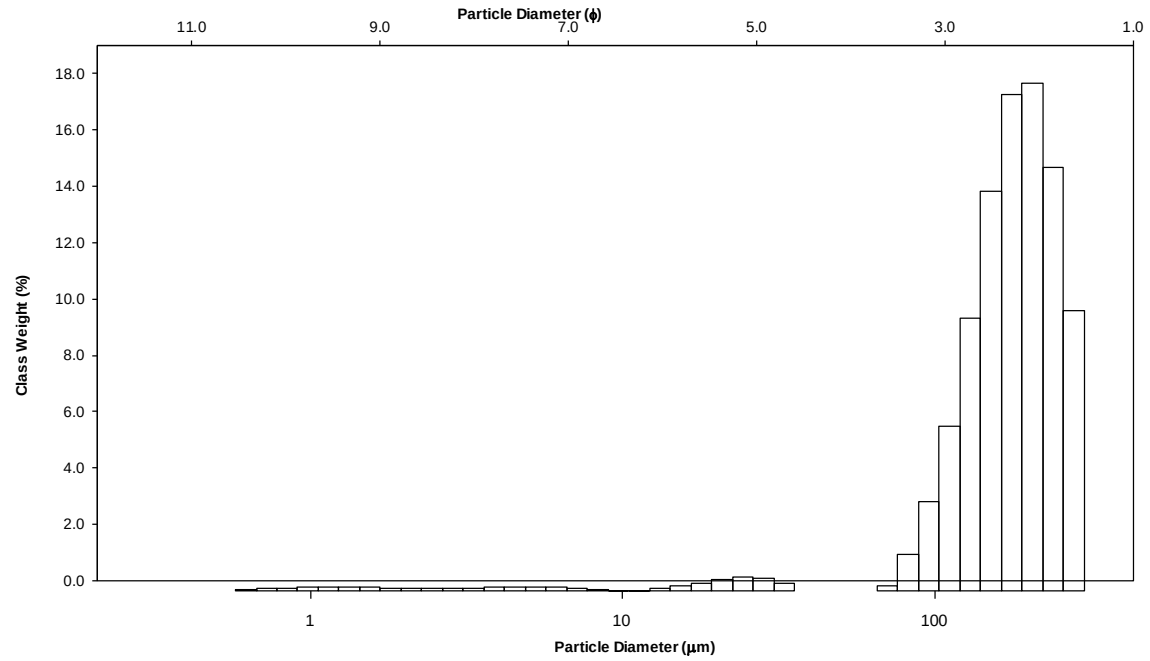

Appendix 2- Surface Samples' Minerology results

Performed in XPowder 2004 Software Version 0.4.0.2.

Samples			DNA 1		DNA2		DNA3		DNA4		DNA5		DNA6		DNA7		DNA8		DNA9		DNA10		DNA11		DNA12		DNA13		DNA14		DNA15		DNA16		DNA17		DNA18		DNA19		DNA20	
Mineral	Reflectant Power	d A	%	Crystalinity (nm)	%	Crystalinity (nm)	%	Crystalinity (nm)	%	Crystalinity (nm)	%	Crystalinity (nm)	%	Crystalinity (nm)	%	Crystalinity (nm)	%	Crystalinity (nm)	%	Crystalinity (nm)	%	Crystalinity (nm)	%	Crystalinity (nm)	%	Crystalinity (nm)	%	Crystalinity (nm)	%	Crystalinity (nm)	%	Crystalinity (nm)	%	Crystalinity (nm)	%	Crystalinity (nm)	%	Crystalinity (nm)	%	Crystalinity (nm)	%	Crystalinity (nm)
Pyrite	0.5	1.63	0		0		0		0		0		0		0		0		0		0		0		0		0		0		0		0		0		0		0		0	
Halite	1	2.82			0		0		0		0		0		0		0		0				5.615003423	68	6.420251661	61	0		23.08827805	57	0		0		0		0		0		0	
Goetite	0.5	2.68	0		0		0		0		0		0		0		0		0		0		0		0		0		0		0		0		0		0		0		0	
Hematite	0.5	2.7	0		0		0		0		0		0		0		0		0		0		0		0		0		0		0		0		0		0		0		0	
Magnesite	0.4	2.74	0		0		0		0		0		0		0		0		0		0		0		0		0		0		0		0		0		0		0		0	
Siderite	0.6	2.79	0		0		0		0		0		0		0		0		0		0		0		0		0		0		0		0		0		0		0		0	
Dolomite	1	2.88	0		0		0		0		2.212866852	39	0		0		0		0		0		3.32508113	44	2.202410048	26	0		1.77808593	24	0		0		0		0		0		0	
Ankerite	0.9	2.9	0		0		0		0		0		0		0		0		0		0		0		0		0		0		0		0		0		0		0		0	
Calcite	1	3.03	0		0		0		0		25.77595697	46	0		0		0		0		19.80119808	38	50.00919836	33	25.15392344	28	0		35.34946657	44	36.0035263	47	34.91126485	50	32.80551115	44	36.07709855	45	0.415553843	46	1.974852014	52
Plagioclase	1	3.19	0		0		0		0.949415059	45	1.968780145	27	0		0		0		0.686892523	43	1.949522151	23	3.280714253	28	1.280411132	34	0.580055184	54	0		4.293270644	16	2.748533614	23	0.961650848	32	2.133015984	23	0		0	
Feldspar K	1	3.24	1.468949607	35	1.417871846	48	0.985495386	48	0		0		0.74404915	50	0.955985761	45	0.578818848	45	0.751921694	57	0		0		0		0.862857093	56	0		0		0		0		0		0		0.136344276	58	1.128157804	57
Quartz	1.5	3.34	98.53105139	55	98.58212815	55	99.01456461	55	63.1035948	51	21.15982787	51	99.25595085	44	97.12440981	53	99.42118115	56	98.56108578	55	37.80866801	52	15.5530687	50	10.20115519	51	98.55708693	55	7.756480508	49	16.35909482	49	20.35393794	59	10.94138456	49	14.02117052	49	99.45010308	55	96.89898927	56
Aragonite	1	3.4	0		0		0		0		0		0		0		0		0		0		0		0		0		0		0		0		0		0		0		0	
Anhydrite	1	3.5	0		0		0		0		0		0		0		0		0		0		5.16108147	18	3.327932195	11	0		1.375500496	17	0		0		0		0		0		0	
Cristobalite	0.5	4.05	0		0		0		0		0		0		0		0		0		0		0		0		0		0		0		0		0		0		0		0	
Quartz	0.6	4.26	0		0		0		0		0		0		0		0		0		0		0		0		0		0		0		0		0		0		0		0	
Phyllosilicates	0.15	4.45	0		0		0		35.94759014	19	47.84547817	22	0		1.91900431	39	0		0		40.44061177	19	0		51.40221862	20	0		39.15200562	22	43.34410814	24	41.9862636	22	55.28025341	21	47.76874524	22	0		0	
Gypsum	1.5	7.56	0		0		0		0		0		0		0		0		0		0		0		0		0		1.400102883	47	0		0		0		0		0		0	

Appendix 3 - Faunistic density (Ni/g) of all specimens in Core C, sampling depth (m), and total number of specimens obtained in each sample/depth

Depth / Taxa	46	50	54	58	62	66	70	74	78	82	86	90	94	98	116	120	124	128	132	136	140	144	148
Buliminella elegantissima	1	0	0	0	0	0	0	0	0	0	0	0	0	0	0	0	0	0	0	1	1	0	1
Haynesina germanica	291	238	249	258	234	159	213	298	183	201	511	376	228	235	254	190	219	198	342	192	186	220	236
Ammonia tepida	75	77	69	94	76	54	64	75	57	68	154	109	88	55	92	79	51	42	78	51	57	51	59
Brizalina sp	2	0	0	0	2	0	0	0	0	0	1	0	0	0	0	1	0	0	0	0	3	0	1
Bolivina ordinaria	3	2	0	2	1	1	3	0	1	1	0	0	1	1	0	3	4	3	1	2	3	4	10
Elphidium cuvillieri	6	0	2	5	3	4	2	2	2	5	5	1	5	5	12	9	3	2	2	1	7	1	8
Elphidium oceanensis	4	5	5	7	8	8	0	4	3	7	4	2	2	0	11	14	3	7	5	6	5	10	0
Elphidium granosum	1	3	0	7	0	0	5	0	3	2	13	4	4	9	22	4	4	2	9	1	7	6	16
Elphidium sp	0	4	0	0	0	0	0	3	0	0	0	2	8	12	0	3	0	0	0	0	0	4	13
Elphidium complanatum	0	0	1	0	0	0	0	0	0	0	0	2	0	0	0	0	0	0	0	0	0	0	0
Bulimina elongata	0	0	0	0	1	1	0	0	0	0	0	0	0	0	0	0	0	1	0	1	0	0	0
Asterigerinata mamilla	0	0	0	0	0	1	0	1	0	0	0	0	0	0	0	0	0	0	1	0	0	0	0
Spirillina vivipara	0	0	0	0	0	0	1	0	0	0	0	0	0	0	0	0	0	0	0	0	0	2	1
Lagena sulcata	0	0	0	0	0	0	0	1	0	0	0	0	0	0	0	0	0	0	0	0	0	0	0
Planorbulina mediterranensis	0	0	0	0	0	0	0	1	0	0	0	1	1	0	0	0	0	0	0	0	0	0	0
Uvigerina peregrina	0	0	0	0	0	0	0	0	0	1	0	0	0	0	0	0	0	0	0	0	0	0	0
Textularia sp	0	0	0	0	0	0	0	0	0	1	1	0	0	0	0	0	0	1	0	0	0	0	1
Rosalina bradyi	0	0	0	0	0	0	0	0	0	0	1	0	0	0	0	0	0	0	0	0	0	0	0
Spirillina sp	0	0	0	0	0	0	0	0	0	0	1	1	0	0	0	0	0	0	0	0	0	0	0
Bulimina marginata	0	0	0	0	0	0	0	0	0	0	1	0	0	0	0	0	0	0	0	0	0	0	0
Stainforthia complanata	0	0	0	0	0	0	0	0	0	0	0	0	0	1	0	0	0	0	0	0	0	0	0
Quinqueloculina laevigata	0	0	0	0	0	0	0	0	0	0	0	0	0	0	0	1	0	0	0	5	0	0	0
Fissurina sp (1,2,3)	0	0	0	0	0	0	0	0	0	0	0	0	0	0	0	0	6	10	6	7	5	0	0
Stilostomella sp	0	0	0	0	0	0	0	0	0	0	0	0	0	0	0	0	1	1	2	0	0	0	0
Brizalina striatula	0	0	0	0	0	0	0	0	0	0	0	0	0	0	0	0	1	0	0	0	0	0	0
Triloculina trigonula	0	0	0	0	0	0	0	0	0	0	0	0	0	0	0	0	0	0	0	1	0	0	0
Quinqueloculina sp	0	0	0	0	0	0	0	0	0	0	0	0	0	0	0	0	0	0	0	1	11	0	0
Cornuloculina sp	0	0	0	0	0	0	0	0	0	0	0	0	0	0	0	0	0	0	0	0	1	0	0
Cornuspira involvens	0	0	0	0	0	0	0	0	0	0	0	0	0	0	0	0	0	0	0	0	1	0	0
Nonionella stella	0	0	0	0	0	0	0	0	0	0	0	0	0	0	0	0	0	0	0	0	0	0	1
Quinqueloculina stelligera	0	0	0	0	0	0	0	0	0	0	0	0	0	0	0	0	0	0	0	0	0	0	9
Total individuals per sample/depth	383	329	326	373	325	228	288	385	249	286	692	498	337	318	391	304	292	267	446	269	287	298	356

Appendix 4 - Faunistic density (Ni/g) of all specimens in Core D, sampling depth (m), and total number of specimens obtained in each sample/depth

Depth	27	31	34	38	41	45	48	52	55	59	62	66	69	73	76	80	83	87	90	94	97	101	104	108	111	115	118	122	125	129	132	136	139	143	146	150	153	157	160
Buliminella elegantissima	0	0	0	1	0	0	0	0	0	2	0	0	0	1	1	0	0	0	0	0	0	0	0	0	0	0	0	0	0	0	0	1	2	1	0	0	0	1	0
Haynesina germanica	86	81	78	46	52	84	66	84	48	166	55	57	67	92	88	99	26	12	7	166	198	73	223	189	165	217	105	83	261	220	183	167	125	198	143	115	206	224	195
Ammonia tepida	180	175	193	186	215	267	193	159	177	40	11	43	71	117	156	144	20	8	5	33	21	16	11	52	33	32	129	14	39	41	73	86	109	91	84	119	96	70	57
Brizalina sp	0	1	0	3	0	0	0	2	0	0	0	1	0	0	0	1	0	0	0	0	0	0	0	0	0	0	0	0	0	0	0	8	12	2	3	0	4	9	4
Bolivina ordinaria	0	0	0	0	1	0	0	1	0	1	1	0	0	0	0	3	0	0	0	7	0	0	1	3	2	3	0	0	2	1	7	11	4	9	5	25	2	8	24
Elphidium cuvillieri	6	15	3	6	16	12	1	9	27	2	0	2	4	5	4	0	0	0	0	1	1	0	0	1	0	0	8	0	0	0	2	11	0	7	7	2	2	0	1
Elphidium oceanensis	27	25	17	28	21	14	21	10	16	1	0	0	7	12	18	7	0	1	2	2	1	0	0	5	0	0	12	1	0	0	0	0	8	4	8	7	0	0	3
Elphidium granosum	9	0	10	8	7	16	12	11	2	0	0	0	0	4	8	12	0	2	1	3	1	0	0	0	0	0	7	0	0	0	0	0	5	0	0	0	0	6	3
Elphidium sp	12	5	11	0	9	20	0	2	0	0	0	0	0	0	6	8	0	0	0	0	0	4	0	0	0	1	3	0	0	0	0	0	0	0	0	0	10	0	0
Elphidium complanatum	3	2	0	0	0	0	3	1	1	0	0	0	0	0	0	0	0	0	0	0	0	0	0	0	0	0	0	0	0	0	0	0	0	0	0	0	0	0	0
Bulimina elongata	0	0	0	2	0	2	0	0	1	0	0	0	1	0	0	0	0	0	0	0	0	0	0	0	0	0	0	0	0	0	0	2	0	0	0	0	1	0	0
Asterigerinata mamilla	0	0	0	1	1	1	2	3	1	0	0	0	1	0	1	1	1	0	0	1	0	0	0	1	0	1	0	0	0	0	1	0	0	0	2	2	0	3	1
Spirillina vivipara	0	0	0	0	0	0	0	0	0	0	0	0	0	0	1	0	0	0	0	0	0	0	0	0	0	0	0	0	0	0	0	0	1	1	0	1	2	0	0
Lagena sulcata	0	0	1	0	0	0	0	0	0	0	0	0	0	1	0	0	0	0	0	0	0	0	0	0	0	0	0	0	0	0	0	0	0	0	0	0	0	0	0
Planorbulina mediterranensis	2	1	0	1	2	0	0	0	0	0	0	0	1	0	0	1	0	0	0	0	0	0	0	0	0	0	0	0	0	0	0	0	0	0	3	0	0	0	0
Uvigerina peregrina	0	0	1	2	0	2	4	0	1	0	0	0	0	0	0	0	0	0	0	0	0	0	0	0	0	0	0	0	0	0	0	0	0	1	0	0	0	0	0
Textularia sp	0	0	0	0	0	0	0	0	0	0	0	0	0	0	0	0	0	0	0	0	0	0	0	0	0	0	0	0	0	0	5	5	2	3	1	1	2	1	2
Rosalina bradyi	3	2	1	4	3	0	0	0	0	0	0	0	1	0	4	1	0	0	0	0	0	0	0	0	0	0	1	0	0	0	0	0	1	0	0	0	0	0	0
Fissurina sp (1,2,3)	0	0	0	0	0	0	0	0	0	0	0	3	1	0	0	0	0	2	0	3	0	3	13	16	6	0	9	5	5	7	12	22	6	8	5	9	3	1	0
Stilostomella sp	0	0	0	1	0	0	0	0	0	0	0	0	0	0	0	0	0	0	0	0	0	0	0	0	0	0	0	0	0	0	1	0	0	0	0	0	1	0	0
Triloculina trigonula	0	1	0	0	0	0	0	0	0	0	0	0	0	4	0	1	0	0	0	0	0	0	0	0	0	0	0	0	0	0	0	0	0	0	0	0	0	0	0
Quinqueloculina sp	6	0	2	1	0	0	2	2	2	0	0	0	0	0	5	1	0	0	0	0	0	0	0	1	0	1	0	0	0	0	0	0	0	0	0	0	1	0	0
Cornuloculina sp	0	0	0	0	1	0	0	0	0	0	0	0	0	0	0	0	0	0	0	0	0	0	0	0	0	0	0	0	0	0	0	0	0	0	0	0	0	0	0
Nonionella stella	0	0	0	0	0	0	0	0	0	0	0	0	0	0	0	0	0	0	0	0	0	0	0	0	0	0	0	0	0	0	0	0	0	2	1	0	0	0	0
Quinqueloculina stelligera	0	0	0	1	2	0	0	1	0	0	0	0	0	0	0	0	0	0	0	0	0	0	0	0	0	0	0	0	0	0	0	0	0	0	0	0	0	0	0
Nonion fabum	4	1	2	1	2	2	0	1	0	1	0	0	0	0	0	0	0	0	0	0	0	0	0	0	0	0	0	0	0	0	0	0	0	0	0	0	0	0	0
Adelosina sp	2	0	0	1	0	2	0	0	0	1	0	0	0	1	0	0	0	0	0	0	0	0	0	0	0	0	1	0	0	0	0	0	0	0	0	0	0	0	0
Quinqueloculina seminulum	2	0	0	2	4	1	0	3	0	0	0	0	0	4	0	2	0	0	1	0	0	0	0	0	0	0	1	0	0	0	0	0	0	0	0	0	0	0	0
Elphidium crispum	0	0	3	0	3	1	2	0	0	0	0	0	0	0	0	0	1	0	0	0	0	0	0	0	0	0	0	0	0	0	0	0	0	0	0	0	0	0	0
Oolina squamosa	0	0	0	0	0	0	0	0	0	0	0	0	0	0	0	0	0		0	0	1	0	0	0	0	0	0	0	0	0	0	0	0	0	0	0	0	0	0
Cassidulina laevigata	0	0	0	0	0	0	0	0	0	0	0	0	0	0	0	0	0	0	0	0	0	0	0	0	0	0	0	0	0	0	3	0	0	0	1	1	1	0	0
Cassidulina minuta	0	0	0	0	0	0	0	0	0	0	0	0	0	0	0	0	0	0	0	0	0	0	0	0	0	0	0	0	0	0	0	0	0	0	0	0	0	1	0
Total individuals per sample/depth	342	309	322	295	339	424	306	289	276	214	67	106	154	241	292	281	48	25	16	216	223	96	248	268	206	255	276	103	307	269	287	313	275	327	263	282	331	324	290

Appendix 5 - Faunistic density (Ni/g) of all specimens in surface samples, and total number of specimens obtained in each sample

Sample / Taxa	DÑA10	DÑA11	DÑA12	DÑA15	DÑA16	DÑA17	DÑA18	DÑA20
Bulimina elongata	0	0	0	0	0	0	0	2
Elphidium crispum	0	0	0	0	0	0	0	10
Quinqueloculina seminulum	0	0	0	0	0	0	0	6
Rosalina bradyi	0	0	0	0	1	0	0	6
Nonion fabum	0	0	0	1	0	0	0	1
Stilostomella sp	0	0	0	0	2	0	0	1
Quinqueloculina steligera	0	0	0	4	6	0	3	10
Quinqueloculina sp	0	0	0	4	1	0	0	27
Rosalina bradyi	0	0	0	0	0	0	0	1
Brizalina sp	0	0	0	1	6	0	0	2
Elphidium granosum	0	0	0	1	0	0	0	1
Elphidium cuvillieri	0	0	0	1	0	0	0	2
Planorbulina mediterranensis	0	0	0	1	0	0	0	2
Elphidium complanatum	0	0	0	0	0	0	0	3
Ammonia tepida	32	33	0	20	175	0	7	58
Haynesina germanica	16	33	32	45	16	4	8	14
Ammonia var becarii	0	0	0	0	0	0	0	75
Lagena sp	0	0	0	0	0	0	0	1
Asterigerinata mamila	0	0	0	2	0	0	1	1
Bolivina ordinaria	16	0	0	1	15	0	2	1
Cornuloculina sp	0	0	0	0	0	0	2	0
Fissurina spp	0	0	0	1	2	0	4	0
Trochammina inflata	0	0	0	0	6	213	3	0
Quinqueloculina laevigata	0	0	0	0	0	0	3	0
Jadammina macrescens	0	0	0	0	0	56	0	0
Cassidulina laevigata	0	0	0	0	1	0	0	0
Elphidium sp	0	0	16	0	5	0	0	0
Textularia sp	0	0	0	0	6	0	0	0
Nonionella stella	0	0	0	0	4	0	0	0
Hopkinsina atlantica	0	0	0	0	6	0	0	0
Ammotium sp	0	0	0	0	2	0	0	0
Cornuspira involvens	0	0	0	0	1	0	0	0
Miliammina fusca	0	0	0	1	17	0	0	0
Buliminella elegantissima	0	0	0	0	1	0	0	0
Cassidulina minuta	0	0	0	1	0	0	0	0
Total individuals per sample	64	66	48	84	273	273	33	224

Appendix 6 – Relative Abundance (%) of species with relative abundances >1% in Core C, sampling depth (m),

Depth / Taxa	46	50	54	58	62	66	70	74	78	82	86	90	94	98	116	120	124	128	132	136	140	144	148
Haynesina germanica	75.6	72.3	76.4	69.2	72.0	69.7	74.0	77.4	73.5	70.3	73.8	75.5	67.7	73.9	65.0	62.5	75.0	74.2	76.7	71.4	64.8	73.8	66.3
Ammonia tepida	19.5	23.4	21.2	25.2	23.4	23.7	22.2	19.5	22.9	23.8	22.3	21.9	26.1	17.3	23.5	26.0	17.5	15.7	17.5	19.0	19.9	17.1	16.6
Brizalina sp	0.5	0.0	0.0	0.0	0.6	0.0	0.0	0.0	0.0	0.0	0.1	0.0	0.0	0.0	0.0	0.3	0.0	0.0	0.0	0.0	1.0	0.0	0.3
Bolivina ordinaria	0.8	0.6	0.0	0.5	0.6	0.4	1.0	0.0	0.4	0.3	0.0	0.0	0.3	0.3	0.0	1.0	1.4	1.1	0.2	0.7	1.0	1.3	2.8
Elphidium cuvillieri	1.6	0.0	0.6	1.3	0.3	1.8	0.7	0.5	0.8	1.7	0.7	0.2	1.5	1.6	3.1	3.0	1.0	0.7	0.4	0.4	2.4	0.3	2.2
Elphidium oceanensis	1.0	1.5	1.5	1.9	0.9	3.5	0.0	1.0	1.2	2.4	0.6	0.4	0.6	0.0	2.8	4.6	1.0	2.6	1.1	2.2	1.7	3.4	0.0
Elphidium granosum	0.3	0.9	0.0	1.9	2.5	0.0	1.7	0.0	1.2	0.7	1.9	0.8	1.2	2.8	5.6	1.3	1.4	0.7	2.0	0.4	2.4	2.0	4.5
Elphidium sp	0.0	1.2	0.0	0.0	0.0	0.0	0.0	0.8	0.0	0.0	0.0	0.4	2.4	3.8	0.0	1.0	0.0	0.0	0.0	0.0	0.0	1.3	3.7
Quinqueloculina laevigata	0.0	0.0	0.0	0.0	0.0	0.0	0.0	0.0	0.0	0.0	0.0	0.0	0.0	0.0	0.0	0.3	0.0	0.0	0.0	1.9	0.0	0.0	0.0
Fissurina sp (1,2,3)	0.0	0.0	0.0	0.0	0.0	0.0	0.0	0.0	0.0	0.0	0.0	0.0	0.0	0.0	0.0	0.0	2.1	3.7	1.3	2.6	1.7	0.0	0.0
Quinqueloculina sp	0.0	0.0	0.0	0.0	0.0	0.0	0.0	0.0	0.0	0.0	0.0	0.0	0.0	0.0	0.0	0.0	0.0	0.0	0.0	0.4	3.8	0.0	0.0
Quinqueloculina stelligera	0.0	0.0	0.0	0.0	0.0	0.0	0.0	0.0	0.0	0.0	0.0	0.0	0.0	0.0	0.0	0.0	0.0	0.0	0.0	0.0	0.0	0.0	2.5

Appendix 7 – Relative Abundance (%) of species with relative abundances >1% in Core D, sampling depth (m),

Depth/Taxa	27	31	34	38	41	45	48	52	55	59	62	66	69	73	76	80	83	87	90	94	97	101	104	108	111	115	118	122	125	129	132	136	139	143	146	150	153	157	160
Haynesina germanica	25.1	26.2	23.9	15.6	15.3	19.8	21.6	29.1	17.4	77.6	82.1	53.8	43.5	38.2	30.1	35.0	54.2	48.0	43.8	76.9	88.8	76.0	89.9	70.5	80.1	85.1	38.0	80.6	85.0	81.8	63.8	53.4	45.5	60.6	54.4	40.8	62.2	69.1	67.2
Ammonia tepida	52.6	56.6	59.0	63.1	63.4	62.8	63.1	55.0	64.1	18.7	16.4	40.6	46.1	48.5	53.4	50.9	41.7	32.0	31.3	15.3	9.4	16.7	4.4	19.4	16.0	12.5	46.7	13.6	12.7	15.2	25.4	27.5	39.6	27.8	31.9	42.2	29.0	21.6	19.7
Brizalina sp	0.0	0.3	0.0	1.0	0.0	0.0	0.0	0.7	0.0	0.0	0.0	0.9	0.0	0.0	0.0	0.4	0.0	0.0	0.0	0.0	0.0	0.0	0.0	0.0	0.0	0.0	0.0	0.0	0.0	0.0	0.0	2.6	4.4	0.6	1.1	0.0	1.2	2.8	1.4
Bolivina ordinaria	0.0	0.0	0.0	0.0	0.3	0.0	0.0	0.3	0.0	0.5	1.5	0.0	0.0	0.0	0.0	1.1	0.0	0.0	0.0	3.2	0.0	0.0	0.4	1.1	1.0	1.2	0.0	0.0	0.7	0.4	2.4	3.5	1.5	2.8	1.9	8.9	0.6	2.5	8.3
Elphidium cuvillieri	1.8	4.9	0.9	2.0	4.7	2.8	0.3	3.1	9.8	0.9	0.0	1.9	2.6	2.1	1.4	0.0	0.0	0.0	0.0	0.5	0.4	0.0	0.0	0.4	0.0	0.0	2.9	0.0	0.0	0.0	0.7	3.5	0.0	2.1	2.7	0.7	0.6	0.0	0.3
Elphidium oceanensis	7.9	8.1	5.2	9.5	6.2	3.3	6.9	3.5	5.8	0.5	0.0	0.0	4.5	5.0	6.2	2.5	0.0	4.0	12.5	0.9	0.4	0.0	0.0	1.9	0.0	0.0	4.3	1.0	0.0	0.0	0.0	0.0	2.9	1.2	3.0	2.5	0.0	0.0	1.0
Elphidium granosum	2.6	0.0	3.1	2.7	2.1	3.8	3.9	3.8	0.7	0.0	0.0	0.0	0.0	1.7	2.7	4.2	0.0	8.0	6.3	1.4	0.4	0.0	0.0	0.0	0.0	0.0	2.5	0.0	0.0	0.0	0.0	0.0	1.8	0.0	0.0	0.0	0.0	1.9	1.0
Elphidium sp	3.5	1.6	3.4	0.0	2.7	4.7	0.0	0.7	0.0	0.0	0.0	0.0	0.0	0.0	2.1	2.8	0.0	0.0	0.0	0.0	0.0	4.2	0.0	0.0	0.0	0.4	1.1	0.0	0.0	0.0	0.0	0.0	0.0	0.0	0.0	0.0	3.0	0.0	0.0
Asterigerinata mamilla	0.0	0.0	0.0	0.3	0.3	0.2	0.7	1.0	0.4	0.0	0.0	0.0	0.6	0.0	0.3	0.4	2.1	0.0	0.0	0.5	0.0	0.0	0.0	0.4	0.0	0.4	0.0	0.0	0.0	0.0	0.3	0.0	0.0	0.0	0.8	0.7	0.0	0.9	0.3
Planorbulina mediterranensis	0.6	0.3	0.0	0.3	0.6	0.0	0.0	0.0	0.0	0.0	0.0	0.0	0.6	0.0	0.0	0.4	0.0	0.0	0.0	0.0	0.0	0.0	0.0	0.0	0.0	0.0	0.0	0.0	0.0	0.0	0.0	0.0	0.0	0.0	1.1	0.0	0.0	0.0	0.0
Uvigerina peregrina	0.0	0.0	0.3	0.7	0.0	0.5	1.3	0.0	0.4	0.0	0.0	0.0	0.0	0.0	0.0	0.0	0.0	0.0	0.0	0.0	0.0	0.0	0.0	0.0	0.0	0.0	0.0	0.0	0.0	0.0	0.0	0.0	0.0	0.3	0.0	0.0	0.0	0.0	0.0
Textularia sp	0.0	0.0	0.0	0.0	0.0	0.0	0.0	0.0	0.0	0.0	0.0	0.0	0.0	0.0	0.0	0.0	0.0	0.0	0.0	0.0	0.0	0.0	0.0	0.0	0.0	0.0	0.0	0.0	0.0	0.0	1.7	1.6	0.7	0.9	0.4	0.4	0.6	0.3	0.7
Rosalina bradyi	0.9	0.6	0.3	1.4	0.9	0.0	0.0	0.0	0.0	0.0	0.0	0.0	0.6	0.0	1.4	0.4	0.0	0.0	0.0	0.0	0.0	0.0	0.0	0.0	0.0	0.0	0.4	0.0	0.0	0.0	0.0	0.0	0.4	0.0	0.0	0.0	0.0	0.0	0.0
Fissurina sp (1,2,3)	0.0	0.0	0.0	0.0	0.0	0.0	0.0	0.0	0.0	0.0	0.0	2.8	0.6	0.0	0.0	0.0	0.0	8.0	0.0	1.4	0.0	3.1	5.2	6.0	2.9	0.0	3.3	4.9	1.6	2.6	4.2	7.0	2.2	2.4	1.9	3.2	0.9	0.3	0.0
Triloculina trigonula	0.0	0.3	0.0	0.0	0.0	0.0	0.0	0.0	0.0	0.0	0.0	0.0	0.0	1.7	0.0	0.4	0.0	0.0	0.0	0.0	0.0	0.0	0.0	0.0	0.0	0.0	0.0	0.0	0.0	0.0	0.0	0.0	0.0	0.0	0.0	0.0	0.0	0.0	0.0
Quinqueloculina sp	1.8	0.0	0.6	0.3	0.0	0.0	0.7	0.7	0.7	0.0	0.0	0.0	0.0	0.0	1.7	0.4	0.0	0.0	0.0	0.0	0.0	0.0	0.0	0.4	0.0	0.4	0.0	0.0	0.0	0.0	0.0	0.0	0.0	0.0	0.0	0.0	0.3	0.0	0.0
Nonion fabum	1.2	0.3	0.6	0.3	0.6	0.5	0.0	0.3	0.0	0.5	0.0	0.0	0.0	0.0	0.0	0.0	0.0	0.0	0.0	0.0	0.0	0.0	0.0	0.0	0.0	0.0	0.0	0.0	0.0	0.0	0.0	0.0	0.0	0.0	0.0	0.0	0.0	0.0	0.0
Quinqueloculina seminulum	0.6	0.0	0.0	0.7	1.2	0.2	0.0	1.0	0.0	0.0	0.0	0.0	0.0	1.7	0.0	0.7	0.0	0.0	6.3	0.0	0.0	0.0	0.0	0.0	0.0	0.0	0.4	0.0	0.0	0.0	0.0	0.0	0.0	0.0	0.0	0.0	0.0	0.0	0.0
Elphidium crispum	0.0	0.0	0.9	0.0	0.9	0.2	0.7	0.0	0.0	0.0	0.0	0.0	0.0	0.0	0.0	0.0	2.1	0.0	0.0	0.0	0.0	0.0	0.0	0.0	0.0	0.0	0.0	0.0	0.0	0.0	0.0	0.0	0.0	0.0	0.0	0.0	0.0	0.0	0.0
Cassidulina laevigata	0.0	0.0	0.0	0.0	0.0	0.0	0.0	0.0	0.0	0.0	0.0	0.0	0.0	0.0	0.0	0.0	0.0	0.0	0.0	0.0	0.0	0.0	0.0	0.0	0.0	0.0	0.0	0.0	0.0	0.0	1.0	0.0	0.0	0.0	0.4	0.4	0.3	0.0	0.0

Appendix 8 – Relative Abundance (%) of species with relative abundances >1% in surface samples

Sample/Taxa	DÑA10	DÑA11	DÑA12	DÑA15	DÑA16	DÑA17	DÑA18	DÑA20
Bulimina elongata	0.0	0.0	0.0	0.0	0.0	0.0	0.0	0.9
Elphidium crispum	0.0	0.0	0.0	0.0	0.0	0.0	0.0	4.4
Quinqueloculina seminulum	0.0	0.0	0.0	0.0	0.0	0.0	0.0	2.7
Rosalina bradyi	0.0	0.0	0.0	0.0	0.4	0.0	0.0	3.1
Nonion fabum	0.0	0.0	0.0	1.2	0.0	0.0	0.0	0.4
Stilostomella sp	0.0	0.0	0.0	0.0	0.8	0.0	0.0	0.4
Quinqueloculina steligera	0.0	0.0	0.0	4.7	2.3	0.0	9.1	4.4
Quinqueloculina sp	0.0	0.0	0.0	4.7	0.4	0.0	0.0	12.0
Rosalina bradyi	0.0	0.0	0.0	0.0	0.0	0.0	0.0	0.4
Brizalina sp	0.0	0.0	0.0	1.2	2.3	0.0	0.0	0.9
Elphidium granosum	0.0	0.0	0.0	1.2	0.0	0.0	0.0	0.4
Elphidium cuvillieri	0.0	0.0	0.0	1.2	0.0	0.0	0.0	0.9
Planorbulina mediterranensis	0.0	0.0	0.0	1.2	0.0	0.0	0.0	0.9
Elphidium complanatum	0.0	0.0	0.0	0.0	0.0	0.0	0.0	1.3
Ammonia tepida	50.0	50.0	0.0	23.5	64.9	0.0	21.2	25.7
Haynesina germanica	25.0	50.0	66.6	52.9	4.9	1.5	24.2	6.2
Ammonia var becarii	0.0	0.0	0.0	0.0	0.0	0.0	0.0	33.2
Asterigerinata mamila	0.0	0.0	0.0	2.4	0.0	0.0	3.0	0.4
Bolivina ordinaria	25.0	0.0	0.0	1.2	5.7	0.0	6.1	0.4
Cornuloculina sp	0.0	0.0	0.0	0.0	0.0	0.0	6.1	0.0
Fissurina spp	0.0	0.0	0.0	1.2	0.8	0.0	12.1	0.0
Trochammina inflata	0.0	0.0	0.0	0.0	2.3	78.0	9.1	0.0
Quinqueloculina laevigata	0.0	0.0	0.0	0.0	0.0	0.0	9.1	0.0
Jadammina macrescens	0.0	0.0	0.0	0.0	0.0	20.5	0.0	0.0
Elphidium sp	0.0	0.0	33.3	0.0	1.9	0.0	0.0	0.0
Textularia sp	0.0	0.0	0.0	0.0	2.3	0.0	0.0	0.0
Nonionella stella	0.0	0.0	0.0	0.0	1.5	0.0	0.0	0.0
Hopkinsina atlantica	0.0	0.0	0.0	0.0	2.3	0.0	0.0	0.0
Ammotium sp	0.0	0.0	0.0	0.0	0.8	0.0	0.0	0.0
Miliammina fusca	0.0	0.0	0.0	1.2	5.7	0.0	0.0	0.0
Cassidulina minuta	0.0	0.0	0.0	1.2	0.0	0.0	0.0	0.0